

THESIS FOR THE DEGREE OF DOCTOR OF PHILOSOPHY

MgB₂ hot-electron bolometer mixers for sub-mm wave
astronomy

EVGENII NOVOSELOV



CHALMERS

Terahertz and Millimetre Wave Laboratory
Department of Microtechnology and Nanoscience - MC2
Chalmers University of Technology
Göteborg, Sweden, 2017

MgB₂ hot-electron bolometer mixers for sub-mm wave astronomy

EVGENII NOVOSELOV

© Evgenii Novoselov, 2017

ISBN 978-91-7597-575-7

Löpnummer: 4256

i serien Doktorsavhandlingar vid Chalmers tekniska högskola
Ny serie (ISSN 0346-718X)

Technical Report MC2-360

ISSN 1652-0769

Chalmers University of Technology

Department of Microtechnology and Nanoscience - MC2

Terahertz and Millimetre Wave Laboratory

SE-412 96 Göteborg, Sweden

Phone: +46 (0) 31 772 1000

Cover:

Left: HPCVD system deposition chamber. Center upper left: SEM image of spiral antenna coupled MgB₂ HEB. Center upper right: TEM image of 5 nm thick HPCVD grown MgB₂ film on SiC substrate. Center: Cold plate of LHe cryostat. Center lower left: SEM image of HPCVD grown MgB₂ film on Al₂O₃ substrate. Center lower right: 3D CAD image of MgB₂ HEB. Upper right: Chamber view during MgB₂ film deposition. Lower right: mixer block with Si lens. Designed by Niia Silaeva.

Printed by Chalmers Reproservice

Göteborg, Sweden, May 2017

Per aspera ad astra

Abstract

Spectroscopy and photometry in the terahertz (THz) range of remote space objects allows for a study of their chemical composition, because this range covers rotational lines from simple molecules and electron transition lines from atoms and ions. Due to high spectral resolution, THz heterodyne receivers allow for studying dynamical properties of space objects manifested in doppler-shifted emission lines. Niobium nitride (NbN) hot-electron bolometer (HEB) mixers currently used at frequencies >1 THz, provide a typical gain bandwidth (GBW) of 3 GHz, and consequently, a noise bandwidth (NBW) of 4 GHz. This property severely limits the functionality of astronomical instruments. Moreover, the low critical temperature ($T_c = 8\text{--}11$ K) of NbN ultrathin films necessitates usage of liquid helium (LHe) for device cooling, which reduces lifetime of spaceborne missions.

In this thesis, a study of HEB mixers dedicated for sub-mm wave astronomy applications made from magnesium diboride (MgB_2) ultrathin films is presented. It is shown that MgB_2 HEB mixers reach a unique combination of low noise, wide noise bandwidth, and high operation temperature when 8 nm thick MgB_2 films ($T_c = 30$ K) are used. The hybrid physical chemical vapour deposition (HPCVD) technique allows for reproducible deposition of such thin films. The high T_c of MgB_2 (39 K), and consequently, short (3 ps) electron-phonon interaction time result in a GBW of up to 10 GHz and possibility of operation at temperatures >20 K, where compact cryocoolers are available. The GBW was observed to be almost independent on both bias voltage and bath temperature. A NBW of 11 GHz with a minimum double sideband (DSB) receiver noise temperature of 930 K is achieved at a 1.63 THz local oscillator (LO) and a 5 K bath temperature. At 15 K and 20 K, noise temperatures are 1100 K and 1600 K, respectively. From 0.69 THz to 1.63 THz noise increases by only 12%, and hence, low noise performance is expected even at higher frequencies. The minimum receiver noise temperature is achieved in a quite large range of both bias voltages (5–10 mV) and LO power. Compared to initial results, higher sensitivity and larger NBW are due to a larger HEB width (lower contact resistance), applied *in-situ* contact cleaning, and a smaller film thickness. The increase of noise temperature when operation temperature rises from 5 K to 20 K is due to a reduction of conversion gain by 2–4 dB caused by the reduced LO power absorbed in the HEB. The output noise of the HEB remains the same (120–220 K depending on the bias point).

Keywords: conversion gain, electron-phonon interaction, gain bandwidth, hot-electron bolometer, magnesium diboride, mixer, noise bandwidth, noise temperature, superconductor, thin film, THz detector.

List of Publications

Appended papers

This thesis is based on the following papers:

- [A] S. Bevilacqua, **E. Novoselov**, S. Cherednichenko, H. Shibata, and Y. Tokura, “MgB₂ hot-electron bolometer mixers at terahertz frequencies,” in *IEEE Transactions on Applied Superconductivity*, vol. 25, no. 3, June 2015, Art. no. 2301104.
- [B] **E. Novoselov**, S. Bevilacqua, S. Cherednichenko, H. Shibata, and Y. Tokura, “Effect of the critical and operational temperatures on the sensitivity of MgB₂ HEB mixers,” in *IEEE Transactions on Terahertz Science and Technology*, vol. 6, no. 2, pp. 238-244, March 2016.
- [C] **E. Novoselov**, N. Zhang, and S. Cherednichenko, “Study of MgB₂ ultrathin films in submicron size bridges,” in *IEEE Transactions on Applied Superconductivity*, vol. 27, no. 4, June 2017, Art. no. 7500605.
- [D] **E. Novoselov**, N. Zhang, and S. Cherednichenko, “MgB₂ hot electron bolometer mixers for THz heterodyne instruments,” in *Proceedings of SPIE*, vol. 9914, July 2016, Art. no. 99141N.
- [E] **E. Novoselov**, N. Zhang, and S. Cherednichenko, “Wideband THz HEB mixers using HPCVD MgB₂ thin films,” in *Proceedings of 41st International Conference on Infrared, Millimeter and Terahertz Waves*, Copenhagen, Denmark, 25-30 September 2016.
- [F] **E. Novoselov** and S. Cherednichenko, “Broadband MgB₂ hot-electron bolometer THz mixers operating up to 20 K,” in *IEEE Transactions on Applied Superconductivity*, vol. 27, no. 4, June 2017, Art. no. 2300504.
- [G] **E. Novoselov** and S. Cherednichenko, “Low noise terahertz MgB₂ hot-electron bolometer mixers with an 11 GHz bandwidth,” in *Applied Physics Letters*, vol. 110, no. 3, January 2017, Art. no. 032601.
- [H] **E. Novoselov** and S. Cherednichenko, “Gain and noise in THz MgB₂ hot-electron bolometer mixers with a 30 K critical temperature,” submitted to *IEEE Transactions on Terahertz Science and Technology*, April 2017.

Other papers and publications

The following papers and publications are not appended to the thesis, either due to contents overlapping of that of appended papers, or due to contents not related to the thesis.

- [a] **E. Novoselov**, N. Zhang, and S. Cherednichenko, “MgB₂ HEB mixers at operation temperatures above liquid helium temperature,” in Proceedings of 27th *International Symposium on Space Terahertz Technology*, Nanjing, China, 12-15 April 2016.
- [b] S. Bevilacqua, **E. Novoselov**, S. Cherednichenko, H. Shibata, and Y. Tokura, “Wideband MgB₂ hot-electron bolometer mixers: IF impedance characterisation and modeling,” in *IEEE Transactions on Applied Superconductivity*, vol. 26, no. 3, April 2016, Art. no. 2300105.
- [c] **E. Novoselov**, S. Bevilacqua, S. Cherednichenko, H. Shibata, and Y. Tokura, “THz low noise mixers for sub-mm astronomy,” in Proceedings of 3rd *Swedish Microwave Days*, Linköping, Sweden, 15-16 March 2016, p. 50.
- [d] S. Bevilacqua, **E. Novoselov**, S. Cherednichenko, H. Shibata, and Y. Tokura, “Characterisation and Modeling of MgB₂ HEBs IF impedance,” in Proceedings of 3rd *Swedish Microwave Days*, Linköping, Sweden, 15-16 March 2016, p. 55.
- [e] **E. Novoselov**, S. Bevilacqua, S. Cherednichenko, H. Shibata, and Y. Tokura, “Noise measurements of the low T_c MgB₂ HEB mixer at 1.6 THz and 2.6 THz,” in Proceedings of 26th *International Symposium on Space Terahertz Technology*, Cambridge, USA, 16-18 March 2015, Art. no. P-31.
- [f] S. Cherednichenko, **E. Novoselov**, S. Bevilacqua, H. Shibata, and Y. Tokura, “Study of MgB₂ HEB mixers vs the LO frequency and the bath temperature,” in Proceedings of 26th *International Symposium on Space Terahertz Technology*, Cambridge, USA, 16-18 March 2015, Art. no. M2-1.
- [g] S. Cherednichenko, S. Bevilacqua, and **E. Novoselov**, “THz hot-electron bolometer mixers,” in Proceedings of 39th *International Conference on Infrared, Millimeter and Terahertz Waves*, Tucson, USA, 14-19 September 2014.
- [h] N. Balbekin, **E. Novoselov**, P. Pavlov, V. Bespalov, and N. Petrov, “Nondestructive monitoring of aircraft composites using terahertz radiation,” in *Proceedings of SPIE*, vol. 9448, March 2015, Art. no. 94482D.
- [i] V.G. Bespalov, A.A. Gorodetskii, Y.V. Grachev, S.A. Kozlov, and **E.V. Novoselov**, “Pulse terahertz reflectometer,” in *Scientific and Technical Journal of Information Technologies, Mechanics, and Optics*, vol. 71, no. 1, pp. 19-23, January-February 2011, (in russian).

- [j] **E.V. Novoselov** and V.G. Bespalov, “Design of the tunable mirror objective for pulse terahertz reflectometer spectrograph-intravisor,” in *Scientific and Technical Journal of Information Technologies, Mechanics, and Optics*, vol. 70, no. 6, pp. 6-9, November-December 2010, (in russian).
- [k] A.A. Andreev, V.G. Bespalov, A.A. Gorodetskii, S.A. Kozlov, V.N. Krylov, G.V. Lukomskii, **E.V. Novoselov**, N.V. Petrov, S.E. Putilin, and S.A. Stumpf, “Generation of ultrabroadband terahertz radiation under optical breakdown of air by two femtosecond pulses of different frequencies,” in *Optics and Spectroscopy*, vol. 107, no. 4, pp. 538-544, October 2009.

Notations and abbreviations

Notations

2Δ	Superconducting energy gap
$2\Delta_{dirty}$	Dirty limit superconducting energy gap
$2\Delta_{\pi}$	Superconducting energy π -gap
$2\Delta_{\sigma}$	Superconducting energy σ -gap
\hbar	Dirac constant
α	Thermometer local sensitivity
β	Acoustic phonon transmission coefficient
γ	Electron specific heat coefficient
ΔT	Temperature change
ΔU_0	DC voltage response
ϵ	Permittivity
λ	Wavelength
λ_L	Penetration depth
μ_0	Permeability of vacuum
ξ	Coherence length
ρ_{295K}	Room temperature resistivity
θ	Electron temperature
τ	Bolometer time constant
τ_{θ}	Electron temperature relaxation time
τ_{θ}^*	Modified electron temperature relaxation time
τ_e	Effective bolometer time constant
τ_{ep}	Electron phonon interaction time
τ_{esc}	Phonon escape time
τ_{mix}	Mixer time constant
τ_{pe}	Phonon electron interaction time
Φ_0	Flux quantum
χ	Power exchange function
ω	Angular frequency
ω_i	Imaginary frequency
ω_{IF}	Intermediate angular frequency
ω_{LO}	Local oscillator angular frequency
ω_0	Response rate
ω_s	Signal angular frequency
B	Bandwidth

C	Heat capacitance
C'	Dimensionless self heating parameter
C_0	Self heating parameter
c_e	Electron specific heat
c_p	Phonon specific heat
d	Film thickness
f_g	Gain bandwidth frequency
f_{IF}	Intermediate frequency
f_n	Noise bandwidth frequency
G	Thermal conductance
G_d	Dynamic thermal conductance
G_e	Effective thermal conductance
G_{IF}	IF chain gain
G_m	Mixer conversion gain
G_{tot}	Receiver conversion gain
I	Current
I_0	Bias current
I_c	Critical current
J_c	Critical current density
J_d	Depairing current density
k_B	Boltzmann constant
L	Bolometer length
L_{opt}	Optical losses
n	Atomic density
N_{out}	Output noise power
P	Power
P_{cold}	Cold load intermediate frequency output power
P_{hot}	Hot load intermediate frequency output power
P_{IF}	Intermediate frequency signal power
P_{LO}	Local oscillator power
P_{out}	Intermediate frequency output power
P_s	Signal power
R	Resistance
R_0	Bolometer resistance
R_L	Load resistance
R_{ons}	Onset resistance
R_S	Sheet resistance
R_t	Thermometer resistance
R_v	Voltage responsivity
R_{295K}	Room temperature resistance
RRR	Residual resistance ratio
r	Etching rate
S/N	Signal to noise ratio
T	Temperature
t	Time
T_b	Bolometer temperature
T_{bath}	Reservoir temperature
T_c	Critical temperature
T_D	Debye temperature
T_{FL}	Thermal fluctuation noise

T_J	Johnson noise
T_{IF}	IF chain noise temperature
T_m	Mixer noise temperature
T_{opt}	Equivalent noise temperature of optical components
T_{out}	Mixer output noise temperature
T_p	Phonon temperature
T_{rec}	Receiver noise temperature
T_{REF}	Equivalent noise temperature at the reference state
u	Speed of sound
U	Voltage
U_0	Bias voltage
U_{LO}	Voltage amplitude of the local oscillator
U_s	Voltage amplitude of the signal
W	Bolometer width
Z	Bolometer impedance

Abbreviations

2-T	Two-temperature
3D	Three-dimensional
AFM	Atomic force microscope
Al ₂ O ₃	Sapphire
Ar	Argon
Au	Gold
B	Boron
B ₂ H ₆	Diborane
BCS	Bardeen-Cooper-Schrieffer
BH ₃	Borane
BWO	Backward-wave oscillator
CAD	Computer-aided design
CH ₂ F ₂	Difluoromethane
CH ₂ O ₂	Formic acid
DC	Direct current
DSB	Double sideband
FIR	Far Infrared
GaAs	Gallium arsenide
GBW	Gain bandwidth
GHz	10 ⁹ Hz
H ₂	Hydrogen
HCl	Hydrogen chloride
HDPE	High-density polyethylene
HEB	Hot electron bolometer
HEMT	High-electron-mobility transistor
HPCVD	Hybrid physical chemical vapour deposition
IF	Intermediate frequency
IR	Infrared
InP	Indium phosphide
InSb	Indium antimonide
I-V	Current versus voltage
LHe	Liquid helium
LNA	Low noise amplifier
LO	Local oscillator
LSB	Lower sideband
MBE	Molecular beam epitaxy
Mg	Magnesium
MgO	Magnesium oxide
MgB ₂	Magnesium diboride
N ₂	Nitrogen
NbN	Niobium nitride
NbTiN	Niobium titanium nitride
NBW	Noise bandwidth
O ₂	Oxygen
PLD	Pulsed laser deposition
RF	Radio frequency
R-T	Resistance versus temperature
SEM	Scanning electron microscope

SD	Schottky diode
Si	Silicon
SiC	Silicon carbide
SiN _x	Silicon nitride
SiO ₂	Silicon dioxide
SIS	Superconductor-insulator-superconductor tunnel junction
SSPD	Superconducting single-photon detector
SQUID	Superconducting quantum interference device
TEM	Transmission electron microscope
THz	10 ¹² Hz
Ti	Titanium
USB	Upper sideband
UV	Ultraviolet
XRD	X-ray diffractometer
YIG	Yttrium iron garnet

Contents

Abstract	v
List of Publications	vii
Notations and abbreviations	x
1 Introduction	1
2 Background	5
2.1 Bolometric receiver	5
2.1.1 Direct detection	6
2.1.2 Frequency mixing	8
2.2 Superconducting HEB mixers	9
2.2.1 Photoresponse of phonon-cooled HEB mixers	9
2.2.2 The lumped element HEB model	11
2.2.2.1 Conversion gain	11
2.2.2.2 Noise temperature	12
2.2.3 Two-temperature model	13
2.3 THz heterodyne receivers design	14
3 MgB₂ superconducting ultrathin films	17
3.1 MgB ₂ thin films	17
3.2 Chalmers HPCVD system	19
3.2.1 System design	20
3.2.2 Safety	22
3.3 HPCVD grown ultrathin films	23
3.4 Films thinning down using Ar ⁺ ion beam milling	28
4 MgB₂ HEB design and fabrication	31
4.1 E-beam lithography based process	31
4.2 UV lithography based process	34
5 HEB mixers characterisation techniques	37
5.1 Sensitivity characterisation	37
5.1.1 Y-factor technique	38
5.1.2 U-factor technique	40
5.2 GBW characterisation	43
5.3 S/N ratio characterisation	43

6	MgB₂ HEBs THz characterisation results	47
6.1	Devices fabricated from MBE grown films	47
6.1.1	DC characterisation	47
6.1.2	Direct detection characterisation	48
6.1.3	Mixer sensitivity characterisation	49
6.2	Devices fabricated from HPCVD grown films	53
6.2.1	Gain bandwidth characterisation	53
6.2.2	Mixer sensitivity characterisation	56
6.2.2.1	Initial results	56
6.2.2.2	Low noise MgB ₂ HEB mixers	57
6.2.3	Further improvement	62
7	Conclusion and future outlook	65
8	Summary of appended papers	69
	Acknowledgments	73
	Bibliography	75
	Appended Papers	95

Chapter 1

Introduction

The 0.1–10 THz part of electromagnetic spectrum between the microwave and infrared (IR) bands is referred to as terahertz (THz) range [1, 2]. Despite technological difficulties (the THz gap), this region has proven to be of great interest for medical [3] and security [4] sensing, communication [5], and Earth and Space science [6]. The THz range covers rotational lines from simple molecules and the ground state fine-structure emission lines from atoms and ions [7]. This is of great interest for astronomy [8], because of the possibility to study physics, dynamics, and chemistry of galaxies, star-formation regions, the interstellar medium, comets, asteroids, outer planet atmospheres, etc.

In order to resolve fine structure of molecular emission lines, heterodyne receivers with a high spectral resolution ($\lambda/\Delta\lambda \approx 10^6\text{--}10^7$) are required [9, 10]. For such applications several types of devices have been used as a mixer element for a heterodyne receiver, e.g. Schottky diodes (SD) [11], superconductor-insulator-superconductor tunnel junctions (SIS) [12], hot-electron bolometers (HEB) [13]. At frequencies above 1 THz HEBs are devices of choice (see Figure 1.1). Superconducting HEB mixers were introduced in Ref. [14] after the discovery of the electron-heating effect in superconducting films [15]. Until recently, the state-of-the-art phonon-cooled HEBs were fabricated using niobium nitride (NbN) and niobium titanium nitride (NbTiN) ultrathin films. HEB mixers are highly sensitive THz detectors providing a low receiver noise temperature from 300 K at 1.3 THz local oscillator (LO) [16] to 1150 K at 5.25 THz LO [17]. They were employed in many receivers for astronomical and atmospheric science observation programs launched in recent years, e.g. RLT [18], APEX [19, 20], the Herschel Space Observatory [21, 22], TELIS [23, 24], STO/STO-2 [25–29], and SOFIA [30–32]. They were also chosen for a number of current programs and programs under development, such as ASTE [33, 34], DATE5 [16, 35], SMILES-2 [36, 37], GUSSTO [38], Millimetron [39, 40], FIRSPEX [41], and OST [42].

NbN HEB mixers typically have a gain bandwidth (GBW) of ≈ 3 GHz (NbTiN HEB mixers have even smaller GBW of ≈ 2 GHz). As a result, the receiver noise temperature increases towards higher intermediate frequencies (IF) and doubles already at an IF of ≈ 4 GHz. Therefore, the number of scientific tasks in sub-mm wave astronomy which can be performed with HEB mixers is limited [43].

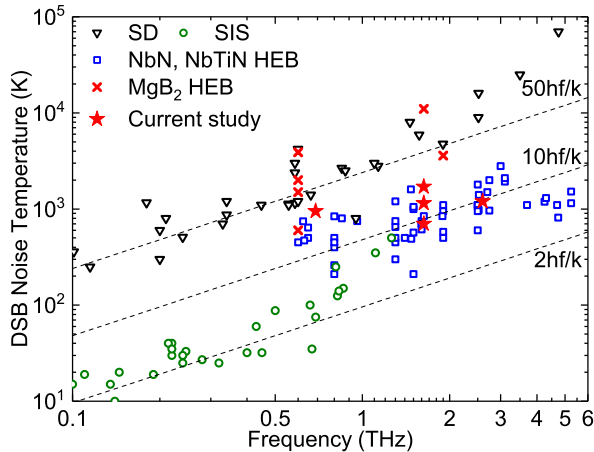


Fig. 1.1: State-of-the-art noise temperature versus LO frequency for different THz mixer technologies: SD [44–69]; SIS [70–90]; NbN, NbTiN HEB [16, 17, 19, 31–35, 91–121]; and MgB₂ HEB [122–126].

Figure 1.2(a) demonstrates a mapping of Galaxy M82 by the HIFI instrument of the Hershel Space Observatory [43]. The high spectral resolution and sensitivity of the HIFI instrument allowed for observation of very weak (<5 K) frequency-shifted emissions from the two arms of the galaxy. Measured spectra at 0.57 THz (CO line) and 1.9 THz (CII line) are shown in Figure 1.2(b). One arm of the galaxy is moving towards us and the other from us, which results in the existence of two main velocity components: the blue-shifted and the red-shifted emission lobes, which are clearly seen on the left spectrum in Figure 1.2(b). The large difference between relative to the Earth velocities of the Galaxy M82 arms of 400 km/s resulted in the rather broad 1.9 THz CII spectral line (2.5 GHz). The nominal IF bandwidth of the used receivers (2.4 GHz) was just enough to fit this spectral line, but it did not allow to get the baseline of the signal properly. At the same time, the observation at higher frequencies might be interesting due to the smaller beam size. For example, the beam at 1.9 THz was almost four times smaller than at 0.57 THz (red bars on Figure 1.2(a)). Moreover, emission lines for some molecules exist only at higher frequencies. At 4.7 THz such velocity difference will result in ≈ 6 GHz broad lines, which is well above a typical NbN HEB mixer bandwidth. On the other hand, a superconducting critical temperature (T_c) of 8–11 K limits NbN HEB mixer operation to liquid helium (LHe) temperatures (<6 K). The lack of 4K cryocoolers qualified for space application necessitates of LHe utilization that leads to very limited spaceborne mission lifetimes. In order to improve the functionality of HEB mixers, other superconducting materials must be used, e.g. magnesium diboride (MgB₂).

The discovery of superconductivity in MgB₂ [127] with the highest T_c among intermetallic compounds (bulk $T_c = 39$ K) and fast progress in thin film deposition techniques [128–130] opened new opportunities in HEB development. For the first time heterodyne mixing using a MgB₂ HEB with a T_c of 22 K made from a molecular beam epitaxy (MBE) grown [130] 20 nm thick

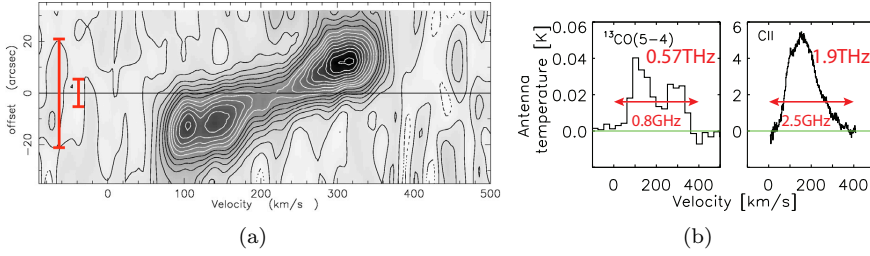


Fig. 1.2: Observation of Galaxy M82 by the Hershel Space Observatory (a) Position-velocity diagram of the Nucleus of M82. The two red bars show the largest (44'' at 0.57 THz) and the smallest (12'' at 1.9 THz) beams in observations. (b) Observed spectra of Galaxy M82: CO line at 0.57 THz by SIS mixers (left) and CII line at 1.9 THz by HEB mixers (right). The same velocity range corresponds to about three times wider signal bandwidth at 1.9 THz than at 0.57 THz. Illustrations from Ref. [43].

film on a silicon (Si) substrate was reported in 2007 [122]. The device had a rather high receiver noise temperature of 11 000 K at 1.6 THz but the GBW was already 2.3 GHz at 0.6 THz despite such a thick film.

In subsequent works by *Bevilacqua et al.* [123, 124, 131] the GBW of MgB₂ HEB mixers made from MBE grown films on c-cut sapphire (Al₂O₃) substrates was studied the most. The large dimensions of initial HEBs (100–500 μm²) and consequently high LO power requirements forced the utilization of low frequency (0.35–0.6 THz) sources providing more output power for device characterisation. Therefore, a large superconducting energy gap necessitated the use of high bath temperatures of up to few degrees below the T_c in order to make the gap smaller than the energy of photons. The maximum GBW of 3.4 GHz was achieved with a 10 nm thick device with a T_c of 14 K [124]. And the possibility to increase the GBW up to 8–10 GHz using 3–5 nm thick MgB₂ HEB mixers with a T_c >30 K was suggested [123]. Fabrication of smaller devices (3–42 μm²) that requires less LO power allowed for the study of MgB₂ HEB mixers sensitivity in a wide range of bath temperatures [123, 124]. The minimum noise temperature of 800 K at 0.6 THz was demonstrated with a device with a T_c of 8.5 K [123]. A HEB mixer with a T_c of 15 K had a higher noise temperature of 1500 K, but it was also shown that the noise temperature remains constant at bath temperatures ranging from 4.2 K up to 10.5 K [124]. The need for fabrication of submicron size MgB₂ HEB mixers for operation at higher LO frequencies was highlighted [124].

In parallel work on MgB₂ HEB mixers by *Cunnane et al.* [125, 126, 132] devices made from hybrid physical-chemical vapour deposition (HPCVD) grown [133] films on silicon carbide (SiC) substrates were studied. A GBW greater than 8 GHz was demonstrated with a 15 nm thick HEB mixer with a T_c of 33 K. The best noise performance achieved for HEB mixers made from HPCVD grown films was 2000 K at 0.6 THz [126]. This device had a noise bandwidth (NBW) of 6.5 GHz and the noise temperature had a minimal dependence on a bath temperature up to 20 K. At 1.9 THz, the noise temperature of such device increased to 3600 K.

The research presented in this thesis addresses the problem of limited bandwidth and low operation temperature of THz HEB mixers. The increase of bandwidth and operation temperature is required without sacrificing the low noise performance. The low noise temperature and the large bandwidth were shown for MgB₂ HEB mixers separately, but devices simultaneously demonstrating both of these features were not achieved. **The achievement of sensitivity and bandwidth superior to NbN HEB mixers and operation at bath temperatures above the LHe temperature by fabrication of submicron size MgB₂ HEB mixers was the main goal of this work.**

- The performance of HEB mixer is mainly affected by the quality of superconducting thin film used for device fabrication. **The primary goal** was to develop the process for growth of MgB₂ ultrathin (5-10 nm thick) films with a T_c above 30 K, low roughness, high homogeneity, and applicable for fabrication of submicron size structures.
- **The second goal** was the development of HEB fabrication process capable for submicron size device fabrication, preserving superconducting film quality, and providing a high yield and a high robustness.
- **Third**, the fabricated HEB mixers should be tested at THz frequencies. The dependence of their intrinsic parameters on LO frequency and power, a T_c , and a bath temperature should be studied in order to find the way for further MgB₂ HEB mixers improvement and their optimization for specific tasks.

The thesis is structured in 6 chapters. **Chapter 2** contains an overview of: bolometer detection principles, heterodyne mixing, HEB modeling, and design of heterodyne receivers utilizing HEB mixers. **Chapter 3** describes the HPCVD technique used for MgB₂ ultrathin film deposition and the study of achieved films. The electron beam (e-beam) and ultraviolet (UV) lithography HEB fabrication processes are presented in **Chapter 4**. **Chapter 5** provides the detailed description of the measurement setup and techniques used for device characterization at THz frequencies. The summary of THz characterization results is given in **Chapter 6**. Finally, **Chapter 7** summarises the results of this work and provides the future outlook.

Chapter 2

Background

This chapter provides an overview of: bolometer operation principles and main characteristics which determine the bolometer performance. Total power and frequency selective detection regimes of bolometer operation are described and discussed. The lumped HEB mixer model and the two-temperature (2-T) model of electron-phonon relaxation are presented as well as an overview of heterodyne receivers designs.

2.1 Bolometric receiver

A simple bolometer consists of three parts. Figure 2.1(a) represents these parts: an absorber where an incident power is absorbed and thermalized; a perfectly coupled thermometer which measures changes of the absorber temperature; and a weak thermal link connecting the absorber and a heat sink to return the absorber into the initial state in an absence of incident power. The absorber is characterised by a heat capacity C , the thermal link by a thermal conductivity G and the heat sink by a temperature T_{bath} .

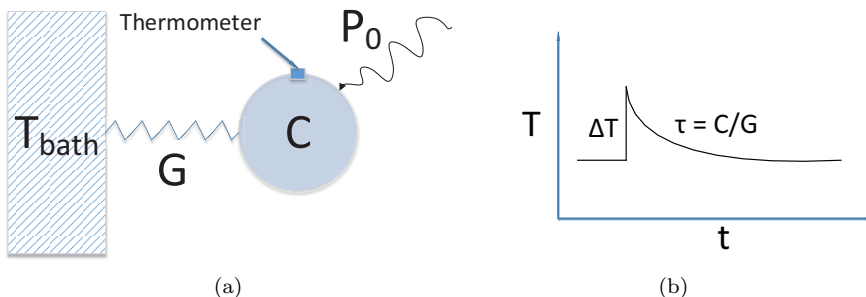


Fig. 2.1: (a) Schematic of simple bolometer consisting of an absorber with a heat C , a thermometer and a weak link with a thermal conductivity G connecting the absorber to a heat sink with a temperature T_{bath} . (b) Schematic representation of bolometer working principle. An incoming radiation with a total power P_0 increases bolometer temperature by $\Delta T = P_0/G$. After the incoming radiation is removed the bolometer temperature decays back with a time constant $\tau = C/G$.



Fig. 2.2: Schematic of total power detection.

This device can be used to measure a steady power input P_0 which gives a temperature increase of $\Delta T = P_0/G$ with an assumption of uniform heating of the bolometer. In case of a variable power $P(t)$ the dynamics of the bolometer temperature T_b can be described by a heat balance equation:

$$C \frac{dT_b}{dt} + G(T_b - T_{bath}) = P(t) \quad (2.1)$$

When the bolometer is no longer irradiated, i.e. $P(t) = 0$, its temperature relaxes back to T_{bath} . Then Equation 2.1 can be solved as:

$$T_b(t) = T_{bath} + \Delta T e^{-\frac{t}{\tau}} \quad (2.2)$$

where $\tau = C/G$ is a bolometer time constant.

2.1.1 Direct detection

Being irradiated by the input power P_0 the receiver produces a direct current (DC) voltage response ΔU_0 which is proportional to the power of incoming radiation (see Figure 2.2). In this case the receiver measures the total power of incoming radiation independently on frequency in the whole band where the receiver is sensitive. The total power detector is characterised by a voltage responsivity:

$$R_v = \frac{\Delta U_0}{P_0} \quad (2.3)$$

An electrical resistance thermometer (thermistor) (see Figure 2.3) might be used to measure the temperature of bolometer. In the electrical resistance thermometer a change in temperature is converted into a change in resistance R_t , which is converted into voltage changes with a readout current. The temperature of such a bolometer irradiated by an incident signal (ω_s) with a power $P(t) = P_0 + P_1 e^{i\omega_s t}$ changes as $T_b = T_0 + T_1 e^{i\omega_s t}$. The voltage responsivity of bolometer with a thermistor biased with a constant current I_0 is [134]:

$$R_v = \frac{I_0 \frac{dR_t}{dT}}{G_d - I_0^2 \left(\frac{dR_t}{dT} \right) + i\omega_s C} \quad (2.4)$$

where $G_d = dP/dT$ is a dynamic thermal conductance at the temperature T_0 . Equation 2.4 is valid if the load resistance $R_L \gg R_t$. The bolometer responsivity is influenced by the thermal feedback which can be expressed as the effective thermal conductance $G_e = G_d - I_0^2 (dR_t/dT)$. The thermal feedback also modifies the measured bolometer time constant $\tau_e = C/G_e$. It is

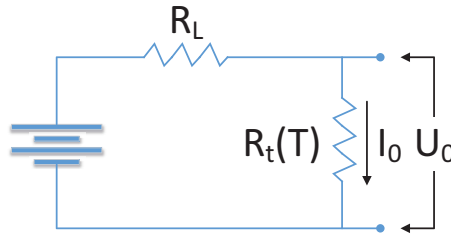


Fig. 2.3: Bias circuit of electrical resistance thermometer. I_0 is the bias current, U_0 the bias voltage, R_L the load resistance, $R_t(T)$ the temperature dependent thermometer resistance.

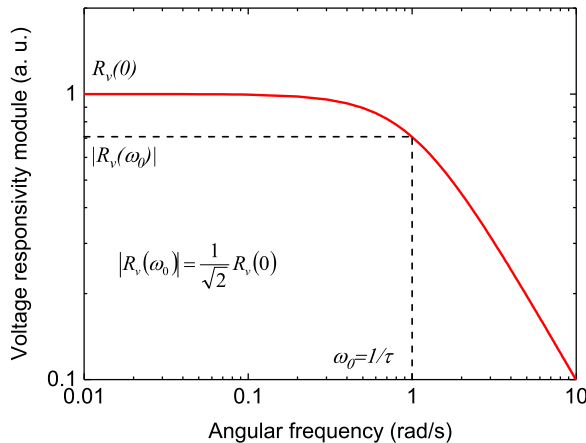


Fig. 2.4: Voltage responsivity versus frequency.

convenient to define a local sensitivity for the thermometer $\alpha = R_t^{-1}(dR_t/dT)$ evaluated at T_0 . With new definitions the voltage responsivity becomes:

$$R_v = \frac{I_0 R_t \alpha}{G_e (1 + i\omega_s \tau_e)} \quad (2.5)$$

The module of voltage responsivity:

$$|R_v| = \frac{R_v(0)}{\sqrt{1 + \omega_s^2 \tau_e^2}} \quad (2.6)$$

where $R_v(0) = I_0 R_t \alpha / G_e$ is the zero frequency responsivity, is plotted in Figure 2.4. The bolometer time constant τ_e determines the bolometer response rate ($\omega_0 = 1/\tau_e$).

The absorber and thermistor could be combined in one structure as in case of microbolometer which is a thin film resistor with a high temperature coefficient of resistance. The microbolometers were realized in different geometries in order to reduce a thermal coupling of the microbolometer to the heat sink, e.g. placing on a thin membrane [135] or making free-standing bridge bolome-

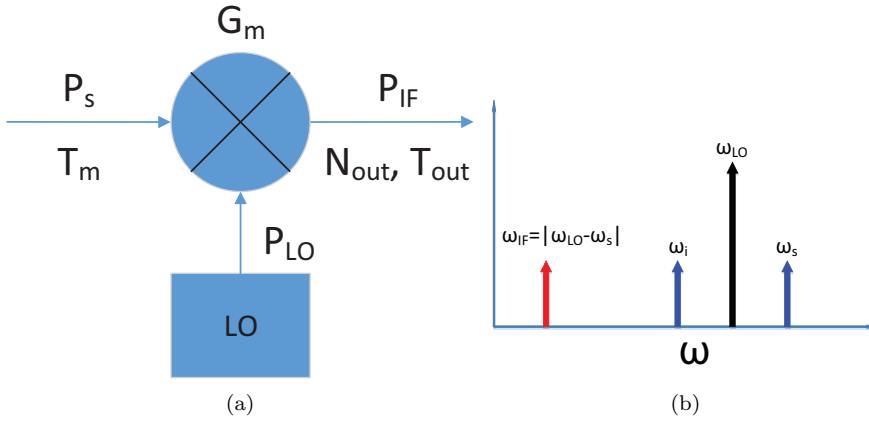


Fig. 2.5: (a) Schematic of down-converting mixer. (b) Schematic of down-conversion in a frequency domain.

ters [136]. A lower thermal coupling results in a higher voltage responsivity, but simultaneously the response rate is decreasing.

The total power detector may be a very efficient radiation detector but it does not provide any spectral information. In order to perform spectrometry a narrow band-pass filter is placed at the receiver input, e.g. an interferometer. However, the size of interferometer scales with its resolution. So the maximum practical spectral resolution which might be achieved in THz range using interferometer is $\approx 10^3$.

2.1.2 Frequency mixing

Heterodyne receivers have some advantages over direct detection receivers. First, both amplitude and phase information are preserved. Second, a high frequency narrow band-pass filter is not required at the receiver input in order to achieve a high spectral resolution. In heterodyne receivers a down-converting mixer mixes an incident signal (ω_s), which in a general case might be represented as a sum of frequency components, with a monochromatic radiation (ω_{LO}) from an LO (see Fig. 2.5). The total radio frequency (RF) voltage $U(t)$ across the mixer is:

$$U(t) = U_s(\cos(\omega_s t)) + U_{LO}(\cos(\omega_{LO} t)) \quad (2.7)$$

where U_s and U_{LO} are amplitudes of signal and LO voltages, respectively. Bolometers with a thermistor could be used as mixing elements for heterodyne receivers. The total power dissipated in the bolometer is:

$$P(t) = \frac{U(t)^2}{2R_t} \quad (2.8)$$

Inserting Equation 2.7 into 2.8 and taking into account that the bolometer temperature can not follow high frequency terms $2\omega_s$, $2\omega_{LO}$ and $\omega_s + \omega_{LO}$ the

total dissipated power becomes:

$$P(t) = P_s + P_{LO} + 2\sqrt{P_s P_{LO}} \cos(\omega_{IF} t) \quad (2.9)$$

where $P_s = U_s^2/2R_t$, $P_{LO} = U_{LO}^2/2R_t$, and $\omega_{IF} = |\omega_s - \omega_{LO}|$ which should be less than $1/\tau_e$. As it follows from Equation 2.9 the IF output P_{IF} at a frequency ω_{IF} can be produced by either an Upper Sideband (USB) $\omega_s = \omega_{LO} + \omega_{IF}$ or a Lower Sideband (LSB) $\omega_i = \omega_{LO} - \omega_{IF}$ (see Figure 2.5(b)). Mixers sensitive to both USB and LSB are called Double Sideband (DSB). The performance of mixer is characterised by a mixer conversion gain:

$$G_m = \frac{P_{IF}}{P_s} \quad (2.10)$$

Another important figure of merit for the mixer is noise. The mixer itself produces noise at the output with a power N_{out} . This noise might be represented with the output noise temperature T_{out} using the Johnson-Nyquist equation:

$$T_{out} = \frac{N_{out}}{k_B B} \quad (2.11)$$

where k_B is the Boltzmann constant and B a bandwidth. Using the mixer conversion gain the output noise temperature T_{out} might be referred to the mixer input in case of DSB mixer as:

$$T_m = \frac{T_{out}}{2G_m} \quad (2.12)$$

A factor “2” in Equation 2.12 comes from a DSB operation of HEB mixer and an assumption that a sideband ratio is one.

2.2 Superconducting HEB mixers

The term “hot electrons” is used to describe a non-equilibrium state of electrons inside the bolometer, i.e. an effective elevation of electron temperature. The first HEB mixer was realised using a doped semiconductor indium antimonide (InSb) [134]. Despite a good sensitivity, devices based on InSb had quite small bandwidth due to the time constants of the order of microseconds [137]. After the discovery of electron-heating effect in superconducting films [15] superconductors emerged as a material for HEB mixers [14]. The resistance of a superconductor is strongly affected by the electron temperature in a region close to a T_c , which explains the HEBs’ high sensitivity. HEB mixers made from NbN films were successfully implemented [138] allowing for the achievement of a typical bandwidth of up to 4 GHz [139].

2.2.1 Photoresponse of phonon-cooled HEB mixers

Two types of superconducting HEB mixers differing by the dominating mechanism of electron cooling were reported: phonon-cooled [14] and diffusion-cooled [140]. In a phonon-cooled HEB a thin superconducting film deposited on a substrate acts as an absorber. The film cools down through the substrate,

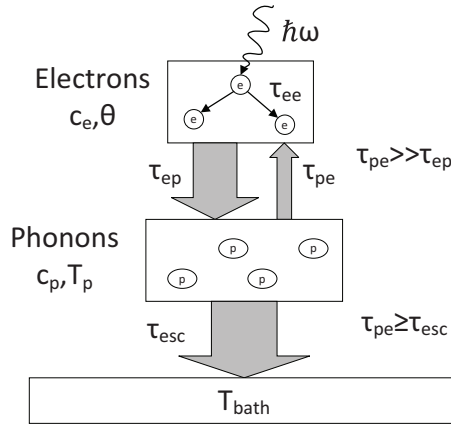


Fig. 2.6: Energy transfer and intrinsic relaxation times in a phonon-cooled HEB [141].

which plays a role of a heat sink. A thermal link between them is a thermal boundary resistance. The superconducting film acts also as a resistive thermometer. The thermalisation scheme of such a device is depicted in Figure 2.6.

In order to operate as a receiver the HEB is cooled down below its T_c where a thermal coupling between phonons and electrons is weak and the electron-electron interaction is strong. The interaction time between electrons τ_{ee} is shorter than other characteristic time constants, which makes possible to present the HEB as a 2-T system. The first (electron) subsystem consists of quasiparticles and has a temperature θ and a specific heat c_e . The second (phonon) subsystem is formed by phonons in a superconducting film and has a temperature T_p and a specific heat c_p . The heat exchange between electron and phonon subsystems is done with characteristic time constants τ_{ep} and τ_{pe} . In an equilibrium state this interaction times relates as $\tau_{pe} = \tau_{ep}c_p/c_e$ and in order to achieve electron cooling τ_{ep} should be less than τ_{pe} . Then instead of one heat balance equation 2.1 a system of heat balance equations might be written as [142]:

$$c_e \frac{d\theta}{dt} = P(t) - c_e \frac{\theta - T_p}{\tau_{ep}} \quad (2.13)$$

$$c_p \frac{dT_p}{dt} = c_e \frac{\theta - T_p}{\tau_{ep}} - c_p \frac{T_p - T_{bath}}{\tau_{esc}} \quad (2.14)$$

where τ_{esc} is an escape time of phonons from the superconducting film into the substrate:

$$\tau_{esc} = \frac{4d}{\beta u} \quad (2.15)$$

where d is a superconductor thickness, u a speed of sound and β an acoustic phonon transmission coefficient. The phonon escape time τ_{esc} should be less than the electron-phonon interaction time τ_{ep} to prevent heat accumulation in the phonon subsystem. The reverse energy flow carried by the phonons from the substrate into the superconductor is neglected.

Close to the T_c the electron specific heat as a function of the electron temperature is:

$$c_e(\theta) = \gamma\theta \quad (2.16)$$

where γ is the electron specific heat coefficient. The phonon specific heat at an arbitrary phonon temperature in the Debye approximation is given by [143]:

$$c_p(T_p) = 9nk_B \left(\frac{T_p}{T_D}\right)^3 \int_0^{\frac{T_D}{T_p}} \frac{e^x x^4}{(e^x - 1)^2} dx \quad (2.17)$$

where n is an atomic density and T_D the Debye temperature. The phonon temperature T_p is $\approx 0.9 \times \theta$ and could be estimated from the heat balance equations (Equations 2.13 and 2.14) [144].

2.2.2 The lumped element HEB model

In order to analyse the HEB behavior, lumped element model previously developed for NbN HEBs [14] can be used. The model assumes that the electron temperature along the superconducting film is uniform and RF radiation and both DC power have the same effect on the HEB. However, this assumption was not completely true and development of the hot-spot models [145–147] was required. In the hot-spot models the electron temperature profile along the superconducting film was taken into account. Compared to the standard model, modifications of the heat balance equation were done. This modifications allowed for the correct modeling of HEB noise and current versus voltage (I-V) curves, while the standard model requires experimental curves for modeling.

2.2.2.1 Conversion gain

Using standard lumped element formalism expression for the HEB voltage responsivity might be written as [148]:

$$R_v(f_{IF}) = \frac{R_L I_0}{R_L + R_0} \frac{\frac{C_0}{\chi}}{1 - C_0 I_0^2 \frac{R_L - R_0}{R_L + R_0}} \frac{1}{1 + i \frac{f_{IF}}{f_g}} = R_v(0) \frac{1}{1 + i \frac{f_{IF}}{f_g}} \quad (2.18)$$

where R_0 is the HEB DC resistance at the bias point, f_g the HEB 3 dB gain roll-off frequency (GBW), and $C_0 = dR/dP$ (P is a sum of dissipated DC and LO powers). An assumption that the impedance of a HEB at the high-frequency limit $Z(\infty)$ is equal to R_0 was done. For Nb HEBs it was shown that a real part of $Z(f_{IF})$ goes to R_0 at frequencies >1 GHz [149]. For MgB₂ HEBs a similar investigation on the IF impedance was performed recently [150]. It was shown that a real part of HEB impedance approaches differential resistance dU/dI at low frequencies and R_0 at higher frequencies similar to NbN HEBs [151]. A power exchange function χ is introduced in a similar way as in [152]. It is defined as a ratio of the RF and DC power changes required to keep the device resistance constant. As a general rule a HEB resistance is more sensitive to a DC power than to an RF power, which results in conversion functions larger than one. It was demonstrated that χ typically takes values from 3 to 1 decaying moving to higher biases [146, 151].

The mixer conversion gain is given by [148]:

$$G_m(f_{IF}) = \frac{2P_{LO}R_v^2(f_{IF})}{R_L} \quad (2.19)$$

where P_{LO} is an absorbed LO power.

Inserting Equation 2.18 into 2.20 the mixer conversion gain predicted by the standard model is calculated as:

$$G_m(f_{IF}) = \frac{2P_{LO}R_L I_0^2}{(R_L + R_0)^2} \frac{(\frac{C_0}{\chi})^2}{(1 - C_0 I_0^2 \frac{R_L - R_0}{R_L + R_0})^2} \frac{1}{1 + (\frac{f_{IF}}{f_g})^2} = G_m(0) \frac{1}{1 + (\frac{f_{IF}}{f_g})^2} \quad (2.20)$$

where $G_m(0)$ is a mixer conversion gain at zero IF.

Another assumption made in this theory is that the resistance of HEB depends on the electron temperature. Because the temperature is linearly proportional to the dissipated power, then $R = C_0 P$. After some mathematical derivations it was shown that [149]:

$$C_0 = \frac{1}{I_0^2} \frac{\frac{dU}{dI} - R_0}{\frac{dU}{dI} + R_0} = \frac{C'}{I_0^2} \quad (2.21)$$

where C' is a dimensionless self-heating parameter.

2.2.2.2 Noise temperature

The main noise sources in a HEB mixer are Johnson noise and thermal fluctuation noise [14]. Output noise temperatures T_J and T_{FL} produced by each noise component might be calculated [153] according to the Mather's nonequilibrium theory of bolometer detector [154] as:

$$T_J(f_{IF}) = \frac{4R_L R_0 \theta}{(R_L + R_0)^2 (1 - C_0 I_0^2 \frac{R_L - R_0}{R_L + R_0})^2} \quad (2.22)$$

$$T_{FL}(f_{IF}) = \frac{I_0^2 R_L (\frac{\partial R}{\partial \theta})^2 \frac{4\theta^2}{c_e V} \tau_\theta}{(R_L + R_0)^2 (1 - C_0 I_0^2 \frac{R_L - R_0}{R_L + R_0})^2} \frac{1}{1 + (2\pi f_{IF} \tau_\theta^*)^2} \quad (2.23)$$

where V is the HEB volume and τ_θ^* the electron temperature relaxation time modified by the electro-thermal feedback:

$$\tau_\theta^* = \frac{\tau_\theta}{1 - C_0 I_0^2 \frac{R_L - R_0}{R_L + R_0}} \quad (2.24)$$

The DSB mixer input noise temperature which also includes noise from the IF chain T_{IF} is [153]:

$$T_m(f_{IF}) = \frac{T_J + T_{FL} + T_{IF}}{2G_m(0)(1 + (\frac{f_{IF}}{f_g})^2)^{-1}} \quad (2.25)$$

The thermal fluctuation noise depends on the IF as $(1 + (2\pi f_{IF} \tau_\theta^*)^2)^{-1}$. Since τ_θ^* and a mixer time constant $\tau_{mix} = (2\pi f_g)^{-1}$ basically are equal, Equation 2.25 could be rewritten as:

$$T_m(f_{IF}) = \frac{T_{FL}(0) + (T_J + T_{IF}) (1 + (\frac{f_{IF}}{f_g})^2)}{2G_m(0)} \quad (2.26)$$

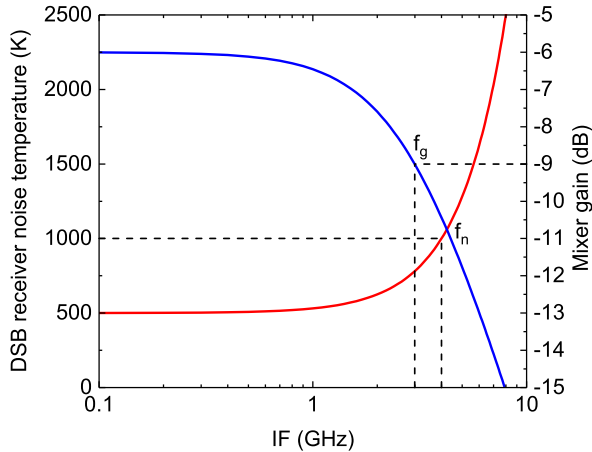


Fig. 2.7: HEB mixer noise temperature and conversion gain versus IF.

And then defining a new parameter f_n as a mixer NBW:

$$f_n = f_g \sqrt{\frac{T_{FL} + T_J + T_{LNA}}{T_J + T_{LNA}}} \quad (2.27)$$

the final equation becomes:

$$T_m(f_{IF}) = T_m(0) \left(1 + \left(\frac{f_{IF}}{f_n}\right)^2\right) \quad (2.28)$$

where $T_m(0)$ is a mixer noise temperature at zero IF. It should be noted that according Equation 2.27 f_n is always larger than f_g , because the radicand is larger than 1 (see Figure 2.7).

2.2.3 Two-temperature model

In the low temperature limit when c_e is much larger than c_p the electron temperature relaxation could be described with a single time constant τ_θ [155]:

$$\tau_\theta = \tau_{ep} + \tau_{esc} \frac{c_e}{c_p} \quad (2.29)$$

while in a general case a relation between τ_θ , τ_{ep} and τ_{esc} is more complicated.

A two-temperature approach (2-T model) was used in order to describe the response of superconducting films to a modulated electro-magnetic radiation [142]. Taking into account the effect of self-heating electrothermal feedback [156] the HEB conversion gain as a function of IF is [124]:

$$G_m(f_{IF}) \propto \left| \frac{C'}{\xi(f_{IF}) - C' \frac{R_L - R_0}{R_L + R_0}} \right|^2 \quad (2.30)$$

where

$$\xi(\omega) = \frac{(1 + j\omega\tau_1)(1 + j\omega\tau_2)}{(1 + j\omega\tau_0)} \quad (2.31)$$

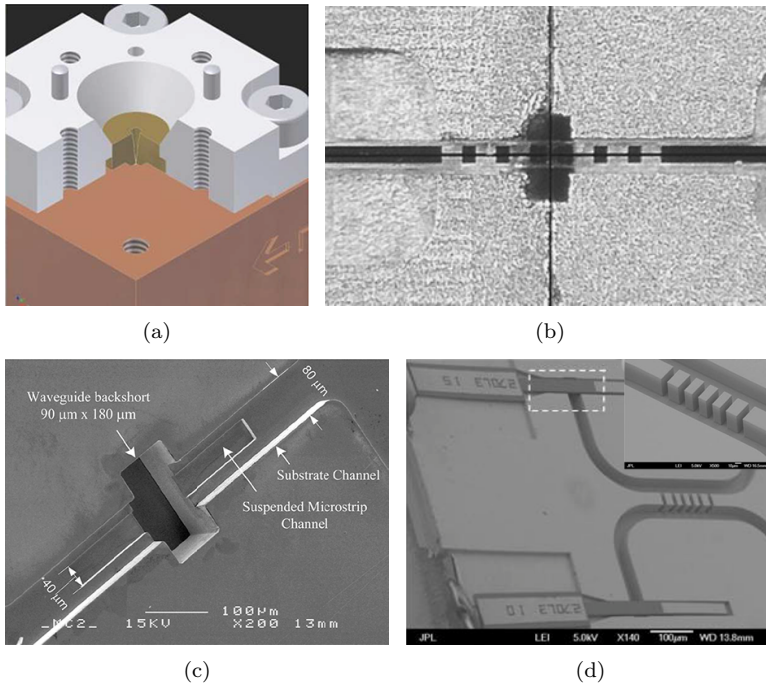


Fig. 2.8: Waveguide HEB heterodyne receivers. (a) Three-dimensional (3D) computer-aided design (CAD) image: sectioned cut of a feed horn antenna. Illustration from [31]. (b) SEM image of a HEB mixer mounted on the waveguide mixer block. Illustration from [115]. (c) SEM image of a microchannel with a backshort. Illustration from [19]. (d) SEM image of a 90° hybrid coupler. Illustration from [111].

$$\tau_3^{-1} = \tau_{esc}^{-1} + \tau_{ep}^{-1} \frac{C_e}{C_p} \quad (2.32)$$

$$\tau_{1,2}^{-1} = \frac{\tau_3^{-1} + \tau_{eph}^{-1}}{2} \left[1 \pm \sqrt{1 - 4 \frac{(\tau_3^{-1} + \tau_{ep}^{-1})^{-2}}{\tau_{esc} \tau_{ep}}} \right] \quad (2.33)$$

However, simplified Equation 2.29 gives a good understanding of a trade-off in HEB mixer development. As it is seen from Equation 2.15 it is required to reduce the film thickness to achieve the shorter phonon escape time. Unfortunately, reduction of film thickness leads to decrease of T_c , i.e. due to a large amount of defects in a film bottom layer. NbN with a bulk T_c of 16 K has only a 8–11 K T_c in 3–5 nm films. The reduction of T_c consequently leads to an increase of electron-phonon interaction time.

2.3 THz heterodyne receivers design

The HEB itself operates just as a mixing element. In order to use HEB in a heterodyne receiver the problem of effective signal and LO radiation coupling

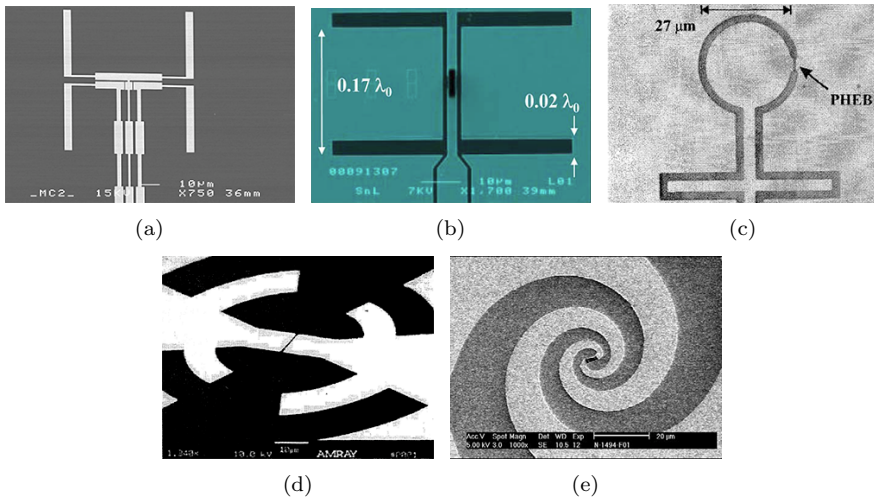


Fig. 2.9: Integrated planar antennas. (a) Double dipole antenna. Illustration from [157]. (b) Double slot antenna. Illustration from [98]. (c) Slot-ring antenna. Illustration from [158]. (d) Log-periodic antenna. Illustration from [159]. (e) Spiral antenna. Illustration from [97].

into device, DC biasing and IF signal redout should be solved. There are two main approaches for the receiver design that differ by the manner radiation is coupled into the device: waveguide coupling and quasi-optical coupling.

In the waveguide coupling approach a feed horn antenna (see Figure 2.8(a)) is used for radiation coupling from the free space into a machined waveguide with a mounted device (see Figure 2.8(b)). The HEBs integrated with a probe antenna are typically fabricated on thin substrates. The tunable element (backshort) could be used to maximize radiation coupling from the waveguide into the device (see Figure 2.8(c)). The optimal frequency range for radiation coupling for the waveguide receiver is defined by the antenna and waveguide geometry. The drawback of this receiver type is that the waveguide dimensions scale down for higher frequencies and fabrication becomes more challenging. High frequency operation also necessitates a reduction of substrate thickness due to increasing waveguide losses and substrate modes formation. However, waveguide HEB mixers have been successfully developed for frequencies up to 4.7 THz [19, 31, 33, 111, 115]. In waveguide receivers axial and lateral positions of the mixer beam are determined only by the feed horn antenna (i.e. by the machining tolerances only). However, the mixer chip mounting in the correct position for maximum coupling could be challenging. Using waveguide approach it is possible to avoid thin film beam splitter utilization for combining signal and LO radiation. The balanced scheme used to improve receiver stability could be realized easily using built in machined hybrid coupler as shown in Figure 2.8(d) [111].

In the quasi-optical coupling approach a lithographic planar antenna directly integrated with a HEB is used. Figure 2.9 demonstrates several types of integrated planar antennas used with HEB mixers, e.g. a double dipole an-

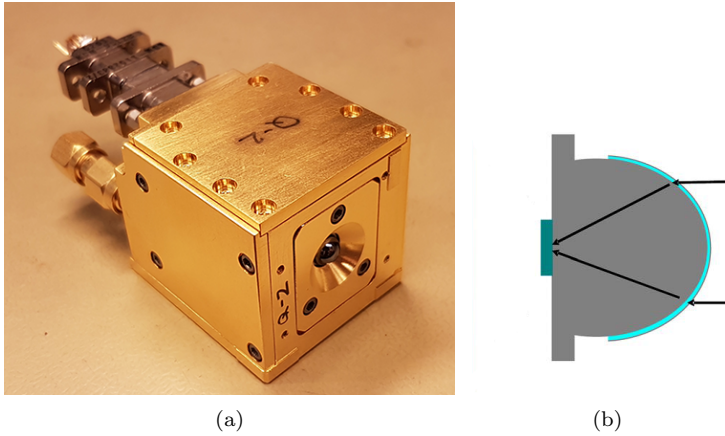


Fig. 2.10: (a) Quasi-optical mixer block used for HIFI instrument of The Hershel Space Observatory. (b) Elliptical dielectric lens with a planar antenna integrated HEB mixer attached. Illustration from [98].

tenna [157], a double slot antenna [98], a slot-ring antenna [158], a log-periodic antenna [159] and a spiral antenna [97]. The spiral antenna is a good choice for a laboratory study of devices at different LO frequencies, because it has a constant real impedance in a broad frequency range. The impedance of a HEB can be easily matched to the antenna impedance by choosing the right HEB geometry. Unfortunately, real spiral antennas have an elliptical polarization, while the radiation of LO source are typically linear polarized. That results in LO coupling losses (at least 50%) and complexity of loss estimation of a beam splitter used for combining signal and LO radiation.

For a planar antenna on a dielectric substrate coupling into the substrate is $\epsilon^{3/2}$ times (ϵ is the dielectric substrate permittivity) higher than into the air. The incoming radiation then should be fed from the substrate side. In this case the radiation propagating at the angles larger than the critical angle will be trapped in the substrate, so an additional beam handling is required. In order to avoid this problem, hyperhemispherical and elliptical dielectric lenses are typically used [160]. The planar antenna integrated HEB mixer is attached to the back side of the lens and packed in a mixer block (see Figure 2.10). The antenna gain in case of hyperhemispherical lens is increased by n_l^2 (n_l is the lens dielectric refractive index). In practice, hyperhemispherical and elliptical lenses can be realized approximately by using a hemispherical lens and a dielectric plate of required thickness placed between the hemisphere and the substrate. Use of lenses results in losses caused by the reflection of radiation at the lens/air interface. Reflection losses could be reduced by applying antireflection coating [161]. Application of Parylene C antireflection coating allows for reduction of the reflection losses from 1 dB to 0.2 dB [93].

Chapter 3

MgB₂ superconducting ultrathin films

In this chapter the detailed description of HPCVD method, the deposition system design, and the study of achieved films presented in [Paper C] and [Paper D] are summarized.

3.1 MgB₂ thin films

In order to increase operation temperature and to improve IF bandwidth of HEB mixers, superconducting materials with a higher T_c , which can provide a shorter electron-phonon interaction time are required. MgB₂ is one of these materials. Thinner films provide shorter phonon escape time from the film into the substrate, which is another important limitation for the HEB mixers IF bandwidth. Hence, both high T_c and small thickness superconducting films are desirable. The superconductivity in MgB₂ was reported in 2001 [127]. MgB₂ is a conventional intermetallic compound superconductor with the highest T_c for a traditional phonon mediated superconductor of 39 K reported so far. The crystalline structure of MgB₂ is shown in Figure 3.1. It consists of hexagonal magnesium (Mg) layers and honeycomb boron (B) layers in-between. The hexagonal unit cell has the following lattice parameters $a = b = 3.086 \text{ \AA}$, $c = 3.524 \text{ \AA}$ [127]. Despite MgB₂ is a conventional Bardeen-Cooper-Schrieffer (BCS) superconductor, it exhibits a double superconducting gap structure with $2\Delta_\sigma \approx 4k_B T_c$ and $2\Delta_\pi \approx 1.3k_B T_c$ [162]. In the dirty limit, due to strong interband and intraband scattering two superconducting gaps merge into one energy gap $2\Delta_{dirty}$ whose temperature dependance deviates from curve predicted by BCS theory [163]. A penetration depth (λ_L) of 34.5 nm and coherence length (ξ) of 8 nm were reported for MgB₂ [164, 165]. Using the Ginzburg-Landau formula for the depairing current density $J_d = \Phi_0 / (\sqrt{3}\pi\mu_0\lambda_L^2\xi)$, where Φ_0 is the flux quantum and μ_0 the permeability of vacuum, it is estimated to be $\approx 3 \times 10^9 \text{ A/cm}^2$.

The discovery of superconductivity in MgB₂ immediately brought a great interest to MgB₂ thin films [128, 166, 167]. Several techniques for *in-situ* thin film growth were proposed, e.g. pulsed laser deposition (PLD) [128], MBE

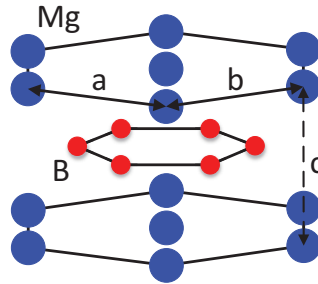


Fig. 3.1: MgB_2 crystal structure. Honeycomb boron layers are in between of hexagonal magnesium layers [127].

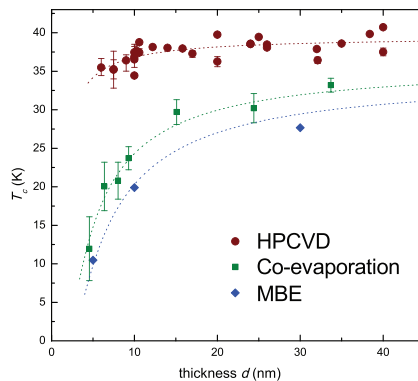


Fig. 3.2: Comparison of different MgB_2 thin film deposition techniques: MBE [174], co-evaporation [175], and HPCVD [172, 176, 177]. Illustration from Ref. [177].

[168], HPCVD [129], sputtering [169], e-beam and thermal co-evaporation [170]. The HPCVD grown MgB_2 films have a higher T_c compared to films with the same thickness grown by other techniques (see Figure 3.2). Unfortunately, deposition systems utilizing HPCVD method are not commercially available.

The most suitable substrates for MgB_2 thin film deposition are Al_2O_3 and SiC with a lattice mismatch with MgB_2 of $\sim 11\%$ (30° in-plane rotation) [171] and $\sim 0.42\%$ [172], respectively. SiC is a more preferable substrate for MgB_2 thin film deposition due to a better film/substrate lattice match which results in a reduced number of defects in bottom layers of the film. This leads to a better phonon transparency of the film/substrate interface. It should be also noted, that both thermodynamic calculations [173] and experimental results [129] show that layers of magnesium oxide (MgO) form at the film/substrate interface, when Al_2O_3 substrates are used. More common substrates for microelectronics industry, such as Si and silicon dioxide (SiO_2), react with Mg to form silicides [173] and therefore require the use of appropriate buffer layers.

Significant progress in ultrathin MgB_2 film deposition allowed for fabri-

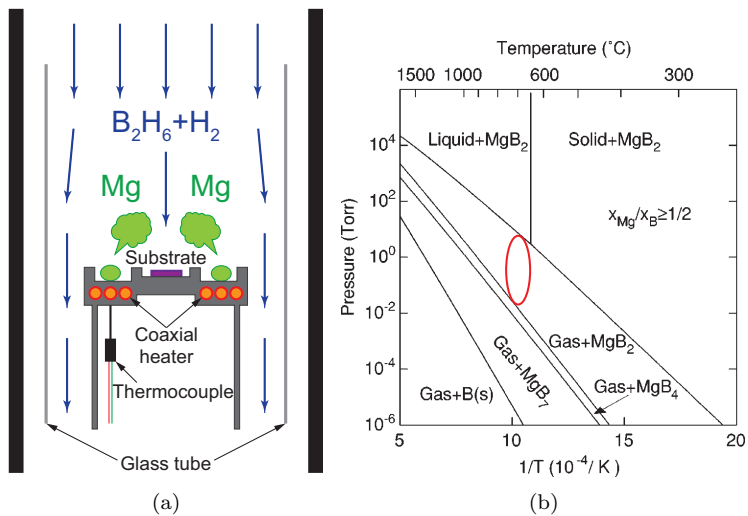


Fig. 3.3: (a) Schematic drawing of the HPCVD system's deposition chamber. (b) Pressure-temperature phase diagram for the Mg-B system. Illustration from Ref. [167].

cation of different types of superconducting electronic devices, e.g. HEB mixers [122], superconducting single-photon detectors (SSPD) [178], superconducting quantum interference devices (SQUID) [179]. MgB_2 thin films are of the great interest for HEB fabrication due to a potential possibility to achieve a wider IF bandwidth and higher operation temperatures compared to NbN HEB mixers. The shorter electron-phonon interaction time was measured in a thin MgB_2 film on a Si substrate (3 ps) [162] in comparison to NbN (12 ps). The possibility to deposit very thin films (6–8 nm) with a high T_c of 34–37 K has been demonstrated [172, 180]. However, no HEBs made utilizing such thin films have been reported to date. The recently reported results on MgB_2 HEB mixers were achieved with devices fabricated from MBE grown films on Al_2O_3 [123, 124, 131] substrates and HPCVD grown films on SiC substrates [125, 126, 132].

3.2 Chalmers HPCVD system

Initial studies of MgB_2 HEB mixers were performed using MBE grown films on *c*-cut Al_2O_3 substrates provided by NTT Basic Research Laboratories [181]. Typically, the T_c of MBE grown films is much lower than for HPCVD grown films, but the film surface is smoother, which is essential for the device fabrication and performance. The film deposition process included co-evaporation of Mg and B in a high-vacuum chamber at $280^{\circ}C$ and subsequent Ar atmosphere annealing in a rapid-annealing furnace. Films were covered *in-situ* with a 20 nm Au layer to reduce contact resistance between a MgB_2 film and metal layers deposited during device fabrication and to prevent film degradation during storage and initial device fabrication steps. A HPCVD method developed

for MgB_2 thin film growth can provide high quality ultrathin superconducting films that can maintain a high T_c even when few nanometers thick. On the other hand, the availability of in-house source of thin films is of a great advantage for device development. Therefore, a custom made HPCVD system was constructed at Chalmers University of Technology for MgB_2 ultrathin film deposition as a part of the project on MgB_2 HEB mixers development.

3.2.1 System design

The HPCVD technique utilizing a combination of both physical and chemical vapor deposition was proposed specifically for MgB_2 thin film growth. The Mg source is an evaporative flux from solid Mg and the B source is a diborane (B_2H_6) gas. In brief, in this process both the Mg pellets and the substrate are placed on a heater (either resistive or inductive) while a mixture of hydrogen (H_2) and B_2H_6 gases is supplied into the chamber as shown in Figure 3.3(a). The B_2H_6 gas decomposes above the heated substrate into borane (BH_3) gas. The borane molecules are adsorbed on the substrate surface and react with evaporated Mg to form an MgB_2 film. The film growth usually occurs at temperatures ranging from $650^\circ C$ to $760^\circ C$ [129, 133, 172, 182], which is above the Mg melting point of $650^\circ C$ (the area marked with a red oval in Figure 3.3(b)). As one can see, in order to form the correct crystalline phase (MgB_2) both the Mg partial pressure and the temperature should fall in a quite tight area in the phase diagram. This necessitate very fine tuning of deposition parameters.

The system photos are presented in Figure 3.4. H_2 , B_2H_6 (5% diluted in H_2), and purging nitrogen (N_2) gases are supplied to the deposition chamber using a computer controlled gas panel consisting of pneumatic valves and mass-flow controllers (see Figure 3.4(a)). A pirani gauge is mounted on the deposition chamber to monitor the pressure during system pumping. A throttle valve operated through a controller with a capacitance manometer is used to set the desired process pressure. A kinetic trap (see Figure 3.4(c)) after the deposition chamber is installed in order to protect following system components from residuals of the deposited material carried by the gas flow. A fore-vacuum pump and a scrubber used for B_2H_6 disposal are placed behind a main cabinet in an utility room (see Figure 3.4(d)).

A schematic of the MgB_2 HPCVD system chamber is presented in Figure 3.3(a). A quartz tube prevents material deposition on water cooled chamber metal walls. Both the substrate and pieces of solid Mg are placed on a heater. A coaxial heating wire is clamped between an upper and a bottom parts of the heater under an area where magnesium is placed (see Figure 3.4(b)). In contrast to the previously presented resistive heater designs the coaxial wire itself is hidden inside the heater, which reduces contamination of the wire during depositions and increases the heater life time. Due to a temperature gradient the temperature of the central part where the substrate is placed is 50 K lower than under Mg pellets. A thermocouple is attached to the bottom part of the heater to monitor the temperature during the deposition process.

The MgB_2 thin film deposition procedure is following:

1. The chamber is pumped to the base pressure (10^{-3} Torr).

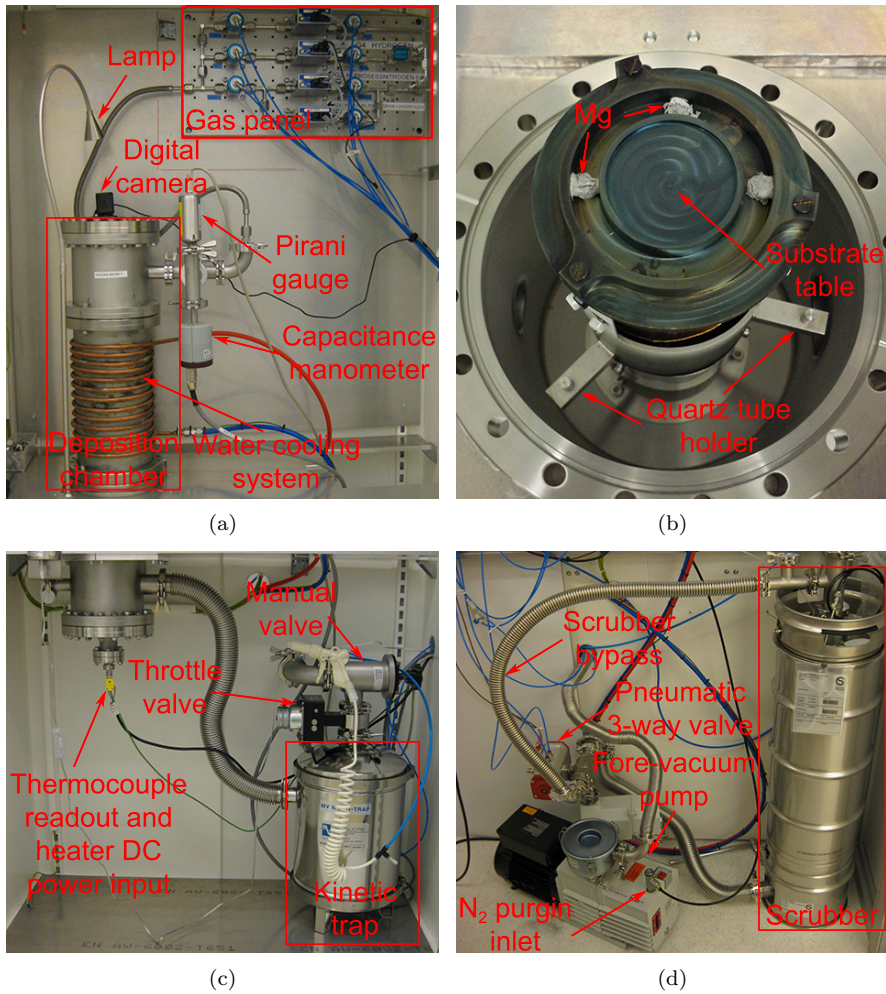


Fig. 3.4: Chalmers in-house built MgB₂ HPCVD system. (a) Top part front view. (b) Deposition chamber inside view (c) Bottom part front view. (d) The utility room view.

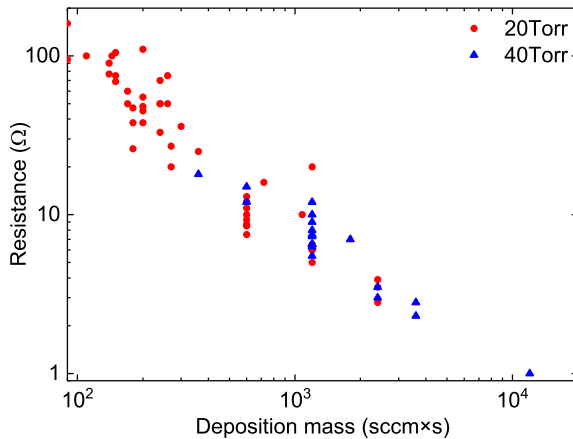


Fig. 3.5: MgB₂ film resistance measured on 5×5 mm² size test wafers (SiC) versus deposition mass. Films are deposited at either 20 Torr or 40 Torr.

2. The chamber is flushed with H₂ gas and pumped again to the base pressure.
3. The chamber is filled with H₂ gas (400 sccm) to the desired pressure (typically 20 Torr).
4. Solid Mg and the substrate are heated to about 700°C.
5. The B₂H₆ gas mixture is turned on for the desired time.
6. After the deposition is finished the heater is turned off and the substrate is cooled down.
7. The chamber is flushed several times with N₂ gas in order to remove possible remaining B₂H₆ gas.

3.2.2 Safety

During the HPCVD deposition system design and construction several safety issues had to be solved. The gases used in the system are dangerous for the personnel and laboratory environment. The gas panel, the deposition chamber, and other main system components are placed inside the ventilated cabinet. Furthermore, the gas panel is covered with a metal shield and has additional ventilation exhaust with a higher flow to form a negative pressure difference in case of a gas leakage. The cabinet doors have switches connected to an inter-lock system preventing process gases supply when doors are opened. The output of the pressure controller is also connected to the inter-lock system such as gas supply is possible only if the pressure inside the deposition chamber is below 300 Torr.

B₂H₆ is a pyrophoric gas and can self-inflate even at a room temperature. Moreover, B₂H₆ has a toxic effect primarily due to its irritant properties. In

Table 3.1: HPCVD MgB₂ HEB thickness (d), size (W×L), critical temperature (T_c), resistance at room temperature (R_{295K}), resistivity (ρ_{295K}), and critical current density (J_c)

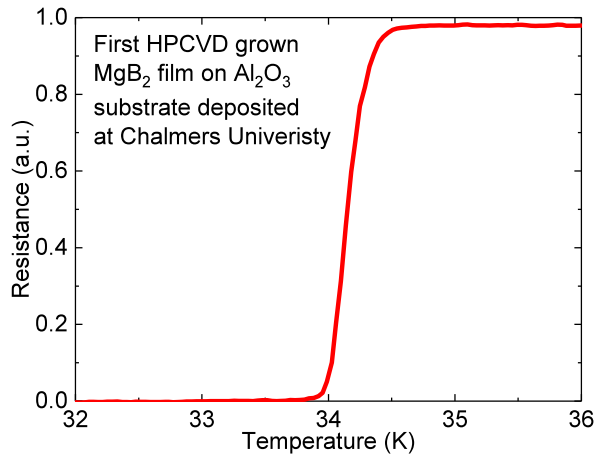
Device	d(nm)	W×L (μm ²)	T _c (K)	R _{295K} (Ω)	ρ _{295K} (μΩ × cm)	J _c (10 ⁷ A/cm ²)
E2-1	30	1×1	39.6	39	117	8.8
E2-2	30	1×1	39.4	40	120	11.0
E3-2	20	0.5×0.5	38.6	25	50	10.5
E3-8	20	0.8×0.8	39.2	20	40	12.0
E6-4	12	1×1	33.5	44	53	2.0
E6-7	12	1×1.5	34.5	67	54	2.9
E8-2	10	0.3×0.3	34.0	52	52	2.5
E8-7	10	0.5×0.5	32.5	87	87	1.2
E10-7	8	1×1	30.0	196	157	0.9
E10-8	8	1×1	31.0	230	182	1.2
E15-7	5	1×1	32.5	130	65	2.8

order to avoid an exposure of laboratory environment to B₂H₆, which is highly undesirable, a remotely controlled bypass line with a B₂H₆ gas sensor was installed after the fore-vacuum pump (see Figure 3.4(d)). After the completion of film deposition procedure the system exhaust is switched to the bypass to make sure there is no B₂H₆ gas left in the chamber. The inter-lock system prevents switching to the bypass during the deposition process.

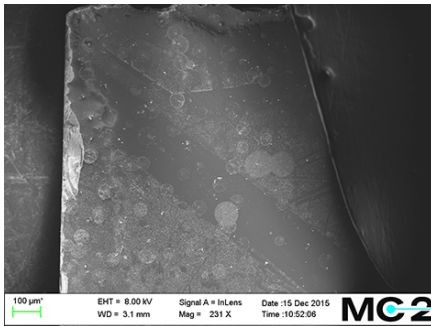
H₂ is a flammable gas and can self-explode in a certain concentration with oxygen (O₂). H₂ gas cleaned from B₂H₆ is mixed at the scrubber exhaust with N₂ to prevent formation of explosive concentrations of the oxyhydrogen. Another N₂ gas line is connected to an oil return inlet of the fore-vacuum pump in order to avoid accumulation of H₂ in the pump oil. The pump N₂ gas line has a lower flow and is always turned on, while the exhaust N₂ gas line with a higher gas flow is turned on only during the HPCVD system operation. The N₂ gas flows are controlled with gas flow meters which are also connected to the inter-lock system.

3.3 HPCVD grown ultrathin films

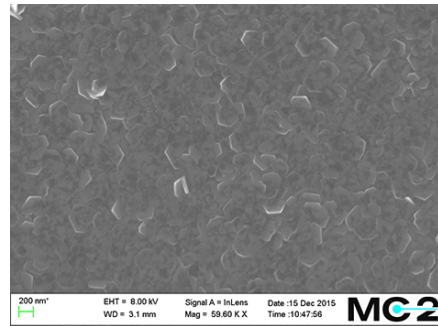
In the HPCVD process film thickness is defined by a B₂H₆ flow rate and a deposition time. As a measure of the deposited material amount a product of the B₂H₆ flow rate and the deposition time, so called deposition mass, can be used. Immediately after the chamber is opened, resistance of the deposited film is measured using multimeter from corner to corner of the substrate. The resistance was found to be inversely proportional to the deposition mass over two orders of magnitude, which suggests a good connectivity of the obtained films. Initially, MgB₂ thin films were grown on Al₂O₃ substrates. Even the first film deposition using the newly built system was successful, and film with a T_c of 34 K was achieved (see Figure 3.6(a)). A T_c of grown films ranged from 33 K (15 nm) to 37 K (40 nm) with a distinct double transition for thinner films. The film surface was covered with lots of spots and particles (see Figure



(a)



(b)



(c)

Fig. 3.6: First HPCVD grown MgB_2 films on Al_2O_3 substrates deposited at Chalmers University (20 sccm, 120 s, 40 Torr). (a) The resistance versus temperature curve for the first film. (b) SEM image of the second film. (c) High magnification SEM image of the second film.

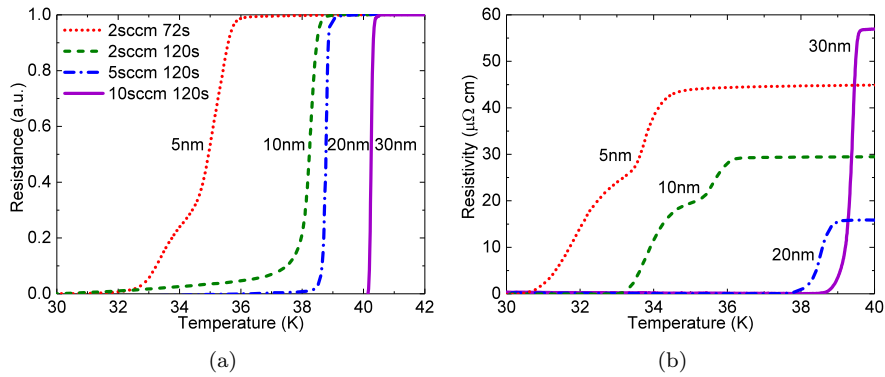


Fig. 3.7: (a) Resistance versus temperature curve for HPCVD grown MgB_2 films on SiC substrates after the deposition. (b) Resistivity versus temperature curve for bridges fabricated from HPCVD grown MgB_2 films on SiC substrates.

3.6(b)). HPCVD films are assumed to grow in a Volmer-Weber mode and large (300 nm in diameter) hexagonal crystallites corresponding to the MgB_2 unit cell are clearly distinguishable in scanning electron microscope (SEM) image (see Figure 3.6(c)). For MgB_2 films on Al_2O_3 substrates the residual resistance ratio ($\text{RRR} = R_{295\text{K}}/R_{\text{ons}}$, where $R_{295\text{K}}$ is the room temperature resistance and R_{ons} the onset resistance) was 1.5–2.5 suggesting a high defect concentration. The RRR values are much lower than value (about 10) reported previously for clean MgB_2 films [133].

Further deposition process development and optimisation were performed using SiC substrates. The discussed films have a T_c ranging from 35 K (5 nm thick) to 41 K (30 nm thick) (see Figure 3.7(a)). The RRR of the films is ranging from 2 to 6 indicating an improvement of film quality. The film surface was also studied with atomic force microscope (AFM). The measured mean square roughness (see Figure 3.8(d)) was about 1 nm, which is lower than for previously reported HPCVD as grown ultrathin MgB_2 films [183]. A low roughness is one of the key characteristics affecting fabrication of micro- and nanostructures in thin films. We observed that reduction of the deposition pressure from 80 Torr to 20 Torr continuously leads to smoother film surfaces. For deposition pressures above 30 Torr a droplet formation occurs in the deposition chamber resulting in rougher films. Therefore, most of the discussed films used for HEB fabrication were grown at a pressure of 20 Torr. Film epitaxial growth is confirmed by both the transmission electron microscope image (see Figure 3.8(b)) and MgB_2 epitaxial response in X-ray diffractometer (XRD) scan (see Figure 3.8(c)).

Film DC parameters in patterned microstructures were studied in several batches of HEBs fabricated using either ultraviolet (UV) or electron beam (e-beam) lithography based process (see Chapter 4). Summary of DC measurement results for devices selected for THz characterisation are summarised in Table 3.1. MgB_2 films were covered with a 20 nm gold (Au) layer using magnetron sputtering directly after the deposition. This Au layer was used both to protect the deposited film from degradation in the atmosphere as well as

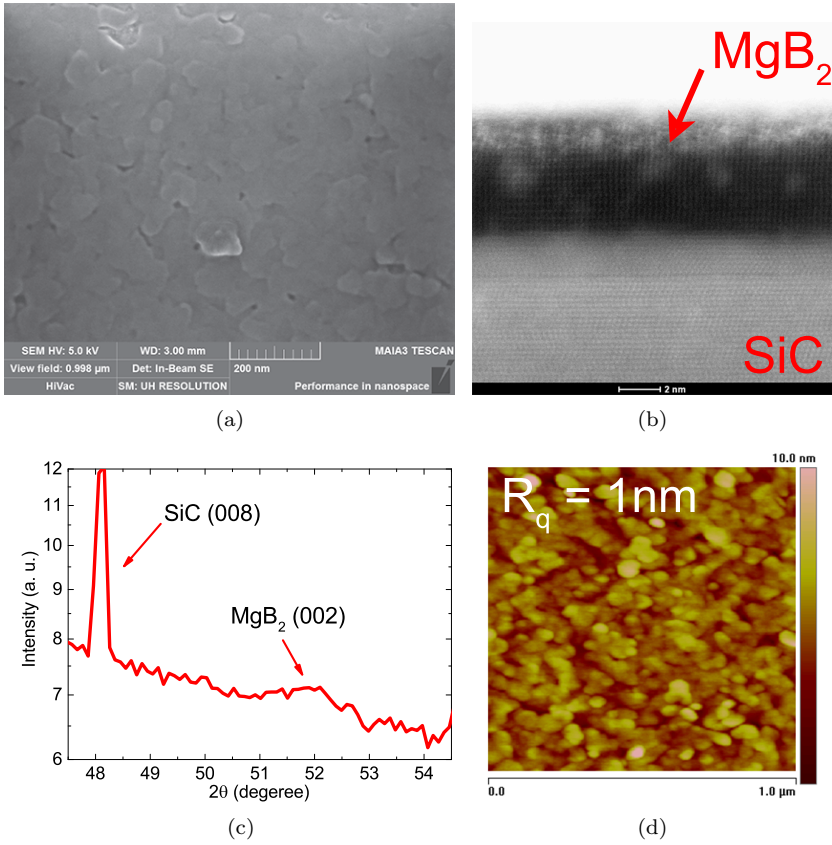


Fig. 3.8: A 5 nm thick as grown MgB_2 film. (a) SEM image. (b) TEM image. (c) XRD scan. (d) AFM image.

to be able to use the same fabrication process previously developed for HEBs made from MBE grown films [Paper A], [Paper B]. For batches E1-E8 a 2 nm thick Ti layer was deposited prior the 20 nm Au layer deposition to improve a layer adhesion. Since batch E9 the *in-situ* precleaning with argon plasma was used to remove the native oxide, improve the Au layer adhesion, and reduce contact resistance. There was no Ti layer used in the last case.

There are several tools to measure the conductive film thickness: contact and optical surface profilometers, AFM, TEM, ellipsometer, etc. Ellipsometry is a non-invasive method, however it requires preliminary knowledge of the MgB_2 film optical properties. Initially, for the deposition process development, film thickness was measured both with a contact profilometer and an AFM on MgB_2 films etched away on a fraction of the substrate using a hydrochloric (HCl) acid. Later, selected samples have been also studied using TEM to investigate the film/substrate interface as well as to measure MgB_2 film thickness. All thicknesses presented in Table 3.1 were confirmed with TEM measurements, except for device E2-2 for which it was estimated from the deposition rate.

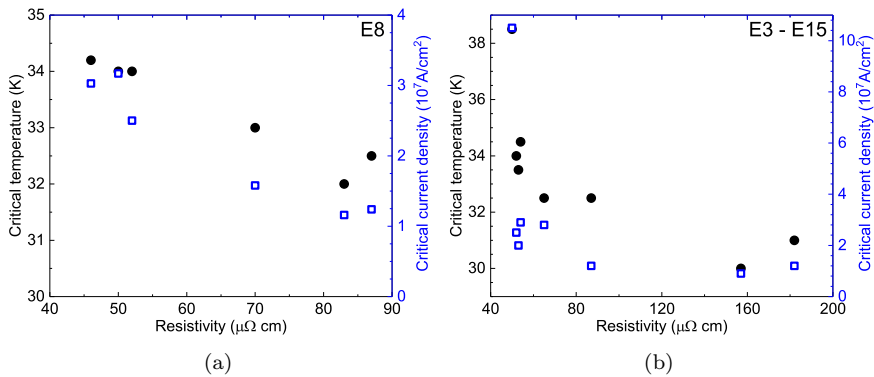


Fig. 3.9: Critical temperature and critical current density versus resistivity measured for the devices (a) from the same batch and (b) from batches of various thickness.

At room temperature sheet resistance of unpatterned films was measured with a four-point probe technique. Then by knowing the film thickness from TEM measurements the room temperature resistivity was calculated both for unpatterned films and for microstructures. These values correspond to the previously published resistivity values for films of similar thickness [180, 183–185]. The resistivity obtained from resistance of submicron size bridges (see Table 3.1) was ranging from $50 \mu\Omega\text{cm}$ (for a 20 nm thick film) till $182 \mu\Omega\text{cm}$ (for a 8 nm thick film). It is a factor of 2 higher than e.g. in Ref. [184] and [185], but much smaller bridges have been used. The high resistivity of the 30 nm thick film could be explained by a higher (40 Torr) deposition pressure, while the origin of the low resistivity in the 5 nm thick film is unclear.

The film resistivity affects design of HEB mixers. In order to provide the best performance, the impedance of HEB should be matched to the impedance of the integrated planar antenna (in our case a 100Ω spiral antenna). With a resistivity of about $50\text{--}100 \mu\Omega\text{cm}$ the aspect ratio of HEB (width/length) should be less than 1. Together with a requirement keeping a bolometer area small (due a limited available LO power) it will lead to the reduction of bolometer width in the design (in comparison to HEB mixers made from MBE grown MgB_2 films [Paper A], [Paper B]). That will increase the contact resistance between the HEB and the metal antenna, which subsequently increases the noise temperature.

In order to better understand the nature of the increased resistivity in thin films, the critical current density (J_c) has to be discussed. Whereas a T_c for thicker films remains the same in microbridges, for films thinner than 10 nm a T_c is reduces by a few degrees. Nevertheless, all films show excellent superconducting transition. The J_c values obtained from I-V characteristics of fabricated devices are presented in Table 3.1. For the 30 nm and 20 nm thick films the J_c is about $1 \times 10^8 \text{ A/cm}^2$ (at 4.2K), hence is one of the highest J_c reported so far for MgB_2 thin films. ($\approx 10\%$ of the depairing current). Even for films thinner than 10 nm the J_c is $(1\text{--}3) \times 10^7 \text{ A/cm}^2$. The same or higher resistivity and J_c of our films can possibly be explained by the lower deposition

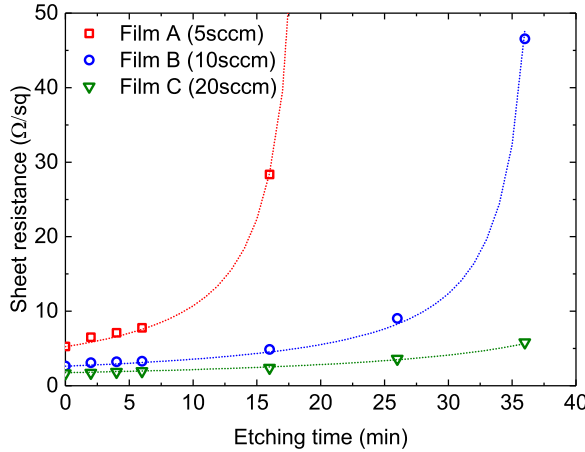


Fig. 3.10: Sheet resistance measured using four-point probe technique versus etching time. Deposition time and deposition pressure are 120 s and 20 Torr, respectively.

rate in the discussed HPCVD system as compared to [184], which facilitate more uniform and homogenous MgB₂ film growth [186].

As mentioned above the J_c in submicron size bridges made from films thinner than 10 nm is lower than for thicker films. However, it is approximately a factor of 10 higher than for the previously reported microbridges made from MBE and HPCVD grown MgB₂ films. The high yield (above 75%) allowed for the study of correlation between the resistivity and the J_c of the submicron size bridges made from the same 10 nm thick film (see Figure 3.9(a)). The lower resistivity corresponds to the higher J_c . The same correlation is observed also for the T_c measured in submicron size bridges after the fabrication (see Figure 3.9(a)). The spread of parameters suggests that the 10 nm film is quite inhomogeneous over the substrate area. The same dependence (see Figure 3.9(b)) of T_c and J_c on resistivity is observed for the devices made from films of various thickness (Table 3.1).

3.4 Films thinning down using Ar⁺ ion beam milling

Recently, argon ion (Ar⁺) beam milling was proposed as a technique for achieving ultrathin MgB₂ film from initially grown thicker films [180, 184, 185]. In order to study the effect of a thinning down on our HPCVD grown MgB₂ films, three films of various thickness were grown. The films were deposited with the same deposition parameters (20 Torr, 120 s) except B₂H₆ gas flows: Film A (5 sccm), Film B (10 sccm), and Films C (20 sccm). The etching utilizing Oxford Ionfab 300 Ion Beam System (2 sccm Ar gas flow, 13 mA beam current, 350 V beam voltage, and 30° tilt) was performed in several steps with sheet resistance measurements between them. Three steps with a duration of 2 min each followed by three steps with a duration of 10 min each. The film sheet resistance was measured with the four-point probe technique (see Figure

3.10). Due to the higher deposition mass, Film C should be approximately twice thicker than Film B and approximately four times thicker than Film A. Film B and Film C reach the same sheet resistance as Film A after approximately 20 min and 40 min of milling, respectively. Film A has completely gone after about 16–20 min of etching. The dependence of sheet resistance on etching time suggests that expected relations between film thicknesses based on the gas flows is correct.

Assuming that both the film resistivity and the etching rate are constant along the film vertical profile the sheet resistance is $R_s = r/(d-\rho t)$, where r is the etching rate, and t the etching time. Fit to the experimental data gives the etching rate of 1–1.2 nm/min. This value corresponds to the etching rate observed during HEB fabrication. Film thicknesses for Film A, Film B, and Film C used for fitting are 20 nm, 40 nm, and 60 nm, respectively, and close to the values estimated using the deposition mass. It is still of a great interest how the milling will affect film homogeneity, film surface, and submicron structures in HPCVD grown MgB₂ films.

Chapter 4

MgB₂ HEB design and fabrication

Several batches of submicron and micrometer scale HEBs were fabricated from superconducting MgB₂ films grown by either MBE or HPCVD. An e-beam lithography based fabrication process was used for submicron size devices designed for noise performance characterisation, which is sensitive to the limited available LO power. For GBW characterisation micrometer scale devices were fabricated using UV lithography based process. Since GBW measurements are performed at lower frequencies (more LO power is available) and elevated bath temperatures (less LO power is needed), large size devices are acceptable.

In this chapter, the detailed description of device fabrication processes is presented.

4.1 E-beam lithography based process

The HEBs were fabricated using superconducting MgB₂ films either provided by NTT Basic Research Laboratories (MBE grown films) or deposited at Chalmers University of Technology (HPCVD grown films). The HEB chip design is shown in Figure 4.1. A broadband spiral antenna was chosen as the most suitable antenna type for HEB characterisation since the same device could be tested at various frequencies.

The fabrication of devices from MBE grown films was challenging. The bolometer high frequency impedance should be close to the spiral antenna impedance of $90\ \Omega$ in order to provide high efficiency coupling of THz radiation. Due to the high resistance of used MBE grown MgB₂ films ($\approx 1000\ \Omega/\square$ for 20 nm thick films) the bolometer should be short and wide to fulfill this requirement. A desirable aspect ratio is about 10:1, e.g. a $2\ \mu\text{m}$ wide bolometer should be $0.2\ \mu\text{m}$ in length. For such tasks the e-beam lithography allows pattern transfer with feature size down to 5 nm and provides more flexibility than projection UV lithography. In addition, since MgB₂ degrades during exposure to water and oxygen [187, 188], some kind of protection to preserve the quality of MgB₂ films during the processing should be considered, e.g. a SiN_x or SiO₂ passivation layer. The fabrication procedure developed for MBE grown MgB₂

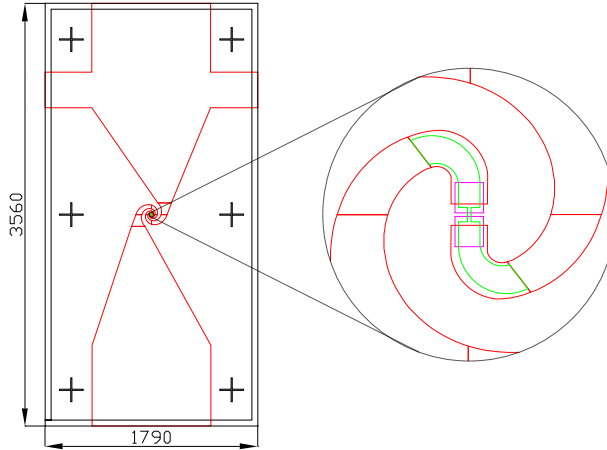


Fig. 4.1: The design of MgB_2 HEB mixer including alignment marks. The dimensions are given in microns.

films was also used for the fabrication of devices down to $0.3 \mu m$ in size from HPCVD grown films.

The fabrication procedure utilizing e-beam lithography, Ar^+ ion beam milling and lift-off process includes the following steps:

1. **Alignment marks and chip frames:** Initially, alignment marks for pattern alignment at subsequent processing steps and chip frames are fabricated. After the e-beam lithography, metal evaporation (10 nm titanium (Ti), 150 nm Au, and 30 nm Ti) and lift-off are performed (see Figure 4.2(a)). The chip frame is used both for short circuiting of bolometers and avoiding possible device damaging by the electrostatic charge; and cutting lines definition for the wafer dicing. The top Ti layer is used to protect structures during Ar^+ ion beam milling steps.
2. **Contact pads:** Contact pads defining the bolometer length are patterned. After the e-beam lithography, metal evaporation (10 nm Ti, 100 nm Au, and 60 nm Ti) and lift-off are performed (see Figure 4.2(b)). The top Ti layer is used to protect structures during Ar^+ ion beam milling steps.
3. **Spiral antenna:** The broadband planar spiral antenna is patterned. The antenna center part is overlapping with contact pads. After the e-beam lithography, metal evaporation (10 nm Ti, 270 nm Au, and 70 nm Ti) and lift-off are performed (see Figure 4.2(c)). The top Ti layer is used to protect structures during Ar^+ ion beam milling steps.
4. **Thin Au layer removal and passivation:** The 20 nm thick protective Au layer was etched away using Ar^+ ion beam milling (see Figure 4.2(d)). To prevent the degradation of the MgB_2 film during the rest of processing steps, immediately after the etching, the wafer was passivated with 40 nm thick SiN_x film by RF magnetron sputtering process (see Figure 4.2(e)).

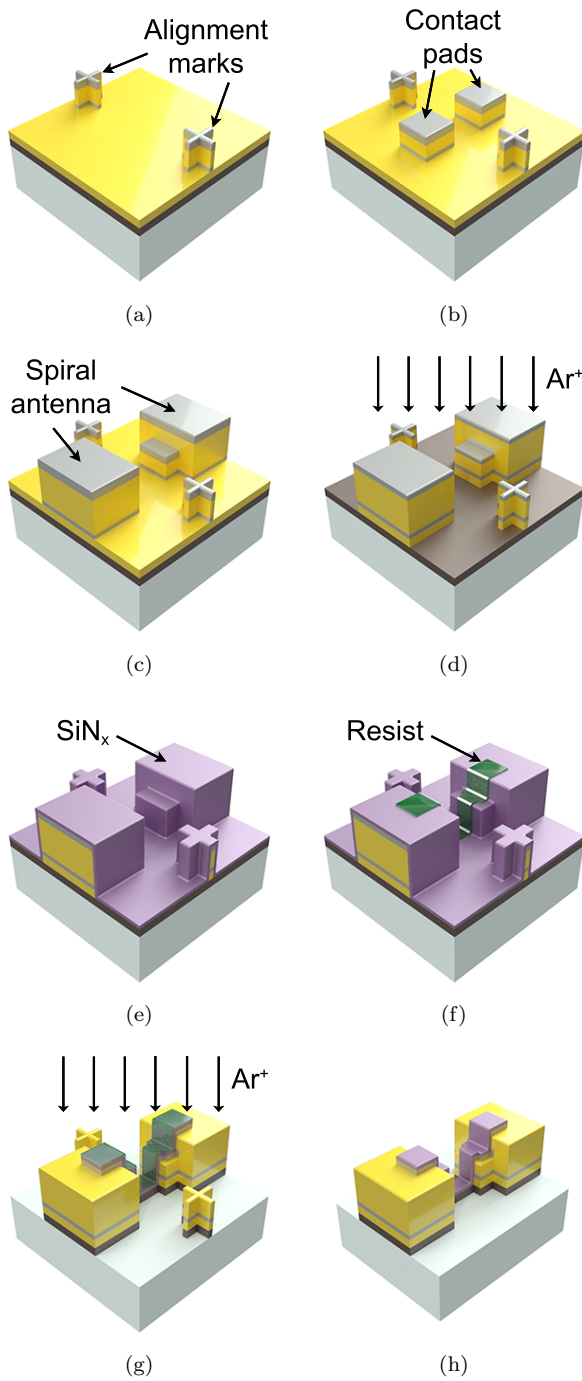


Fig. 4.2: Fabrication process sequence using e-beam lithography. (a) Alignment marks. (b) Contact pads. (c) Spiral antenna. (d) Thin Au layer removal. (e) Passivation with SiN_x . (f) Bolometer width patterning. (g) Ar^+ ion beam milling with a resist mask. (h) Final device.

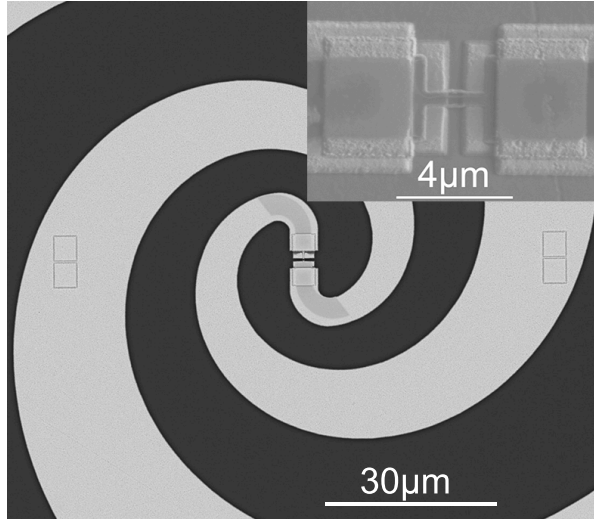


Fig. 4.3: SEM images of MgB_2 HEB made using e-beam lithography based fabrication process.

5. **Width definition and etching:** For the bolometer width definition etching mask was patterned using negative e-beam resist (see Figure 4.2(f)). The SiN_x passivation and MgB_2 film were etched away except from the bolometer area protected by the resist (see Figure 4.2(g)).
6. **Dicing:** Finally, the wafer covered for mechanical protection with photoresist was cut into $1.5 \times 3.3 \text{ mm}^2$ chips with the diamond dicing saw along the frame lines and washed in acetone to remove resist residuals (see Figure 4.2(h)).

The SEM image of the device fabricated using e-beam lithography based process is presented in Figure 4.3. The SEM picture in the inset of Figure 4.3 was done during the preparation of one of the samples for TEM analysis.

4.2 UV lithography based process

In order to acquire information about film parameters in microstructure during HPCVD process optimization faster, the UV lithography based process was used for HEB fabrication. Compared to the approximately one week required for fabrication when e-beam based process is applied, just 1-2 days are needed for UV lithography based process which involves less steps. The fabrication sequence is as following:

1. **HEB length definition:** Initially, the bolometer length and alignment marks are defined with an image reversal photoresist which provides negative slope profile (see Figure 4.4(a)). The patterning was followed by metal evaporation (10 nm Ti, 270 nm Au) and lift-off steps (see Figure 4.4(b)).

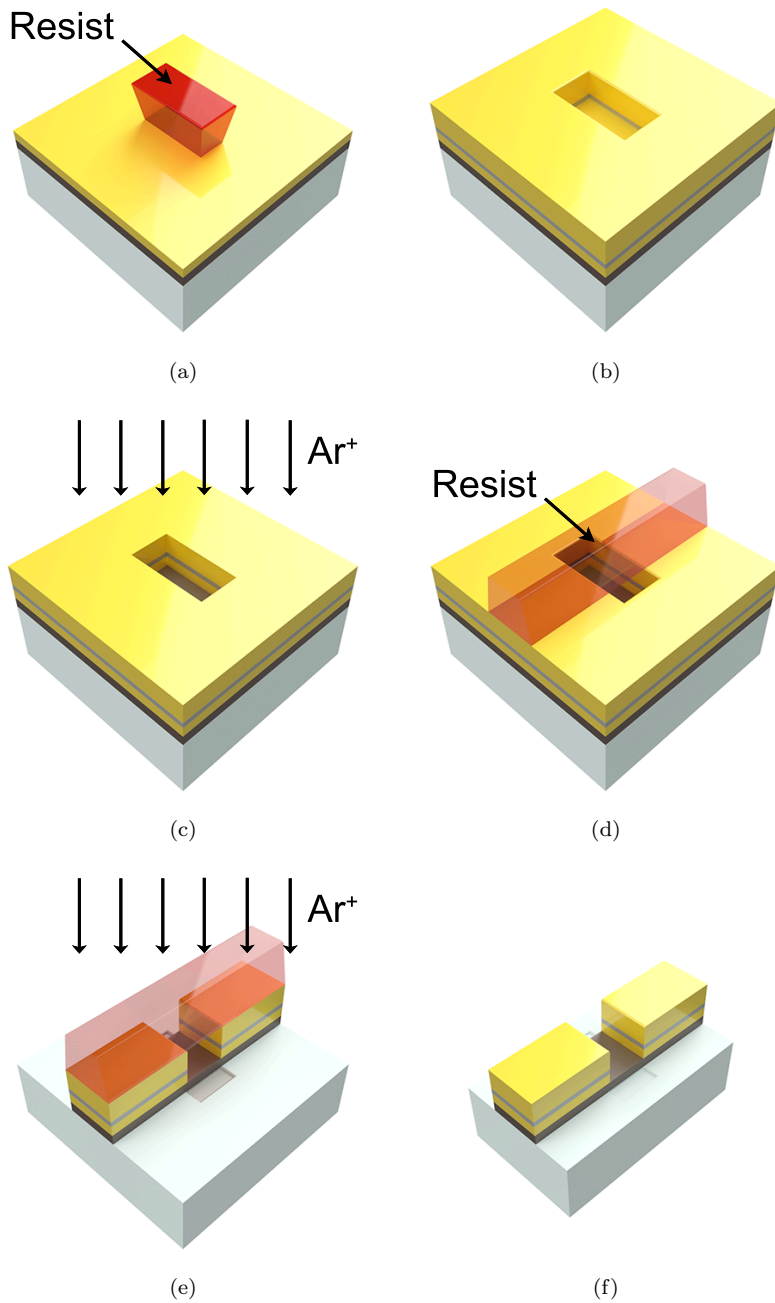


Fig. 4.4: Fabrication process sequence using UV lithography. (a) HEB length definition with resist. (b) Lift-off process. (c) Thin Au layer removal. (d) HEB width and spiral antenna definition with resist. (e) Ar^+ ion beam milling with a resist mask. (f) Final device.

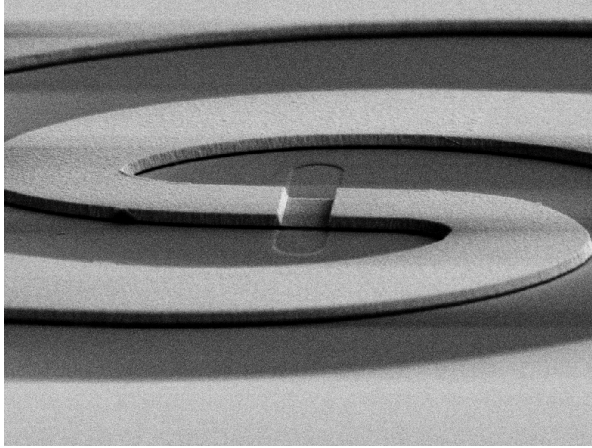


Fig. 4.5: SEM image of MgB_2 HEB made using UV-lithography based fabrication process [Paper A].

2. **Thin Au layer removal:** At this stage the 20 nm thick protective Au layer was etched away using Ar^+ ion beam milling (see Figure 4.4(c)).
3. **Spiral antenna definition:** Next, the spiral antenna with the inner part corresponding to the bolometer width and chip frames were patterned with positive photoresist (see Figure 4.4(d)). Then the developed photoresist was used as an etching mask for Ar^+ ion beam milling. The metal and MgB_2 layers were etched away down to the substrate (see Figure 4.4(e)).
4. **Dicing:** Finally, the wafer covered with photoresist for mechanical protection was cut into $1.3 \times 3.5 \text{ mm}^2$ chips with the diamond dicing saw along the frame lines and washed in acetone to remove resist residuals (see Figure 4.4(f)).

The SEM image of the device fabricated using UV lithography based process is presented in Figure 4.5. The UV lithography does not allow for features below $1 \mu\text{m}$ in size, so such the devices were used mostly for DC characterisation and heterodyne mixing experiments. The HPCVD grown MgB_2 films have lower resistance ($50\text{--}200 \Omega/\square$ for $5\text{--}10 \text{ nm}$ thick films) compared to MBE grown films, so the required aspect ratio of device dimensions is about 1:1. The available LO power is limiting the maximum width of our HEBs to couple of microns. From another side fabrication of narrow HEBs is not desirable due to a higher contact resistance. As a result, low noise MgB_2 HEB mixers could be fabricated using UV lithography based process in most of the cases. However, extra fabrication step for bolometer microbridge passivation is required in order to improve device robustness.

Chapter 5

HEB mixers characterisation techniques

In order to characterise HEB mixers, fabricated chips have to be placed in a complex measurement setup which provides cooling to cryogenic temperatures, effective coupling of signal and LO radiation, voltage biasing, and readout of IF signal. The sensitivity figure of merit for mixers is a receiver input noise temperature which can be measured using the Y-factor technique. Losses and noise of measurement setup components affect measured receiver noise. Therefore, noise contribution of these components has to be analysed in order to study noise performance of HEB mixers themselves. The intrinsic mixer parameters (conversion gain and output noise temperature) can be measured with the U-factor technique using the achieved receiver noise temperature. Mixing of radiation from two sources, when the frequency of one source (LO) is fixed and the frequency of another source is tuned (signal) allows for the direct measurement of mixer GBW. However, the calibration of IF chain and tunable source output power is required.

This chapter describes techniques used for MgB₂ HEB mixers THz characterisation.

5.1 Sensitivity characterisation

In order to provide effective radiation coupling into devices, fabricated MgB₂ HEBs were mounted in a mixer block with a 5 mm elliptical Si lens (see Figure 5.1(a)). The mixer block was placed inside a cryostat (see Figure 5.2(a)) providing cooling down to LHe temperatures. A parabolic off-axis mirror was placed inside the cryostat to focus an incident radiation into the device in order to improve radiation coupling from a LO. A Zitex™ IR block filter was mounted on a 4K screen of the cryostat. A bias-T followed the mixer block to apply a voltage bias to the device and to separate an IF response (see Fig. 5.2(a)). Several amplifiers were used in the IF chain to measure the IF response. One cryogenic low-noise amplifier (LNA) was used inside the LHe cryostat (Chalmers 1.5–4.5 GHz indium phosphide (InP) LNA) in order to amplify a low power IF signal. Two room temperature LNAs were used

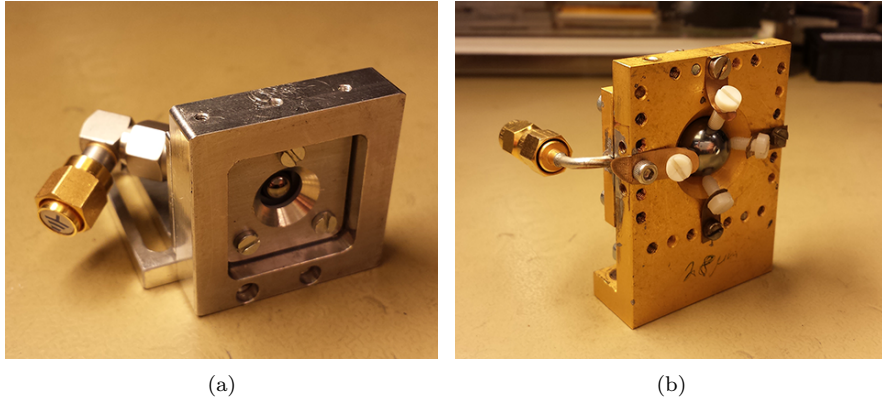


Fig. 5.1: Mixer blocks used for (a) sensitivity characterisation and (b) GBW measurements.

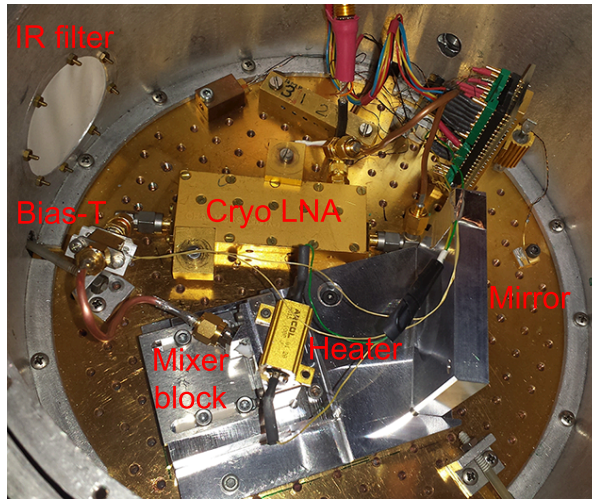
outside the cryostat (Chalmers 1.5–4.5 GHz Gallium arsenide (GaAs) LNA and MITEQ 0.1–10 GHz LNA) to amplify the IF signal further in order to overcome the noise floor. For the characterisation of HEBs with large noise bandwidth cryogenic and room temperature SiIn1.5–4.5GHz band LNAs were substituted with a set of Chalmers 1.0–9.0 GHz InP LNAs.

The schematics of experimental setup is presented in Figure 5.2(b). A far-infrared (FIR) gas laser radiation (LO beam) was combined with signal from either hot or cold loads (Eccosorb sheets) using a Mylar® beam splitter. The emission lines of the FIR gas laser used for mixer sensitivity characterisation were 0.69 THz (formic acid (CH_2O_2) line), 1.63 THz, and 2.56 THz (difluoromethane (CH_2F_2) lines). A high-density polyethylene (HDPE) window let the incoming radiation enter the cryostat. The amplified IF signal was measured through a tunable 50 MHz band-pass YIG-filter with a powermeter. A Goly cell connected to the oscilloscope (not presented in Figure 5.2(b)) was placed behind the beam splitter to monitor the FIR gas laser output power during experiments. Various bath temperatures were used during tests. The temperature of boiling LHe under the standard conditions (4.2 K) were used as a base temperature. Pumping of helium vapour was performed to decrease a bath temperature down to 2 K. A resistive heater mounted directly on the mixer block was used for measurements at elevated bath temperatures up to 30 K (see Fig. 5.2(a)).

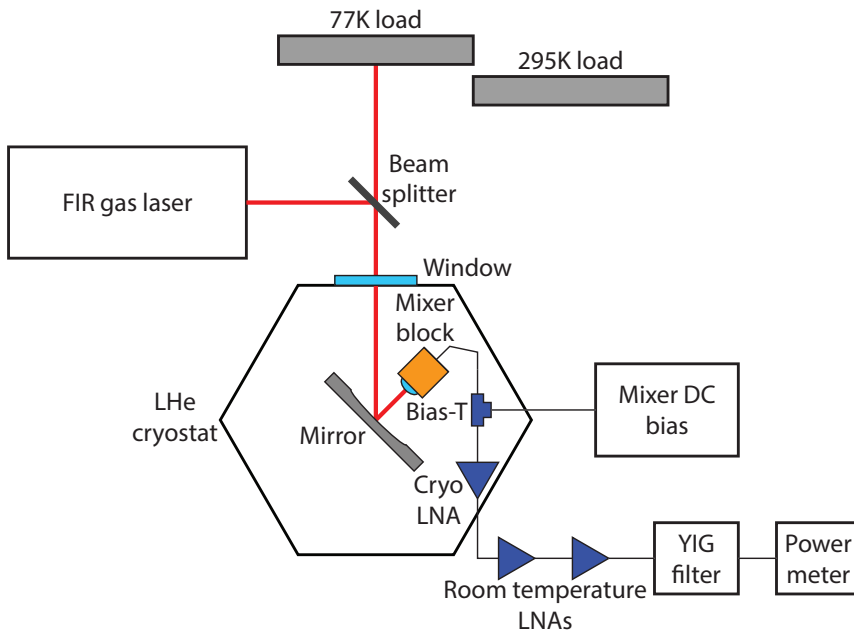
5.1.1 Y-factor technique

In order to measure the DSB receiver noise temperature T_{rec} the standard Y-factor technique [189] was used. Y is a ratio between receiver output powers with the hot P_{hot} and the cold P_{cold} loads (in this case 295 K and 77 K, respectively):

$$Y = \frac{P_{hot}}{P_{cold}} = \frac{2G_{tot}G_{IF}k_B(T_{rec} + T_{295K})B}{2G_{tot}G_{IF}k_B(T_{rec} + T_{77K})B} = \frac{T_{rec} + T_{295K}}{T_{rec} + T_{77K}} \quad (5.1)$$



(a)



(b)

Fig. 5.2: Mixer noise and gain characterisation. (a) The cold plate of LHe cryostat. (b) The schematic of measurement setup.

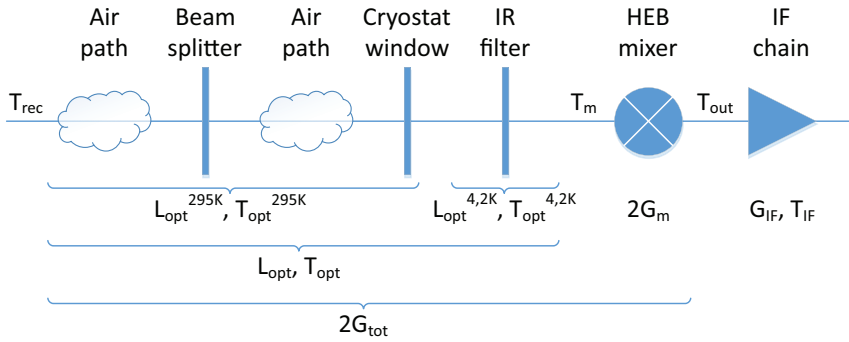


Fig. 5.3: Losses and equivalent noise temperatures of optical and electrical components in the signal path.

where G_{tot} is the total receiver gain, G_{IF} the IF chain gain, T_{IF} the IF chain input noise temperature, B the bandwidth, and T_{295K} , T_{77K} the Callen-Welton temperatures [190] of hot and cold loads. The noise temperature then could be calculated as:

$$T_{rec} = \frac{T_{295K} - Y T_{77K}}{Y - 1} \quad (5.2)$$

Since THz superconducting mixers (e.g. HEB mixers) are characterised in a complex set-up, both the loss and the noise contributions of optical components have to be analysed. That allows for de-embedding of the mixer input noise temperature. Figure 5.3 represents the signal path through the optical and electrical components in the receiver. A contribution of optical elements to a noise temperature can be calculated using the general formula for lossy components $T_{eq} = (L-1)T$ (where L is a component loss and T is a Callen-Welton temperature of component) and then deducted from the measured noise temperature (Table 5.1). The losses in the Si lens were treated as a part of mixer loss and was not deducted from the noise temperature. The DSB receiver noise temperature is then:

$$T_{rec} = T_{opt} + T_m L_{opt} + \frac{T_{IF}}{2G_{tot}} \quad (5.3)$$

where T_{opt} is the noise contribution of optical components and L_{opt} the optical losses.

5.1.2 U-factor technique

In order to measure both the mixer conversion gain and the output noise temperature, the U-factor technique [94] was applied. The U-factor is defined as a ratio between receiver output powers when the receiver is in an operating state and a reference state which can be characterised by an equivalent temperature T_{REF} . As a reference state either a superconducting state or a normal state could be used. In a superconducting state a HEB works as a microwave short and reflects all power coming from an IF chain ($T_{REF} = T_{IF}$). A normal

Table 5.1: Optical losses along the signal path at 0.69 THz ($L_{0.69THz}$) and 1.63 THz ($L_{1.63THz}$).

Component	$L_{0.69THz}$ (dB)	$L_{1.63THz}$ (dB)
Air path (50 cm)	0.03	0.55
Cryostat window (1 mm HDPE)	0.7	0.7
IR filter (2 Zitex™ sheets)	0.6	0.6
Si lens reflection	1	1
Total	2.33	2.85

state could be achieved by a heavy pumping of HEB with the LO. For a HEB in a normal state an output power is determined mostly by the thermal noise with an effective temperature which is equal to the electron temperature of HEB in this state (i.e. about T_c). In both reference states, an output power of the receiver is determined by a sum of the reference and the IF chain noise temperatures:

$$U = \frac{2 G_{tot} (T_{rec} + T_{295K})}{T_{IF} + T_{REF}} \quad (5.4)$$

In this case the mixer conversion gain could be calculated as:

$$G_m = G_{tot} L_{opt} = \frac{U (T_{IF} + T_{REF})}{2 (T_{rec} + T_{295K})} L_{opt} \quad (5.5)$$

Using Equations 2.12 and 5.3, Equation 5.4 could be rewritten as:

$$U = \frac{T_{out} + T_{IF} + 2 G_{tot} (T_{opt} + T_{295K})}{T_{IF} + T_{REF}} \quad (5.6)$$

Finally, the mixer output noise temperature becomes:

$$T_{out} = U (T_{IF} + T_{REF}) - T_{IF} - 2 G_{tot} (T_{opt} + T_{295K}) \quad (5.7)$$

Another way to obtain the mixer conversion gain and the output noise temperature is to calculate it directly from the IF response of HEB mixer at an operation state:

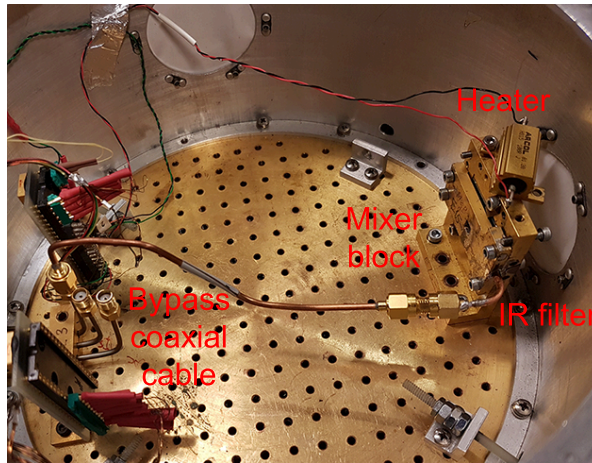
$$P_{out} = k_B B (T_{295K} + T_{rec}) \frac{2 G_m G_{IF}}{L_{opt}} \quad (5.8)$$

where G_{IF} is an IF chain gain. If both the gain and the noise temperature of the IF chain are well known, the mixer conversion gain could be derived from Equation 5.8 as:

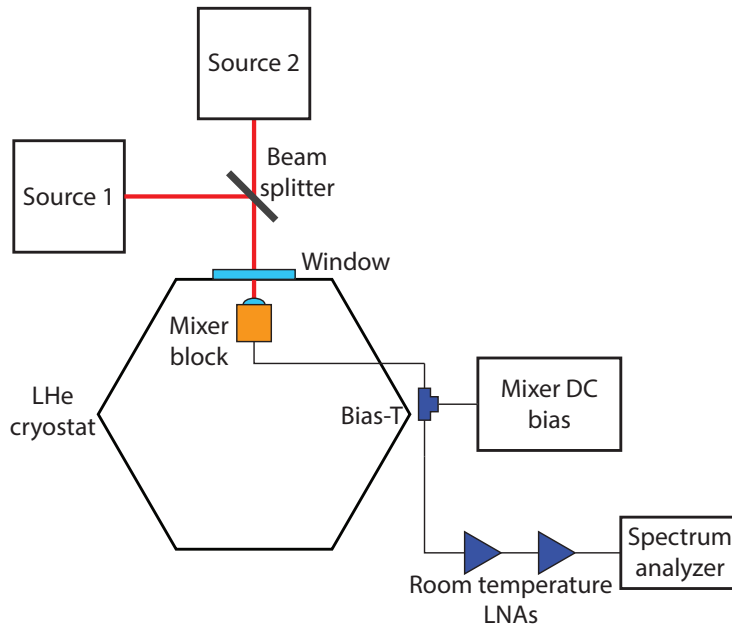
$$G_m = \frac{P_{out} L_{opt}}{2 k_B B (T_{295K} + T_{rec}) G_{IF}} \quad (5.9)$$

In this case, the mixer output noise temperature is:

$$T_{out} = \frac{P_{out} L_{opt}}{2 k_B B G_{IF}} - T_{IF} - \frac{2 G_m (T_{295K} + T_{opt})}{L_{opt}} \quad (5.10)$$



(a)



(b)

Fig. 5.4: Mixer GBW characterisation. (a) The cold plate of LHe cryostat. (b) The schematic of measurement setup.

5.2 GBW characterisation

For GBW measurements, MgB₂ HEB mixers were mounted in a mixer block with a 12 mm elliptical Si lens (see Figure 5.1(b)). The mixer block was placed in the LHe cryostat just in front the cryostat window. The mixer block output was connected directly to the cryostat output bypassing both the bias-T and the cryogenic LNA (see Figure 5.4(a)). The same resistive heater was mounted on the mixer block to perform measurements at elevated bath temperatures.

The full measurement setup schematics is presented in Figure 5.4(b). Radiation from two sources was combined using the Mylar[®] beam splitter. The frequency of Source 1 was fixed while the frequency of Source 2 was tuned. Either the FIR laser at 0.69 THz line or the backward wave oscillator (BWO) at 0.4 THz were used as a fixed frequency source. SD based frequency multiplier sources for corresponding frequency were used as a tunable frequency source. For GBW measurements at 0.1 THz, a Gunn diode source and a tunable high-electron-mobility transistor (HEMT) based frequency multiplier source were utilized. Signals from both sources were mixed by rectangular waveguide directional coupler with a horn antenna at the output for quasi-optical coupling of combined radiation into the receiver. Another broadband (20 kHz–45 GHz) bias-T was placed outside the cryostat to apply a voltage bias to the device and to separate the IF response. Two broadband MITEQ (0.1–20 GHz) LNAs followed the bias-T. The amplified mixing signal P_{IF} was measured with a spectrum analyser:

$$P_{IF} = P_s \frac{1}{L_{opt}} G_m G_{IF} \quad (5.11)$$

The gain of entire IF chain (except for the mixer unit) was measured with a noise figure analyser. Variation of tunable THz sources output power was measured both with HEB direct detection response on amplitude modulated THz signal and the Golay cell. After measurements, both calibrations were applied to recorded curves in order to obtain the IF response of HEB mixers themselves.

5.3 S/N ratio characterisation

The mixer characterisation using the Y-factor technique is practical for noise temperatures less than 10 000 K ($Y = 0.1$ dB). For lower Y-factor values the stability of the LO source becomes more critical. Device characterisation well outside the optimal bias regions and LO pumping levels (and at bath temperatures close to the T_c) becomes problematic without proper LO source stabilization. Therefore, heterodyne mixing was utilized in order to measure mixer signal to noise (S/N) ratio, which could be done in a broader conditions range. The experiments were performed using the FIR gas laser at 0.69 THz as an LO. The Schottky diode based frequency multiplier source was used as a signal source. The absolute power of the signal source (including mixer-to-source beam mismatch losses) was of no importance at that stage. However, the output power of the signal source was kept constant during experiments. After the cryogenic LNA, the IF signal was split into two branches outside the cryostat: 1) with the room temperature LNAs and the band-pass YIG-filter

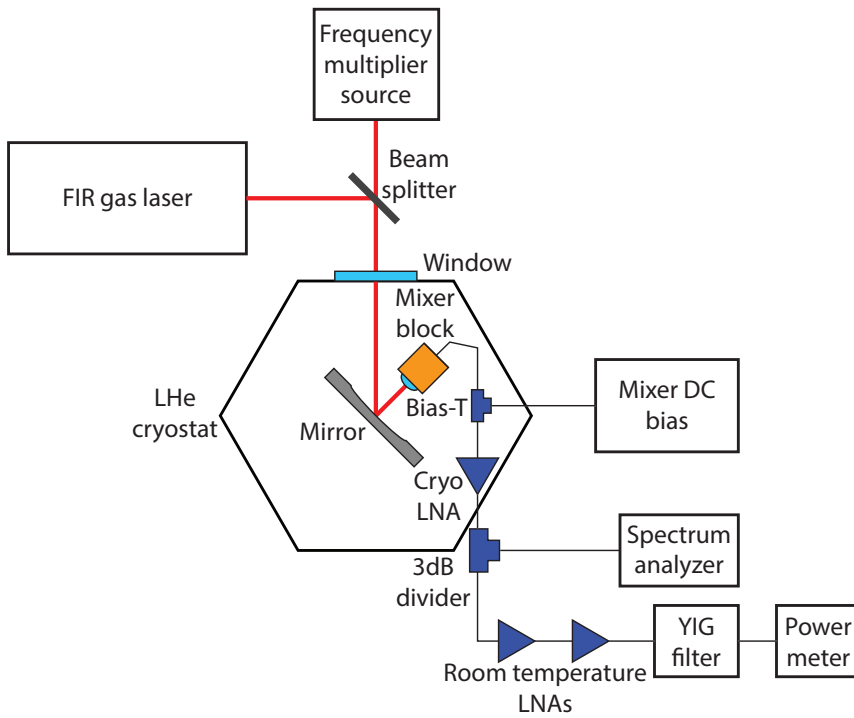


Fig. 5.5: Schematic of measurement setup for S/N ratio characterisation.

(for output noise measurements); and 2) directly fed into the spectrum analyser (for mixing signal measurements). The YIG-filter was set at 2 GHz. In order to exclude any effect from the signal source on the output noise measurements the signal source frequency was detuned by 2.5 GHz from the LO.

The mixing signal P_{IF} was recorded along with the receiver output noise power P_{out} for the same operation points. Since the incident power from the signal source, the optical losses, and the IF chain gain were constant through the experiments, variation of the P_{IF} are due to changes of the mixer gain (see Equation 5.11). Therefore, the mixer gain (in relative units) can be compared at different LO pumping levels and bath temperatures.

By using Equations 2.12 and 5.3, Equation 5.8 could be rewritten as:

$$P_{out} = k_B B \left(\frac{2 G_m T_{295K}}{L_{opt}} + T_{out} + \frac{T_{IF}}{G_{IF}} \right) G_{IF} \quad (5.12)$$

In case of $T_{IF} \ll T_{out}$, the receiver output noise is mostly proportional to the mixer output noise temperature (see Equation 5.12). The S/N ratio then is calculated as:

$$S/N = \frac{P_{IF}}{P_{out}} \quad (5.13)$$

Chapter 6

MgB₂ HEBs THz characterisation results

This chapter summarises the results on THz characterisation of MgB₂ HEB mixers fabricated from both MBE and HPCVD grown MgB₂ superconducting thin films. The results are presented in [Paper A], [Paper B], [Paper D], [Paper E], [Paper F], [Paper G], and [Paper H].

6.1 Devices fabricated from MBE grown films

6.1.1 DC characterisation

One device from each of the three batches B14, N1, N3 was chosen THz characterisation (see Table 6.1). HEB B14-1 discussed below was 10 nm thick and $1 \times 1 \mu\text{m}^2$ in size with a T_c of 8.5 K. HEB N3-2 was 20 nm thick and $1 \times 0.2 \mu\text{m}^2$ in size with a T_c of 22.5 K. HEB N1-2 was 20 nm thick and $1 \times 0.5 \mu\text{m}^2$ in size with a T_c of 22 K. The resistance versus temperature (R-T) curves (see Figure 6.1(a)) were measured in a dip-stick for all HEBs. The devices were biased at

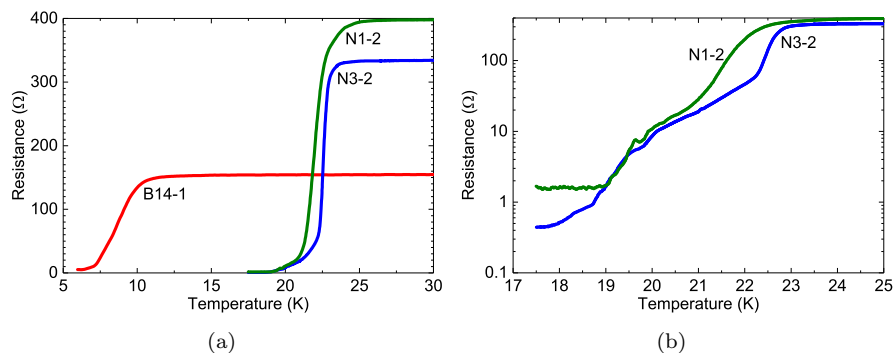


Fig. 6.1: R-T curves (a) for HEBs B14-1, N1-2, and N3-2 and (b) in logarithmic scale for HEBs N1-2 and N3-2. (Data adopted from [Paper B])

Table 6.1: MBE MgB₂ HEB thickness (d), size (W×L), critical temperature (T_c), resistance at room temperature (R_{295K}), resistivity (ρ_{295K}), and critical current density (J_c). (Data adopted from [Paper A] and [Paper B])

Device	d(nm)	W×L (μm ²)	T _c (K)	R _{295K} (Ω)	ρ _{295K} (μΩcm)	J _c (10 ⁷ A/cm ²)
B14-1	10	1×1	8.5	160	160	0.7
N1-2	20	1×0.5	22.0	400	850	5.5
N3-2	20	1×0.2	22.5	330	1650	5.0

a constant current (typically 10 μA) and cooled down from room temperature (295 K) to the LHe temperature (4.2 K). The 10 nm and 20 nm films used for device fabrication were from different batches deposited under different conditions, which affected the film quality. The presence of the double transition on R-T curves for devices N3-2 and N1-2 (see Figure 6.1(b)) suggests that the electrical contact between MgB₂ and Au was rather good (the proximity effect) [191]. One order of magnitude higher sheet resistance for the 20 nm thick devices could be explained by the fact that both surface roughness and film inhomogeneity start to play a significant role for devices with submicron dimensions. The resistivity measured in HEBs N3-2 and N1-2 is also one order of magnitude higher than values reported for 20 nm MBE films previously (100–200 μΩ × cm) [181]. Device B14-1 had much smaller critical current density than two other devices, which together with a lower T_c suggests poorer film quality. The critical current density measured in device B14-1 is in the same ballpark as values reported for devices of similar size [124], while the critical current densities measured in devices N3-2 and N1-2 are of one order of magnitude higher because of the rapid annealing used for the film fabrication [181].

Results of DC measurements are very different from the data acquired with the devices fabricated from HPCVD grown films (see Chapter 3). The resistivity of these 10–20 nm films was much smaller (50–90 μΩcm), whereas critical current density was higher ((2–12)×10⁷ A/cm² in submicron size bridges).

6.1.2 Direct detection characterisation

Some preliminary pumping tests of HEB N1-2 were conducted prior to the noise measurements in order to study the effect of THz radiation on the device. For pumping experiments, the cryostat was placed directly in front of the FIR gas laser front panel. The I-V curves for HEB N1-2 are given in Figure 6.2. The mixer was pumped to the I-V curve close to the optimum with the total available LO power estimated to be ~100 μW in front of the cryostat (Curve 3 in Figure 6.2(a)). A high T_c of 22–23 K according to the BCS theory corresponds to 8 meV σ-gap (or 1.9 THz, 2Δ = ħω, where ħ is the Dirac constant), where a conduction prevails for dirty samples [192, 193]. However, at 1.63 THz the switching similar to the one of NbN devices under the pumping at frequencies below the superconducting gap frequency was not observed. It was demonstrated experimentally, that for the MgB₂ thin film in dirty limit with a T_c as high as 33 K absorption of radiation occurs in a superconducting gap

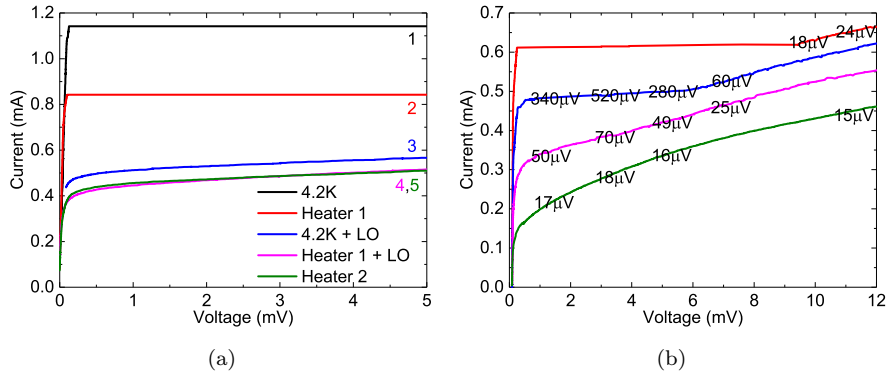


Fig. 6.2: I-V curves for HEB N1-2. (a) Curve 1: 4.2 K without LO pumping; Curve 2: Heater 1 without LO pumping; Curve 3: 4.2 K the maximum LO pumping; Curve 4: Heater 1 with the maximum LO pumping; Curve 5: Heater 2, the heating was increased until curve 5 coincided with curve 4. (b) The numbers in the field represent the voltage response on the lock-in amplifier at 1.63 THz. (Data adopted from [Paper A])

of 1.3 THz [194]. Curves 4 (2) correspond to the increased bath temperature with (without) LO pumping, respectively. For Curve 5 LO was switched off and a bath temperature was further increased by the resistive heater until it overlapped with Curve 4. The identity of Curves 4 and 5 demonstrate that 1.63 THz radiation has the same effect on a HEB as the rise of a bath temperature.

Direct detection experiments were performed in order to estimate which I-V curve corresponds to the HEB's maximum sensitivity to the THz radiation. The voltage response of HEB N1-2 on amplitude modulated THz radiation was recorded for a set of bath temperatures and bias points (see Figure 6.2(b)). The FIR gas laser radiation was attenuated by ~ 20 dB to reach a small signal limit, when the THz radiation has no visible effect on I-V curves. The FIR gas laser radiation was modulated with the chopper 20 Hz. With the HEB in a current biased mode, a lock-in amplifier with a separate voltage pre-amplifier was used to measure voltage response of the HEB. The maximum responsivity was achieved at bias points ranging from 2 mV to 4 mV and from 0.3 mA to 0.5 mA, i.e. at 25-35% of the critical current at 4.2 K. Taking into account optical losses, the maximum responsivity at 1.63 THz can be estimated to be in a range of 1-2 kV/W.

6.1.3 Mixer sensitivity characterisation

HEB B14-1 had a T_c of 8.5 K, relatively low for MgB_2 . Therefore, this device could be directly compared to NbN HEBs. LO pumped I-V curves of B14-1 at both 4.2 K and 2 K are presented in Figure 6.3. The minimum DSB receiver noise temperature corrected for optical losses versus the IF for device B14-1 at 4.2 K is presented in Figure 6.4(a). The I-V curves of B14-1 under LO pumping at 2 K are presented in Figure 6.3(b). The reduction of bath

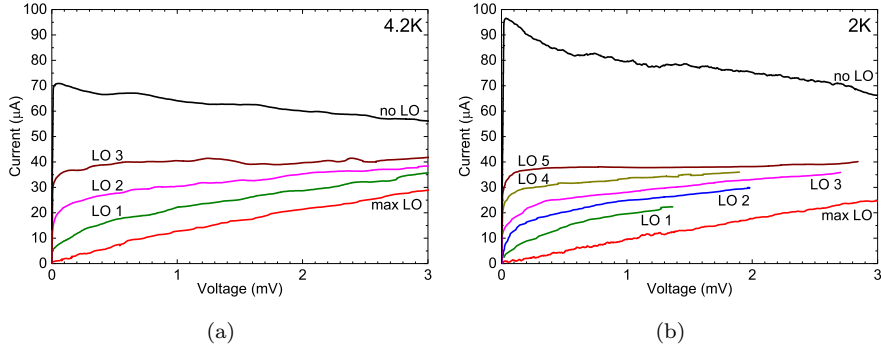


Fig. 6.3: (a) I-V curves for HEB B14-1: under 1.63 THz LO pumping (a) at 4.2 K (LO2 is an optimal I-V curve) and (b) at 2 K (LO3 is an optimal I-V curve). (Data adopted from [Paper B])

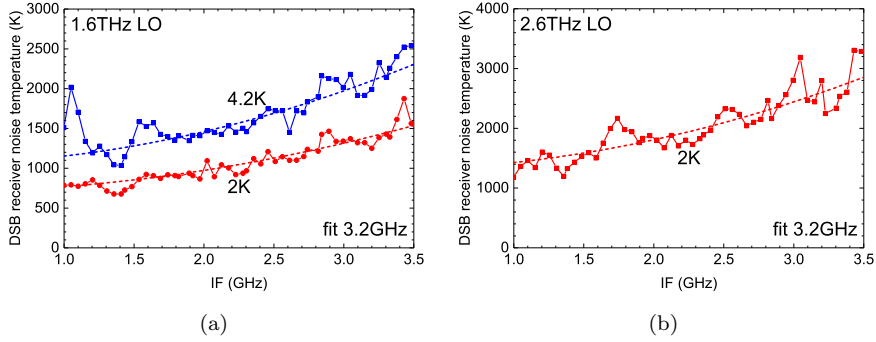


Fig. 6.4: DSB receiver noise temperature corrected for optical losses versus IF for HEB B14-1 (a) at 1.63 THz (the bias points are $U_0 = 0.8$ mV $I_0 = 28$ μ A at 4.2 K and $U_0 = 1.3$ mV $I_0 = 23$ μ A at 2 K) and (b) 2.6 THz (the bias point is $U_0 = 1.38$ mV and $I_0 = 31$ μ A at 2 K). (Data adopted from [Paper B])

temperature resulted in a $\sim 30\%$ increase of the critical current and a $\sim 30\%$ reduction of the receiver noise temperature (see Figure 6.4(a)). The corrected DSB noise temperature acquired with Y-factor measurements for HEB B14-1 was fitted with Equation 2.28. The values of $T_m(0)$ and f_N obtained from a fit are 1050 K and 3.2 GHz for 4.2 K; 700 K and 3.2 GHz for 2 K.

The LO power, required to reach the minimum receiver noise temperature, was calculated using the isotherm method (LO2 curve in Figure 6.3(a)) was 70 nW. The isotherm method assumes that both DC and LO powers have similar effect on HEB resistance [149]. At 2 K the required LO power was estimated to be 80 nW. The LO power required for the minimum noise is in the same ballpark as one reported for NbN HEB mixers.

The available LO power was enough to pump the device into the normal state and to perform U-factor measurements. The noise temperature of the IF chain was determined by the noise temperature of the first LNA which was

Table 6.2: Mixer conversion gains (G_m) and output noise temperatures (T_{out}) for HEB B14-1 at $f_{IF} = 1.8$ GHz calculated using Equations 5.5 and 5.7 with superconducting and normal reference states, and using Equations 5.9 and 5.10. (*Data adopted from [Paper B]*)

T_{bath} (K)	“superconducting”		“normal”		“gain”	
	G_m (dB)	T_{out} (K)	G_m (dB)	T_{out} (K)	G_m (dB)	T_{out} (K)
4.2	-19.1	31	-19.6	27	-19.9	26
2	-18.2	21	-18.1	22	-18.9	18

mounted on the cryostat’s cold plate. The gain of this LNA was 30 dB and the noise temperature was ≈ 2 K. For the whole IF chain the noise temperature was estimated to be not exceeding 3 K. The total gain of the IF chain, used for the gain method calculation, was 77 dB at 1.8 GHz.

At 4.2 K, at the optimal operation point of $U_0 = 0.8$ mV $I_0 = 28 \mu\text{A}$ the U-factor was 8.2 dB for the superconducting state reference and 4.7 dB for the normal state reference. An uncorrected DSB receiver noise temperature of 2500 K and $T_{REF} = 9$ K were taken for calculation using Equations 5.5 and 5.7. At 2 K, the following values were used for the mixer conversion gain and the output noise calculation ($U_0 = 1.3$ mV $I_0 = 23 \mu\text{A}$ bias point): U-factor for a superconducting state reference of 7.2 dBm, U-factor for a normal state reference of 4.2 dBm, a receiver noise temperature of 1500 K and $T_{REF} = 9.3$ K. Mixer conversion gains and output noise temperatures, calculated using all three methods, are summarized in Table 6.2. The values obtained by all three methods are very close to each other, which can be interpreted as a confirmation of reliability. While changing the bath temperature from 4.2 K to 2 K the mixer conversion gain increased by ~ 1 dB, whereas the mixer output noise temperature decreased by 5–10 K. Both of these facts lead to a decrease of the receiver noise temperature. It is of interest to compare this device to a NbN HEB mixer since T_c s are quite close. The reported conversion gain for NbN HEB was -12 dB with a mixer output noise temperature of about 40 K [94, 139]. The U-factor measurements for HEB B14-1 were performed at a 1.8 GHz IF which is quite close to the 3-dB roll-off frequency. Therefore, a correction of about +2 dB should be applied. The receiver noise temperatures and NBWs are in the same ballpark.

Characterisation of MgB_2 HEBs with a higher T_c , in a mode where LO frequency is higher than superconducting gap frequency, requires operation at higher bath temperatures or utilization of LO sources with higher frequencies. Therefore, preliminary Y-factor measurements were performed with HEB B14-1 at 2.6 THz and 2 K. The available output power from the FIR gas laser at this frequency was lower compared to 1.63 THz but still enough to pump the device. The DSB receiver noise temperature versus the IF ($U_0 = 1.38$ mV $I_0 = 31 \mu\text{A}$) is presented in Figure 6.4(b). The fit with Equation 2.28 gives a zero IF noise temperature of 1250 K and NBW of 3.2 GHz. At 2.6 THz, the receiver noise temperature of HEB B14-1 appeared to be higher compared to a 1.63 THz LO.

The same experimental setup was used for HEB N3-2 characterisation and

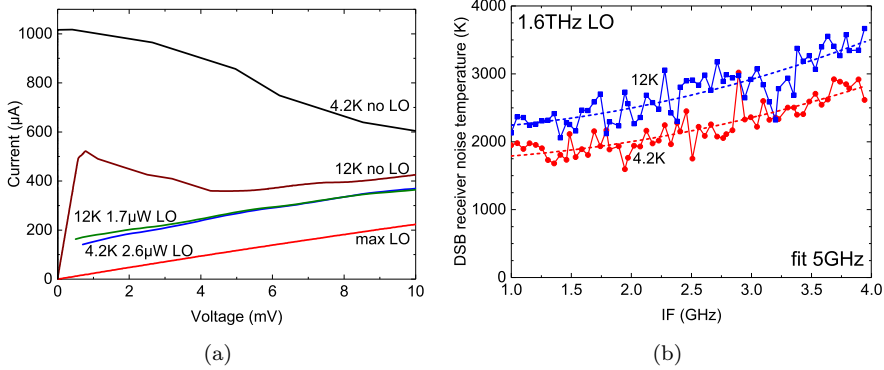


Fig. 6.5: (a) I-V curves for HEB N3-2 with (without) 1.63 THz LO at 12 K and 4.2 K. (b) DSB receiver noise temperatures corrected for optical losses versus IF for HEB N3-2 at 1.63 THz and, 4.2 K (circles) and 12 K (squares). The bias points are $U_0 = 1.6$ mV $I_0 = 180 \mu A$ and $U_0 = 1.8$ mV, $I_0 = 200 \mu A$, respectively. (Data adopted from [Paper B])

a thin plastic film was placed between the mixer block and the cryostat cold plate to minimize a LHe boiling rate during “heated” tests. The I-V curves for HEB N3-2 at 4.2 K and 12 K with and without 1.6 THz LO pumping are presented in Figure 6.5(a). At a bath temperature of about 12 K the HEB critical current has reduced to the half of its value at 4.2 K. The required LO power for the minimum noise operation at 12 K is $1.7 \mu W$ compared to $2.6 \mu W$ at 4.2 K. The measured receiver noise temperatures across a 1–4 GHz IF band for bath temperatures of 4.2 K and 12 K fitted with Equation 2.28 are presented in Figure 6.5(b). Measurements were performed at bias points of $U_0 = 1.6$ mV $I_0 = 180 \mu A$ and $U_0 = 1.8$ mV, $I_0 = 200 \mu A$ for 4.2 K and 12 K, respectively. At certain IFs the mixer response on a hot-cold load was unstable, which resulted in errors in noise temperature measurements (e.g. at 3.2 GHz for 12 K and 1.9 GHz, 2.9 GHz for 4.2 K). The corrected receiver noise temperature increased from 1700 K to 2150 K with an increase of bath temperature but a NBW of 5 GHz remained unchanged.

A direct measurement of GBW at frequencies >1 THz is problematic due to a low availability of coherent sources with a tunable frequency. One of the possible solutions is a use of BWOs or multiplier sources with frequencies <1 THz. For NbN HEB mixers made from ultrathin films a typical critical temperature is about 9 K. This T_c gives a superconducting gap frequency of about 0.6 THz at 4.2 K. Hence, NbN devices work with mentioned power sources in the regime where the LO frequency is higher than the gap frequency. Consequently, this mixing experiments could be extrapolated to higher frequencies. For devices with a high T_c (and hence, large superconducting gap) such low frequency mixing experiments can not be extrapolated to higher frequencies because of slightly different mechanism of mixer operation. In this case, low frequency THz radiation is absorbed only in a normal domain of HEB bridge where a superconducting gap is suppressed by a DC power. Instead of mixing experiments for N3-2 U-factor measurements were performed across the IF band in

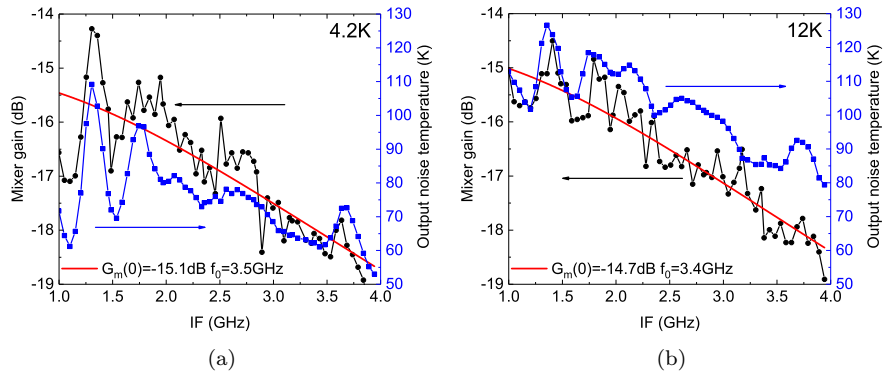


Fig. 6.6: Conversion gain (circles) and output noise temperature (squares) versus the IF for HEB N3-2 at 1.63 THz and (a) 4.2 K, $U_0 = 1.6 \text{ mV}$, $I_0 = 180 \mu\text{A}$ and (b) 12 K, $U_0 = 1.8 \text{ mV}$, $I_0 = 200 \mu\text{A}$. (Data adopted from [Paper B])

order to extract the GBW. Moreover, this method provides both the mixer conversion gain and the output noise temperature. The results of U-factor measurements for 4.2 K and 12 K are presented in Figure 6.6. Higher ripples for IFs < 1.5 GHz correspond to the region of LNA's high return loss. Experimental data were fitted with Equation 2.20. The zero IF mixer conversion gain and the GBW achieved from the fit are -15.1 dB and 3.4 GHz; -14.7 dB and 3.5 GHz at 4.2 K and 12 K, respectively. The HEB shows almost the same conversion gain and GBW at both bath temperatures, but the output noise at 12 K is higher, which resulted in a higher receiver noise temperature. The similar effect of bath temperature was observed for HEB B14-1.

6.2 Devices fabricated from HPCVD grown films

6.2.1 Gain bandwidth characterisation

GBW measurements were performed at three LO frequencies of 0.1 THz, 0.4 THz, and 0.69 THz. The first two frequencies were expected to be below the superconducting gap frequency at 4.2 K, so the tested HEBs were heated up to 25–35 K in order to suppress the superconducting gap. The GBW was observed to be almost independent on both the bias voltage and the bath temperature. The higher output power of 0.1 THz LO allowed for GBW measurements of thicker devices at a wider range of bath temperatures and device sizes. Figure 6.7 presents I-V curves measured in LHe cryostat and the mixing signal at 0.1 THz for 30 nm thick HEB E2-2 with a T_c of 39.5 K. The mixing signal curves taken at different bias points and bath temperatures coincide perfectly. HEBs E3-8 (20 nm thick, $T_c = 38.5 \text{ K}$) and E6-4 (12 nm thick, 33.5 K) were tested at various LO frequencies. Figure 6.8 demonstrates that the GBW of these devices is independent on the LO frequency at least in 0.1–0.69 THz range.

The summary of GBW measurements performed for the HEBs of various thickness is plotted in Figure 6.9. A GBW of 6.8 GHz was observed for HEB

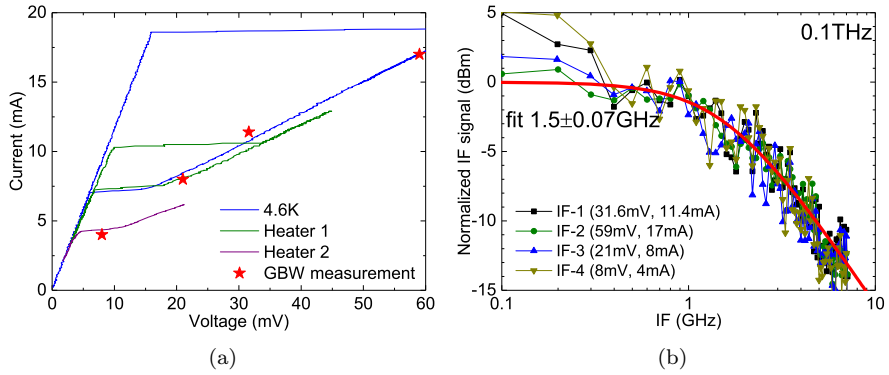


Fig. 6.7: GBW of HEB E2-2 (30 nm thick, $T_c = 39.5$ K). (a) I-V curves measured in LHe cryostat at various bath temperatures and (b) mixing signal at 0.1 THz at various bias points. (Data adopted from [Paper E])

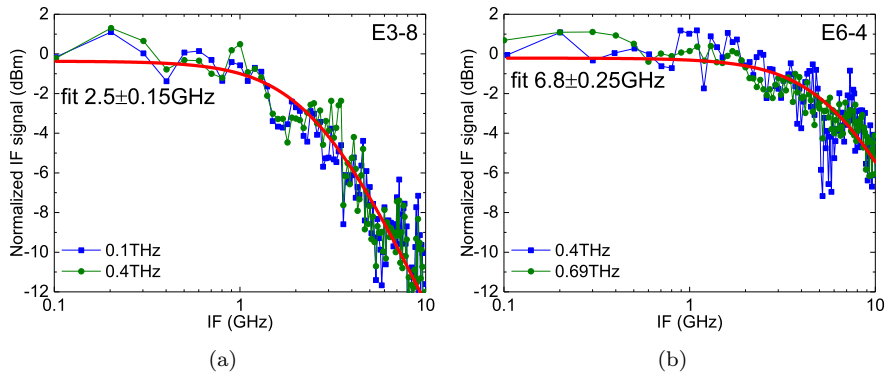


Fig. 6.8: GBW of HEBs (a) E3-8 (20 nm thick, $T_c = 38.5$ K) at 0.1 THz and 0.4 THz LOs and (b) E6-4 (12 nm thick, $T_c = 33.5$ K) at 0.4 THz and 0.69 THz.

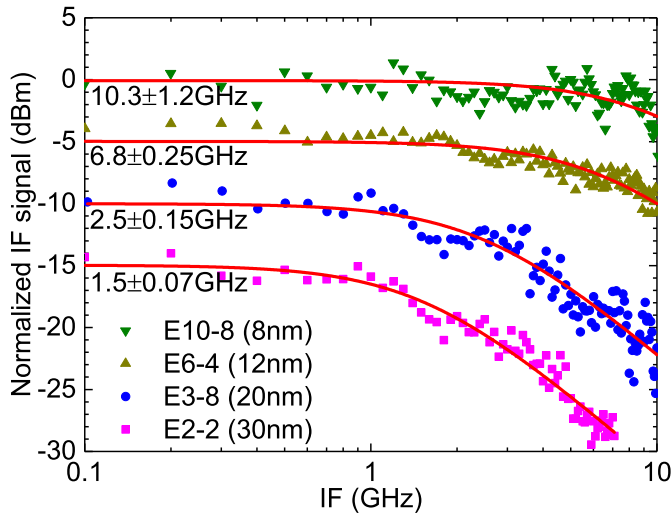


Fig. 6.9: Normalized IF signal of four MgB₂ HEB mixers measured at 0.1 THz (E2-2), 0.4 THz (E3-8), and 0.69 THz (E6-4, E10-8).

Table 6.3: HPCVD MgB₂ HEB thickness (d), critical temperature (T_c), GBW, time constant (τ), electron and phonon heat capacities ratio (c_e/c_{ph}) and critical current density (J_c)

Device	d(nm)	T_c (K)	GBW (GHz)	τ (ps)	c_e/c_{ph}	τ_{ep} (ps)	τ_{esc} (ps)
E2-2	30	39.5	1.5±0.1	106	0.57	3.5±1	22±2
E3-8	20	38.5	2.5±0.15	64	0.59	4±1	20±1.5
E6-4	12	33.5	6.8±0.25	24	0.73	5±0.5	5±0.5
E10-8	8	31.0	10.3±1.2	16	0.82	6±0.2	3±1

E6-4 made from the 12 nm thick MgB₂ film. The GBW is about 2-3 times larger than for typical phonon-cooled NbN HEB mixers made from 3–5 nm thick NbN films. The critical temperatures of the discussed HEBs were in the range of 30–40 K where similar electron-phonon interaction times are expected. Therefore, the increase of GBW for thinner films is expected to be defined mostly by the reduction of the phonon escape time.

In order to estimate these characteristic times, a fit to experimental data was done with the 2-T model (see Chapter 2) similar to Ref. [124]. The same Debye temperature (750 K) and electron specific heat (3 mJ/mol K²) were used for fitting. The HEB parameters and the results are summarized in Table 6.3. The characteristic times follow expected trends (an increase of electron-phonon interaction time and a reduction of escape time). The estimated phonon escape times are twice shorter compared to the escape times measured for HEBs fabricated from MBE grown films [124] suggesting a better acoustic matching at a film/substrate interface. It is obvious that in order to archive more reliable results for device thinner than 10 nm measurements should be performed up

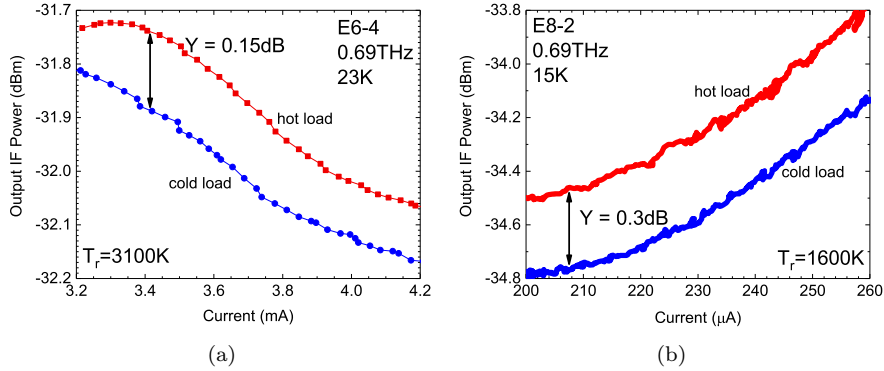


Fig. 6.10: DSB receiver noise temperature measured by Y-factor technique for HEBs (a) E6-4 and (b) E8-2. (Data adopted from [Paper D] and [Paper F])

to higher IFs (at least 20 GHz), which requires a fabrication of a new mixer block and a re-calibration of the whole IF chain.

6.2.2 Mixer sensitivity characterisation

6.2.2.1 Initial results

The GBW characterisation provides some useful information about potential devices performance. However, it was not the main goal of the study since the ultimate characteristics of HEB mixers are receiver noise temperature and NBW. At first stages, sensitivity characterisation was challenging. Initial devices were made from films thicker than 10 nm with high $T_{c,s}$ (close to the bulk value) and high critical current densities. For LO pumping to expected optimal I-V curves, a thick beam splitter (200 μm) with a high transmission loss was used. The available LO power was still not enough to pump the device at 4.2 K, so the bath temperature had to be raised above 20 K. The thick beam splitter and elevated bath temperatures used for device characterisation resulted in a quite high measured DSB receiver noise temperature of 6000 K (see Figure 6.10(a)) for HEB E6-4, which after applying correction for optical losses becomes 3100 K. Better results were achieved for batch E8 made from a 10 nm thick film. Corrected for optical losses DSB receiver noise temperature of 1600 K (see Figure 6.10(b)) was measured for HEB E8-2 with a T_c of 32 K at 0.69 THz and 15 K. At 20 K the noise temperature increased to 2500–3000 K.

For HEB E8-7 the receiver noise temperature was measured versus the IF. Recorded I-V curves are shown in Figure 6.11(a). The I-V curve under the optimal LO power (the highest Y-factor) is IV-opt. The corresponding output IF power curve (Figure 6.11(a), PV-opt) varies with bias voltage with a maximum at about 0.5 mV. The lowest receiver noise temperature was obtained at bias voltages slightly above the maximum on the PV-opt curve (1–2 mV). In the normal state, I-V curve IV-norm is totally linear with a resistance of 50 Ω equal to the resistance near the beginning of superconducting transition. The output IF power curve (PV-norm) is also bias independent indicating that the HEB is in a normal state. The noise temperature is approximately 2000 K in

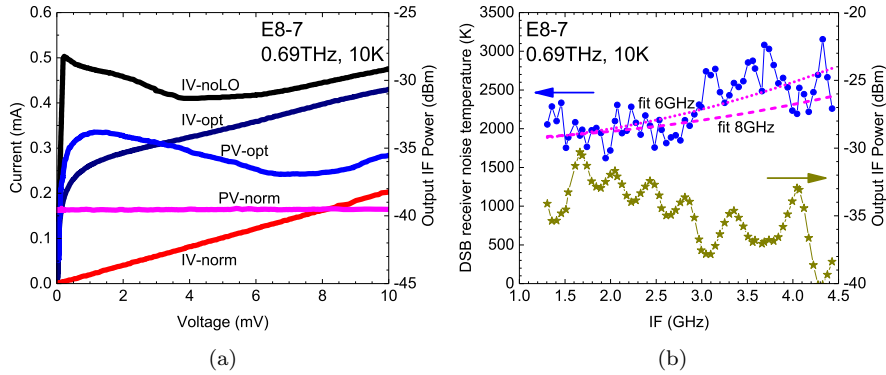


Fig. 6.11: HEB E8-7 (a) IV curves: IV-noLO - in the mixer block at 10 K; IV-opt - under the optimal LO power; IV-norm - pumped by the LO into the normal state. Output IF power versus bias voltage curves measured at 2 GHz: PV-opt corresponds to the optimal LO (IV-opt); PV-norm corresponds to the normal state (IV-norm). (b) DSB receiver noise temperature (circles) and the output power (stars) versus the IF. The dotted and dashed lines are fits for 6 GHz and 8 GHz NBWs, respectively. (Data adopted from [Paper F])

a 1.3–3 GHz IF range (see Figure 6.11(b)). The output IF power versus the IF curve exhibits some notches in 3–4 GHz range and at 4.3 GHz, which is also accompanied by the rise of noise temperature (see Figure 6.11(b)). It could be associated with the cryogenic LNA and leads to a reduced NBW of 6–8 GHz. For further measurements, the cryogenic LNA was replaced.

6.2.2.2 Low noise MgB₂ HEB mixers

Significant progress, comparing to the initial results, was achieved with MgB₂ HEB mixers $1 \times 1 \mu\text{m}^2$ in size with a T_c of 30 K fabricated from a 8 nm thick HPCVD grown film for which Ar⁺ cleaning was applied (see Chapter 3). These devices had room temperature resistances of $\approx 200 \Omega$ (see Figure 6.12). I-V curves for HEB E10-7 are given in Figure 6.13. Device E10-8 from the same batch had very similar critical current and I-V curves as for device E10-7. Therefore, further data would be given for HEB E10-7. Sheet resistance obtained from nanobridges was higher by a factor of 4 compared with sheet resistance measured on this film prior processing. The T_c was reduced by 4 K. The Far Infrared (FIR) gas laser was used as a LO, with emission frequencies of 0.69 THz, 1.63 THz, and 2.56 THz. At 2.56 THz the output power was not sufficient to pump the mixer with a thin beam splitter ($12.5 \mu\text{m}$) and hence, it was only used with a mirror to record I-V curves. With the optimal LO (0.69 THz) power, I-V curves at 5 K, 15 K, and 20 K fully overlap each other, indicating that the LO power at 0.69 THz is absorbed independently of the temperature and the bias voltage (see Figure 6.13(a)). At 5 K, the shape of the IV curves did not depend on the LO frequency from 0.69 THz to 2.56 THz (see Figure 6.13(b)) suggesting that absorption of THz radiation occurs in the π -gap (smaller gap). The same IV curves were achieved by simply rising the bath temperature with the LO turned off. The shapes of the curves are similar

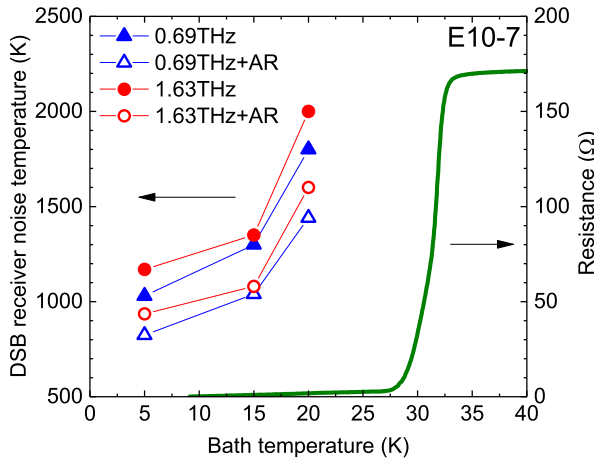


Fig. 6.12: R-T curve for HEB E10-7. Summary of the receiver noise temperature at 0.69 THz (triangles) and 1.63 THz (circles) LOs. Empty symbols are receiver noise temperatures corrected for Si lens losses. (Data adopted from [Paper G])

to those for NbN HEB mixers.

With the 0.69 THz LO, receiver noise temperature was measured using the Y-factor technique at various LO power levels and in a bias voltage range up to 25 mV. The corresponding set of I-V curves at 5 K (each relates to a certain LO power) is given in Figure 6.14(a). The receiver noise temperature measured along IV-3 is given in Figure 6.14(a) (filled dark blue squares, right ordinate). For a bias voltage of 7 mV the receiver noise temperature is shown as a function of bias current (magenta squares, top abscissa). The lowest noise temperature is obtained in a bias voltage range corresponding to the maximum output noise (5–10 mV). The bias point range for the lowest receiver noise temperature is marked with the red oval (IV-3 to IV-5). As the mixer temperature increases, the optimal LO power range shrinks. At 20 K the lowest receiver noise was achieved only around IV-3. For the given set of I-V curves, which excessively covers the optimal LO-bias voltage range, the mixer output noise (see Figure 6.14(b)) increases continuously as the LO power is reduced from the heavily overpumped state (IV-7) till the underpumped state (IV-1) is reached. The mixer gain starts to saturate just above IV-5, i.e. above the optimal bias zone. The resulting S/N ratio (see Figure 6.14(d)) has a maximum at curves IV-3 to IV-5. The $(A \cdot \log(T_{rec}))$ for IV-3 is also plotted in Figure 6.14(d), where A is a fitting parameter for plotting. The logarithm of $1/T_{rec}$ follows closely the S/N ratio curve, as it is expected from Equation 5.13:

$$\log(S/N) \approx \log\left(\frac{P_{IF}}{k_B B T_{rec}}\right) \propto -\log(T_{rec}) \quad (6.1)$$

demonstrating that the bias voltage and LO power optimization for both S/N ratio and receiver noise temperature coincides across the I-V plane. This fact illustrates that, despite the broadband antenna is used for the HEB mixer, the direct detection effect (shift of the bias point due to the switch between hot and cold loads) does not have any impact on the choice of the mixer

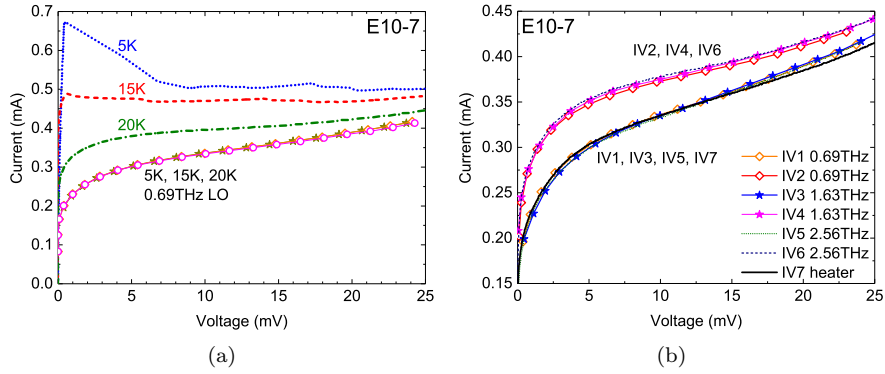


Fig. 6.13: HEB E10-7 I-V curves (a) in the cryostat at 5 K (no LO, blue solid), at 15 K (no LO, red dashed), at 20 K (no LO, green dash-dotted), three fully overlapping IV curves at the optimal LO power at 5 K, 15 K, and 20 K; (b) at different LO power levels (at 5 K): under the 0.69 THz, 1.63 THz, and 2.56 THz LO pumping, IV7 (black solid) at an elevated temperature without LO pumping. (Data adopted from [Paper G])

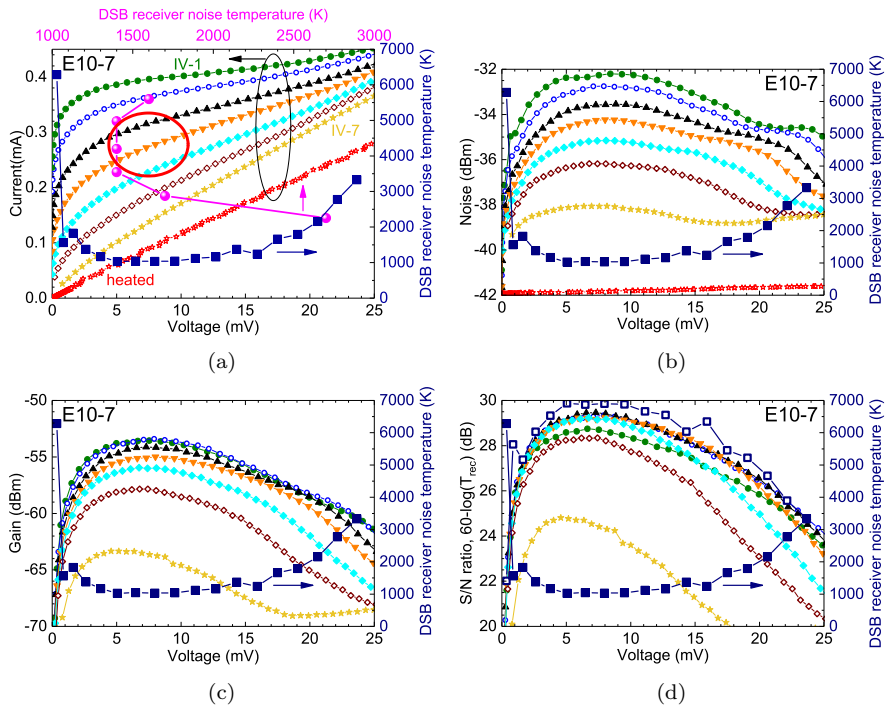


Fig. 6.14: HEB E10-7 with 0.69 THz LO pumping and at 5 K. The area of the highest S/N ratio is marked on the I-V plane. (Data adopted from [Paper H])

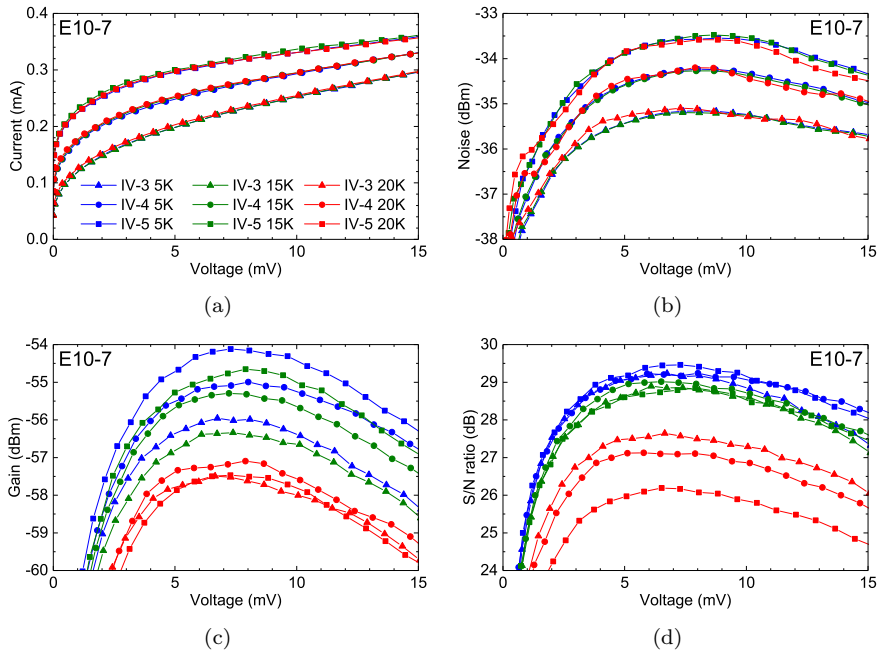


Fig. 6.15: Close comparison of the I-V, P_{out} -V, G-V, and S/N-V curves for HEB E10-7 (0.69 THz and 5 K, 15 K, and 20 K) at the bias voltages and LO power levels corresponding to the highest S/N ratio. (Data adopted from [Paper H])

operation point. In a 3 THz band, a black body at 295 K (77 K) emits ≈ 2.8 nW (≈ 1.6 nW) in the single spatial mode [12]. This is $\approx 1\%$ of a typical optimal LO power for NbN HEB mixers, and hence, this radiation has a significant impact on a mixer bias point especially at smaller bias voltages. For NbN HEB mixers this effect can either decrease or increase the apparent Y-factor (receiver noise temperature). However, for the discussed MgB_2 HEB mixers the direct detection effect is negligible.

The three sets of I-V curves at 5 K, 15 K, and 20 K (corresponding to IV-3, IV-4, and IV-5) are plotted in Figure 6.15(a). For the matching I-V curves, the output noise power versus bias voltage curves also totally overlap each other, which means that the mixer output noise temperature is independent on a bath temperature. In Figure 6.16(a), the output noise power at the same bias point (7 mV and 200 μ A) is plotted as a function of bath temperature. In contrast to the output noise, mixer gain has decreased at higher temperatures (Figure 6.15(c)). The absorbed LO power was calculated using the isotherm method (see Figure 6.16(a)). The logarithm of absorbed LO power is plotted in Figure 6.16(a) (magenta diamonds) along with the mixer conversion gain (red squares). A reduction of mixer gain (by 2.5 dB) from 5 K to 20 K is proportional to a reduction of LO power (by 2.4 dB) for the given I-V curve, as it would be expected from the HEB mixer lumped element model. The logarithm of the receiver noise temperature follows exactly the same temperature trend as the S/N ratio (green triangles and filled stars in Figure 6.16(a)).

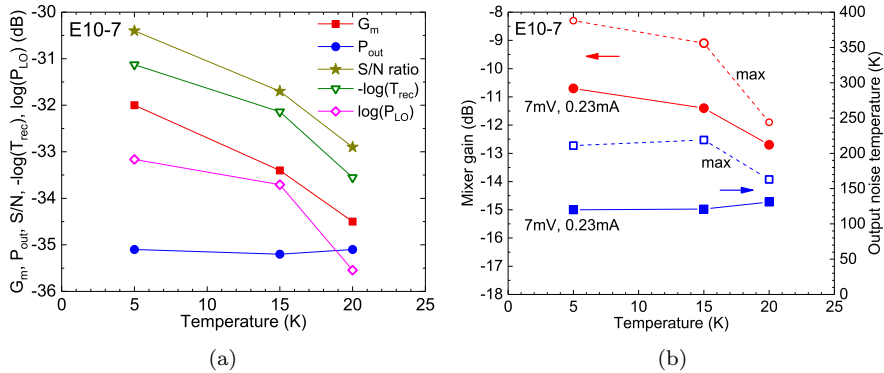


Fig. 6.16: (a) Mixer gain (from mixing experiments) (red squares), mixer output noise (blue circles), S/N ratio (yellow stars), logarithm of $1/T_{rec}$ (empty green triangles), and logarithm of absorbed LO power (empty magenta diamonds) at 0.69 THz versus temperature. Mixer characteristics were measured at the same bias point (7 mV and 0.23 mA) for all bath temperatures. (b) Mixer gain and output noise temperature as a function of bath temperature (from U-factor technique). Filled symbols are at a 7 mV and 0.23 mA bias point. Open symbols are at the point of the maximum output noise temperature providing the same receiver noise temperature as at the discussed bias point. (Data adopted from [Paper H])

Mixer gain (filled circles) and output noise temperature (filled squares) calculated using the U-factor technique with a normal reference state are plotted in Figure 6.16(b) for 5 K, 15 K, and 20 K (all at the same bias point of 7 mV and 0.23 mA). Mixer gain is inversely proportional to the temperature, whereas output noise remains almost the same. This is also confirmed by the mixing experiment, as it can be seen in Figure 6.16(a). As follows from Figure 6.14(a) the receiver noise temperature is constant over quite a wide range of LO power. Across this range (IV5-IV3), both mixer gain and output noise vary by a factor of 2: from 120 K to 220 K and from -10.7 dB to -8.3 dB, respectively (see Figure 6.16(b)). Apart from a lower LO power, the operation at IV3 has an advantage of higher output noise. With an output noise of 220 K, the IF LNA noise becomes much less critical for the overall receiver noise temperature. This is particularly important for the broadband IF LNAs which optimization can now be focused on input matching (no need for an isolator) rather than on the noise. In Figure 6.16(b) both maximum output noise temperature and corresponding mixer gain (within the minimum receiver noise zone) are plotted for 5 K, 15 K, and 20 K mixer temperatures.

In order to obtain the HEB NBW, the noise temperature was measured across a wide IF band with a step of 50 MHz. Both 1.5–4.5 GHz and 1.0–9.0 GHz IF LNAs were used for the experiments. Measurements with the 1.5–4.5 GHz LNA were intended to verify whether HEB-LNA interference might be affecting obtained results. In Figure 6.17(a), the receiver noise temperature measured with the 1.5–4.5 GHz LNA at both 0.69 THz and 1.63 THz LOs is shown. The noise temperature increases proportionally over the whole IF range, indicating that NBW is the same at both LOs, and hence supporting

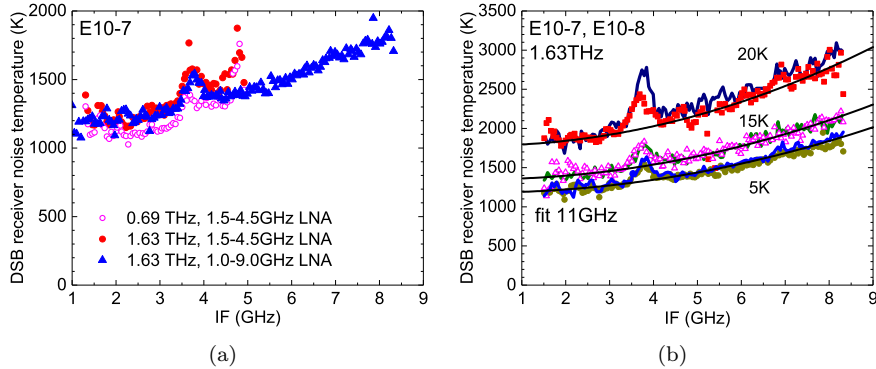


Fig. 6.17: (a) HEB E10-7 receiver noise temperature versus the IF recorded at 5 K. Filled symbols: 1.63 THz. Open symbols: 0.69 THz. Circles: 1.5–4.5 GHz LNA. Triangles: 1.0–9.0 GHz LNA. (b) The receiver noise temperature (at 1.63 THz) as a function of IF recorded at 5 K, 15 K, and 20 K. Results for HEBs E10-7 (line) and E10-8 (symbols) are shown. (*Data adopted from [Paper H]*)

the idea of heterodyne response bolometric nature in discussed devices. The noise temperature at lower IFs as measured with the 1.5–4.5 GHz LNA fully overlaps with the data obtained using the 1.0–9.0 GHz LNA. The hump at 3.7 GHz is present at both data sets and originates from the bias-T used for experiments. The noise temperature spectrum at 1.63 THz was measured at 5 K, 15 K, and 20 K for both HEBs E10-7 and E10-8 (see Figure 6.17(b)). The fitting curves are for an 11 GHz NBW. The summary of measured receiver noise temperatures measured at both 0.69 THz and 1.63 THz LO frequencies is given in Figure 6.12. Considering a possible reduction of reflection losses at the Si lens by 20% with an anti-reflection coating the minimum noise temperatures at 5 K are 830 K (0.69 THz) and 930 K (1.63 THz). At 15 K, the noise temperature rises by 20% from its value at 5 K. At 20 K, the noise temperature rises by 75%. As it can be noticed, the noise temperature difference between 0.69 THz and 1.63 THz is about 12%, which is similar to the rate observed for NbN HEB mixers at higher LO frequency.

6.2.3 Further improvement

As it is demonstrated in Figure 6.16(a)), devices with a higher T_c are needed in order to increase mixer gain and consequently improve noise performance at higher bath temperatures. HEB E15-7 with a T_c of 33 K made from a 5 nm thick HPCVD grown MgB₂ film has demonstrated a lower noise temperature at 20 K compared to HEBs from batch E10 ($T_c = 33$ K) (see Figure 6.18). For device E15-7, a significant increase of the noise temperature (2500 K) was observed only at 25 K. At 30 K, the noise temperature of 15 000 K was estimated using S/N ratio approach. In order to push further the high temperature operation of MgB₂ HEB mixers, devices with even higher T_c have to be utilized. Most likely, it would be possible to achieve only by increasing the film thickness, which would lead to a NBW reduction. Another direction to improve

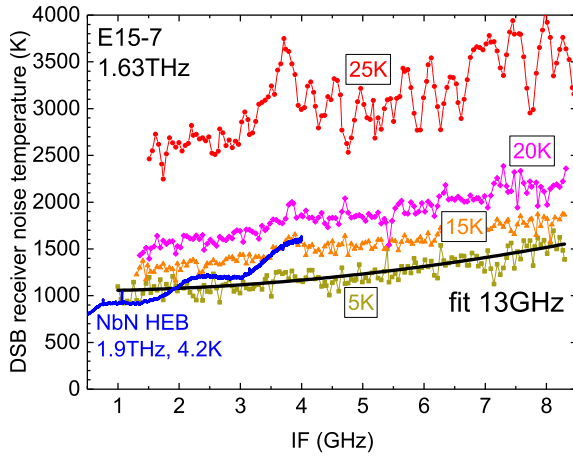


Fig. 6.18: HEB E15-7 receiver noise temperature (at 1.63 THz) versus the IF recorded at 5 K, 15 K, 20 K, and 25 K. The NbN HEB mixer data is from Ref. [32].

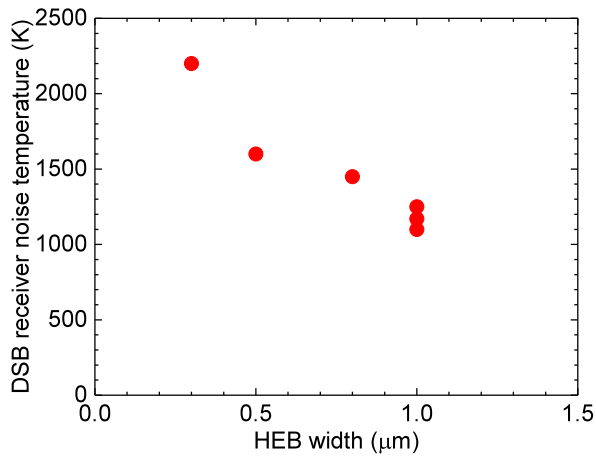


Fig. 6.19: MgB₂ HEB DSB receiver noise temperature versus HEB width.

MgB_2 HEB mixer noise performance is to decrease the contact resistance between the film and Au antenna. The observed dependence of noise temperature on device width (see Figure 6.19) suggests that the contact resistance has a significant contribution. The contact resistance might be reduced either by increasing HEB width, which will, unfortunately, lead to increase of required LO power, or by changing the fabrication procedure to improve the film/antenna contact.

However, MgB_2 HEB mixer already demonstrate noise performance comparable with state-of-the-art NbN HEB mixers but with a three times larger NBW (see Figure 6.18). Despite NbN HEB mixers can have lower noise temperature than the discussed MgB_2 HEB mixers at IFs below 1 GHz, the noise temperatures averaged over the IF bandwidth are in the same ballpark.

Chapter 7

Conclusion and future outlook

In this thesis, study of the novel HEB mixers for THz frequencies based on MgB₂ thin films have been discussed. **MgB₂ HEBs of submicron sizes were fabricated and characterised at THz frequencies.** Transition to submicron sizes has reduced LO power requirements and allowed for the pumping of MgB₂ HEBs to optimal I-V curves at the LHe temperature using available FIR gas laser. **Study of HEBs made from MBE grown MgB₂ films shows that both the output noise temperature and the conversion gain of HEB mixers are proportional to the T_c.** This is valid for the optimal operation conditions: optimal LO power and DC bias. At the same time, utilization of films with a higher T_c results in a broader NBW. Already having reached a T_c of 22 K, HEB mixers can operate above 12 K with only a 25% increase of the noise temperature, compared to that at 4.2 K. **MgB₂ HEB mixers can have a noise temperature as low as 700 K.** Three different methods for mixer conversion gain estimation: the gain method and U-factor methods with superconducting and normal reference states, were applied and compared. Good agreement with an error margin of ±0.5 dB was demonstrated, which indicates the reliability of methods.

An HPCVD system was constructed and launched at Chalmers University of Technology. It is applicable for ultrathin film deposition down to 5 nm without a need for post-processing. Both the low resistivity of 50–90 μΩcm and the high J_c of up to 1.2×10⁸ A/cm² indicate a rather good quality of the achieved films. The micron and submicron size HEB mixers can be fabricated from these films with a high yield (above 75%). The best deposited films that were used in fabrication of HEBs, were only 5 nm thick with a T_c of 33 K and a J_c of (1–3)×10⁸ A/cm².

MgB₂ HEB mixers possess a unique combination of low noise, wide noise bandwidth, and high operation temperature when 5–8 nm thick superconducting MgB₂ films are used with a T_c of 30–33 K. It was demonstrated that compared to the gain bandwidth (GBW) of NbN HEB mixer (≈3 GHz), **the GBW for HEBs made from 8 nm thick HPCVD grown MgB₂ films was 10 GHz.** The GBW was inversely proportional to the film thickness and independent on both the bias voltage, the bath temperature, and LO fre-

quency (from 0.1 THz to 0.69 THz), which simplifies device characterisation. **A NBW of 11 GHz with a minimum receiver noise temperature of 930 K at 1.63 THz and 5 K was achieved.** At 15 K and 20 K, the noise temperature was 1100 K and 1600 K, respectively. From 0.69 THz to 1.63 THz the noise has increased by only 12%. The minimum noise temperature was achieved in a quite large range of bias voltages (5–10 mV) and LO power. **A similar noise temperature of \approx 1000 K and a larger NBW of 13 GHz were achieved with HEB mixers with a T_c of 33 K made from 5 nm thick films.** Such devices have demonstrated a better noise performance at 20 K (1500 K), and operation at 25 K with a noise temperature of 2500 K. At 30 K the noise temperature was estimated to be 15 000 K.

Previously, a receiver noise temperature of 1600 K and a NBW of 6–8 GHz was measured for a 10 nm thick devices. An improvement of sensitivity and NBW was due to a larger bolometer width (lower contact resistance), applied in-situ contact cleaning, and a smaller film thickness. An increase of noise temperature at elevated bath temperatures is determined by a reduction of mixer conversion gain (less LO power is absorbed in the bolometer), while output noise of the HEB remains the same. A high output noise temperature (210 K), compared to values reported for NbN HEB mixers (60 K), lowers demands for the low noise IF chain. Instead of cryogenic LNAs at LHe temperature, LNAs at room temperature or LNAs mounted on higher stages of cryocooling system might be used. In this case cryocoolers with a smaller cold plate and lower cooling power can be utilized, which is important for spaceborne telescopes where resources are always limited. Fabricated devices with a SiN_x passivation demonstrated high robustness and did not lose their properties after continuous storage in a nitrogen atmosphere. However, for a space applications special reliability tests would be required.

Good sensitivity and a large bandwidth as well as operation at elevated bath temperature have been achieved in HEBs from several batches. A combination of these parameters in one device would provide a perfect instrument for the sub-mm wave astronomy. MgB_2 HEB mixers have shown a potential to substitute current NbN (NbTiN) HEB mixers in certain applications, e.g. observation of wide doppler broadened emission from extra-galactic objects or operation on spaceborne satellite based telescopes utilizing light weight closed cycle cryocoolers. For utilization in future space missions, further investigation is required. The following steps in MgB_2 HEB mixer development should be performed:

- Despite a small increase of noise temperature was demonstrated when LO frequency increased from 0.69 THz to 1.63 THz, the low noise performance should still be demonstrated at higher frequencies, up to 5 THz.
- HPCVD process should be improved in order to reduce degradation of T_c with the film thickness reduction in order to achieve low noise operation at bath temperatures >20 K.
- Simultaneously, further development of the process is needed to be able to change the T_c of MgB_2 films without changing other film parameters, e.g. in order to lower the T_c to reduce LO power requirements.
- Modification of fabrication process is required in order to improve the

antenna/film contact and consequently to reduce contact resistance without increasing bolometer width.

- Currently used SiC substrates do not provide a possibility of HEB fabrication on thin membranes for realization of waveguide receivers. Other substrate materials should be tested, e.g. thin SiC on Si substrate.
- Stability of MgB₂ HEB mixers should be investigated by measuring Allan variance. Possibly, the development of receivers utilizing balanced HEB mixers scheme would be required.

Chapter 8

Summary of appended papers

Paper A

MgB₂ hot-electron bolometer mixers at terahertz frequencies

Submicron size HEBs were fabricated with no degradation of the initial film T_c from a 20 nm MgB₂ MBE grown film with a T_c of 22 K. In the direct detection mode, the maximum voltage responsivity was in the range of 1–2 kV/W at 1.63 THz and the optimal bias current is around 1/4-1/3 of the I_c at 4.2 K. 1.63 THz radiation has the same effect on the HEB's IV-curve as a rise in temperature indicating that the response of the device is bolometric.

Contribution: Device layout design. Fabrication process development. Fabrication and responsivity characterisation of HEBs with a higher T_c . Co-writing of the paper.

Paper B

Effect of the critical and operational temperatures on the sensitivity of MgB₂ HEB mixers

Results of the noise and gain bandwidth investigation of HEB mixers made from 10 nm thick MgB₂ films with a T_c of 8.5 K and 20 nm thick MgB₂ film with a T_c of 22.5 K are presented. At an LO frequency of 1.63 THz the minimum receiver noise temperature was 700 K with a NBW of 3.5 GHz and a gain of -18 dB for a device with a T_c of 8.5 K. For a device with a T_c of 22.5 K the corresponding values were 1700 K, 5 GHz and -15 dB. For the latter device the T_r was 2150 K at a bath temperature of 12 K, which is not achievable with Nb-compound based HEB mixers. Different methods for measurements of the HEB mixer gain and the output noise are presented and compared.

Contribution: Device layout design. Fabrication process development. Fabrication of the HEB with a higher T_c , part of THz characterisation of HEBs with low and high T_c . Writing of the paper.

Paper C

Study of MgB₂ ultrathin films in submicron size bridges

A custom built HPCVD system for MgB₂ ultrathin film deposition: construction, deposition process development, and optimization are discussed. Achieved films on SiC substrates have a T_c ranging from 35 K (10 nm thick films) to 41 K (40 nm thick films). The 20 nm thick unpatterned film had a room temperature resistivity of 13 μΩcm, whereas it becomes 50 μΩcm in submicron size bridges with a J_c (4.2 K) up to 1.2×10⁸ A/cm². The lower value of resistivity corresponds to the higher of both T_c and J_c. The surface roughness, measured with an AFM, is approximately 1.5 nm. Possibility of thinning down of MgB₂ film by Ar⁺ ion-beam milling is studied.

Contribution: Participation in designing and construction of the HPCVD system. Thin film characterisation during optimization of film deposition process. Layout design. Fabrication process development. Fabrication of submicron size bridges. DC characterisation of nanobridges. SEM and AFM scans. Writing of the paper.

Paper D

MgB₂ hot electron bolometer mixers for THz heterodyne instruments

Experimental investigation of the MgB₂ HEB mixers for low noise mixing at terahertz frequencies is presented. The GBW measured by mixing of two THz sources is inversely proportional to the film thickness and it is at least 6 GHz for 15 nm thick devices. Performance of MgB₂ HEBs was compared to performance of one of the NbN HEB mixers made for the Herschel Space Observatory (one of the flight units), for which both the GBW and the NBW was measured. MgB₂ HEB mixers show a GBW at least a factor of three broader compared to the NbN HEB measured in the same set-up.

Contribution: Device layout design. Fabrication process development. Fabrication of HEBs. DC and part of THz characterisation of HEBs.

Paper E

Wideband THz HEB mixers using HPCVD MgB₂ thin films

Results of experimental study of the GBW of MgB₂ HEB mixers at 0.1 THz and 0.4 THz are presented. Antenna integrated 0.25–1.5 μm² area devices were made from thin MgB₂ films deposited with a custom made HPCVD system. The GBW was found to be independent on the bias conditions, the bath temperature, and the LO frequency. At 0.69 THz and 23 K the noise temperature of this mixer was 3000 K (corrected for optical losses).

Contribution: Device layout design. Fabrication process development. Fabrication of HEBs. DC and part in THz characterisation of HEBs. Writing of the paper.

Paper F

Broadband MgB₂ Hot-Electron Bolometer THz Mixers operating up to 20 K

Performance of submicron size HEB mixers made from thin MgB₂ superconducting films is discussed. With a superconducting transition temperature of about 30 K, such THz mixers can operate with high sensitivity at temperatures up to 20 K. Due to very small dimensions LO power requirements are rather low. In the IF band of 1–3 GHz the double sideband receiver noise temperature is 1600 K at 10 K operation temperature, 2000 K at 15 K, 2500–3000 K at 20 K. The NBW is estimated to be 6–8 GHz.

Contribution: Device layout design. Fabrication process development. Fabrication of HEBs. DC and part in THz characterisation of HEBs. Co-writing of the paper.

Paper G

Low noise terahertz MgB₂ hot-electron bolometer mixers with an 11 GHz bandwidth

THz HEB mixers with a low noise temperature, a wide NBW, and a high operation temperature made from an 8 nm thick superconducting MgB₂ film are presented. A NBW of 11 GHz with a minimum noise temperature of 930 K at 1.63 THz and 5 K are obtained. At 15 K and 20 K, the noise temperature is 1100 K and 1600 K, respectively. From 0.69 THz to 1.63 THz the receiver noise increases by only 12%. Device current-voltage characteristics are identical when pumped with LOs from 0.69 THz up to 2.56 THz, and match well with IV curves at elevated temperatures. Therefore, the effect of the THz waves on the mixer is totally thermal, due to absorption in the π conduction band of MgB₂.

Contribution: Device layout design. Fabrication process development. Fabrication of HEBs. DC and part in THz characterisation of HEBs. Co-writing of the paper.

Paper H

Gain and noise in THz MgB₂ hot-electron bolometer mixers with a 30 K critical temperature

The detailed study of HEB mixers made from an 8 nm thick superconducting MgB₂ film is presented. Variation of the mixer characteristics such as noise temperature, gain, output noise, and LO power at 5 K, 15 K, and 20 K, and at 0.69 THz and 1.63 THz LO frequencies is investigated. The low noise performance is achieved in quite wide bias point range (5–10 mV). The main reason for the noise temperature to rise at higher temperatures is a reduction of the mixer gain, which occurs proportionally to the LO power reduction. On contrary, the output noise remains constant (for the same bias point). The mixer gain and output noise temperature are in the range of -(8–11) dB and 120–220 K, respectively.

Contribution: Device layout design. Fabrication process development. Fabrication of HEBs. DC and part in THz characterisation of HEBs. Co-writing of the paper.

Acknowledgment

This work would never be done without people I have worked with during my PhD studies.

First and foremost, I would like to express my deep gratitude to my supervisor Assoc. Prof. Sergey Cherednichenko for guidance, discussions and help with measurements and data analysis, which made this work possible.

My sincere thanks to my examiner Prof. Jan Stake for his support and for giving me the possibility to do the PhD at the Terahertz and Millimetre Wave Laboratory. Many special thanks to my ex-colleague Dr. Stella Bevilacqua for the fruitful discussions, for guidance and help in the process lab and for assisting me in the measurement lab. In addition, I want to thank Vladimir Drakinskiy for helpful discussions, teaching me in the process lab and giving me lots of hints about the processing.

Prof. Hiroyuki Shibata from KITAMI Institute of Technology, Prof. Yasuhiro Tokura from University of Tsukuba, and NTT Basic Research Laboratories, are acknowledged for the MBE MgB₂ films providing.

Prof. Xiaoxing Xi and Prof. Ke Chen from Temple University, are acknowledged for valuable discussions on HPCVD MgB₂ film technology.

Kiryl Kustanovich, Dr. Tomas Bryllert, and Dr. Andrei Gorodetsky are acknowledged for the help with the thesis proofreading.

I want to thank all the staff of the Nanofabrication Laboratory. In particular, Henrik Frederiksen for the great help with the construction of the HPCVD system.

Special thanks to my parents and friends for encouraging me and their support.

This work was financially supported by the European Research Council (ERC) under the Starting Grant TERAMIX.

Bibliography

- [1] A. Rogalski and F. Sizov, “Terahertz detectors and focal plane arrays,” *Opto-Electronics Review*, vol. 19, no. 3, pp. 346–404, September 2011.
- [2] R. A. Lewis, “A review of terahertz sources,” *Journal of Physics D: Applied Physics*, vol. 47, no. 37, p. 374001, September 2014.
- [3] P. Siegel, “Terahertz technology in biology and medicine,” *IEEE Transactions on Microwave Theory and Techniques*, vol. 52, no. 10, pp. 2438–2447, October 2004.
- [4] M. C. Kemp, P. F. Taday, B. E. Cole, J. A. Cluff, A. J. Fitzgerald, and W. R. Tribe, “Security applications of terahertz technology,” *Proceedings of SPIE*, vol. 5070, pp. 44–52, 2003.
- [5] M. Fitch and R. Osiander, “Terahertz waves for communications and sensing,” *Johns Hopkins APL Technical Digest (Applied Physics Laboratory)*, vol. 25, no. 4, pp. 348–355, 2004.
- [6] T. Phillips and J. Keene, “Submillimeter astronomy,” *Proceedings of the IEEE*, vol. 80, no. 11, pp. 1662–1678, November 1992.
- [7] G. Stacey, “THz Low Resolution Spectroscopy for Astronomy,” *IEEE Transactions on Terahertz Science and Technology*, vol. 1, no. 1, pp. 241–255, September 2011.
- [8] P. Ubertini, N. Gehrels, I. Corbett, P. de Bernardis, M. Machado, M. Griffin, M. Hauser, R. K. Manchanda, N. Kawai, S.-N. Zhang, and M. Pavlinsky, “Future of space astronomy: A global road map for the next decades,” *Advances in space research*, vol. 50, no. 1, pp. 1–55, July 2012.
- [9] J. Zmuidzinas and P. Richards, “Superconducting detectors and mixers for millimeter and submillimeter astrophysics,” *Proceedings of the IEEE*, vol. 92, no. 10, pp. 1597–1616, October 2004.
- [10] H.-W. Hübers, “Terahertz heterodyne receivers,” *IEEE Journal of Selected Topics in Quantum Electronics*, vol. 14, no. 2, pp. 378–391, Mar-Apr 2008.
- [11] I. Mehdi, J. V. Siles, C. Lee, and E. Schlecht, “THz diode technology: status, prospects, and applications,” *Proceedings of the IEEE*, January 2017.

- [12] A. R. Kerr, S. K. Pan, and W. G. Lyons, "The genesis of SIS mixers - the legacy of John Tucker in radio astronomy," in *2015 IEEE MTT-S International Microwave Symposium*, May 2015.
- [13] A. Shurakov, Y. Lobanov, and G. Gol'tsman, "Superconducting hot-electron bolometer: From the discovery of hot-electron phenomena to practical applications," *Superconductor Science and Technology*, vol. 29, no. 2, p. 023001, December 2016.
- [14] E. Gershenson, G. Gol'tsman, I. Gogidze, Y. Gusev, A. Elantev, B. Karasik, and A. Semenov, "Millimeter and submillimeter range mixer based on electronic heating of superconductive films in the resistive state," *Superconductivity*, vol. 10, no. 3, pp. 1582–1597, October 1990.
- [15] E. Gershenson, M. Gershenson, G. Gol'tsman, A. Semyonov, and A. Sergeev, "Heating of electrons in superconductor in the resistive state due to electromagnetic radiation," *Solid State Communications*, vol. 50, no. 3, pp. 207–212, 1984.
- [16] K. Zhou, W. Miao, Z. Lou, J. Hu, S. Li, W. Zhang, S. Shi, R. Lefevre, Y. Delorme, and T. Vacelet, "A 1.4 THz quasi-optical NbN superconducting HEB mixer developed for the DATE5 telescope," *IEEE Transactions on Applied Superconductivity*, vol. 25, no. 3, p. 2300805, June 2015.
- [17] W. Zhang, P. Khosropanah, J. Gao, T. Bansal, T. Klapwijk, W. Miao, and S. Shi, "Noise temperature and beam pattern of an NbN hot electron bolometer mixer at 5.25 THz," *Journal of Applied Physics*, vol. 108, no. 9, p. 093102, March 2010.
- [18] D. Marrone, R. Blundell, E. Tong, S. Paine, D. Loudkov, J. Kawamura, D. Lühr, and C. Barrientos, "Observations in the 1.3 and 1.5 THz Atmospheric Windows with the Receiver Lab Telescope," in *16th International Symposium on Space Terahertz Technology*, May 2005, pp. 64–67.
- [19] D. Meledin, A. Pavolotsky, V. Desmaris, I. Lapkin, C. Risacher, V. Perez, D. Henke, O. Nystrom, E. Sundin, D. Dochev, M. Pantaleev, M. Fredrixon, M. Strandberg, B. Voronov, G. Goltsman, and V. Belitsky, "A 1.3-THz balanced waveguide HEB mixer for the APEX telescope," *IEEE Transactions on Microwave Theory and Techniques*, vol. 57, no. 1, pp. 89–98, January 2009.
- [20] C. Risacher, D. Meledin, V. Belitsky, and P. Bergman, "First 1.3 THz Observations at the APEX Telescope," in *20th International Symposium on Space Terahertz Technology*, April 2009, pp. 54–61.
- [21] T. de Graauw et al., "The Herschel-Heterodyne Instrument for the Far-Infrared (HIFI)," *Astronomy & Astrophysics*, vol. 518, p. L6, July-August 2010.
- [22] P. Goldsmith and D. Lis, "Early Science Results From the Heterodyne Instrument for the Far Infrared (HIFI) on the Herschel Space Observatory," *Terahertz Science and Technology, IEEE Transactions on*, vol. 2, no. 4, pp. 383–392, July 2012.

- [23] M. Suttivong, M. Birk, G. Wagner, M. Krocka, M. Wittkamp, P. Haschberger, P. Vogt, and F. Geiger, "Development and characterization of the balloon borne instrument TELIS (TEerahertz and submm LImb Sounder): 1.8 THz receiver," in *19th ESA Symposium on European Rocket and Balloon Programmes and Related Research*, June 2009.
- [24] M. Birk, G. Wagner, G. de Lange, A. de Lange, B. N. Ellison, M. Harman, A. Murk, H. Oelhaf, G. Maucher, and C. Sartorius, "TELIS: TEerahertz and submmw LImb Sounder - Project summary after first successful flight," in *21th International Symposium on Space Terahertz Technology*, March 2010, pp. 195–200.
- [25] C. Walker, C. Kulesa, P. Bernasconi, H. Eaton, N. Rolander, C. Groppi, J. Kloosterman, T. Cottam, D. Lesser, C. Martin, A. Stark, D. Neufeld, C. Lisse, D. Hollenbach, J. Kawamura, P. Goldsmith, W. Langer, H. Yorke, J. Sterne, A. Skalare, I. Mehdi, S. Weinreb, J. Kooi, J. Stutzki, U. Graf, M. Brasse, C. Honingh, R. Simon, M. Akyilmaz, P. Puetz, and M. Wolfire, "The Stratospheric THz Observatory (STO)," *Proceedings of SPIE*, vol. 7733, p. 77330N, July 2010.
- [26] Kawamura, J. and Skalare, A. and Stern, J. and Tong, E., "A 1.5THz waveguide HEB mixer using silicon-on-insulator substrates for the Stratospheric Terahertz Observatory," in *21th International Symposium on Space Terahertz Technology*, March 2010, p. 217.
- [27] Brasse, M. and Graf, U.U. and Honingh, C.E. and Jacobs, K. and Justen, M. and Pütz, P. and Schultz, M. and Stutzki, J., "Receiver optics and 1.9 THz HEB mixers for STO," in *22th International Symposium on Space Terahertz Technology*, April 2011.
- [28] D. Hayton, J. Kloosterman, Y. Ren, T. Kao, J. Gao, T. Klapwijk, Q. Hu, C. Walker, and J. Reno, "A 4.7THz heterodyne receiver for a balloon borne telescope," *Proceedings of SPIE*, vol. 9153, p. 91531R, July 2014.
- [29] Young, A. and Walker, C. and Kulesa, C. and Bernasconi, P. and Dominguez, R. and Siles, J. and Hayton, D. and Gao, J.R. and Peters, W. and Goldsmith, P., "Stratospheric Terahertz Observatory 2016, Sub-orbital flight from McMurdo, Antarctica," in *22th International Symposium on Space Terahertz Technology*, March 2017.
- [30] S. Heyminck, U. U. Graf, R. Güsten, J. Stutzki, H. W. Hübers, and P. Hartogh, "GREAT: the SOFIA high-frequency heterodyne instrument," *Astronomy & Astrophysics*, vol. 542, p. L1, June 2012.
- [31] D. Büchel, P. Pütz, K. Jacobs, M. Schultz, U. Graf, C. Risacher, H. Richter, O. Ricken, H. Hübers, R. Güsten, C. Honingh, and J. Stutzki, "4.7-THz superconducting hot electron bolometer waveguide mixer," *IEEE Transactions on Terahertz Science and Technology*, vol. 5, no. 2, pp. 207–214, March 2015.
- [32] C. Risacher, R. Güsten, J. Stutzki, H. Hübers, D. Büchel, U. Graf, S. Heyminck, C. Honingh, K. Jacobs, B. Klein, T. Klein, C. Leinz,

- P. Pütz, N. Reyes, O. Ricken, H. Wunsch, P. Fusco, and S. Rosner, "First Supra-THz heterodyne array receivers for astronomy with the SOFIA observatory," *IEEE Transactions on Terahertz Science and Technology*, vol. 6, no. 2, pp. 199–211, March 2016.
- [33] L. Jiang, S. Shiba, T. Shiino, K. Shimbo, N. Sakai, T. Yamakura, Y. Irimajiri, P. Ananthasubramanian, H. Maezawa, and S. Yamamoto, "Development of 1.5 THz waveguide NbTiN superconducting hot electron bolometer mixers," *Superconductor Science and Technology*, vol. 23, no. 4, p. 045025, March 2010.
- [34] T. Shiino, L. Jiang, R. Furuya, T. Yamaguchi, S. Shiba, T. Sakai, N. Sakai, Y. Watanabe, O. Ohguchi, H. Maezawa, T. Yamakura, Y. Irimajiri, and S. Yamamoto, "Development of the 1.3–1.5 THz band superconducting HEB mixer receivers for ASTE 10m telescope," April 2011, p. 146.
- [35] K. M. Zhou, W. Miao, S. Shi, R. Lefevre, and Y. Delorme, "Noise temperature and IF bandwidth of a 1.4 THz superconducting HEB mixer," in *2016 URSI Asia-Pacific Radio Science Conference (URSI AP-RASC 2016)*, August 2016, pp. 2010–2012.
- [36] N. Manago, H. Ozeki, and M. Suzuki, "Band selection study for the sub-mm limb sounder SMILES-2," in *IEEE Geoscience and Remote Sensing Symposium 2014*, July 2014, pp. 4153–4156.
- [37] M. Suzuki, N. Manago, H. Ozeki, S. Ochiai, and P. Baron, "Sensitivity study of SMILES-2 for chemical species," p. 96390M, October 2015.
- [38] "Gussto." [Online]. Available: <http://www.as.arizona.edu/gussto>
- [39] W. Wild et al., "Millimetron - a large Russian-European submillimeter space observatory," *Experimental Astronomy*, vol. 23, no. 1, pp. 221–244, March 2009.
- [40] A. V. Smirnov, A. M. Baryshev, P. de Bernardis, V. F. Vdovin, G. N. Gol'tsman, N. S. Kardashev, L. S. Kuz'min, V. P. Koshelets, A. N. Vystavkin, Y. V. Lobanov, S. A. Ryabchun, M. I. Finkel, and D. R. Khokhlov, "The current stage of development of the receiving complex of the Millimetron Space Observatory," *Radiophysics and Quantum Electronics*, vol. 54, no. 8, pp. 557–568, January 2012.
- [41] D. Rigopoulou, M. Caldwell, B. Ellison, C. Pearson, E. Caux, A. Cooray, J. D. Gallego, M. Gerin, J. R. Goicoechea, P. Goldsmith, C. Kramer, D. C. Lis, S. Molinari, V. Ossenkopf-Okada, G. Savini, B. K. Tan, X. Tielens, S. Viti, M. Wiedner, and G. Yassin, "The Far Infrared Spectroscopic Explorer (FIRSPEX): probing the lifecycle of the ISM in the universe," *Proceedings of SPIE*, vol. 9904, p. 99042K, July 2016.
- [42] "Origins space telescope." [Online]. Available: <http://asd.gsfc.nasa.gov/firs/>

- [43] A. F. Loenen, S. Lord, P. Morris, and T. G. Phillips, "Excitation of the molecular gas in the nuclear region of M82," *Astronomy & Astrophysics*, vol. 521, p. L2, October 2010.
- [44] A. R. Kerr, "Low-noise room-temperature and cryogenic mixers for 80–120 GHz," *IEEE Transactions on Microwave Theory and Techniques*, vol. 23, no. 10, pp. 781–787, October 1975.
- [45] E. Carlson, M. Schneider, and T. McMaster, "Subharmonically pumped millimeter-wave mixers," *IEEE Transactions on Microwave Theory and Techniques*, vol. 26, no. 10, pp. 706–715, October 1978.
- [46] P. Siegel, R. Dengler, I. Mehdi, J. Oswald, W. Bishop, T. Crowe, and R. Mattauch, "Measurements on a 215-GHz subharmonically pumped waveguide mixer using planar back-to-back air-bridge Schottky diodes," *IEEE Transactions on Microwave Theory and Techniques*, vol. 41, no. 11, pp. 1913–1921, November 1993.
- [47] I. Mehdi, T. Lee, D. Humphrey, S. Martin, R. Dengler, J. Oswald, A. Pease, R. Smith, and P. Siegel, "600 GHz planar-Schottky-diode subharmonic waveguide mixers," in *1996 IEEE MTT-S International Microwave Symposium Digest*, vol. 1, June 1996, pp. 377–380.
- [48] I. Mehdi, T. Lee, R. Dengler, A. Pease, J. Oswald, D. Humphrey, S. Martin, R. Smith, and P. Siegel, "200 GHz waveguide based subharmonically-pumped mixers with planar Schottky diodes," in *7th International Symposium on Space Terahertz Technology (ISSTT 1996)*, March 1996, pp. 450–461.
- [49] P. Marsh, K. Hong, and D. Pavlidis, "InGaAs-based mm-wave integrated subharmonic mixer exhibiting low input power requirement and low noise characteristics," in *8th International Conference on Indium Phosphide and Related Materials*, April 1996, pp. 57–60.
- [50] A. L. Betz and R. T. Boreiko, "A practical Schottky mixer for 5 THz (Part II)," in *7th International Symposium on Space Terahertz Technology (ISSTT 1996)*, March 1996, pp. 503–510.
- [51] R. Boreiko and A. Betz, "Heterodyne Spectroscopy of the 63 μm OI Line in M42," *The Astrophysical Journal Letters*, vol. 464, no. 1, p. L83, June 1996.
- [52] J. Hesler, T. Crowe, W. Bishop, R. Weikle, R. Bradley, and S.-K. Pan, "The development of planar Schottky diode waveguide mixers at submillimeter wavelengths," in *1997 IEEE MTT-S International Microwave Symposium Digest*, vol. 2, June 1997, pp. 953–956.
- [53] I. Mehdi, S. Marazita, D. Humphrey, L. T.-H., R. Dengler, J. Oswald, A. Pease, S. Martin, W. Bishop, T. Crowe, and P. Siegel, "Improved 240-GHz subharmonically pumped planar Schottky diode mixers for spaceborne applications," *IEEE Transactions on Microwave Theory and Techniques*, vol. 46, no. 12, pp. 2036–2042, December 1998.

- [54] S. Marazita, J. Hesler, R. Feinaugle, W. Bishop, and T. Crowe, "Planar Schottky mixer development to 1 THz and beyond," in *9th International Symposium on Space Terahertz Technology (ISSTT 1998)*, March 1998, pp. 501–510.
- [55] P. Siegel, R. Smith, M. Graidis, and S. Martin, "2.5-THz GaAs monolithic membrane-diode mixer," *IEEE Transactions on Microwave Theory and Techniques*, vol. 47, no. 5, pp. 596–604, May 1999.
- [56] K. Huber, H. Brand, and L.-P. Schmidt, "A broadband low noise heterodyne receiver at 2.5 THz," in *8th International Conference on Terahertz Electronics*, September 2000.
- [57] S. Marazita, W. Bishop, J. Hesler, K. Hui, W. E. Bowen, and T. W. Crowe, "Integrated GaAs Schottky mixers by spin-on-dielectric wafer bonding," *IEEE Transactions on Electron Devices*, vol. 47, no. 6, pp. 1152–1157, June 2000.
- [58] B. Thomas, A. Maestrini, and G. Beaudin, "A low-noise fixed-tuned 300–360-GHz sub-harmonic mixer using planar Schottky diodes," *IEEE Microwave and Wireless Components Letters*, vol. 15, no. 12, pp. 865–867, December 2005.
- [59] E. Schlecht, J. Gill, R. Dengler, R. Lin, R. Tsang, and I. Mehdi, "A unique 520–590 GHz biased subharmonically-pumped Schottky mixer," *IEEE Microwave and Wireless Components Letters*, vol. 17, no. 12, pp. 879–881, December 2007.
- [60] J. Hesler, H. Xu, A. Brissette, and W. Bishop, "Development and characterization of THz planar Schottky diode mixers and detectors," in *19th International Symposium on Space Terahertz Technology (ISSTT 2008)*, April 2008, pp. 224–225.
- [61] B. Thomas, A. Maestrini, J. Gill, C. Lee, R. Lin, I. Mehdi, and P. de Maagt, "A broadband 835–900-GHz fundamental balanced mixer based on monolithic GaAs membrane Schottky diodes," *IEEE Transactions on Microwave Theory and Techniques*, vol. 58, no. 7, pp. 1917–1924, July 2010.
- [62] P. Sobis, N. Wadefalk, A. Emrich, and J. Stake, "A broadband, low noise, integrated 340 GHz Schottky diode receiver," *IEEE Microwave and Wireless Components Letters*, vol. 22, no. 7, pp. 366–368, July 2012.
- [63] H. Zhao, V. Drakinskiy, P. Sobis, J. Hanning, T. Bryllert, A.-Y. Tang, and J. Stake, "Development of a 557 GHz GaAs monolithic membrane-diode mixer," in *2012 International Conference on Indium Phosphide and Related Materials*, August 2012, pp. 102–105.
- [64] B. Thomas, M. Brandt, A. Walber, M. Philipp, H. Gibson, H. Czekala, T. Rose, and V. Kangas, "Submillimetre-wave receiver developments for ICI onboard MetOP-SG and ice cloud remote sensing instruments," in *2012 IEEE International Geoscience and Remote Sensing Symposium*, July 2012, pp. 1278–1281.

- [65] S. A. Retzloff, A. Young, and J. Hesler, "A 1.46 THz Schottky receiver at cryogenic temperatures," in *39th International Conference on Infrared, Millimeter, and Terahertz waves (IRMMW-THz 2014)*, September 2014.
- [66] E. Schlecht, J. Siles, C. Lee, R. Lin, B. Thomas, G. Chattopadhyay, and I. Mehdi, "Schottky diode based 1.2 THz receivers operating at room-temperature and below for planetary atmospheric sounding," *IEEE Transactions on Terahertz Science and Technology*, vol. 4, no. 6, pp. 661–669, November 2014.
- [67] J. Treuttel, L. Gatilova, A. Maestrini, D. Moro-Melgar, F. Yang, F. Tamazouzt, T. Vacelet, Y. Jin, A. Cavanna, J. Mateos, A. Feret, C. Chaumont, and C. Goldstein, "A 520–620-GHz Schottky receiver front-end for planetary science and remote sensing with 1070 K–1500 K DSB noise temperature at room temperature," *IEEE Transactions on Terahertz Science and Technology*, vol. 6, no. 1, pp. 148–155, January 2016.
- [68] T. Reck, A. Zemora, E. Schlecht, R. Dengler, W. Deal, and G. Chattopadhyay, "A 230 GHz MMIC-based sideband separating receiver," *IEEE Transactions on Terahertz Science and Technology*, vol. 6, no. 1, pp. 141–147, January 2016.
- [69] P. J. Sobis, V. Drakinskiy, N. Wadefalk, P.-A. Nilsson, D. Nyberg, A. Hammar, T. Bryllert, H. Zhao, A. Emrich, J. Grahn, and J. Stake, "Ultra low noise 600/1200 GHz and 874 GHz GaAs Schottky receivers for SWI and ISMAR," in *27th International Symposium on Space Terahertz Technology (ISSTT 2016)*, April 2016.
- [70] M. Justen, M. Schultz, T. Tils, R. Teipen, S. Glenz, P. Pütz, C. Honingh, and K. Jacobs, "SIS flight mixers for Band 2 of the HIFI instrument of the Herschel Space Observatory," in *Conference Digest of the Joint Infrared and Millimeter Waves 29th International Conference on Infrared and Millimeter Waves and 12th International Conference on Terahertz Electronics*, September 2004, pp. 437–438.
- [71] A. Karpov, D. Miller, F. Rice, J. Stern, B. Bumble, H. LeDuc, and J. Zmuidzinas, "Low noise NbTiN 1.25 THz SIS mixer for Herschel Space Observatory," in *16th International Symposium on Space Terahertz Technology (ISSTT 2005)*, May 2005, p. 450.
- [72] A. Baryshev, F. Mena, J. Adema, R. Hesper, B. Jackson, G. Gerlofsma, M. Bekema, K. Keizer, H. Schaeffer, J. Barkhof, C. Lodewijk, D. Ludkov, T. Zijlstra, E. van Zeijl, T. Klapwijk, and W. Wild, "ALMA Band 9 cartridge," in *19th International Symposium on Space Terahertz Technology (ISSTT 2008)*, April 2008, pp. 258–262.
- [73] Y. Sekimoto, Y. Iizuka, N. Satou, T. Ito, K. Kumagai, M. Kamikura, M. Naruse, and W. Shan, "Development of ALMA Band 8 (385–500 GHz) cartridge," in *19th International Symposium on Space Terahertz Technology (ISSTT 2008)*, April 2008, pp. 253–257.

- [74] S. Asayama, S. Kawashima, H. Iwashita, T. Takahashi, M. Inata, Y. Obuchi, T. Suzuki, and T. Wada, "Design and development of ALMA Band 4 cartridge receiver," in *19th International Symposium on Space Terahertz Technology (ISSTT 2008)*, April 2008, pp. 244–249.
- [75] B. Billade, O. Nystrom, D. Meledin, E. Sundin, I. Lapkin, M. Fredrixon, V. Desmaris, H. Rashid, M. Strandberg, S. Ferm, A. Pavolotsky, and V. Belitsky, "Performance of the first ALMA Band 5 production cartridge," *IEEE Transactions on Terahertz Science and Technology*, vol. 2, no. 2, pp. 208–214, March 2012.
- [76] S. Mahieu, D. Maier, B. Lazareff, A. Navarrini, G. Celestin, J. Chalain, D. Geoffroy, F. Laslaz, and G. Perrin, "The ALMA Band-7 cartridge," *IEEE Transactions on Terahertz Science and Technology*, vol. 2, no. 1, pp. 29–39, January 2012.
- [77] A. Kerr, S. Pan, S. Claude, P. Dindo, A. Lichtenberger, J. Effland, and E. Lauria, "Development of the ALMA Band-3 and Band-6 sideband-separating SIS mixers," *IEEE Transactions on Terahertz Science and Technology*, vol. 4, no. 2, pp. 201–212, March 2014.
- [78] J. Kooi, R. Chamberlin, R. Monje, A. Kovacs, F. Rice, H. Yoshida, B. Force, K. Cooper, D. Miller, M. Gould, D. Lis, B. Bumble, R. LeDuc, J. Stern, and T. Phillips, "Performance of the Caltech Submillimeter Observatory dual-color 180–720 GHz balanced SIS receivers," *IEEE Transactions on Terahertz Science and Technology*, vol. 4, no. 2, pp. 149–164, March 2014.
- [79] T. Kojima, K. Kuroiwa, T. Takahashi, Y. Fujii, Y. Uzawa, S. Asayama, and T. Noguchi, "Design and performance of mass-produced sideband separating SIS mixers for ALMA Band 4 receivers," *Superconductor Science and Technology*, vol. 28, no. 9, p. 094001, July 2015.
- [80] T. Tamura, T. Noguchi, Y. Sekimoto, W. Shan, N. Sato, Y. Iizuka, K. Kumagai, Y. Niizeki, M. Iwakuni, and T. Ito, "Performance and uniformity of mass-produced SIS mixers for ALMA Band 8 receiver cartridges," *IEEE Transactions on Applied Superconductivity*, vol. 25, no. 3, p. 2400305, June 2015.
- [81] S. Montazeri, P. K. Grimes, C.-Y. E. Tong, W.-T. Wong, and J. C. Bardin, "Direct integration of an SIS mixer with a high-impedance SiGe low noise amplifier," in *26th International Symposium on Space Terahertz Technology (ISSTT 2015)*, March 2015, pp. P–30.
- [82] C. Tong, P. Grimes, J. Weintroub, and R. Blundell, "Ultra-wide IF bandwidth - The next frontier for SIS receivers," in *2015 IEEE MTT-S International Microwave Symposium (IMS 2015)*, May 2015.
- [83] M. Yao, D. Liu, J. Hu, J. Li, and S. Shi, "Study of the input RF noise of a THz superconductor-insulator-superconductor receiver," in *2015 Asia-Pacific Microwave Conference (APMC 2015)*, vol. 2, December 2015.

- [84] A. Khudchenko, A. Baryshev, K. Rudakov, P. Dmitriev, R. Hesper, L. de Jong, and V. Koshelets, "High-gap Nb-AlN-NbN SIS junctions for frequency band 790–950 GHz," *IEEE Transactions on Terahertz Science and Technology*, vol. 6, no. 1, pp. 127–132, January 2016.
- [85] J. Chenu, A. Navarrini, Y. Bortolotti, G. Butin, A. Fontana, S. Mahieu, D. Maier, F. Mattiocco, P. Serres, M. Berton, O. Garnier, Q. Moutote, M. Parioleau, B. Pissard, and J. Reverdy, "The front-end of the NOEMA interferometer," *IEEE Transactions on Terahertz Science and Technology*, vol. 6, no. 2, pp. 223–237, March 2016.
- [86] S. Montazeri, P. Grimes, C. Tong, and J. C. Bardin, "A 220-GHz SIS mixer tightly integrated with a sub-hundred-microwatt SiGe IF amplifier," *IEEE Transactions on Terahertz Science and Technology*, vol. 6, no. 1, pp. 133–140, January 2016.
- [87] Y. Uzawa, Y. Fujii, M. Kroug, K. Makise, A. Gonzalez, K. Kaneko, T. Kojima, A. Miyachi, S. Saito, H. Terai, and Z. Wang, "Development of superconducting THz receivers for radio astronomy," in *41st International Conference on Infrared, Millimeter, and Terahertz waves (IRMMW-THz 2016)*, September 2016.
- [88] A. Khudchenko, R. Hesper, A. Baryshev, J. Barkhof, and F. Mena, "Modular 2SB SIS receiver for 600–720 GHz: Performance and characterization methods," *IEEE Transactions on Terahertz Science and Technology*, vol. 7, no. 1, pp. 2–9, January 2017.
- [89] S. Montazeri, P. Grimes, C. Tong, and J. Bardin, "A wide-band high-gain compact SIS receiver utilizing a 300- μ W SiGe IF LNA," *IEEE Transactions on Applied Superconductivity*, vol. 27, no. 4, p. 1500605, June 2017.
- [90] Y. Fujii, T. Kojima, A. Gonzalez, S. Asayama, M. Kroug, K. Kaneko, H. Ogawa, and Y. Uzawa, "Low-noise integrated balanced SIS mixer for 787–950 GHz," *Superconductor Science and Technology*, vol. 30, no. 2, p. 024001, November 2017.
- [91] R. Wyss, B. Karasik, W. McGrath, B. Bumble, and H. LeDuc, "Noise and bandwidth measurements of diffusion-cooled Nb hot-electron bolometer mixers at frequencies above the superconductive energy gap," in *10th International Symposium on Space Terahertz Technology (ISSTT 1999)*, March 1999, pp. 215–228.
- [92] J. Kawamura, R. Blundell, C. Tong, D. Papa, T. Hunter, S. Paine, F. Patt, G. Gol'tsman, S. Cherednichenko, B. Voronov, and E. Gershenzon, "Superconductive hot-electron-bolometer mixer receiver for 800-GHz operation," *IEEE Transactions on Microwave Theory and Techniques*, vol. 48, no. 4, pp. 683–689, April 2000.
- [93] M. Kroug, S. Cherednichenko, H. Merkel, E. Kollberg, B. Voronov, G. Gol'tsman, H. Huebers, and H. Richter, "NbN hot electron bolometric mixers for terahertz receivers," *IEEE Transactions on Applied Superconductivity*, vol. 11, no. 1, pp. 962–965, March 2001.

- [94] S. Cherednichenko, M. Kroug, H. Merkel, P. Khosropanah, A. Adam, E. Kollberg, D. Loudkov, G. Gol'tsman, B. Voronov, H. Richter, and H.-W. Hübers, "1.6 THz heterodyne receiver for the far infrared space telescope," *Physica C: Superconductivity*, vol. 372-376, no. 1, pp. 427–431, August 2002.
- [95] T. Klapwijk, R. Barends, J. Gao, M. Hajenius, and J. Baselmans, "Improved superconducting hot-electron bolometer devices for the THz range," *Proceedings of SPIE*, vol. 5498, pp. 129–139, October 2004.
- [96] J. Stern, B. Bumble, J. Kawamura, and A. Skalare, "Fabrication of terahertz frequency phonon cooled HEB mixers," *IEEE Transactions on Applied Superconductivity*, vol. 15, no. 2, pp. 499–502, June 2005.
- [97] P. Khosropanah, J. Gao, W. Laauwen, M. Hajenius, and T. Klapwijk, "Low noise NbN hot electron bolometer mixer at 4.3 THz," *Applied Physics Letters*, vol. 91, no. 22, p. 221111, November 2007.
- [98] S. Cherednichenko, V. Drakinskiy, T. Berg, P. Khosropanah, and E. Kollberg, "Hot-electron bolometer terahertz mixers for the Herschel Space Observatory," *Review of Scientific Instruments*, vol. 79, no. 3, p. 034501, March 2008.
- [99] J. Schultz, D. Herald, H. Xu, L. Liu, R. Bass, R. Weikle, and A. Lichtenberger, "The design, fabrication and test results of a 1.6 THz superconducting hot electron bolometer mixer on SOI," *IEEE Transactions on Applied Superconductivity*, vol. 19, no. 3, pp. 297–300, June 2009.
- [100] L. Jiang, S. Shiba, K. Shimbo, N. Sakai, T. Yamakura, M. Sugimura, P. Ananthasubramanian, H. Maezawa, Y. Irimajiri, and S. Yamamoto, "Development of THz waveguide NbTiN HEB mixers," *IEEE Transactions on Applied Superconductivity*, vol. 19, no. 3, pp. 301–304, June 2009.
- [101] W. Zhang, P. Khosropanah, J. Gao, E. Kollberg, K. Yngvesson, T. Bansal, R. Barends, and T. Klapwijk, "Quantum noise in a terahertz hot electron bolometer mixer," *Applied Physics Letters*, vol. 96, no. 11, p. 111113, March 2010.
- [102] Y. Lobanov, C. Tong, A. Hedden, R. Blundell, B. Voronov, and G. Gol'tsman, "Direct measurement of the gain and noise bandwidths of HEB mixers," *IEEE Transactions on Applied Superconductivity*, vol. 21, no. 3, pp. 645–648, June 2011.
- [103] H. Maezawa, T. Yamakura, T. Shiino, S. Yamamoto, S. Shiba, N. Sakai, Y. Irimajiri, L. Jiang, N. Nakai, M. Seta, A. Mizuno, T. Nagahama, and Y. Fukui, "Stability of a quasi-optical superconducting NbTiN hot-electron bolometer mixer at 1.5 THz frequency band," *IEEE Transactions on Applied Superconductivity*, vol. 21, no. 3, pp. 640–644, June 2011.

- [104] I. Tretyakov, S. Ryabchun, M. Finkel, A. Maslennikova, N. Kaurova, A. Lobastova, B. Voronov, and G. Gol'tsman, "Low noise and wide bandwidth of NbN hot-electron bolometer mixers," *Applied Physics Letters*, vol. 98, no. 3, p. 033507, January 2011.
- [105] P. Pütz, C. Honingh, K. Jacobs, M. Justen, M. Schultz, and J. Stutzki, "Terahertz hot electron bolometer waveguide mixers for GREAT," *Astronomy & Astrophysics*, vol. 542, p. L2, June 2012.
- [106] F. Boussaha, J. Kawamura, J. Stern, A. Skalare, and V. White, "A low noise 2.7 THz waveguide-based superconducting mixer," *IEEE Transactions on Terahertz Science and Technology*, vol. 2, no. 3, pp. 284–289, May 2012.
- [107] S. Shiba, Y. Irimajiri, T. Yamakura, H. Maezawa, N. Sekine, I. Hosako, and S. Yamamoto, "3.1-THz heterodyne receiver using an NbTiN hot-electron bolometer mixer and a quantum cascade laser," *IEEE Transactions on Terahertz Science and Technology*, vol. 2, no. 1, pp. 22–28, January 2012.
- [108] Y. Irimajiri, A. Kawakami, I. Morohashi, N. Sekine, S. Ochiai, S. Tanaka, I. Hosako, and M. Yasui, "Development of a low noise heterodyne receiver at 3 THz," in *37th International Conference on Infrared, Millimeter, and Terahertz Waves (IRMMW-THz 2012)*, September 2012.
- [109] L. Jiang, C. Li, T. Shiino, and S. Yamamoto, "Intrinsic mixing behavior of superconducting NbTiN hot electron bolometer mixers based on in situ technique," *Physica C: Superconductivity*, vol. 485, pp. 120–124, February 2013.
- [110] J. Kloosterman, D. Hayton, Y. Ren, T. Kao, J. Hovenier, J. Gao, T. Klapwijk, Q. Hu, C. Walker, and J. Reno, "Hot electron bolometer heterodyne receiver with a 4.7-THz quantum cascade laser as a local oscillator," *Applied Physics Letters*, vol. 102, no. 1, p. 011123, January 2013.
- [111] F. Boussaha, J. Kawamura, J. Stern, and C. Jung-Kubiak, "2.7 THz balanced waveguide HEB mixer," *IEEE Transactions on Terahertz Science and Technology*, vol. 4, no. 5, pp. 545–551, September 2014.
- [112] W. Miao, W. Zhang, Z. Lou, Y. Ren, S. Li, K. Zhang, Q. Yao, T. Kao, Q. Hu, and S. Shi, "A 3.7 THz third-order distributed feedback quantum cascade laser as the local oscillator of a superconducting hot electron bolometer receiver," in *31th URSI General Assembly and Scientific Symposium (URSI GASS 2014)*, August 2014.
- [113] P. Pütz, D. Büchel, K. Jacobs, M. Schultz, and C. Honingh, "1.9 THz waveguide HEB mixers for the upGREAT low frequency array," in *26th International Symposium on Space Terahertz Technology (ISSTT 2015)*, March 2015, pp. M2–3.
- [114] W. Miao, Z. Lou, G.-Y. Xu, J. Hu, S.-L. Li, W. Zhang, K.-M. Zhou, Q.-J. Yao, K. Zhang, W.-Y. Duan, S.-C. Shi, R. Colombelli, B. H.E., and

- R. D.A., "Demonstration of a fully integrated superconducting receiver with a 2.7 THz quantum cascade laser," *Optics Express*, vol. 23, no. 4, pp. 4453–4458, February 2015.
- [115] T. Shiino, R. Furuya, T. Soma, Y. Watanabe, T. Sakai, L. Jiang, H. Maezawa, T. Yamakura, N. Sakai, and S. Yamamoto, "Low-noise 1.5 THz waveguide-type hot-electron bolometer mixers using relatively thick NbTiN superconducting film," *Japanese Journal of Applied Physics*, vol. 54, no. 3, p. 033101, February 2015.
- [116] A. Kawakami, Y. Irimajiri, Y. Uzawa, S. Tanaka, S. Ochiai, and I. Hosako, "Fabrication of 3 THz superconducting hot electron bolometer mixers," in *26th International Symposium on Space Terahertz Technology (ISSTT 2015)*, March 2015, pp. P–18.
- [117] K. Zhou, W. Miao, J. Hu, S. Li, R. Lefevre, Y. Delorme, and S. Shi, "Performance of a 1.3-THz twin-slot antenna superconducting HEB mixer integrated with different elliptical lenses," in *2015 Asia-Pacific Microwave Conference (APMC 2015)*, December 2015.
- [118] S. Jiang, X. Jia, B. Jin, L. Kang, W. Xu, J. Chen, and P. Wu, "Superconducting detectors for terahertz imaging," in *40th International Conference on Infrared, Millimeter, and Terahertz waves (IRMMW-THz 2015)*, August 2015.
- [119] W. Zhang, W. Miao, K. M. Zhou, X. H. Guo, J. Q. Zhong, and S. C. Shi, "High sensitive THz superconducting hot electron bolometer mixers and transition edge sensors," *Proceedings of SPIE*, vol. 10030, p. 1003009, November 2016.
- [120] I. Tret'yakov, N. Kaurova, B. Voronov, V. Anfert'ev, L. Revin, V. Vaks, and G. Gol'tsman, "The influence of the diffusion cooling on the noise band of the superconductor NbN hot-electron bolometer operating in the terahertz range," *Technical Physics Letters*, vol. 42, no. 6, pp. 563–566, July 2016.
- [121] W. Miao, W. Zhang, K. Zhou, H. Gao, K. Zhang, W. Duan, Q. Yao, S. Shi, Y. Delorme, and R. Lefevre, "Investigation of the performance of NbN superconducting HEB Mixers of different critical temperatures," *IEEE Transactions on Applied Superconductivity*, vol. 27, no. 4, p. 2200304, June 2017.
- [122] S. Cherednichenko, V. Drakinskiy, K. Ueda, and M. Naito, "Terahertz mixing in MgB₂ microbolometers," *Applied Physics Letters*, vol. 90, no. 2, January 2007.
- [123] S. Bevilacqua, S. Cherednichenko, V. Drakinskiy, J. Stake, H. Shibata, and Y. Tokura, "Low noise mgb₂ terahertz hot-electron bolometer mixers," *Applied Physics Letters*, vol. 100, no. 3, p. 033504, January 2012.
- [124] S. Bevilacqua, S. Cherednichenko, V. Drakinskiy, H. Shibata, Y. Tokura, and J. Stake, "Study of IF bandwidth of MgB₂ phonon-cooled hot-electron bolometer mixers," *IEEE Transactions on Terahertz Science and Technology*, vol. 3, no. 4, pp. 409–415, July 2013.

- [125] D. Cunnane, J. Kawamura, M. Wolak, N. Acharya, T. Tan, X. Xi, and B. Karasik, "Characterization of MgB₂ superconducting hot electron bolometers," *Applied Superconductivity, IEEE Transactions on*, vol. 25, no. 3, p. 2300206, June 2015.
- [126] D. Cunnane, J. H. Kawamura, M. A. Wolak, N. Acharya, X. X. Xi, and B. S. Karasik, "Optimization of parameters of MgB₂ hot-electron bolometers," *Applied Superconductivity, IEEE Transactions on*, vol. 27, no. 4, p. 2301104, June 2017.
- [127] J. Nagamatsu, N. Nakagawa, T. Muranaka, Y. Zenitani, and J. Akimitsu, "Superconductivity at 39K in magnesium diboride," *Nature*, vol. 410, no. 6824, pp. 63–64, March 2001.
- [128] W. N. Kang, H.-J. Kim, E.-M. Choi, C. U. Jung, and S.-I. Lee, "MgB₂ superconducting thin films with a transition temperature of 39 Kelvin," *Science*, vol. 292, no. 5521, pp. 1521–1523, May 2001.
- [129] X. Zeng, A. Pogrebnyakov, A. Kotcharov, J. Jones, X. Xi, E. Lysczek, J. Redwing, X. Shengyong, Q. Li, J. Lettieri, D. Schlom, W. Tian, X. Pan, and Z.-K. Liu, "In situ epitaxial MgB₂ thin films for superconducting electronics," *Nature Materials*, vol. 1, no. 1, pp. 35–38, September 2002.
- [130] K. Ueda and M. Naito, "In situ growth of superconducting MgB₂ thin films by molecular-beam epitaxy," *Journal of Applied Physics*, vol. 93, no. 4, pp. 2113–2120, February 2003.
- [131] S. Bevilacqua, S. Cherednichenko, V. Drakinskiy, H. Shibata, A. Hammar, and J. Stake, "Investigation of MgB₂ HEB mixer gain bandwidth," in *IRMMW-THz 2011 - 36th International Conference on Infrared, Millimeter, and Terahertz Waves*, October 2011.
- [132] D. Cunnane, J. Kawamura, B. Karasik, M. Wolak, and X. Xi, "Development of hot-electron THz bolometric mixers using MgB₂ thin films," *Proceedings of SPIE*, vol. 9153, p. 91531Q, July 2014.
- [133] X. Xi, A. Pogrebnyakov, S. Xu, K. Chen, Y. Cui, E. Maertz, C. Zhuang, Q. Li, D. Lamborn, J. Redwing, Z. Liu, A. Soukiassian, D. Schlom, X. Weng, E. Dickey, Y. Chen, W. Tian, X. Pan, S. Cybart, and R. Dynes, "MgB₂ thin films by hybrid physical-chemical vapor deposition," *Physica C: Superconductivity*, vol. 456, no. 1-2, pp. 22–37, June 2007.
- [134] F. Arams, C. Allen, B. Peyton, and E. Sard, "Millimeter mixing and detection in bulk InSb," *Proceedings of the IEEE*, vol. 54, no. 4, pp. 612–622, April 1966.
- [135] N. Chi-Anh, H.-J. Shin, K.-T. Kim, Y.-H. Han, and S. Moon, "Characterization of uncooled bolometer with vanadium tungsten oxide infrared active layer," *Sensors and Actuators A: Physical*, vol. 123-124, pp. 87–91, September 2005.

- [136] A. J. Miller, A. Luukanen, and E. N. Grossman, "Micromachined antenna-coupled uncooled microbolometers for terahertz imaging arrays," *Proceedings of SPIE*, vol. 5411, pp. 18–24, September 2004.
- [137] T. G. Phillips and K. B. Jefferts, "A low temperature bolometer heterodyne receiver for millimeter wave astronomy," *Review of Scientific Instruments*, vol. 44, no. 8, pp. 1009–1014, August 1973.
- [138] Y. P. Gousev, G. N. Gol'tsman, A. D. Semenov, E. M. Gershenzon, R. S. Nebosis, M. A. Heusinger, and K. F. Renk, "Broadband ultrafast superconducting NbN detector for electromagnetic radiation," *Journal of Applied Physics*, vol. 75, no. 7, April 1994.
- [139] S. Cherednichenko, P. Khosropanah, E. Kollberg, M. Kroug, and H. Merkel, "Terahertz superconducting hot-electron bolometer mixers," *Physica C: Superconductivity*, vol. 372-376, no. 1, pp. 407–415, August 2002.
- [140] D. E. Prober, "Superconducting terahertz mixer using a transition-edge microbolometer," *Applied Physics Letters*, vol. 62, no. 17, pp. 2119–2121, April 1993.
- [141] A. Semenov, G. Gol'tsman, and R. Sobolewski, "Hot-electron effect in superconductors and its applications for radiation sensors," *Superconductor Science and Technology*, vol. 15, no. 4, pp. R1–R16, March 2002.
- [142] N. Perrin and C. Vanneste, "Response of superconducting films to a periodic optical irradiation," *Phys. Rev. B*, vol. 28, pp. 5150–5159, November 1983.
- [143] J. S. Blakemore, *Solid State Physics (2nd ed)*. Cambridge, UK: University press, 1985.
- [144] J.-L. Luo, J. Zhang, Z.-J. Chen, H.-Y. Bai, Y.-P. Wang, J.-B. Meng, D. Jin, R. Z.-A., G.-C. Che, and Z.-X. Zhao, "Low temperature specific heat of superconducting MgB₂," *Chinese Physics Letters*, vol. 18, no. 6, pp. 820–821, 2001.
- [145] H. Merkel, P. Khosropanah, P. Yagoubov, and E. Kollberg, "A hot-spot mixer model for phonon-cooled NbN hot electron bolometric mixers," *Applied Superconductivity, IEEE Transactions on*, vol. 9, no. 2, pp. 4201–4204, June 1999.
- [146] H. Merkel, P. Khosropanah, D. Wilms Floet, P. Yagoubov, and E. Kollberg, "Conversion gain and fluctuation noise of phonon-cooled hot-electron bolometers in hot-spot regime," *Microwave Theory and Techniques, IEEE Transactions on*, vol. 48, no. 4, pp. 690–699, April 2000.
- [147] H. Merkel, P. Khosropanah, S. Cherednichenko, K. Yngvesson, A. Adam, and E. Kollberg, "A two-dimensional hot-spot mixer model for phonon-cooled hot electron bolometers," *Applied Superconductivity, IEEE Transactions on*, vol. 11, no. 1, pp. 179–182, March 2001.

- [148] B. S. Karasik and A. Elantev, "Analysis of the noise performance of a hot-electron superconducting bolometer mixer," in *6th International Symposium on Space Terahertz Technology*, March 1995, pp. 229–246.
- [149] H. Ekström, B. Karasik, E. Kollberg, and K. Yngvesson, "Conversion gain and noise of niobium superconducting hot-electron-mixers," *IEEE Transactions on Microwave Theory and Techniques*, vol. 43, no. 4, pp. 938–947, April 1995.
- [150] S. Bevilacqua, E. Novoselov, S. Cherednichenko, H. Shibata, and Y. Tokura, "Wideband MgB₂ hot-electron bolometer mixers: IF impedance characterisation and modeling," *IEEE Transactions on Applied Superconductivity*, vol. 26, no. 3, pp. 1–5, April 2016.
- [151] J. W. Kooi, J. J. A. Baselmans, M. Hajenius, J. R. Gao, T. M. Klapwijk, P. Dieleman, A. Baryshev, and G. de Lange, "IF impedance and mixer gain of NbN hot electron bolometers," *Journal of Applied Physics*, vol. 101, no. 4, p. 044511, February 2007.
- [152] H. Merkel, P. Yagoubov, P. Khosropanah, and E. Kollberg, "An accurate calculation method of the absorbed LO power in hot electron bolometric mixers," in *1998 IEEE Sixth International Conference on Terahertz Electronics Proceedings (THZ 98)*, September 1998, pp. 145–148.
- [153] P. Khosropanah, H. Merkel, S. Yngvesson, A. Adam, S. Cherednichenko, and E. Kollberg, "A distributed device model for phonon-cooled HEB mixers predicting IV characteristics, gain, noise and IF bandwidth," in *11th International Symposium on Space Terahertz Technology*, May 2000, pp. 474–488.
- [154] J. C. Mather, "Bolometer noise: nonequilibrium theory," *Appl. Opt.*, vol. 21, no. 6, pp. 1125–1129, March 1982.
- [155] B. S. Karasik and A. I. Elantiev, "Noise temperature limit of a superconducting hot electron bolometer mixer," *Applied Physics Letters*, vol. 68, no. 6, pp. 853–855, February 1996.
- [156] R. Nebosis, A. Semenov, Y. Gousev, and K. Renk, "Rigorous analysis of a superconducting hot-electron bolometer mixer: Theory and comparison with experiment," in *7th International Symposium on Space Terahertz Technology (ISSTT 1996)*, March 1996, pp. 601–613.
- [157] S. Cherednichenko, V. Drakinskiy, J. Baubert, B. Lecomte, F. Dauplay, J.-M. Krieg, Y. Delorme, A. Feret, H.-W. Hübers, A. D. Semenov, and G. N. Gol'tsman, "2.5 THz multipixel heterodyne receiver based on NbN HEB mixers," *Proceedings of SPIE*, vol. 6275, p. 62750I, June 2006.
- [158] E. Gerecht, D. Gu, X. Zhao, J. Nicholson, F. Rodriguez-Morales, and S. Yngvesson, "Development of NbN terahertz HEB mixers coupled through slot-ring antennas," in *15th International Symposium on Space Terahertz Technology (ISSTT 2004)*, April 2004, pp. 33–40.

- [159] E. Gerecht, C. Musante, H. Jian, Y. Zhuang, K. Yngvesson, J. Dickinson, T. Goyette, J. Waldman, P. Yagoubov, G. Gol'tsman, B. Voronov, and E. Gershenzon, "Improved characteristics of NbN HEB mixers integrated with log-periodic antennas," in *10th International Symposium on Space Terahertz Technology (ISSTT 1999)*, March 1999, pp. 200–207.
- [160] E. Grossman, "Lithographic antennas for submillimeter and infrared frequencies," in *Proceedings of International Symposium on Electromagnetic Compatibility*, August 1995, pp. 102–107.
- [161] H.-W. Hübers, J. Schubert, A. Krabbe, M. Birk, G. Wagner, A. Semenov, G. Gol'tsman, B. Voronov, and E. Gershenzon, "Parylene anti-reflection coating of a quasi-optical hot-electron-bolometric mixer at terahertz frequencies," *Infrared Physics & Technology*, vol. 42, no. 1, pp. 41–47, February 2001.
- [162] Y. Xu, M. Khafizov, L. Satrapinsky, P. Kus, A. Plecenik, and R. Sobolewski, "Time-resolved photoexcitation of the superconducting two-gap state in MgB₂ thin films," *Physical Review Letters*, vol. 91, no. 19, p. 197004, November 2003.
- [163] Y. Naidyuk, I. Yanson, L. Tyutrina, N. Bobrov, P. Chubov, W. Kang, H.-J. Kim, E.-M. Choi, and S.-I. Lee, "Superconducting energy gap distribution in c-axis oriented MgB₂ thin film from point contact study," *Journal of Experimental and Theoretical Physics Letters*, vol. 75, no. 5, pp. 238–241, March 2002.
- [164] B. Jin, T. Dahm, C. Iniotakis, A. Gubin, E.-M. Choi, H. Kim, L. S.-I., W. Kang, S. Wang, Y. Zhou, A. Pogrebnyakov, J. Redwing, X. Xi, and N. Klein, "Dependence of penetration depth, microwave surface resistance and energy gap of MgB₂ thin films on their normal-state resistivity," *Superconductor Science and Technology*, vol. 18, no. 1, p. L1, November 2005.
- [165] R. Cubitt, M. R. Eskildsen, C. D. Dewhurst, J. Jun, S. M. Kazakov, and J. Karpinski, "Effects of two-band superconductivity on the flux-line lattice in magnesium diboride," *Physical Review Letters*, vol. 91, p. 047002, July 2003.
- [166] C. Eom, M. Lee, J. Choi, L. Belenky, X. Song, L. Cooley, M. Naus, S. Patnaik, J. Jiang, M. Rikel, A. Polyanskii, A. Gurevich, X. Cai, S. Bu, S. Babcock, E. Hellstrom, D. Larbalestier, N. Rogado, K. Regan, M. Hayward, T. He, J. Slusky, K. Inumaru, M. Haas, and R. Cava, "High critical current density and enhanced irreversibility field in superconducting mgb₂ thin films," *Nature*, vol. 411, no. 6837, pp. 558–560, May 2001.
- [167] Z.-K. Liu, D. Schlom, Q. Li, and X. Xi, "Thermodynamics of the Mg-B system: Implications for the deposition of MgB₂ thin films," *Applied Physics Letters*, vol. 78, no. 23, pp. 3678–3680, June 2001.

- [168] K. Ueda and M. Naito, "As-grown superconducting MgB₂ thin films prepared by molecular beam epitaxy," *Applied Physics Letters*, vol. 79, no. 13, pp. 2046–2048, September 2001.
- [169] A. Saito, A. Kawakami, H. Shimakage, and Z. Wang, "As-grown MgB₂ thin films deposited on Al₂O₃ substrates with different crystal planes," *Superconductor Science and Technology*, vol. 15, no. 9, pp. 1325–1329, 2002.
- [170] H. Shimakage, A. Saito, K. A., and Z. Wang, "Optimizing preparation of as-grown MgB₂ thin films made using the co-evaporation method," *Physica C: Superconductivity*, vol. 392-396, Part 2, pp. 1291–1295, 2003.
- [171] S. D. Bu, D. M. Kim, J. H. Choi, J. Giencke, E. E. Hellstrom, D. C. Larbalestier, S. Patnaik, L. Cooley, C. B. Eom, J. Lettieri, D. G. Schlom, W. Tian, and X. Q. Pan, "Synthesis and properties of c-axis oriented epitaxial MgB₂ thin films," *Applied Physics Letters*, vol. 81, no. 10, pp. 1851–1853, November 2002.
- [172] Y. Zhang, Z. Lin, Q. Dai, D. Li, Y. Wang, Y. Zhang, Y. Wang, and Q. Feng, "Ultrathin MgB₂ films fabricated on Al₂O₃ substrate by hybrid physical-chemical vapor deposition with high T_c and J_c," *Superconductor Science and Technology*, vol. 24, no. 1, p. 015013, January 2011.
- [173] Z.-J. Liu, S. Zhou, X. Xi, and Z.-K. Liu, "Thermodynamic reactivity of the magnesium vapor with substrate materials during MgB₂ deposition," *Physica C: Superconductivity*, vol. 397, no. 3-4, pp. 87–94, October 2003.
- [174] H. Shibata, T. Maruyama, T. Akazaki, H. Takesue, T. Honjo, and Y. Tokura, "Photon detection and fabrication of MgB₂ nanowire," *Physica C: Superconductivity*, vol. 468, no. 15-20, pp. 1992–1994, September 2008.
- [175] H. Shimakage, M. Tatsumi, and Z. Wang, "Ultrathin MgB₂ films fabricated by the co-evaporation method at high Mg evaporation rates," *Superconductor Science and Technology*, vol. 21, no. 9, p. 095009, July 2008.
- [176] Y. Wang, C. Zhuang, X. Sun, X. Huang, Q. Fu, Z. Liao, D. Yu, and Q. Feng, "Ultrathin epitaxial MgB₂ superconducting films with high critical current density and T_c above 33 K," *Superconductor Science and Technology*, vol. 22, no. 12, p. 125015, October 2009.
- [177] C. Zhang, Y. Wang, D. Wang, Y. Zhang, Z.-H. Liu, Q.-R. Feng, and G. Z.-Z., "Suppression of superconductivity in epitaxial MgB₂ ultrathin films," *Journal of Applied Physics*, vol. 114, no. 2, p. 023903, July 2013.
- [178] H. Shibata, T. Akazaki, and Y. Tokura, "Fabrication of MgB₂ Nanowire Single-Photon Detector with Meander Structure," *Applied Physics Express*, vol. 6, no. 2, p. 023101, February 2013.
- [179] D. Cunnane, E. Galan, K. Chen, and X. X. Xi, "Planar-type MgB₂ SQUIDS utilizing a multilayer process," *Applied Physics Letters*, vol. 103, no. 21, p. 212603, November 2013.

- [180] M. A. Wolak, N. Acharya, D. P. Cunnane, B. S. Karasik, and X. X. Xi, "Ultrathin MgB₂ films for hot electron bolometer mixers fabricated by HPCVD and ion milling," in *26th International Symposium on Space Terahertz Technology*, March 2015, pp. P-43.
- [181] H. Shibata, T. Akazaki, and Y. Tokura, "Ultrathin MgB₂ films fabricated by molecular beam epitaxy and rapid annealing," *Superconductor Science and Technology*, vol. 26, no. 3, p. 035005, March 2013.
- [182] C. G. Zhuang, S. Meng, C. Y. Zhang, Q. R. Feng, Z. Z. Gan, H. Yang, Y. Jia, H. H. Wen, and X. X. Xi, "Ultrahigh current-carrying capability in clean MgB₂ films," *Journal of Applied Physics*, vol. 104, no. 1, p. 013924, May 2008.
- [183] M. Wolak, N. Acharya, T. Tan, D. Cunnane, B. Karasik, and X. Xi, "Fabrication and characterization of ultrathin MgB₂ films for hot-electron bolometer applications," *Applied Superconductivity, IEEE Transactions on*, vol. 25, no. 3, pp. 1-5, June 2015.
- [184] N. Acharya, M. Wolak, T. Tan, N. Lee, A. Lang, M. Taheri, D. Cunnane, B. Karasik, and X. Xi, "MgB₂ ultrathin films fabricated by hybrid physical chemical vapor deposition and ion milling," *APL Materials*, vol. 4, no. 8, p. 086114, August 2016.
- [185] N. Acharya, M. Wolak, T. Melbourne, D. Cunnane, B. Karasik, and X. Xi, "As-grown versus ion-milled MgB₂ ultrathin films for THz sensor applications," *IEEE Transactions on Applied Superconductivity*, vol. 27, no. 4, p. 2300304, June 2017.
- [186] C. Zhuang, K. Chen, J. Redwing, Q. Li, and X. Xi, "Surface morphology and thickness dependence of the properties of MgB₂ thin films by hybrid physical-chemical vapor deposition," *Superconductor Science and Technology*, vol. 23, no. 5, p. 055004, April 2010.
- [187] Y. Cui, J. Jones, A. Beckley, R. Donovan, D. Lishego, E. Maertz, A. Pogrebnyakov, P. Orgiani, J. Redwing, and X. Xi, "Degradation of MgB₂ thin films in water," *IEEE Transactions on Applied Superconductivity*, vol. 15, no. 2, pp. 224-227, June 2005.
- [188] R. K. Singh, Y. Shen, R. Gandikota, J. M. Rowell, and N. Newman, "Effect of stoichiometry on oxygen incorporation in MgB₂ thin films," *Superconductor Science and Technology*, vol. 21, no. 1, p. 015018, January 2008.
- [189] W. Mumford and E. Scheibe, *Noise performance factors in communication systems*. Dedham, MA: Horizon House-Microwave, 1968.
- [190] H. Callen and T. Welton, "Irreversibility and generalized noise," *Physical Review*, vol. 83, pp. 34-40, July 1951.
- [191] G. Reppel and E. Saur, "Superconducting proximity effect of NbN," *Journal of Low Temperature Physics*, vol. 17, no. 3-4, pp. 287-293, November 1974.

- [192] I. Mazin, O. Andersen, O. Jepsen, O. Dolgov, J. Kortus, A. Golubov, A. Kuz'menko, and D. M. van der, "Superconductivity in MgB_2 : Clean or dirty?" *Physical Review Letters*, vol. 89, no. 10, p. 107002, September 2002.
- [193] M. Putti, V. Braccini, E. Galleani, F. Napoli, I. Pallecchi, A. S. Siri, P. Manfrinetti, and A. Palenzona, "Two-band effects in the transport properties of MgB_2 ," *Superconductor Science and Technology*, vol. 16, no. 2, pp. 188–192, February 2003.
- [194] J. H. Jung, K. W. Kim, H. J. Lee, M. W. Kim, T. W. Noh, W. N. Kang, H.-J. Kim, E.-M. Choi, C. U. Jung, and S.-I. Lee, "Far-infrared transmission studies of a c-axis-oriented superconducting MgB_2 thin film," *Phys. Rev. B*, vol. 65, p. 052413, January 2002.

Paper A

MgB₂ hot-electron bolometer mixers at terahertz frequencies

S. Bevilacqua, E. Novoselov, S. Cherednichenko, H. Shibata, and Y. Tokura

IEEE Transactions on Applied Superconductivity, vol. 25, no. 3, June 2015, Art. no. 2301104.

MgB₂ Hot-Electron Bolometer Mixers at Terahertz Frequencies

Stella Bevilacqua, *Student Member, IEEE*, Evgenii Novoselov, Sergey Cherednichenko, Hiroyuki Shibata, and Yasuhiro Tokura

Abstract—In this paper, we compare the performance of MgB₂ Hot-Electron Bolometer Mixers operating at Local Oscillator frequencies of 0.6 and 1.63 THz. The minimum noise temperatures that were obtained are 700 and 1150 K for 0.6 and 1.63 THz, respectively. The receiver noise bandwidth is of the order of 2.2–3 GHz for 10-nm-thick HEB devices with a T_c of 8.5 K. Sub-micrometer size HEBs were also fabricated with no degradation of the initial film quality when a 20-nm MgB₂ film with a T_c of 22 K was used. In the direct detection mode, the maximum voltage responsivity is in the range of 1–2 kV/W at 1.63 THz and the optimal bias current is around 1/4–1/3 of the I_c at 4.2 K.

Index Terms—HEB mixer, hot-electron bolometer, MgB₂, terahertz detector, thin film.

I. INTRODUCTION

THE PART of the electromagnetic wave spectrum of 0.1–10 THz (3 mm–30 μm) is frequently addressed as the terahertz (THz) range [1]. Despite difficulties to build components and systems for these frequencies, THz heterodyne receivers play important roles in astronomical and atmospheric science applications. [2]. As an example, the Herschel Space Observatory [3] with an overall frequency coverage of 60–670 μm allowed observation of star-formation activities, physics and chemistry of the interstellar medium, spectroscopic and photometric study of comets, asteroids and outer planet atmospheres and their satellites [4].

Several types of devices are used as mixer elements for heterodyne detection: Schottky diodes, SIS junctions, hot-electron bolometers (HEBs). In contrast to Schottky diode mixers, HEBs have much lower noise temperature and three orders of magnitude lower LO power requirements [5], [6]. HEBs could be used at higher frequencies than SIS mixers (1.3 THz upper limit). Typically, phonon-cooled HEBs are made from ultrathin films of NbN [7], but novel materials could be implemented for HEB fabrication to improve their parameters. Magnesium diboride (MgB₂) discovered in 2001 [8] has the highest critical temperature (T_c = 39 K) among intermetallic compounds.

Manuscript received August 12, 2014; accepted October 22, 2014. Date of publication October 27, 2014; date of current version March 13, 2015. The work at Chalmers University of Technology was supported by the European Research Council (ERC) under a Consolidator type Grant TERAMIX.

S. Bevilacqua, E. Novoselov, and S. Cherednichenko are with the Department of Microtechnology and Nanoscience (MC2), Chalmers University of Technology, 41296 Göteborg, Sweden (e-mail: serguei@chalmers.se).

H. Shibata and Y. Tokura are with NTT Basic Research Laboratories, Kanagawa 243-0198, Japan.

Color versions of one or more of the figures in this paper are available online at <http://ieeexplore.ieee.org>.

Digital Object Identifier 10.1109/TASC.2014.2365134

Recent progress in MgB₂ thin film deposition [9], [10] opens new prospects in fabrication of superconducting electronic devices: hot-electron bolometers (HEB) [11], superconducting single-photon detectors (SSPD) [12], superconducting quantum interference devices (SQUID) [13], etc., because of its high T_c and short electron-phonon relaxation time.

Recently, low noise THz HEB mixers were demonstrated based on thin MgB₂ superconducting films deposited on c – Al₂O₃ substrates using molecular-beam epitaxy [14], [15]. A mixer noise temperature of 600 K with a 3.4 GHz gain bandwidth was measured at 2 K and an LO frequency of 600 GHz. Apart from Al₂O₃, SiC substrates have been shown to result in very high quality MgB₂ superconducting films with a critical temperature in excess of 36 K for thicknesses down to 10 nm [16]. In this work, devices were made from films as thin as 15 nm, where GBW from 5 GHz to 7 GHz (depending on the bias point) have been achieved.

In our paper, we present experimental investigation of the noise and the conversion gain for MgB₂ HEB mixer on Al₂O₃ substrates at both 1.63 THz and 0.6 THz.

II. DEVICE FABRICATION AND EXPERIMENTAL SET-UP

HEB devices discussed in this paper were made of thin MgB₂ films on c-cut sapphire substrates. The lattice structure of this substrate matches very well with the lattice of MgB₂, hence providing high quality thin films. Recently, SiC has been shown to be a better option for this application [10], which we will address later in our research.

MgB₂ films were deposited with Molecular Beam Epitaxy (MBE) at a temperature of 300 °C. Details of the deposition process have been published in [9]. MgB₂ films were covered with 20 nm Au films in-situ. This method prevents MgB₂ films from degradation prior to and during the processing. Furthermore, it is expected to provide a lower contact resistance between the MgB₂ and the Au films. A low contact resistance is especially important considering the extremely high frequencies the devices are made for (> 1 THz).

Devices we discuss here were made from MgB₂ films deposited over a period of two years. Gradually, during process optimization, the critical temperature T_c of our ultra-thin films improved. Film smoothness, stresses, and other parameters have not been investigated and will not be discussed here.

HEBs were integrated with planar spiral antennas made of 300 nm thick gold film deposited on top of the in-situ Au (Fig. 1). The *in-situ* Au layer above the bolometer itself was etched by means of Ar Ion-Beam milling. After fabrication,

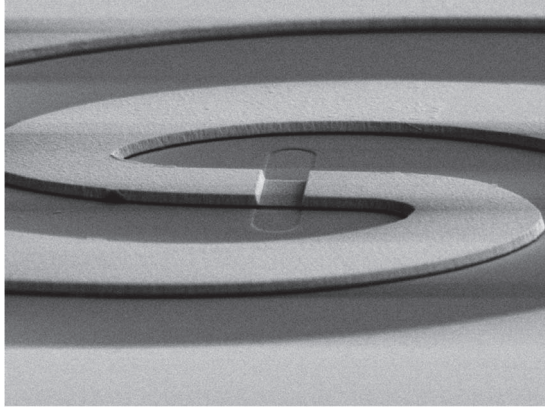


Fig. 1. Scanning Electron Microscope (SEM) image of a spiral antenna integrated HEB (light grey) and the two-point terminals, used to bond the chip to the external [dc and IF (Intermediate Frequency)] circuits. The substrate is dark grey.

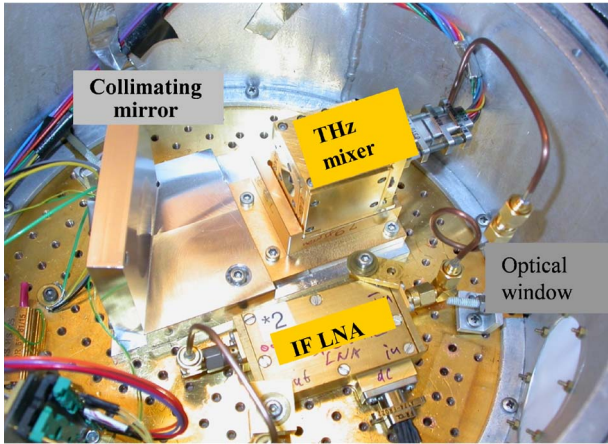


Fig. 2. Photograph of the interior of the test cryostat.

the substrate was diced on individual chips, each including a spiral antenna integrated HEB and the two-point terminals, used to bond the chip to the external [dc and IF (Intermediate Frequency)] circuits.

The HEB chip was clamped on the back side of a Si lens, and packaged in a mixer block with an SMA terminal. In the LHe cooled cryostat, a broadband bias-T and a broadband Low Noise Amplifier (LNA) followed the mixer block (Fig. 2). Outside the cryostat, a pair of extra LNAs, a tunable IF filter (50 MHz instantaneous bandwidth) and a microwave power meter formed the rest of the IF chain.

For the HEB mixer noise temperature measurements, a standard Y-factor technique was applied with two black body loads, at liquid nitrogen and room temperatures. Either a 12 μm or a 50 μm Mylar beam splitter was used to combine the Local Oscillator (LO) and the black body radiation, depending on the HEB size and the power of the LO. As LO sources, both a 0.6 THz Backward Wave Oscillator (BWO) and a 1.63 THz Far Infrared (FIR) gas laser were used. The losses in the beam splitter (0.1 dB), the cryostat window (0.8 dB), and the IR filter (0.6 dB) were measured separately and used for the receiver noise temperature deduction. The Si lens reflection loss was accounted as 1 dB [17], [18]. The LNA noise was not deducted from the noise temperature.

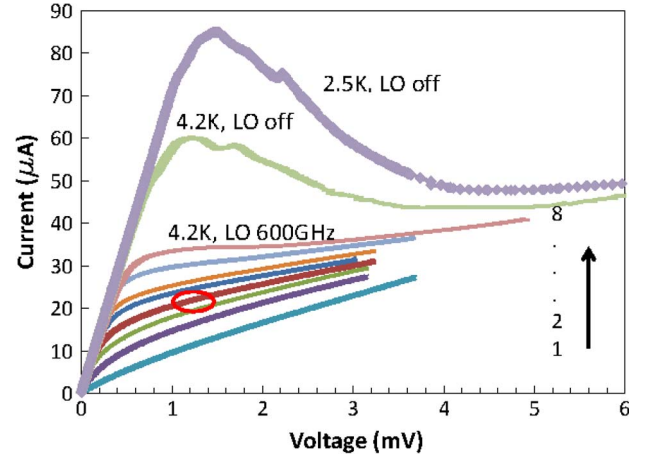


Fig. 3. I - V -curves of HEB mixer (10 nm thick, $T_C = 8.5$ K) at 4.2 K (with and without LO pumping at 600 GHz) and at 2.5 K (without LO). Eight pumped I - V curves are shown and they are labeled 1 through 8 in decreasing LO power.

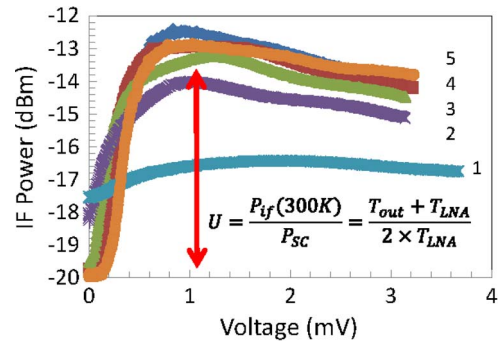


Fig. 4. P - V curves (1.6 GHz) measured at different LO power at 600 GHz. The curves are labeled 1 through 5, corresponding to the numbered I - V curves shown in Fig. 3. The equation explains the definition of the U -factor. Bath temperature is 4.2 K.

III. RESULTS AND DISCUSSION

HEB mixers were tested at LO frequencies of 600 GHz and 1.63 THz. Considering previous publications [14], [15], the goal of the new experiments at 0.6 THz was to confirm the reproducibility of the earlier results. The new devices were also smaller in size (1 $\mu\text{m} \times 1 \mu\text{m}$ vs 3 $\mu\text{m} \times 1.5 \mu\text{m}$ reported earlier). However, we used MgB_2 films from the same film batch as before (10 nm thick, $T_c = 8.8$ K). Current-Voltage (I - V) characteristics of the HEB mixer used for the noise temperature measurements are given in Fig. 3. Despite an increase of the critical current upon cooling from 4.2 K to 2.5 K (achieved by reducing the LHe vapor pressure), the noise temperature improvement was quite small (about 10%). Therefore, all other tests were made at 4.2 K. The lowest noise temperature was obtained at LO power and bias voltage corresponding to the red circle in Fig. 3 (1 mV, 20 μA).

Fig. 4 shows IF power P_{IF} vs bias voltage (P - V curves) for the corresponding I - V curves from Fig. 3. A maximum of the P - V occurs at a bias voltage just below the voltage of the minimum noise temperature. The U -factor [19], [20], defined as a ratio of the P_{IF} with the mixer at the optimal point to the P_{IF} with the mixer in the superconducting state, has been shown to be a useful parameter with which to test the receiver. In the first

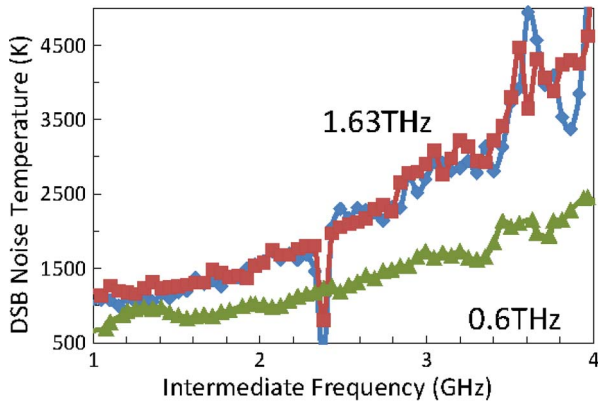


Fig. 5. DSB noise temperature (corrected for the optical loss) at 0.6 THz and 1.63 THz LO frequencies for the device discussed in Figs. 3 and 4.

state, P_{IF} is a sum of the mixer output noise ($k \times B \times T_{out}$), the IF amplifier noise ($k \times B \times T_{LNA}$), and the mixer response to the input load (294 K in this case, $2 \times k \times B \times 294$ K, the factor of 2 here occurs due to the Double Side Band nature of the receiver), k is the Boltzmann constant, and B is the bandwidth of the band pass filter at the output of the IF chain. In the second state, the HEB is in the superconducting state and does not produce any electrical noise. On the other hand, the HEB becomes a perfect short at microwave frequencies, which reflects the amplifier noise (hence, the factor of 2 in the formula for the U-factor, Fig. 3). Therefore, a low U-factor means either a high IF amplifier noise or a low mixer output noise temperature. For a high sensitivity HEB mixer the dominant noise contribution is made by the electron temperature fluctuations, and which is much larger compared to the thermal noise (equal to the electron temperature in the HEB). More detailed discussion can be found in [21].

The measured DSB noise temperature spectrum across the 1–4 GHz IF band is shown in Fig. 5. Similar to as reported earlier [14] the noise bandwidth is approximately 3 GHz. The minimum noise temperature is 700 K (1.1 GHz).

The LNA noise temperature was measured separately and is in the range of 2–3 K. Therefore, from the 7 dB U-factor (see Fig. 4) we can obtain the mixer output noise temperature, which is approximately 25 K. Given the (corrected for the optical loss) DSB noise temperature of 750 K (at 1.6 GHz, see Fig. 5, 650 K without the LNA noise contribution), the mixer gain can be calculated as -19 dB, of which 1.5 dB is the IF impedance mismatch loss ($Z = dV/dI = 170$ Ohm is the IF impedance of the HEB mixer).

The accuracy of the mixer gain and the output noise calculations depends on the IF amplifier gain and noise stability versus the input impedance, which changes when the HEB mixer is switched from the operation point ($Z = 170$ Ohm) to the superconducting state ($Z = 0$). An isolator between the mixer and the amplifier would resolve this issue. However, a cryogenic broadband isolator was not available during the experiments. Our preliminary investigation shows that an error of up to 2 dB can occur for T_{out} and G obtained from the U-factor if we disregard the LNA performance variation.

However, the superconducting state can be replaced by the normal state of the mixer. This state can be achieved when

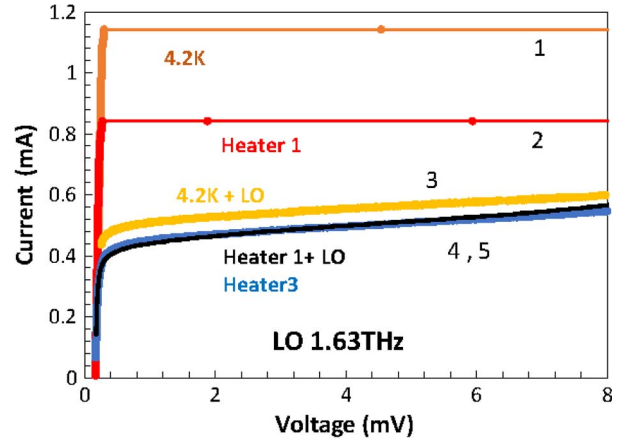


Fig. 6. I - V -curves of a HEB mixer made of 20 nm film with a T_c of 22 K. Curve 1: 4.2 K no LO; Curve 2: Heating-1 no LO; Curve 3: 4.2 K full LO power; Curve 4: Heating-1 with full LO power; Curve 5: No LO, the heating was increased until curve 5 coincided with curve 4.

the mixer is heavily pumped with LO (curves 1 in Figs. 3 and 4). In this case the denominator in the U-factor becomes ($T_{LNA} + T_c$), since in the normal state the temperature fluctuation noise becomes much smaller than the thermal noise, where the effective temperature equals the electron temperature of the HEB. In this case, a mixer gain of -18.5 dB and an output noise of 26 K was obtained. This result is very close to that obtained from the U-factor.

We do not provide I - V characteristics of the mixer pumped with the 1.63 THz LO here, because those were the same as with the 600 GHz LO. This fact can be explained by a relatively low T_c of the devices, which results in a low energy gap, evidently with a characteristic frequency below 600 GHz.

The minimum DSB noise temperature at 1.63 THz LO was 1150 K. The reason for a 50% increase in noise temperature compared to that measured at 600 GHz is not clear at the moment. A contact resistance between the Au antenna and the MgB₂ bolometer might still exist despite the in-situ deposition of the Au layer. This could be the reason for an increase of optical loss at higher LO frequencies.

The same exercise with the U-factor, considering the noise temperature at 1.63 THz, gives a mixer gain of -21 dB. The fact that the U-factor is the same as for the 600 GHz LO agrees with fact that the shape of the I - V curves during pumping with both LOs are the same.

We can note that for NbN HEB mixers (at 0.6 THz and 1.63 THz) the mixer conversion gain from -13 dB to -14 dB, and the mixer output noise from 40 K to 60 K was reported [20].

At 1.63 THz the noise bandwidth is about 2.2–2.5 GHz. Since the given noise temperature includes the contribution of the LNA, the LNA fraction increases by an increase of the optical or the mixer loss. Thereby, the receiver (the mixer + the LNA) noise bandwidth is reduced. A similar effect has also been observed for NbN HEB mixer [20].

Earlier we have shown that the noise bandwidth for MgB₂ HEB mixers increases when higher T_c MgB₂ films are used [15]. After optimization of the MgB₂ film deposition, the critical temperature increased to 20–25 K. Using a 20 nm MgB₂ film a set of devices was fabricated with a T_c of 22 K. The I - V

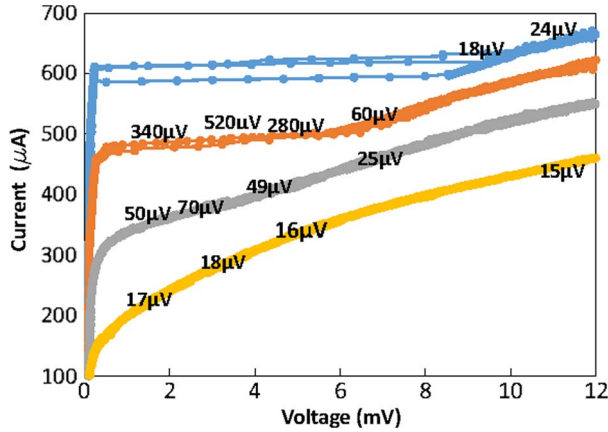


Fig. 7. I - V -curves of the heated HEB Mixer (see Fig. 6). The numbers in the field represent the voltage response at 1.63 THz as measured with the lock-in amplifier.

curves for one such device are given in Fig. 6. The bolometer dimensions are $1 \mu\text{m} \times 0.4 \mu\text{m}$. With the total available power of the FIR laser (estimated as $100 \mu\text{W}$ in front of the cryostat), the mixer was pumped to an I - V -curve which should be close to the optimum (curve 3 in Fig. 6). However, for the noise temperature measurements with a thin beam splitter, the LO power at the cryostat will be greatly reduced. Therefore, the mixer has to be operated at a higher temperature. In Fig. 6, curves 4 and 2 correspond to an increased temperature with and without LO pumping. For curve 5, LO was switched off and the mixer temperature was further increased until it overlapped with curve 4. As can be seen, curves 4 and 5 are identical. Therefore, at “Heater-1” the 1.63 THz radiation has the same effect on the HEB as a rise in temperature.

To estimate which I - V curve corresponds to the HEB maximum sensitivity to the THz radiation, a direct detection experiment was conducted. For a set of temperatures, the voltage response of the HEB on the amplitude modulated THz radiation was recorded (Fig. 7). The FIR laser power was attenuated by 20 dB, to reach the small signal limit (there was no visible effect of the laser on the I - V -curve). The laser radiation modulation was accomplished with a chopper (set on 20 Hz). The voltage response of the HEB was measured with a lock-in amplifier. As can be seen in Fig. 7, the maximum responsivity is achieved at a bias range of 2–4 mV and 0.3–0.5 mA, i.e. at a current which is about 1/4–1/3 of the critical current at 4.2 K. Considering the known optical losses, the maximum responsivity can now be calculated to be in a range of 1–2 kV/W at 1.63 THz. With this information, noise temperature measurements will have to be conducted in the near future.

IV. CONCLUSION

With this work we demonstrate that low noise performance can be repeatedly achieved for MgB_2 HEB mixers, both for

1 THz and for the above. The minimum noise temperatures obtained are 700 K at 0.6 THz and 1150 K at 1.63 THz LO frequencies. The noise bandwidth is of the order of 2.2–3 GHz for devices 10 nm thick with a T_c of 8.5 K. For HEBs with a T_c of 22 K we observe that the effect of the THz LO on the I - V -curves is nearly the same as of HEB heating. The maximum direct detection responsivity is in the range of 1–2 kV/W at 1.63 THz and the optimal bias current is 1/4–1/3 of the I_c at 4.2 K.

REFERENCES

- [1] P. H. Siegel, “Terahertz technology,” *IEEE Trans. Microw. Theory Techn.*, vol. 50, no. 3, pp. 910–928, Mar. 2002.
- [2] G. W. Schwaab, “Heterodyne spectrometers,” *Infrared Phys. Tech.*, vol. 40, no. 3, pp. 207–218, Jun. 1999.
- [3] T. de Graauw *et al.*, “The Herschel-Heterodyne Instrument for the Far-Infrared (HIFI),” *Astron. Astrophys.*, vol. 518, pp. L6:1–L6:7, Jul. 2010.
- [4] P. Ubertini *et al.*, “Future of space astronomy: A global road map for the next decades,” *Adv. Space Res.*, vol. 50, no. 1, pp. 1–55, Jul. 2012.
- [5] B. S. Karasik, W. R. McGrath, and R. A. Wyss, “Optimal choice of material for HEB superconducting mixers,” *IEEE Trans. Appl. Supercond.*, vol. 9, no. 2, pp. 4213–4216, Jun. 1999.
- [6] J. Zmuidzinas and P. L. Richards, “Superconducting detectors and mixers for millimeter and submillimeter astrophysics,” *Proc. IEEE*, vol. 92, no. 10, pp. 1597–1616, Oct. 2004.
- [7] S. Cherednichenko, V. Drakinskiy, T. Berg, P. Khosropanah, and E. Kollberg, “Hot-electron bolometer terahertz mixers for the herchel space observatory,” *Rev. Sci. Instrum.*, vol. 79, no. 3, Mar. 2008, Art. ID. 034501.
- [8] J. Nagamatsu, N. Nakagawa, T. Muranaka, Y. Zenitani, and J. Akimitsu, “Superconductivity at 39 K in magnesium diboride,” *Nature*, vol. 410, no. 6824, pp. 63–64, Feb. 2001.
- [9] H. Shibata, T. Akazaki, and Y. Tokura, “Ultrathin MgB_2 films fabricated by molecular beam epitaxy and rapid annealing,” *Supercond. Sci. Technol.*, vol. 26, no. 3, Jan. 2013, Art. ID. 035005.
- [10] C. G. Zhuang, K. Chen, J. M. Redwing, Q. Li, and X. X. Xi, “Surface morphology and thickness dependence of the properties of MgB_2 thin films by hybrid physical-chemical vapor deposition,” *Supercond. Sci. Technol.*, vol. 23, no. 5, May 2010, Art. ID. 055004.
- [11] S. Cherednichenko, V. Drakinskiy, K. Ueda, and M. Naito, “Terahertz mixing in MgB_2 microbolometers,” *Appl. Phys. Lett.*, vol. 90, no. 2, Jan. 2007, Art. ID. 023507.
- [12] H. Shibata, T. Akazaki, and Y. Tokura, “Fabrication of MgB_2 nanowire single-photon detector with meander structure,” *Appl. Phys. Exp.*, vol. 6, no. 2, Feb. 2013, Art. ID. 023101.
- [13] D. Cunnane, E. Galan, K. Chen, and X. X. Xi, “Planar-type MgB_2 SQUIDS utilizing a multilayer process,” *Appl. Phys. Lett.*, vol. 103, no. 23, Nov. 2013, Art. ID. 212 603.
- [14] S. Bevilacqua *et al.*, “Low noise MgB_2 terahertz hot-electron bolometer mixers,” *Appl. Phys. Lett.*, vol. 100, no. 3, Jan. 2012, Art. ID. 033504.
- [15] S. Bevilacqua *et al.*, “Study of IF bandwidth of MgB phonon-cooled hot-electron bolometer mixers,” *IEEE Trans. Terahertz Sci. Technol.*, vol. 3, no. 4, pp. 409–415, Jul. 2013.
- [16] D. Cunnane, J. Kawamura, B. S. Karasik, M. A. Wolak, and X. X. Xi, “Development of hot-electron THz bolometric mixers using MgB_2 thin films,” in *Proc. SPIE*, Jul. 23, 2014, vol. 9153, p. 91531Q.
- [17] A. J. Gatesman, J. Waldman, M. Ji, C. Musante, and S. Yngvesson, “An anti-reflection coating for silicon optics at terahertz frequencies,” *IEEE Microw. Guided Wave Lett.*, vol. 10, no. 7, pp. 264–266, Jul. 2000.
- [18] M. Kroug, S. Cherednichenko *et al.*, “NbN HEB mixer for terahertz heterodyne receivers,” *IEEE Trans. Appl. Supercond.*, vol. 11, no. 1, pp. 962–965, Mar. 2001.
- [19] H. Ekström *et al.*, “Gain and noise bandwidth of NbN hot-electron bolometric mixers,” *Appl. Phys. Lett.*, vol. 70, no. 24, pp. 3296–3298, Jun. 1997.
- [20] S. Cherednichenko *et al.*, “1.6 THz heterodyne receiver for the far infrared space telescope,” *Phys. C, Supercond.*, vol. 372–376, pt. 1, pp. 427–431, Aug. 2002.
- [21] H. Ekström and B. Karasik, “Electron temperature fluctuation noise in hot-electron superconducting mixers,” *Appl. Phys. Lett.*, vol. 66, no. 23, pp. 3212–3214, Jun. 1995.

Paper B

Effect of the critical and operational temperatures on the sensitivity of MgB₂ HEB mixers

E. Novoselov, S. Bevilacqua, S. Cherednichenko, H. Shibata, and Y. Tokura

IEEE Transactions on Terahertz Science and Technology, vol. 6, no. 2, pp. 238-244, March 2016.

Effect of the Critical and Operational Temperatures on the Sensitivity of MgB₂ HEB Mixers

Evgenii Novoselov, Stella Bevilacqua, Sergey Cherednichenko, Hiroyuki Shibata, and Yasuhiro Tokura

Abstract—In this paper, we present a study of the noise and the gain of MgB₂ hot-electron bolometer mixers with different critical temperatures (T_c) and at various operation temperatures. At a local oscillator (LO) frequency of 1.63 THz the minimum input receiver noise temperature (T_r) was 700 K with a gain of -18 dB for a device with a T_c of 8.5 K. For a device with a T_c of 22.5 K the corresponding values were 1700 K and -19 dB. For the latter device the T_r was 2150 K at a bath temperature of 12 K, which is not achievable with Nb-compound based HEB mixers. We present and compare different methods for measurements of the HEB mixer gain and the output noise.

Index Terms—Bolometer, conversion gain, hot-electron bolometer (HEB), MgB₂, noise temperature, sub-mm astronomy, THz mixer.

I. INTRODUCTION AND BACKGROUND

HOT-ELECTRON bolometer (HEB) mixers have been proven to be a class of highly sensitive terahertz (THz) detection elements (from 1.3 THz to 5.3 THz) employed in many receivers for astronomical and atmospheric science observation programs launched in recent years, including RLT [1], APEX [2], [3], Herschel [4], [5], TELIS [6], [7], SOFIA [8], [9]. They are also chosen for different programs under development, such as ASTE [10], DATE5 [11].

Until recently, the state-of-the-art phonon-cooled HEBs were fabricated using either NbN or NbTiN superconducting ultrathin films providing a low double sideband (DSB) receiver noise temperature (T_r) at Intermediate Frequencies (IF) less than 2 GHz: from 300 K (corrected for optical losses) at 1.3 THz local oscillator (LO) [11] to 1150 K (in a vacuum setup) at 5.3 THz LO [12]. It has been shown that at frequencies over 3 THz the quantum noise term starts “to take over” other terms and becomes dominant at higher frequencies [13], [14].

Due to a limited electron temperature relaxation rate in thin NbN and NbTiN films, HEB mixers have a gain bandwidth (GBW) < 4 GHz. As a result, a T_r increases towards higher IFs and doubles already at IF of 4–5 GHz. Therefore, the number

of scientific tasks in radio astronomy that can be performed with HEB mixers becomes limited. Furthermore, a superconducting critical temperature (T_c) of 8–11 K limits the NbN and NbTiN HEB mixer operation to liquid helium (LHe) temperatures (≤ 4.2 K). 4 K cryocoolers qualified for space application are *rarae aves*, which necessitates utilization of LHe and leads to the reduction of the spaceborn mission lifetime. The discovery of superconductivity in MgB₂ [15] with the highest T_c among intermetallic compounds (bulk $T_c = 39$ K) and recent progress in ultrathin film deposition [16], [17] opened new opportunities in HEB development [18]–[23].

In previously published work there have been two main goals in MgB₂ HEB mixer development: a large GBW and a low T_r . A GBW of 2–3 GHz was reported both for thicker films with a higher T_c (20 nm, 20 K) and for thin films with a much lower T_c (10 nm, 9 K) [18], [19]. A possibility of achieving a GBW of 8–10 GHz with HEB mixers made from thin films with a high T_c was also suggested in [20], which was recently confirmed in experimental work by Cunnane *et al.* [22]. In that paper a GBW of 7 GHz (at 9 K) and 8 GHz (at 25 K) was demonstrated for a device made from a 15 nm thick MgB₂ film with a T_c of 33 K. A feasibility of achievement of a low T_r was already demonstrated in the first publications on the MgB₂ HEB mixers, which allowed for measurements of the mixer noise bandwidth (NBW), as a more appropriate criterion for the HEB mixer performance assessment. At the moment the state-of-the-art T_r for MgB₂ devices is 600 K at a 600 GHz LO [19], and 1150 K at a 1.63 THz LO [21]. Both figures were reported for devices made from 10 nm films with a T_c of 9 K and a NBW of 3 GHz. For devices with a higher T_c , a higher T_r was observed (e.g., 1800 K in [20]), but a NBW was more superior (6–7 GHz). For the device with a T_c of 33 K a T_r of 3900 K was measured [22].

So far very few studies have been performed to understand how HEB mixers would operate at temperatures higher than LHe or how mixer performance depends on the bath temperature. A low T_c for NbN thin films (8–10 K for 3–10 nm films) does not facilitate studying HEB mixer operation at higher temperatures [24]. However, MgB₂ HEB mixers offer such a possibility. In [20], it was shown at a 600 GHz LO that for MgB₂ HEB mixers the T_r remained constant up to 11 K ($T_c = 15$ K). However, no further details were provided.

Currently, the highest T_c of our MgB₂ films is about 22–24 K for 20 nm. In this paper, we present an experimental investigation and analysis of the noise temperature, the NBW, and the conversion gain at a 1.63 THz LO with different bath temperatures for devices made from two films with either a 8.5 K or a 22.5 K T_c . We used three methods to obtain the mixer

Manuscript received July 02, 2015; revised October 19, 2015; accepted January 18, 2016. Date of publication March 15, 2016; date of current version March 21, 2016. This work was supported by the European Research Council (ERC). (Corresponding author: Evgenii Novoselov.)

E. Novoselov, S. Bevilacqua, S. Cherednichenko are with the Department of Microtechnology and Nanoscience (MC2), Chalmers University of Technology, SE-41296 Göteborg, Sweden (e-mail: evgenii@chalmers.se).

H. Shibata and Y. Tokura are with NTT Basic Research Laboratories, Morinosato, Atsugi, Kanagawa 243-0198, Japan.

Color versions of one or more of the figures in this paper are available online at <http://ieeexplore.ieee.org>.

Digital Object Identifier 10.1109/TTHZ.2016.2520659

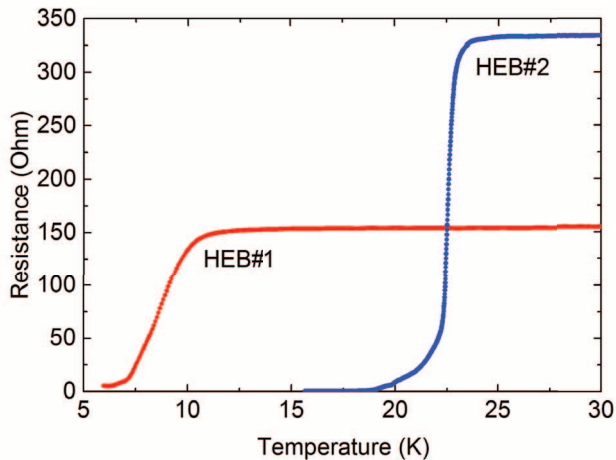


Fig. 1. Resistance versus temperature dependence for the tested devices.

gain, which gave very similar results. Moreover, we present a study of how the most important mixer characteristics, such as the noise temperature and the conversion gain, vary when both the T_c and the film thickness alter over a wide range.

II. DEVICE FABRICATION AND DC CHARACTERIZATION

Two batches of the HEBs were fabricated using MgB_2 films that are 10 and 20 nm thick. Films were deposited on a c-cut sapphire substrate by molecular-beam epitaxy (MBE) and covered *in-situ* with a 20 nm gold layer to prevent film degradation and to reduce contact resistance between the MgB_2 film and the metal layers deposited later. The HEBs were fabricated using e-beam lithography and argon ion beam milling in several steps. Each substrate held 8 HEBs of various dimensions. For the 20 nm film all devices survived during the processing and the dicing, but for the 10 nm film the yield was quite low and only several devices were usable. For radiation coupling into the bolometer, a broadband planar spiral antenna was made from 270 nm gold film in the same process. Devices were passivated with a 40 nm SiN_x for protection from degradation due to both oxidation and exposure to water [25]. One device from the each batch was chosen for tests. The criteria for device selection were: the small size and low critical current density (to fulfil LO power requirement with the available source), and a DC resistance close to 100 Ω (the designed impedance of spiral antenna). HEB#1 discussed below, was 10 nm thick and $1 \times 1 \mu\text{m}^2$ in size, with a T_c of 8.5 K, a transition width of 2.5 K, and a room temperature resistance of 160 Ω . HEB#2 was 20 nm thick and $1 \times 0.2 \mu\text{m}^2$ in size, with a T_c of 22.5 K, a transition width of 0.6 K, and a room temperature resistance of 330 Ω . R-T curves measured in a dip-stick for both HEBs are presented in Fig. 1. The presence of the double transition in the R-T curve for HEB#2 (Fig. 1) suggests that the electrical contact between MgB_2 and Au was quite good.

I - V curves of HEB#1 at 4.2 K (with and without LO pumping) and the corresponding IF response versus the bias voltage (at a 295 K load) are presented in Fig. 2. An LO power required to reach the minimum T_r (LO3 curve in Fig. 2(a) was 70 nW as was calculated using an isothermal method with an assumption that both the direct current (DC) and the LO power have the same effect on the bolometer resistance [26]. The

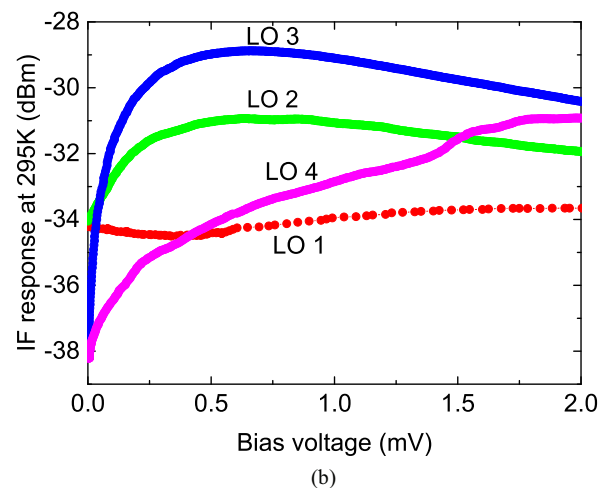
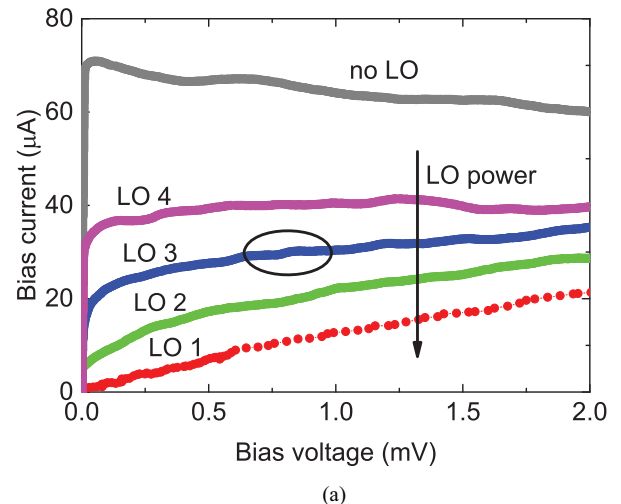


Fig. 2. (a) I - V curves for HEB#1 under different LO (1.63 THz) power at 4.2 K bath temperature, optimal operation points marked with a black ellipse and (b) the corresponding IF response at 295 K load at 1.8 GHz IF.

optimal LO power is in the same order of magnitude as that reported for NbN HEB mixers.

I - V curves of HEB#2 at 4.2 K and 12 K (with and without LO pumping) are presented in Fig. 3. At a bath temperature of about 12 K the HEB critical current (0.5 mA) was around half of its value at 4.2 K (1 mA). The LO power calculated using the isothermal method was either 2.6 μW for 4.2 K bath temperature or 1.7 μW for 12 K. DC parameters of HEB#1 and HEB#2 are summarized in Table I.

III. MEASUREMENT SETUP AND EXPERIMENTAL TECHNIQUE

The HEBs were mounted in mixer blocks with Si lenses and placed on the cold plate of a LHe cryostat sealed with a HDPE window. A ZitexTM IR filter was placed on the 4 K shield of the cryostat. Losses in the optical path from the hot/cold loads to the mixer and equivalent noise temperatures of the corresponding elements are presented in Table II. Reflection loss of the Si lens (1 dB) was not included in the list and it was not accounted for. Therefore, for a specific frequency, both the T_r and conversion gain can be further reduced/increased by application of a proper designed AR layer for the Si lens [27]. In our case, Si lens reflection loss was treated as a part of the mixer

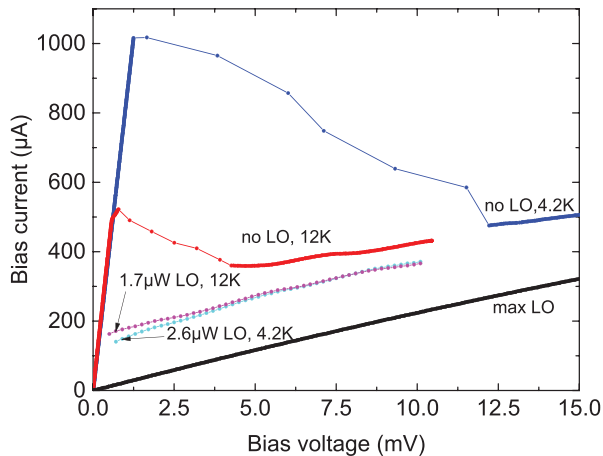


Fig. 3. I - V curves for HEB#2 with and without LO power (1.63 THz) at 12 K and 4.2 K bath temperatures.

TABLE I

MgB₂ HEB SIZE ($W \times L$), THICKNESS (D), CRITICAL TEMPERATURE (T_c), TRANSITION WIDTH (ΔT_c), RESISTANCE AT 300 K ($R_{300\text{K}}$), SHEET RESISTANCE (R_s), RESISTIVITY (ρ), CRITICAL CURRENT AT 4.2 K (I_c) AND CRITICAL CURRENT DENSITY (J_c)

#	$W \times L (\mu\text{m}^2)$	$D (\text{nm})$	$T_c (\text{K})$	$\Delta T_c (\text{K})$	$R_{300\text{K}} (\Omega)$
1	1x1	10	8.5	2.5	160
2	1x0.2	20	22.5	0.6	330
#	$R_s (\Omega/\square)$	$\rho (10^{-6} \Omega \text{ cm})$	$I_c (10^{-6} \text{ A}) @ 4.2\text{K}$	$J_c (10^6 \text{ A/cm}^2)$	
1	160	160	70	0.7	
2	1650	3300	1000	5	

conversion gain (G_m). A bias-T followed the mixer block to apply the voltage bias to the device and to separate the intermediate frequency (IF) response. Three cascaded amplifiers were used in the IF chain to measure the IF response: a 2-4 GHz InP low-noise amplifier mounted on the cryostats' cold plate, a 2-4 GHz GaAs low-noise amplifier at room temperature outside the cryostat, and a broadband (0.1-10 GHz) amplifier at the end. A 3 dB attenuator was placed between the cryostat and the first room temperature LNA to reduce standing waves in the long IF cable. The amplified signal was measured through a tunable (1-9 GHz) YIG-filter (50 MHz bandwidth) with a power meter. Mylar® beam splitters (BS) (of either 12 μm or 3 μm thick) were used to combine the LO and the signal (from the hot/cold loads) beams. Noise measurements were performed with a 1.6 THz LO (a far-infrared (FIR) gas laser) at bath temperatures of 4.2 K, 2.7 K (achieved by helium vapor pumping) and 12 K (achieved by use of a resistive heater mounted on the mixer block). A Golay cell connected to the oscilloscope was placed behind the beam splitter to monitor the FIR gas laser emission power during experiments.

For measurements of the T_r the standard Y-factor technique (295 K/77 K loads) was used. In order to obtain the mixer conversion gain and the mixer output noise temperature, a U-factor

TABLE II
LOSSES (L) AND EQUIVALENT NOISE TEMPERATURES (T_{BQ}) OF OPTICAL COMPONENTS ALONG THE BEAM PATH AT 1.63 THz REFERRED TO THE INPUT OF THE CORRESPONDING COMPONENT. T IS THE PHYSICAL TEMPERATURE OF THE COMPONENT

Component	$T (\text{K})$	$L (\text{dB})$	$T_{\text{eq}} (\text{K})$
Air path (40 cm)	295	1	76.4
Beam splitter (Mylar®)	295	0.1	7.0
Cryostat's window (1mm HDPE)	295	0.7	52.5
IR filter (2 Zitex™ sheets)	4.2	0.6	0.6
Total	-	2.4	137

technique was applied as described in [21] and [29]. In this case, the receiver conversion gain can be calculated as

$$G_{\text{tot}} \equiv \frac{G_m}{L_{\text{opt}}} \equiv \frac{U(T_{\text{LNA}} + T_{\text{REF}})}{2(T_{\text{rec}} + T(295))} \quad (1)$$

where L_{opt} is the optical loss (2.4 dB in our case), T_{LNA} is the IF chain noise temperature. T_{REF} is the reference temperature that depends on the state chosen as the reference to measure the U-factor. For the superconducting state T_{REF} is equal to T_{LNA} , because in this state the HEB acts as a microwave short and hence it reflects the power coming from the IF chain. For the normal state, achieved by pumping with all available LO power (e.g., using a mirror instead of a BS), the noise does not depend on the bias point (LO1 curve on Fig. 2) and it is defined by the Johnson noise of the HEB, so T_{REF} is equal to the HEB electron temperature determined from the R-T curve by DC resistance. The factor “2” in the equation comes from the DSB operation of the mixer with an assumption that the sideband ratio is 1. As follows from (1), the mixer output noise temperature T_{out} can be calculated as

$$T_{\text{out}} = U(T_{\text{LNA}} + T_{\text{REF}}) - T_{\text{LNA}} - 2G_{\text{tot}}T(295 \text{ K}) - 2G_{\text{tot}}T_{\text{REF}} \quad (2)$$

where T_{RF} is the noise contribution of optical components (137 K in our case, see Table II).

Another method to obtain the mixer conversion gain and the mixer output noise temperature is from the output noise of the HEB mixer (P_{IF}) at the operation point and an accurate measurements of the IF chain gain, G_{IF} :

$$G_{\text{tot}} = \frac{P_{\text{IF}}}{2G_{\text{IF}}k_B B(T_{\text{rec}} + T(295))} \quad (3)$$

$$T_{\text{out}} = \frac{P_{\text{IF}}}{2G_{\text{IF}}k_B B - T_{\text{LNA}} - 2G_{\text{tot}}T(295 \text{ K}) - 2G_{\text{tot}}T_{\text{RF}}} \quad (4)$$

where k_B is Boltzmann constant, and B is the bandwidth of the IF filter (see above in this section).

IV. EXPERIMENTAL RESULTS AND DISCUSSION

For HEB#1, the T_r (corrected for optical losses, as in Table II) versus the intermediate frequency at the 4.2 K bath temperature is presented in Fig. 4 (circles).

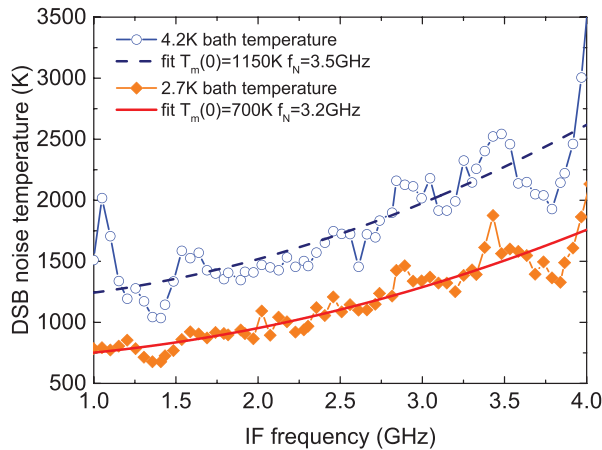


Fig. 4. The DSB receiver noise temperatures (corrected for optical losses) for the HEB#1. The bias points are $U_0 = 0.8$ mV $I_0 = 28$ μ A and $U_0 = 1.3$ mV $I_0 = 23$ μ A at 4.2 K and 2.7 K bath temperatures, respectively.

Equation (5) is usually used to define the receiver NBW [28]:

$$T_r = T_m(0) \left[1 + \left(\frac{f_{IF}}{f_N} \right)^2 \right] \quad (5)$$

where $T_m(0)$ is the noise temperature at zero IF, and f_N is the NBW. Fitting the measured T_r for HEB#1 to (5), both $T_m(0)$ of 1150 K and f_N of 3.5 GHz were obtained.

T_r was also measured at a bath temperature of 2.7 K. This resulted in a 30% increase in the HEB critical current (90 μ A) and a 40% reduction of the T_r (Fig. 4). The optimal operation region moved to slightly higher bias voltages. The required LO power calculated with the isothermal method was 80 nW. The T_r corrected for optical losses versus the IF for the optimal operation point at 2.7 K is presented in Fig. 4 (diamonds). Experimental points are fitted to (5) as was done for the data obtained at 4.2 K. It provides the zero IF noise temperature of 700 K and the NBW of 3.2 GHz.

The mixer conversion gain and the mixer output noise temperature were calculated as discussed in Section III using experimental data from Fig. 4 and Fig. 2(b). The noise temperature of the IF chain is determined mostly by the noise temperature of the first amplifier in the chain i.e., by the cold LNA, which is mounted on the cryostat's 4.2 K plate. It has a gain of 30 dB and a noise temperature of 2 K. Therefore, the noise temperature of the whole IF chain was estimated as not to exceed 3 K. The total gain of the entire IF chain, G_{IF} was measured to be 77 dB at 1.8 GHz. Using an IF response at the optimal operation point ($U_0 = 0.8$ mV and $I_0 = 28$ μ A) of -29.4 dBm, a U-factor of either 8.2 dB (reference state is the superconducting state) or 4.7 dB (reference state is the normal state), the $T_r = 2500$ K, and the HEB temperature of $T_{REF} = 9$ K in the normal state, both the mixer conversion gain and the mixer output noise temperature were calculated at 4.2 K with all three methods presented in Section III.

At 2.7 K, the input data for the calculation of the mixer conversion gain and the mixer output noise temperature (at an operation point of $U_0 = 1.3$ mV and $I_0 = 23$ μ A) for HEB#1 were: the IF response $P_{IF} = -30.4$ dBm, the U-factor was either 7.2 dB (reference state is the superconducting state) or 4.2

TABLE III
THE MIXER CONVERSION GAIN (G_m) AND THE OUTPUT NOISE TEMPERATURE (T_{out}) FOR HEB#1 CALCULATED: USING (1) AND (2) EITHER WITH THE SUPERCONDUCTING (i) OR THE NORMAL (ii) STATES AS THE REFERENCE STATE; USING (3) AND (4) (iii). MEASUREMENTS WERE PERFORMED BOTH AT 4.2 K AND 2.7 K BATH TEMPERATURES (T_{bath}). $f_{IF} = 1.8$ GHz

T_{bath} (K)	i		ii		iii	
	G_m (dB)	T_{out} (K)	G_m (dB)	T_{out} (K)	G_m (dB)	T_{out} (K)
4.2	-19.1	31	-19.6	27	-19.9	26
2.7	-18.2	21	-18.1	22	-18.9	18

dB (reference state is the normal state), the $T_r = 1500$ K, and the HEB temperature $T_{REF} = 9.3$ K.

As one can see from Table III the mixer conversion gain and the mixer output noise temperature obtained using three methods are quite close to each other, which we interpret as a confirmation that the methods are correct. As the mixer temperature is reduced from 4.2 to 2.7 K, the mixer conversion gain is increased by approximately 1 dB, whereas the output mixer noise temperature is decreased by 5–10 K. It is of interest to compare these experimental data with physical modelling of the devices, however this will be a subject for a further publication. It is also interesting to compare results of HEB#1 with published data for NbN HEB mixers, since a T_c of NbN thin films (8–10 K) is very close to the T_c of the MgB₂ film used for HEB#1. The reported conversion gain of NbN HEBs is approximately -12 dB [29] with the mixer output noise temperature of approximately 40 K at a 1.63 THz LO. A lower gain and a lower output noise for the MgB₂ HEB mixer (HEB #1) can be a result of a quite large superconducting transition width (see Fig. 1). The GBW of MgB₂ HEB [20] also shows to be a factor of 1.5 smaller, as compared to the NbN HEB mixer from [28]. Therefore, for comparison of the gain and the output noise at 1.8 GHz (approximately the 3 dB gain roll-off frequency for HEB#1) about a +2 dB correction has to be applied for the MgB₂ mixer. Despite this, the T_r for both NbN and MgB₂ HEB mixers falls within the same ballpark.

HEB#2 was tested using the same setup, except that it was mounted in a mixer block with a 5 mm Si lens. The measured T_r spectrum across the 1–4 GHz IF band for the bath temperature of 4.2 K and a fit with (5) are presented in Fig. 5. At certain IFs the mixer response to the hot/cold loads was unstable which resulted in errors in the noise temperature measurements (e.g., at 1.9 and 2.9 GHz). The fitted line corresponds to the zero IF noise temperature of 1700 K and the NBW of 5 GHz.

The mixer conversion gain and the mixer output noise temperature were calculated using the U-factor technique with the normal state as a reference state. Results are shown in Fig. 6. Higher ripples for IF < 1.8 GHz correspond to the IFs with a high LNA return loss. The mixer conversion gain was fitted with a single-pole Lorentzian $G_m(f_{IF}) = G_m(0)/[1 + (f_{IF}/f_g)^2]$, where $G_m(0)$ is the mixer conversion gain at zero IF and f_g is the mixer GBW (3 dB gain roll-off frequency). The fit in Fig. 6(a) corresponds to the zero IF mixer gain of -15.1 dB and

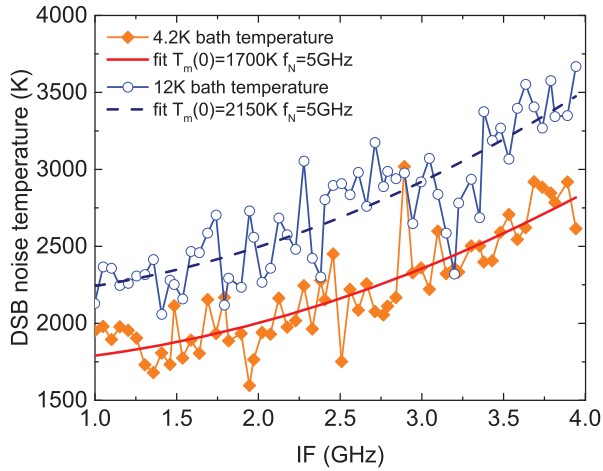
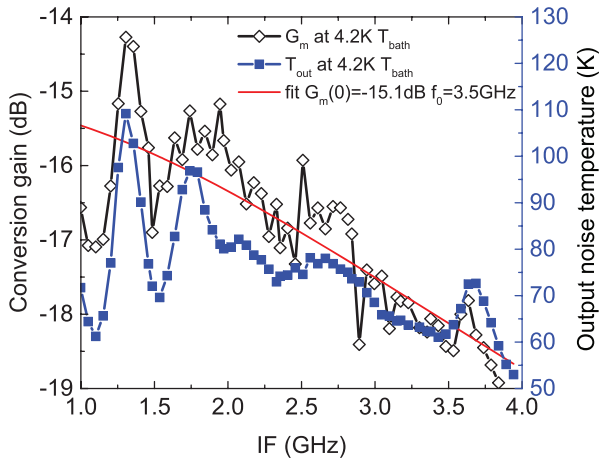
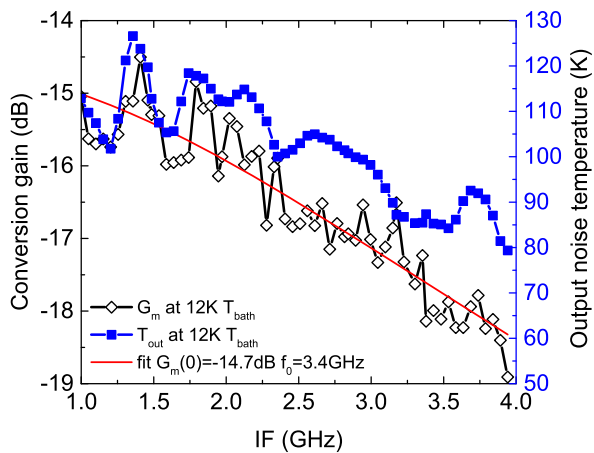


Fig. 5. DSB receiver noise temperatures (corrected for optical losses) at 4.2 K (diamonds) and 12 K (circles) bath temperatures at a 1.63 THz LO for HEB#2. The bias points are $U_0 = 1.8$ mV $I_0 = 200$ μ A and $U_0 = 1.6$ mV $I_0 = 180$ μ A, respectively.



(a)



(b)

Fig. 6. The measured mixer gain (open diamonds) and output mixer noise temperature (squares) of HEB#2 versus IF at a 1.63 THz LO at (a) 4.2 K, $U_0 = 1.6$ mV $I_0 = 180$ μ A and (b) 12 K, $U_0 = 1.8$ mV, $I_0 = 200$ μ A.

a GBW of 3.5 GHz. The same noise and gain measurements as at 4.2 K were conducted at 12 K. Results are shown in Figs. 5 and

TABLE IV
DSB RECEIVER NOISE TEMPERATURE (T_r), THE NOISE BANDWIDTH (F_n), THE MIXER CONVERSION GAIN (G_m), THE GAIN BANDWIDTH (F_g) AND THE OUTPUT MIXER NOISE TEMPERATURE (T_{out}) FOR MIXERS HEB#1, HEB#2 AND NbN HEB MIXER [29]

	HEB#1		HEB#2		NbN HEB[29]
	@2.7K	@4.2K	@4.2K	@12K	@4.2K
T_r , K	700	1150	1700	2150	800
f_n , GHz	3.2	3.5	5	5	-
G_m , dB	-18	-19	-15	-15	-12.3
f_g , GHz	-	-	3.5	3.4	-
T_{out} , K	22	27	80	115	40

6. The fitted zero IF noise temperature, the NBW, the mixer conversion gain and the GBW are 2150 K, 5 GHz, -14.7 dB and 3.4 GHz, respectively. These data show that both the conversion gain and the GBW stays almost the same at both bath temperatures, but the output noise at a higher bath temperature is higher, similar to the behavior observed for the “low” T_c HEB mixer, which results in a higher T_r . The acquired parameters of both HEBs are summarized in Table IV together with values for an NbN HEB mixer [29] for comparison.

Two tested HEB mixers differed, not only in terms of the critical temperature, but also MgB_2 film thickness. As it follows from the HEB mixer theory, and some experiments with NbTiN HEB mixers [10], the film thickness affects the GBW and NBW of the device due to a longer phonon escape time. However, it should not affect the noise temperature (at $IF \ll GBW$) unduly. Our experimental data shows that this is also the case for MgB_2 HEB mixers.

V. CONCLUSION

This study shows that for superconducting films with a higher T_c both the output noise temperature and the conversion gain of HEB mixers increase as compared to the films with a lower T_c . This is valid for the optimal operation conditions. At the same time films with a higher T_c provide a broader NBW, as has been discussed in previous works. Already having reached a T_c of 22 K, the HEB mixer can operate above 12 K with only a 25% increase of the receiver noise temperature, compared to that at 4.2 K. Achieving the HEB mixers with a $T_c > 30 - 35$ K will push the HEB operation temperature above 20 K with no or very small sensitivity reduction. In addition, we have demonstrated that the quality of MgB_2 is not critically important to achieving low noise temperature in the 2–4 K temperature range and $IF < 2$ GHz.

In this work we achieved a mixer noise temperature and a noise bandwidth comparable to NbN HEBs using quite low quality MgB_2 thin films with a “low” T_c (compared to a T_c of 39 K for the bulk MgB_2 or 33–38 K for the high quality MgB_2 films). The required LO power in this case is approximately 100 nW, which can be easily realized with the available

source technologies for frequencies, even above 2 THz. Fabricated devices demonstrated high robustness and did not lose their properties after 1.5 years of storage in a nitrogen atmosphere. However, more specific tests would be required for space application.

Three different methods were applied to estimate the mixer conversion gain of the same HEB mixer. Good agreement with an error margin of ± 0.5 dB (which is within the accuracy of these measurements) between methods, indicates that the obtained mixer gain values are correct.

REFERENCES

- [1] D. P. Marrone *et al.*, "Observations in the 1.3 and 1.5 THz atmospheric windows with the receiver lab telescope," in *Proc. 16th Int. Symp. Space THz Technol. (ISSTT)*, Gothenburg, Sweden, 2005, pp. 64–67.
- [2] D. Meledin *et al.*, "A 1.3 THz balanced waveguide HEB mixer for the APEX telescope," *IEEE Trans. Microw. Theory Techn.*, vol. 57, no. 1, pp. 89–98, Jan. 2009.
- [3] C. Risacher *et al.*, "First 1.3 THz observations at the APEX telescope," in *Proc. 20th Int. Symp. Space THz Technol. (ISSTT)*, Charlottesville, VA, USA, 2009, pp. 54–61.
- [4] T. de Risacher *et al.*, "The Herschel-heterodyne instrument for the far-infrared (HIFI)," *Astron. Astrophys.*, vol. 518, Jul.-Aug. 2010, Art no L6.
- [5] P. F. Goldsmith and D. C. Lis, "Early science results from the heterodyne instrument for the far infrared (HIFI) on the herchel space observatory," *IEEE Trans. THz Sci. Technol.*, vol. 2, no. 3, pp. 383–392, Jul. 2012.
- [6] N. Suttiwong *et al.*, "Development and characterization of the balloon borne instrument telis (Terahertz and submm limb Sounder): 1.8 THz receiver," in *Proc. 19th ESA Symp. Eur. Rocket and Balloon Programmes and Related Res. (PAC)*, Bad Reichenhall, Germany, 2009, pp. 165–168.
- [7] M. Birk *et al.*, "TELIS: Terahertz and subMMW Limb sounder—Project summary after first successful flight," in *Proc. 21th int. Symp. Space THz Technol. (ISSTT)*, Oxford, U.K., 2010, pp. 195–200.
- [8] S. Heyminck *et al.*, "GREAT: The SOFIA high-frequency heterodyne instrument," *Astron. Astrophys.*, vol. 542, Jun. 2012, Art no. L1.
- [9] D. Buchel *et al.*, "4.7-THz superconducting hot electron bolometer waveguide mixer," *IEEE Trans. THz Sci. Technol.*, vol. 5, no. 2, pp. 207–214, Mar. 2015.
- [10] L. Jiang *et al.*, "Development of 1.5 THz waveguide NbTiN superconducting hot electron bolometer mixers," *Supercond. Sci. Technol.*, vol. 23, no. 4, Apr. 2010, Art no 045025.
- [11] K. M. Zhou *et al.*, "A 1.4 THz quasi-optical NbN superconducting HEB mixer developed for the DATE5 telescope," *IEEE Trans. Appl. Supercond.*, vol. 25, no. 3, Jun. 2015, Art. no. 2300805.
- [12] W. Zhang *et al.*, "Noise temperature and beam pattern of an NbN hot electron bolometer mixer at 5.25 THz," *J. Appl. Phys.*, vol. 108, no. 9, Nov. 2010, Art no 093102.
- [13] E. L. Kollberg and K. S. Yngvesson, "Quantum-noise theory for terahertz hot electron bolometer mixers," *IEEE Trans. Microw. Theory Techn.*, vol. 54, pp. 2077–2089, May 2006.
- [14] W. Zhang *et al.*, "Quantum noise in a terahertz hot electron bolometer mixer," *Appl. Phys. Lett.*, vol. 96, no. 11, Nov. 2010, Art no 111113.
- [15] J. Nagamatsu *et al.*, "Superconductivity at 39 K in magnesium diboride," *Nature*, vol. 410, no. 6824, pp. 63–64, Feb. 2001.
- [16] H. Shibata *et al.*, "Ultrathin MgB₂ films fabricated by molecular beam epitaxy and rapid annealing," *Supercond. Sci. Technol.*, vol. 26, no. 3, Mar. 2013, Art no 035005.
- [17] Y. Zhang *et al.*, "Ultrathin MgB₂ films fabricated on Al₂O₃ substrate by hybrid physical-chemical vapor deposition with high T_c and J_c," *Supercond. Sci. Technol.*, vol. 24, no. 1, 2011, Art no 015013.
- [18] S. C. Cherednichenko *et al.*, "Terahertz mixing in MgB₂ microbolometers," *Appl. Phys. Lett.*, vol. 90, no. 2, Jan. 2007, Art no 023507.

- [19] S. Bevilacqua *et al.*, "Low noise MgB₂ terahertz hot-electron bolometer mixers," *Appl. Phys. Lett.*, vol. 100, no. 3, Jan. 2012, Art no 033504.
- [20] S. Bevilacqua *et al.*, "Study of IF bandwidth of MgB₂ phonon-cooled hot-electron bolometer mixers," *IEEE Trans. THz Sci. Technol.*, vol. 3, no. 3, pp. 409–415, Jul. 2013.
- [21] S. Bevilacqua *et al.*, "MgB₂ hot-electron bolometer mixers at terahertz frequencies," *IEEE Trans. Appl. Supercond.*, vol. 25, no. 3, Jun. 2015, Art no 2301104.
- [22] D. Cunnane *et al.*, "Development of hot-electron THz bolometric mixers using MgB₂ thin films," *Proc. SPIE*, vol. 9153, Jul. 2014, Paper 91531Q, 10 pp..
- [23] D. Cunnane *et al.*, "Characterization of MgB₂ superconducting hot electron bolometers," *IEEE Trans. Appl. Supercond.*, vol. 25, Jun. 2015, Art no 2300206.
- [24] S. Cherednichenko *et al.*, "Local oscillator power requirement and saturation effects in NbN HEB mixers," in *Proc. 12th int. Symp. Space THz Technol. (ISSTT)*, San Diego, CA, USA, 2001, pp. 273–285.
- [25] H. Y. Zhai *et al.*, "Degradation of superconducting properties in MgB₂ films by exposure to water," *Supercond. Sci. Tech.*, vol. 14, no. 7, pp. 425–428, Jul. 2001.
- [26] B. S. Karasik, "Optimal choice of material for HEB superconducting mixers," *IEEE Trans. Appl. Supercond.*, vol. 9, no. 2, pp. 4213–4216, Jun. 1999.
- [27] A. J. Gatesman *et al.*, "An anti-reflection coating for silicon optics at terahertz frequencies," *IEEE Microw. Guided Wave Lett.*, vol. 10, no. 7, pp. 264–266, Jul. 2000.
- [28] S. Cherednichenko *et al.*, "Terahertz superconducting hot-electron bolometer mixers," *Physica C*, vol. 372–376, no. 1, pp. 407–415, Aug. 2002.
- [29] S. Cherednichenko *et al.*, "1.6 THz heterodyne receiver for the far infrared space telescope," *Physica C*, vol. 372–376, no. 1, pp. 427–431, Aug. 2002.



Evgenii Novoselov was born in Saint-Petersburg, Russia, in 1988. He received the B.Sc. and M.Sc. (*summa cum laude*) from The Saint-Petersburg National Research University of Information Technologies, Mechanics and Optics (NRU ITMO), in 2009 and 2011, respectively, and is currently working toward the Ph.D. degree from the Terahertz Millimeter Wave Laboratory at Chalmers University of Technology, working on MgB₂ Hot Electron Bolometers.

During his studies at the university, he worked at the research center "Femtosecond optics and femtotechnology" (NRU ITMO) (2007–2011). There he participated in a number of projects on the development of terahertz spectrography and reflectometry using TDS. After completing his master degree, he joined LLC "TELROS Integration", Saint-Petersburg, Russia, as a communication systems design engineer (2011–2013).



Stella Bevilacqua was born in Pizza Armerina, Italy, in 1981. She received the B.Sc. degree in electronic engineering from the University of Catania, Italy, in 2006. She did her thesis work during a four-month period with the Smart-Card group of the MPG division of Catania STMicroelectronics. She received the M.Sc. degree in microelectronic engineering from the University of Catania with the master thesis: "Fabrication and characterization of Graphene field-effect transistors (GFETs) in 2010, and the Ph.D. degree from the Department of Microtechnology and Nanoscience, Chalmers University of Technology, Göteborg, Sweden, in 2014.

Currently, she is a Post-Doc at the Department of Terahertz Millimeter Wave Laboratory, Chalmers University of Technology, Göteborg, Sweden, working on MgB₂ Hot Electron Bolometers.



Sergey Cherednichenko was born in 1970 in Mariupol, Ukraine. He received his Diploma (with Hons) in physics from Taganrog State Pedagogical Institute, in 1993, and the Ph.D. degree in physics from Moscow State Pedagogical University, in 1999.

He is currently with the Department of Microtechnology and Nanoscience at Chalmers University of Technology Göteborg, Sweden. From 2000 to 2006, he was involved in development of terahertz band superconducting mixers for the Herschel Space Observatory; and from 2008 till 2009 in the water vapor radiometer for ALMA. Since 2007, he has been an Associate Professor with the Department of Microtechnology and Nanoscience, Chalmers University of Technology. His research interests include terahertz heterodyne receivers and mixers, photon detectors; THz antennas and optics; thin superconducting films and their application for THz and photonics; and material properties at THz frequencies.



Hiroyuki Shibata received the B.S., M.S., and Ph.D. degrees in physics from Waseda University, Tokyo, Japan, in 1985, 1987, and 1997, respectively.

In 1987, he joined NTT Basic Research Laboratories, Kanagawa, Japan, where he has been working on the physics, material development, and device fabrication of superconductors. He is currently a senior research scientist at NTT Basic Research Laboratories. He has been a guest professor at Osaka University since 2008.

Dr. Shibata is a member of the Physical Society of Japan, the Japan Society of Applied Physics, and the Institute of Electronics, Information and Communication Engineers.



Yasuhiro Tokura received the B.S., M.S., and Ph.D. degrees from the University of Tokyo in 1983, 1985, and 1998, respectively.

In 1985, he joined NTT Musashino Electrical Communications Laboratories, Kanagawa, Japan. He is currently a research professor at NTT Basic Research Laboratories and a professor at the University of Tsukuba. His current research concerns the theory of quantum transport and non-equilibrium dynamics in semiconductor nano/meso-structures.

Dr. Tokura is a member of the Physical Society of Japan and the Japan Society of Applied Physics.

Paper C

Study of MgB₂ ultrathin films in submicron size bridges

E. Novoselov, N. Zhang, and S. Cherednichenko

IEEE Transactions on Applied Superconductivity, vol. 27, no. 4,
June 2017, Art. no. 7500605.

Study of MgB₂ Ultrathin Films in Submicron Size Bridges

Evgenii Novoselov, Naichuan Zhang, and Sergey Cherednichenko

Abstract—We discuss a custom built hybrid physical chemical vapor deposition system for MgB₂ ultrathin film deposition: construction, deposition process development, and optimization. Achieved films on SiC substrates have a critical temperature (T_c) ranging from 35 K (10-nm-thick films) to 41 K (40-nm-thick films). The 20-nm-thick unpatterned film had a room temperature resistivity of $13 \mu\Omega\cdot\text{cm}$, whereas it becomes $50 \mu\Omega\cdot\text{cm}$ in submicrometer size bridges with a critical current density J_c (4.2 K) up to $1.2 \times 10^8 \text{ A/cm}^2$. The lower value of resistivity corresponds to the higher of both T_c and J_c . The surface roughness, measured with an atomic force microscope, is approximately 1.5 nm.

Index Terms—Hot-electron bolometer, HPCVD, magnesium diboride, superconductivity, thin film.

I. INTRODUCTION

HETERODYNE receivers are required in order to achieve a high spectral resolution in sub-mm astronomy observations [1]. The most sensitive mixers used in heterodyne instruments for the frequency range above 1 THz are superconducting hot-electron bolometer (HEB) mixers [2]–[4]. Widely used NbN HEB mixers provide a noise temperature close to ten times the quantum limit and a gain bandwidth (GBW) of 2-3GHz. However, for many astronomical tasks a larger GBW is required [5].

In order to improve the IF bandwidth of HEB mixers, materials with a higher critical temperature (T_c) that provide a shorter electron-phonon interaction time, would be of advantage. MgB₂ is an example of such a material [6]. HEB mixers made from molecular beam epitaxy (MBE) grown MgB₂ films on sapphire have been successfully realized and tested [7]–[10]. Unfortunately, with the MBE process a great reduction of T_c occurs for films thinner than 20 nm, whereas for HEB mixers both a high T_c and a small thickness are desirable. A hybrid physical chemical vapor deposition (HPCVD) method developed for MgB₂ thin films can provide ultra-thin superconducting films of high quality [11], [12]. With such films a gain bandwidth of up to 10 GHz and HEB operation up to 20 K [13] (where compact cryocoolers could be used) can be achieved. This study addresses optimization of the HPCVD method for HEB mixer fabrication.

Manuscript received September 6, 2016; accepted December 4, 2016. Date of publication December 20, 2016; date of current version January 24, 2017. This work was supported by the European Research Council.

The authors are with the Department of Microtechnology and Nanoscience, Chalmers University of Technology, Göteborg SE-41296, Sweden (e-mail: evgenii@chalmers.se; naichuan@student.chalmers.se; serguei@chalmers.se).

Color versions of one or more of the figures in this paper are available online at <http://ieeexplore.ieee.org>.

Digital Object Identifier 10.1109/TASC.2016.2642052

II. MGB₂ THIN FILMS

Superconductivity in MgB₂ was reported in 2001 [14]. It immediately triggered a great interest to MgB₂ film deposition. Several methods for deposition of thin MgB₂ films have been demonstrated, including pulsed laser deposition (PLD), MBE, and HPCVD.

MgB₂ is a conventional intermetallic compound superconductor with the highest T_c of 39 K reported so far. An electron-phonon interaction time of 3 ps (much shorter, in comparison to the one in NbN (12 ps)) was measured in thin MgB₂ films [15]. MgB₂ consists of hexagonal magnesium (Mg) layers with honeycomb boron (B) layers in between. The hexagonal unit cell has the following lattice constants $a = 3.086 \text{ \AA}$, $c = 3.524 \text{ \AA}$. Therefore, the most suitable substrates for MgB₂ thin film deposition are sapphire (Al₂O₃) and silicon carbide (SiC). For Al₂O₃ with the lattice constant of $a = 4.758 \text{ \AA}$ Al₂O₃/MgB₂ lattice mismatch is $\sim 11\%$ (30° in-plane rotation). For SiC ($a = 3.070 \text{ \AA}$) the lattice mismatch is even smaller ($\sim 0.42\%$). A better film/substrate lattice match reduces the number of defects in a bottom layer of the film. This leads to a better phonon transparency of the film/substrate interface. Thinner films provide a shorter phonon escape time from the film into the substrate, which is another important limiting factor for the HEB mixers gain bandwidth. Films as thin as 10 nm were reported in [16] with a T_c of 36 K (almost the same as for the bulk). No devices made using such films have been reported to date.

Local Oscillator power is known to increase with the HEB in-plane dimensions. Therefore, a micrometer and sub-micrometer size HEBs are usually fabricated in order to match the reduced output power of THz LO sources. This maximum size restriction imposes a strong limitation on the superconducting film morphology. Uniform films with a smooth surface are of advantage for reproducible HEB mixer fabrication. As-deposited thin MgB₂ films have previously been characterized with a high concentration of defects leading to a high resistivity and a low critical current density (J_c). This is particularly seen in microstructured (patterned) films. Recently, a method for obtaining thin films from thinning down thick films was reported [17]. In that work films as thin as 2.9 nm with a T_c of 36 K were made. However, it is still a question how this films will behave when patterned in submicron structures.

Our goal was to investigate degradation of superconducting properties (T_c and J_c) as well as normal state resistance for ultra-thin MgB₂ films in sub-micrometer size bridges, similar to those used in HEB mixers.

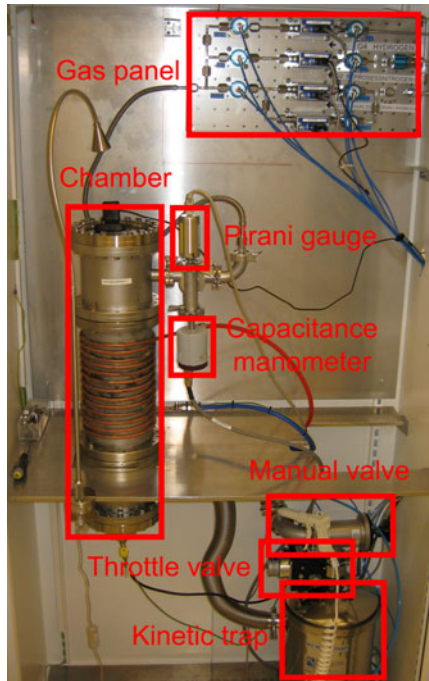


Fig. 1. Chalmers in-house built MgB_2 HPCVD system.

III. CHALMERS HPCVD SYSTEM

A custom made HPCVD system was built at Chalmers University of Technology for deposition of MgB_2 thin films. The system photo is shown in Fig. 1. Gases (hydrogen (H_2), diborane (B_2H_6) (5% in H_2), and purging nitrogen (N_2)) are supplied to the deposition chamber using a computer controlled gas panel consisting of pneumatic valves and mass-flow controllers (MFCs). The MgB_2 deposition occurs only when B_2H_6 flows through the chamber. At 650°C solid Mg pellets melt providing the required high Mg gas pressure.

Above the hot substrate B_2H_6 decomposes and reacts with Mg. As a result, MgB_2 is deposited on the substrate, whereas excess Mg remains in the gas phase. The region where this process occurs is shown with a circle on the phase diagram (see Fig. 2). As one can see, in order to form MgB_2 both the Mg partial pressure and the temperature should fall in a quite tight area in the phase diagram.

A pirani gauge is mounted on the deposition chamber to monitor the pressure during pumping to the base pressure. A capacitance manometer and a throttle valve are connected to a pressure controller to set the desired process pressure. A kinetic trap follows the deposition chamber in order to protect both the throttle valve and the fore-vacuum pump from residuals of the deposited material carried by the gas flow. The fore vacuum pump and the scrubber used for B_2H_6 disposal are placed outside the main cabinet in the utility room. For safety reasons H_2 gas is cleaned from B_2H_6 and mixed with N_2 to prevent formation of dangerously explosive concentrations of the oxyhydrogen.

A schematic of the MgB_2 HPCVD system chamber is presented in Fig. 3. A quartz tube prevents material deposition on water cooled chamber metal walls. Both the substrate and the pieces of solid Mg are placed on the heater. A coaxial heating

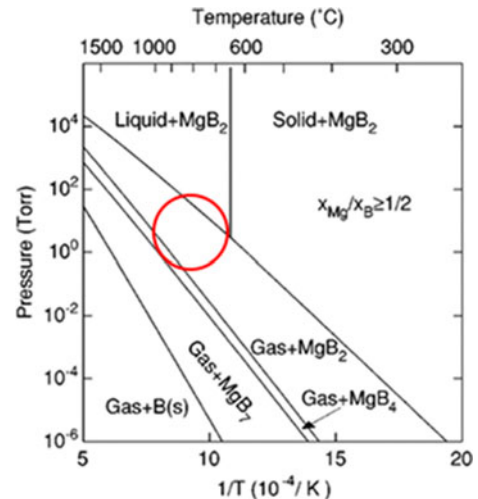


Fig. 2. Pressure-temperature phase diagram for the Mg-B [18].

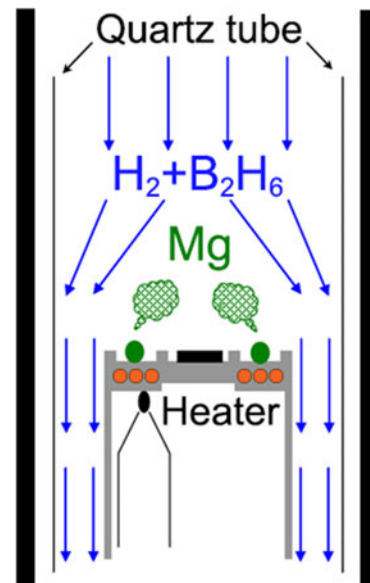


Fig. 3. Schematic drawing of the HPCVD system's deposition chamber.

wire is clamped between the upper and the bottom parts of the heater such that it occurs just under the area where magnesium is placed. In contrast to the previously presented resistive heater designs the coaxial wire itself is hidden inside the heater, which reduces contamination of working parts during the deposition and increases the heater life time. Due to a finite temperature gradient the temperature of the central part where the substrate is placed is 50 K lower than under Mg pellets. A thermocouple is attached to the bottom part of the holder to monitor the temperature during the deposition process.

The sequence for MgB_2 thin film deposition is as following. First, the chamber is pumped till the base pressure is reached ($\sim 10^{-3}$ Torr). Then, it is flushed with H_2 and pumped again to the base pressure. The chamber is filled with H_2 (400 sccm) to a pressure of 20–40 Torr set by the throttle valve. Mg and the substrate are heated to about $690\text{--}720^\circ\text{C}$, which is above the melting point of Mg (650 K). After this, the B_2H_6 mixture is

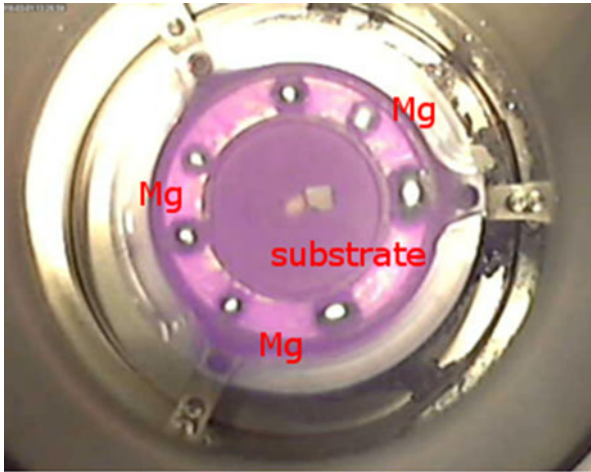


Fig. 4. Chamber view during the deposition process.

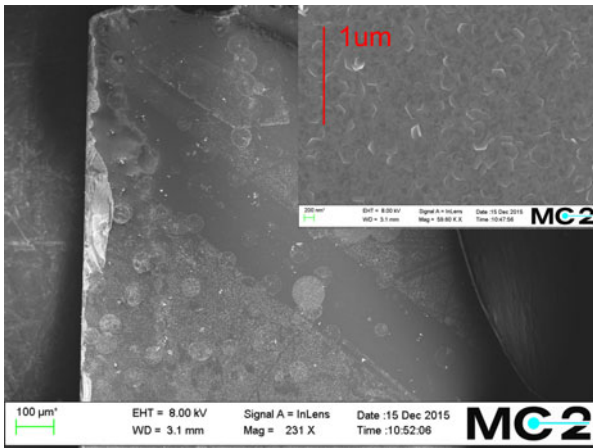


Fig. 5. SEM image of Film 2 (20 sccm 120 s 40 Torr) deposited on the sapphire substrate.

turned on. The chamber view during the deposition process is presented in Fig. 4. After the deposition the heater is turned off and the substrate is cooled down. Before the chamber is opened, it is flushed several times with N_2 in order to clean the chamber from remaining B_2H_6 .

IV. THIN FILMS CHARACTERIZATION

First MgB_2 thin films were deposited on sapphire substrates. The films thickness is defined by the B_2H_6 flow rate and the flow time. The film thickness was measured both with a contact profilometer and an atomic force microscope (AFM). For this purpose, MgB_2 is etched away on a fraction of the substrate using HCl acid (15–40 s etching time, depending on the thickness). The T_c of deposited films ranged from 33 K (15 nm) to 37 K (40 nm) and showed a distinct double transition. Films were very inhomogeneous with lots of spots and particles (see Fig. 5). HPCVD films grow in Volmer-Weber mode and distinct crystallites are seen on the SEM image in the inset in Fig. 5. Another important parameter is the residual resistance ratio ($\text{RRR} = R_{300\text{K}}/R_{50\text{K}}$). For MgB_2 films on sapphire substrates RRR was 1.5–2.5 indicating a high concentration of defects (RRR is about 10 for clean MgB_2 films [12]).

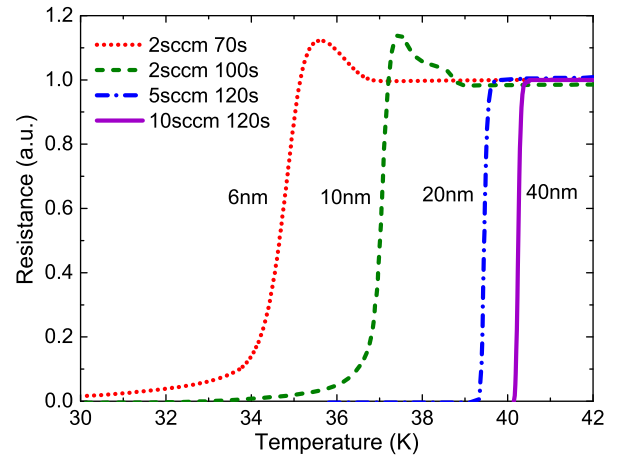


Fig. 6. Normalized R-T curves for MgB_2 films deposited at various B_2H_6 gas flows with different deposition times. Deposition pressure is 20 mTorr.

MgB_2 films deposited on SiC substrates had a T_c ranging from of 35 K (10 nm thick) to 41 K (40 nm thick) (see Fig. 6). However, some problem with the film surface cleanness and homogeneity remained. Crystals with different crystal structure were observed on the film surface with the SEM. Formation of such crystallites could be due to insufficient Mg pressure (Fig. 2). After an increase of the Mg amount the problem with the film inhomogeneity was solved. RRR of the films deposited on SiC substrates was ranging from 2 to 6 indicated improvement of film quality. Optimized films were also studied with atomic force microscope (AFM). A 3D plot recorded with the AFM is shown in Fig. 7, together with a SEM image. The measured roughness was about 1.5 nm, which is lower than for previously reported ultra-thin HPCVD MgB_2 films [16]. The low roughness is one of the most important characteristics affecting fabrication of micro- and nanostructures on thin films. We observed that reduction of the deposition pressure from 80 Torr to 20 Torr continuously leads to smoother film surfaces. For deposition pressures above 30 Torr a droplet formation is observed in the deposition chamber, which probably leads to a rougher film. Therefore, all our latest films were made with a pressure of 20 Torr.

Film parameters in microstructure were studied in several batches of HEBs fabricated using either photo- or e-beam lithography, metal evaporation and ion-beam milling techniques. MgB_2 films were covered with a 20 nm Au layer in another machine directly after the deposition. This Au layer was used both to protect the deposited film from degradation in the atmosphere as well as to be able to use the same fabrication process previously developed for HEBs made from MBE films [9], [10]. Measured HEB parameters for three batches made with e-beam lithography are summarised in Table I.

One of the critical film characteristics is the thickness. There are several techniques to measure the conductive film thickness: mechanical and optical surface profilers, AFM, TEM, ellipsometry, etc. Ellipsometry is a non-invasive method (the film is preserved for further studies). However, it requires preliminary knowledge of the MgB_2 film optical properties. Most of our film thickness data originates from the mechanical profilometer and AFM, which both require a film/substrate step to be defined

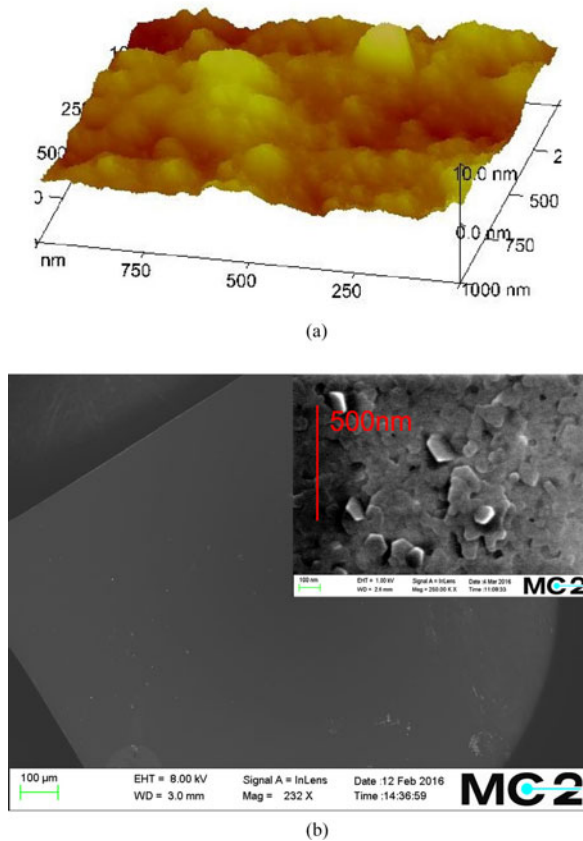


Fig. 7. (a) AFM and (b) SEM images of Film 37 (10 sccm 120 s 40 Torr) deposited on SiC substrate.

TABLE I

MgB₂ HEB SIZE ($W \times L$), THICKNESS (D), CRITICAL TEMPERATURE (T_c), RESISTIVITY IN MICROSTRUCTURE (ρ_{300K}), RESISTIVITY IN FILM (ρ_{FILM}) AND CRITICAL CURRENT DENSITY AT 4.2 K (J_c)

#	$W \times L$ (μm^2)	D (nm)	ρ_{300K} (ρ_{film}) ($\mu\Omega \cdot \text{cm}$)	T_c (K)	J_c ($10^7 \text{A}/\text{cm}^2$)
E2	1×1	$30^{1)}$	$117 - 131^{3)}$ (12)	39.4–39.6	8.8–11.9
E3	0.8×0.8 or 0.5×0.5	$20^{2)}$	40–47 (13)	38.6–39.2	11.6–12.0
E8	0.5×0.5 or 0.3×0.3	$10^{2)}$	46–87 (35)	32.5–34.2	1.2–3.2

1) Determined by deposition rate.

2) Measured by transmission electron microscope (TEM).

3) Rougher film deposited at 40 Torr.

with an etching process. Two samples have also been studied with a Transmission Electron Microscope (TEM) (E3 and E8 in Table I), where the film thickness of 20 nm and 10 nm were measured, respectively.

At room temperature the unpatterned film sheet resistance was measured with a four-point probe technique. With the film thickness knowledge (see above) the room temperature resistivity for unpatterned films of 20 nm and 10 nm thick was calculated to be $13 \mu\Omega \cdot \text{cm}$ and $35 \mu\Omega \cdot \text{cm}$, respectively. These values correspond to the resistivity for the film of the same thicknesses obtained with “thinning-down” technique [17]. Resistivity obtained from resistance of sub-micrometer size bridges (see Table I) was approximately $40\text{--}50 \mu\Omega \cdot \text{cm}$ (20 nm thick film) and $46\text{--}87 \mu\Omega \cdot \text{cm}$

(10 nm thick film). It is a factor of 2 higher than in [17], however we used much smaller bridge dimensions.

To better understand the reasons for an increased resistivity in thin films, the critical current density has to be discussed. As one can observe from Fig. 6 and Table I, the critical temperature for 10 nm and 20 nm thick films is 37 K and 39 K respectively. Whereas T_c for the 20 nm film (E3) remains the same in microbridges, for the 10 nm thick film T_c is reduced to 32–34 K. Nevertheless, both films show excellent superconducting transition. The critical current density is obtained from IV characteristics of microbridges. For the 30 nm and 20 nm thick films J_c is at about $1 \times 10^8 \text{A}/\text{cm}^2$ (4.2 K), hence is one of the highest critical current densities reported for MgB₂ (>10% of the de-pairing current). Even in the 10 nm film the critical current density is $(1 - 3) \times 10^7 \text{A}/\text{cm}^2$, which is the same as for thinned down films [17]. The fact that our as-deposited films have similar resistivity and the same (or higher) J_c can be possibly explained by the lower deposition rate in our HPCVD system as compared to [17]. Lower deposition rates facilitate more uniform MgB₂ film growth [20].

As mentioned above the critical current density in microbridges made from a 10 nm thin film is lower than for thicker films. However, it is approximately a factor of 10 higher than for previously reported microbridges made from MBE and HPCVD grown MgB₂ films [10], [13]. The high yield above 75% allowed for the study of correlation between the resistivity and the critical density for the devices from the same batch (Fig. 8). The lower resistivity corresponds to the higher critical current density. The same behavior is observed also for the critical temperature of the devices (see Fig. 8). These results suggest that the 10 nm film is quite inhomogeneous over the substrate area.

In order to study how the thinning down by Ar⁺ ion-beam milling affects our HPCVD MgB₂ films, three films of various thickness were fabricated. Films were deposited at 20 Torr pressure with 120 s deposition time, but under various B₂H₆ gas flow conditions: Film 61 (10 sccm), Film 62 (20 sccm), and Films 63 (5 sccm). Ion etching was performed in 6 steps: 3 steps of 2 min followed by 3 steps of 10 min. The sheet resistance of each film was measured (at room temperature) with the 4-probe station just after the deposition and after each etching step (see Fig. 9). Based on the deposition parameters, Film 62 was expected to be twice thicker than Film 61, which is twice thicker than Film 63. As one can see Film 61 and Film 62 reach the same sheet resistance as Film 63 after 20 min and 40 min of etching, respectively. Film 63 was completely gone after about 20 min of ion-beam milling. These etching times indicate the correctness of the film thickness relation assumption based on the gas flows.

Assuming that both the etching rate and the resistivity of the film were the same during the ion-beam milling process for all films the dependence of sheet resistance is calculated as $R_s = \rho / (d - r * t)$, where ρ is resistivity, d is film thickness, r is etching rate, and t is etching time. The fit to the experimental data gives the etching rate for selected parameters (2 sccm Ar⁺ flow, 13 mA, 350 V, 30° incidence) of about 1–1.2 nm/min. The value corresponds to the etching rate observed during fabrication of HEBs. Film thicknesses for Film 61, Film 62, and Film 63

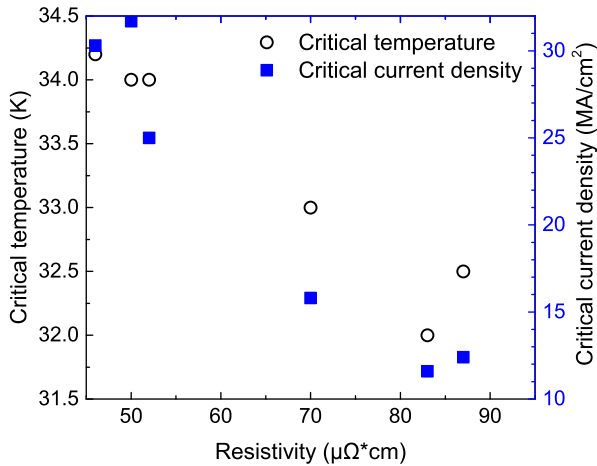


Fig. 8. Critical temperature and critical current density versus resistivity of the film measured for the devices from batch E8.

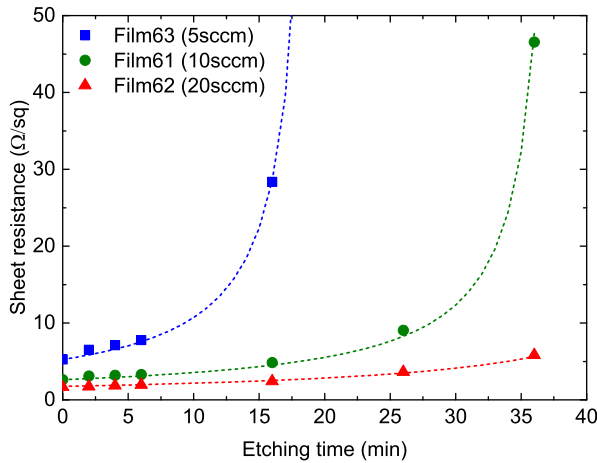


Fig. 9. Sheet resistance versus etching time. Deposition time and deposition pressure are 120 s and 20 Torr, respectively.

used for fitting are 40 nm, 60 nm, and 20 nm, respectively. These values were predicted from relation between different gas flows used for film depositions based on previous film deposition results. For the future it is of great interest how HPCVD MgB_2 films would behave in submicron structure after the milling.

The film resistivity affects the design of HEB mixers. In order to provide the best performance, the resistance of HEB should be matched to the impedance of the integrated planar spiral antenna (100 Ω). With a resistivity of about 50 $\mu\Omega \cdot \text{cm}$ (similar to the previously reported resistivity for the thin MgB_2 films [13]) an aspect ratio of HEB W/L should be less than 1. Together with a requirement from a limited available LO power (keeping a bolometer area small) it will lead to the reduction of bolometer width in the design (compared to HEB mixers made from MBE MgB_2 films [9], [10]). That will increase the contact resistance between the HEB and the metal antenna, which subsequently increases the receiver noise temperature.

V. CONCLUSION

The HPCVD system was successfully constructed and launched at Chalmers University of Technology. The low

resistivity of $\approx 50 \mu\Omega \cdot \text{cm}$ and the high critical current density of up to $1 \times 10^8 \text{ A/cm}^2$ indicates rather good quality of the achieved films. The micron and submicron size HEB mixers have already been fabricated from these films and tested. The maximum IF frequency gain bandwidth of 6 GHz was measured for $1 \times 1.5 \mu\text{m}^2$ device made from 15 nm thick MgB_2 film at 0.4 THz [19]. However, further development of MgB_2 HPCVD process is required to improve stability and repeatability. Of the great interest is a study of the possibility to reduce the thickness of our films by ion-beam milling [17] and to pre-clean MgB_2 films prior the first protective Au layer deposition.

REFERENCES

- [1] H.-W. Hubers, "Terahertz heterodyne receivers," *IEEE J. Sel. Topics Quantum Electron.*, vol. 14, no. 2, pp. 378–391, Mar./Apr. 2008.
- [2] Th. de Graauw *et al.*, "The herschel el-heterodyne instrument for the far-infrared (HIFI)," *Astron. Astrophys.*, vol. 518, Jul./Aug. 2010, Art. no. L6.
- [3] S. Heyminck *et al.*, "GREAT: The SOFIA high-frequency heterodyne instrument," *Astron. Astrophys.*, vol. 542, Jun. 2012, Art. no. L1.
- [4] D. Meledin *et al.*, "A 1.3 THz balanced waveguide HEB mixer for the APEX telescope," *IEEE Trans. Microw. Theory Techn.*, vol. 57, no. 1, pp. 89–98, Jan. 2009.
- [5] A. F. Loenen *et al.*, "Excitation of the molecular gas in the nuclear region of M82," *Astron. Astrophys.*, vol. 521, Oct. 2010, Art. no. L2.
- [6] S. Cherednichenko *et al.*, "Terahertz mixing in MgB_2 microbolometers," *Appl. Phys. Lett.*, vol. 90, no. 2, Jan. 2007, Art. no. 023507.
- [7] S. Bevilacqua *et al.*, "Low noise MgB_2 terahertz hot-electron bolometer mixers," *Appl. Phys. Lett.*, vol. 100, no. 3, Jan. 2012, Art. no. 033504.
- [8] S. Bevilacqua, S. Cherednichenko, V. Drakinskiy, H. Shibata, Y. Tokura, and J. Stake, "Study of IF bandwidth of MgB_2 phonon-cooled hot-electron bolometer mixers," *IEEE Trans. THz Sci. Technol.*, vol. 3, no. 4, pp. 409–415, Jul. 2013.
- [9] S. Bevilacqua, E. Novoselov, S. Cherednichenko, H. Shibata, and Y. Tokura, " MgB_2 hot-electron bolometer mixers at terahertz frequencies," *IEEE Trans. Appl. Supercond.*, vol. 25, no. 3, Jun. 2015, Art. no. 2301104.
- [10] E. Novoselov, S. Bevilacqua, S. Cherednichenko, S. Shibata, and Y. Tokura, "Effect of the critical and operational temperatures on the sensitivity of MgB_2 HEB mixers," *IEEE Trans. THz Sci. Technol.*, vol. 6, no. 2, pp. 238–244, Mar. 2016.
- [11] X. X. Xi *et al.*, "Progress in the deposition of MgB_2 thin films," *Supercond. Sci. Technol.*, vol. 17, no. 5, pp. S196–S201, May 2004.
- [12] X. X. Xi *et al.*, " MgB_2 thin films by hybrid physical-chemical vapor deposition," *Phys. C, Supercond.*, vol. 456, no. 1/2, pp. 22–37, Jun. 2007.
- [13] D. Cunnane *et al.*, "Characterization of MgB_2 superconducting hot electron bolometers," *IEEE Trans. Appl. Supercond.*, vol. 25, no. 3, Jun. 2015, Art. no. 2300206.
- [14] J. Nagamatsu *et al.*, "Superconductivity at 39 K in magnesium diboride," *Nature*, vol. 410, no. 6824, pp. 63–64, Feb. 2001.
- [15] Y. Xu *et al.*, "Time-resolved photoexcitation of the superconducting two-gap state in MgB_2 thin films," *Phys. Rev. Lett.*, vol. 91, no. 19, Nov. 2003, Art. no. 197004.
- [16] M. A. Wolak, N. Acharya, T. Tan, D. Cunnane, B. S. Karasik, and X. Xi, "Fabrication and characterization of ultrathin MgB_2 films for hot-electron bolometer applications," *IEEE Trans. Appl. Supercond.*, vol. 25, no. 3, Jun. 2015, Art. no. 7500905.
- [17] N. Acharya *et al.*, " MgB_2 ultrathin films fabricated by hybrid physical chemical vapor deposition and ion milling," *APL Mater.*, vol. 4, no. 8, Aug. 2016, Art. no. 086114.
- [18] Z.-K. Liu *et al.*, "Thermodynamics of the Mg–B system: Implications for the deposition of MgB_2 thin films," *Appl. Phys. Lett.*, vol. 78, no. 23, pp. 3678–3680, Jun. 2001.
- [19] E. Novoselov, N. Zhang, and S. Cherednichenko, " MgB_2 hot electron bolometer mixers for THz heterodyne instruments," *Proc. SPIE*, vol. 9914, Jul. 2016, Art. no. 99141N.
- [20] C. Zhuang *et al.*, "Surface morphology and thickness dependence of the properties of MgB_2 thin films by hybrid physical-chemical vapor deposition," *Supercond. Sci. Technol.*, vol. 23, no. 5, Apr. 2010, Art. no. 055004.

Paper D

MgB₂ hot electron bolometer mixers for THz heterodyne instruments

E. Novoselov, N. Zhang, and S. Cherednichenko

Proceedings of SPIE, vol. 9914, July 2016, Art. no. 99141N.

MgB₂ hot-electron bolometer mixers for THz heterodyne instruments

Evgenii Novoselov, Naichuan M. Zhang, Sergey Cherednichenko*,
Terahertz and Millimetre Wave Laboratory, Fysikgränd 3, Gothenburg, Sweden 412 98

ABSTRACT

In this work we present experimental investigation of the MgB₂ hot-electron bolometer (HEB) for low noise mixing at terahertz frequencies. A dedicated MgB₂ thin film deposition system was designed and constructed based on Hybrid Physical-Chemical Deposition. Films as thin as 15nm have a superconducting transition at 35K, with a critical current density $>10^7$ A/cm² (at 4.2K) in bridges as narrow as 500nm, indicating on good connectivity in the film. The gain bandwidth (GBW) was measured by mixing of two THz sources. The GBW is proportional to the film thickness and it is at least 6GHz for 15nm thick devices. Performance of MgB₂ HEBs was compared to performance of one of the NbN HEB mixers made for the Herschel Space Observatory (one of the flight units), for which both the GBW and the Noise Bandwidth (NBW) was measured. MgB₂ HEB mixers show a GBW at least a factor of three broader compared to the NbN HEB measured in the same set-up.

Keywords: MgB₂, HEB, hot electron, THz, terahertz, HPCVD, superconducting MgB₂ film

1. INTRODUCTION

Terahertz (THz) frequency range is suitable for observation of molecular emission lines from interstellar medium, galaxies, or planets require heterodyne receivers with high spectral resolution

¹ In order to fulfill these stringent requirements, superconducting mixers are employed based either on Superconductor-Insulator-Superconductor (SIS) junctions or on superconducting hot-electron bolometers (HEB). Providing a times 1-to-3 quantum limit sensitivity, SIS mixers have an upper frequency cut-off frequency which for Nb-NbTiN type junction is at approximately 1.2-1.3THz.² Above this frequency, HEB mixers, based on NbN and NbTiN thin films, offer a much better sensitivity.³ Selection of NbN and NbTiN for HEB mixers is motivated by a fast electron energy relaxation rate, τ which, to a large extent, determines the HEB mixer gain roll-off frequency, $f_o : f_o=1/\tau$. This roll-off frequency defined the maximum mixer gain bandwidth (GBW) if the intermediate frequency (IF) readout starts from zero (it is often not the case, hence the GBW is usually $<f_o$). The electron energy relaxation time is shorter for materials with a short electron-phonon interaction time (τ_{e-ph}) and a fast phonon escape from the film into the substrate (τ_{esc}). For the thinnest reported NbN and NbTiN films (3-5nm) the maximum GBW is about 2-4GHz, depending on the substrate, buffer layers, and (as a very important factor) on the measurement technique.⁴ Ultimately, a large GBW results in a large noise bandwidth (NBW), defined here as an IF where the mixer (or the receiver) noise temperature increases by a factor of two from its value at low IFs. NBW is characterized by measuring the receiver noise temperature as a function of the IF. There are very few experimental reports on the Tr(IF) measurements for NbN HEB mixers covering from well below and up to above of f_o . Recent results which cover IFs from <1GHz to 5GHz show that the NBW of NbN HEB mixer receivers is about 3.5-4GHz (see also results further in this paper).⁵ Observations of extra galactic sources at THz frequencies often require an IF bandwidth broader than that (see on an example of 1.9THz CII observation with the HIFI/Herschel⁶). Attempts to extend the GBW in NbN HEB mixers have not resulted in any repeatable improvements.

THz mixing in MgB₂ bolometers has been reported in 2007⁷. Later, a noise temperature as low as 700K was achieved at 1.6THz.⁸ However, the gain bandwidth was approximately 2GHz and the noise bandwidth of 4GHz. The promise of a much wider GBW (8-10GHz, based on the measured electron-phonon interaction time and the phonon escape time⁹) has not been achieved. The utilized MgB₂ thin films, made by Molecular Beam Epitaxy, were 10-20nm thick with a superconducting transition temperature (T_c) 20-10K. The T_c in bulk MgB₂ is 39K. Therefore, there was a room for improvement in MgB₂ film T_c as well as even thinner films were required.

*serguei@chalmers.se; phone +46317728499; www.chalmers.se

Very promising results in thin MgB_2 film deposition were achieved with Hybrid Physical-Chemical Deposition (HPCVD)¹⁰. Thin films made with HPCVD had higher T_c compared to films of the same thicknesses made of e.g. with MBE. First results for HEB mixers made of such films showed a GBW up to 8GHz (15nm thick, $T_c=33\text{K}$). The receiver noise temperature was rather high, of about 4000K at 600GHz.¹¹

In order to investigate limits for MgB_2 HEB mixers we have built our own deposition system based on the HPCVD method. The goal is to obtain films as thin as 7-10nm with a $T_c > 30\text{K}$. Furthermore, various techniques for HEB contacts have to be explored in order to reduce the contact resistance which appears when the contacts are made with the break of vacuum.

2. MgB_2 FILMS DEPOSITION

MgB_2 films were deposited in the home build HPCVD system, which is similar to described in¹². It consists of three major sections: the gas supply unit, the reactor, and the pumping system (see Figure 1, left). The gas Mass Flow Controllers (MFCs) control supply of H_2 , $\text{H}_2+\text{B}_2\text{H}_6$ (5%), and N_2 . Pure hydrogen is used as a reducing gas (400 sccm), and 5% diborane (1-10 sccm) supplies boron from thermal decomposition of diborane. The reactor is a water cooled 200mm vacuum chamber which contains a heater (the lower section of the heater is shown in Figure 1, right-top). The heater's top section (Figure 1, right-low) has a groove where several pieces of Mg are placed (4-6g in total). The SiC substrate is placed in the central part of the heater, where the temperature is approximately 50 degrees below the peripheral part. At the deposition pressure of 20Torr the given mass of Mg suffices for about 4 min deposition time. Slower Mg evaporation rate results in the reduce Mg partial pressure and hence in formation of other phases of MgB_x .

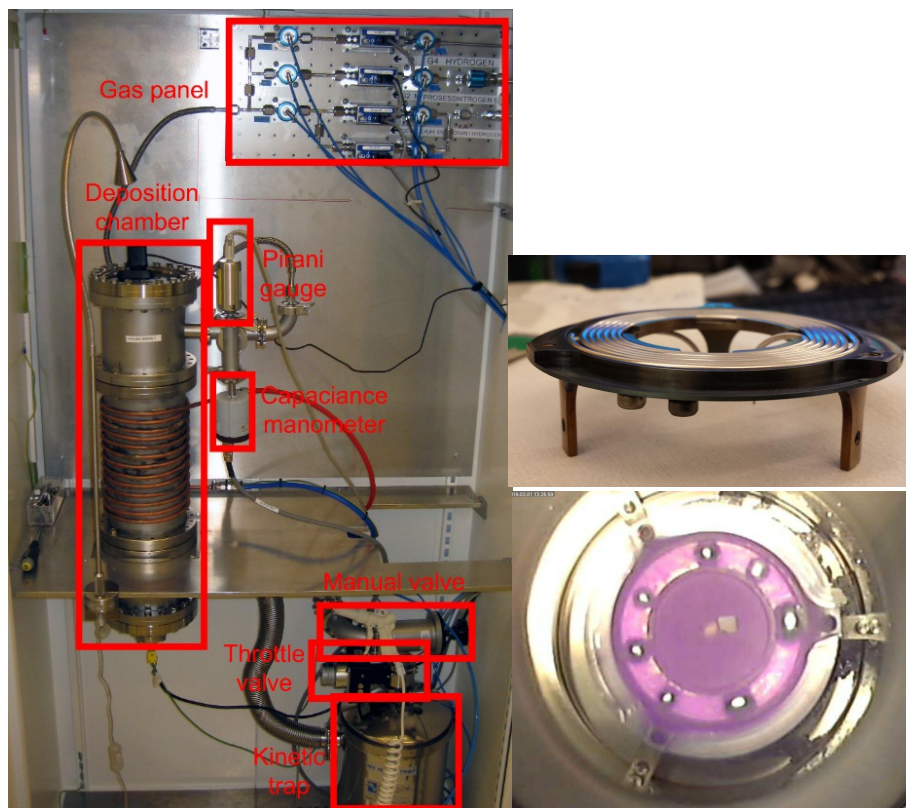


Figure 1. Photograph of the MgB_2 HPCVD system at Chalmers University of Technology. (left) General view with the main sections indicated. (top-right) The heater, with the top part removed. The coaxial heating cable is visible. (lower-right) The top view of the heater during deposition. The Mg pieces are melted and formed shiny bolls. A 5mmx5mm SiC substrate is seen slightly off centered (to the right).

was used for the receiver noise temperature measurements. As an LO source, a FIR gas laser was used at 690GHz. A high output power of the laser allowed us to pump the mixer to the resistive state starting from a 10K bath temperature. Only HEB made of 15nm films were used for the noise temperature measurements. At this stage, no corrections for optical loss (e.g. the beam splitter, the cryostat window, IR filters, etc.) were applied to the obtained receiver noise temperature.

3. RESULTS

The GBW was measured for MgB₂ HEB made of 45nm (E2-1), 35nm (E3-8, E3-2), and 15nm films (E6-7). The critical temperatures of the 45nm and 35nm thick films were >38K, hence such devices were heated up to 35K. The GBW was the same for all temperatures starting from 4.2K. The 15nm thick HEBs were heated up to 30K. Figure 3 shows IF response for four discussed mixers. The temperatures, at which those curves were measured are given in the legend together with the roll-off frequencies of the fitting curves $(1+(f_{if}/f_0)^2)^{-1}$.

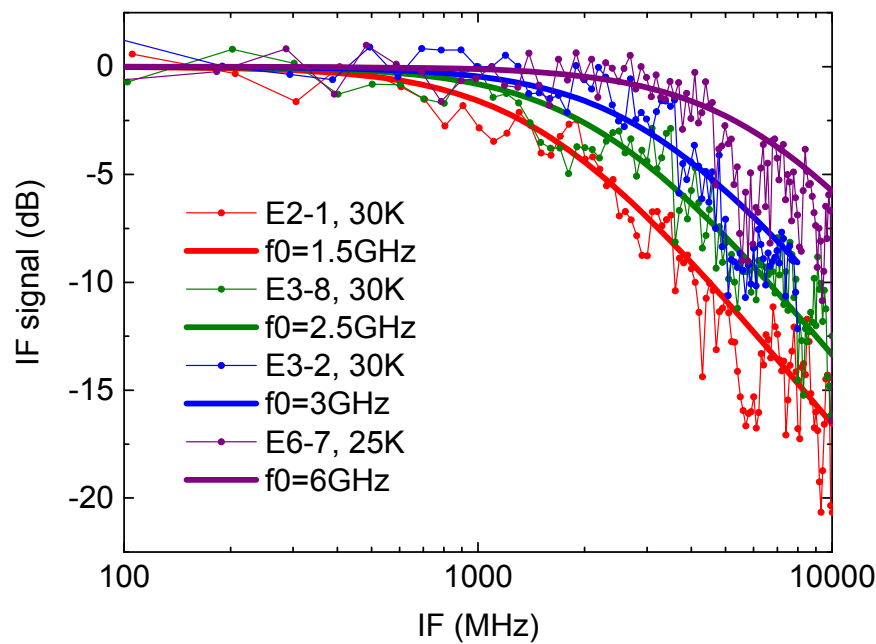


Figure 3. Normalized IF response of four MgB₂ HEB mixers as measured at 400GHz. The film thicknesses were: 45nm (E2-1), 35nm (E3-8 and E3-2), and 15nm films (E6-7). The mixers' temperatures and the gain roll-off frequencies are given in the legend.

The critical temperatures of the discussed mixers were close to each other. Therefore, the increase of the GBW for thinner films can be explained only by the reduction of the phonon escape time, which is proportional to the film thickness in the thin film limit (negligible temperature gradients across the film thickness).

For presented mixers, the IF signal varies only 9dB at the highest IF of 10GHz. Therefore, an error in the IF chain gain calibration of 1-2dB might result in a noticeable error in deduced value of the GBW. Therefore, as an ultimate calibration, we utilized an NbN HEB mixer. This mixer is one of the flight units delivered¹³ by Chalmers University of Technology (in collaboration with Jet Propulsion laboratory (USA), and MSPU (Russian Federation)) for the HIFI instrument of the Herschel Space Observatory as a flight spare unit and for the HIFI Band 6 beam test. This unit was returned back to Chalmers after the successful integration of HIFI and the launch of the Herschel Observatory¹⁴. A remarkable note, after more than a decade after fabrication and integration (in year 2005), the HEB resistance was still the same within 10hm accuracy. The GBW of this mixer (still packed in the flight mixer) unit was now measured in the same set-up as the MgB₂ HEB mixers (the cryostat and the IF chain), except that the 690 GHz LO was used. Resulting IF

response curves for the NbN HEB mixer are given in Figure 4. Two bias points were used: 1mV (the minimum noise temperature point), and 5mV at two LO power levels. At the optimal LO power, the GBW was also measured at a reduced bias of 0.5mV. At the minimum noise point (1mV), which is also a maximum mixer gain point, the GBW was 1.6GHz. The GBW increases to 2.3GHz at the 5mV bias.

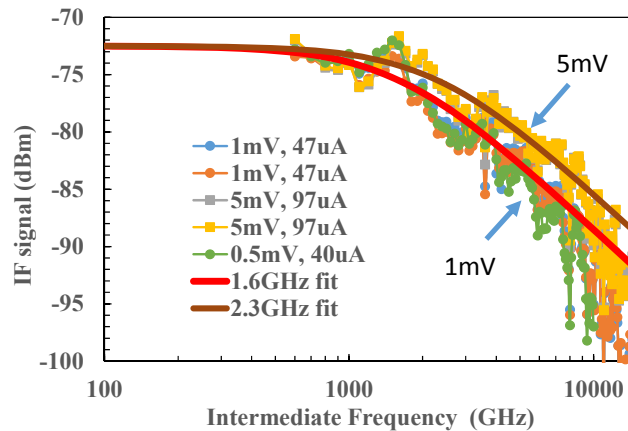


Figure 4. IF response of an NbN HEB mixer in the same set-up as for the MgB₂ HEB mixers. The minimum noise temperature (and the maximum mixer gain) is at about 1mV bias voltage. The NbN HEB mixer GBW increases at higher bias voltages, as it has been reported before.

Increase of the GBW at higher bias voltages is a typical property of NbN HEB mixers. However, previously we had observed a GBW of 3GHz for such mixers (not from this particular batch, though). The Noise Temperature was also measured across an IF band from 0.6GHz to 4GHz as it is shown in Figure 5. The LO was set at 1.63THz since the current NbN HEB mixer is integrated with a 1.6THz Double-Slot Antenna. The fitting curve defines the noise bandwidth, which is 3.5GHz in this case.

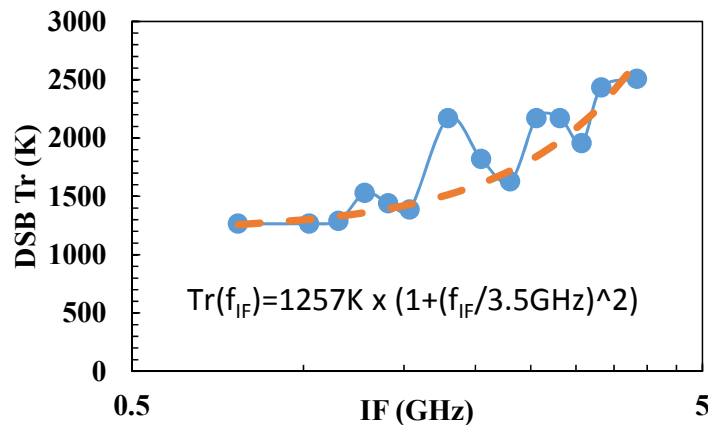


Figure 5. The measured DSB receiver noise temperature for the Herschel FM03 NbN HEB mixer at 1.63THz LO. No corrections for the optical loss were applied. Bias: 1mV, 47μA. The noise temperature is very similar to the one measured with the same sample prior to the delivery in 2005. A different IF LNA was used this time (0.1-5GHz) which allows for measurements from lower IFs. The mixer unit itself has a lower cut-off frequency at 500GHz (the built-in bias-T).

We should note that this is very similar to NbN HEB mixers made for SOFIA and which were tested with a similar cryogenic LNA.⁵ Therefore, both the GBW and the NBW of the Herschel NbN HEB mixers can be considered as the state of the art. Herschel HIFI HEB mixers are optimized for a lower optimal LO power (HEBs are 2μm wide time 0.1 μm long), and hence have a 30% higher noise temperature compared to e.g. 4μm wide HEBs.^{15,13} The IF cryo LNA, used this time, apparently has a worse input impedance matching to the HEB mixers in the 1-2GHz range, resulting in a spike

at 1.7GHz. This one was not seen during the HIFI HEB mixer tests due to different LNAs, designed for a 2-5GHz band. Nevertheless, the obtained GBW matches rather well the NBW for the NbN HEB mixers, where a ratio $NBW/GBW=1.5-2$ has also been reported before. It means, that current MgB_2 HEB mixers have a GBW a factor 3 larger than the state of the art NbN HEB mixer.

We have not conducted an exact measurement of the LO power requirement for MgB_2 HEB mixers. However, comparison with the NbN HEB mixers shows that it is much higher than for NbN HEBs. Using a rather thick beam splitter (200 μm Mylar) we were able to pump an MgB_2 HEB mixer (similar to E6-7, Figure 3) with the 690GHz LO to a smooth IV only for a bath temperature of $>20K$. We will further optimize the LO coupling scheme, however, we were able to obtain the first noise temperature data for devices made of Chalmers MgB_2 films.

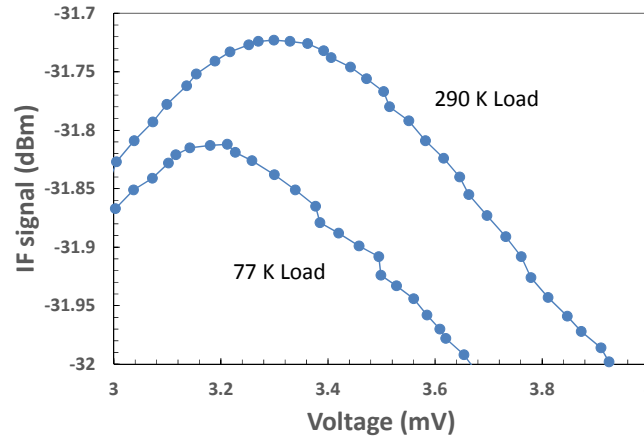


Figure 6. MgB_2 HEB mixer, made of a 15nm thick film. LO frequency is 690GHz. The measured IF response on both the Hot (290K) and the cold (77K) black body loads vs mixer bias voltage. The maximum Y-factor is 0.15dB, corresponding to a receiver noise temperature of 6100K. The mixer temperature is between 22K and 24K (based on comparing the IV to those measured in a dip stick at various temperatures). Correcting for the beam splitter loss, the noise temperature is 4300K.

The IF response (including the IF chain gain) on both the hot (290K) and the cold (77K) black body loads vs the mixer bias voltage is shown in Figure 6. At 3.5mV the Y-factor is 0.15dB, corresponding to a receiver noise temperature of approximately 6100K. The beam splitter reflection loss was measured to be 30% at 690GHz. Therefore, by correcting T_r just for the beam splitter loss we obtain a receiver noise temperature of approximately 4300K. Other optical losses might be also relevant to consider for a proper evaluation of the mixer. However, we will do that in our further investigation. The mixer temperature of about 23K is 1/3 from the HEB critical temperature. Therefore, a lower noise temperature should be expected at lower temperatures, which will be accessible for the tests after improvement of the LO coupling to the mixer.

4. CONCLUSION

MgB₂ HEB mixer technology is a young approach for THz wave detection, compared e.g. to NbN HEB mixers which were under an active investigation by many groups from at least 1995. Nevertheless, performance of HEB mixers made of low T_c MgB₂ films (e.g. 10K) is the same as for state of the art NbN HEB mixers. However, the goal is to obtain this low T_c in a much wider IF band, e.g. up to 8-10GHz. In this work we demonstrate that compared to the NbN HEB mixer (1.6GHz), the GBW for MgB₂ HEB (6GHz) is larger by a about factor of 3. The noise temperature for such MgB₂ devices (4300K) is about factor of 4 higher compared to the NbN HEB. It has been indicated in other publications,¹¹ that due to a fast MgB₂ film surface oxidation, in-situ contact fabrication might be required in order to reduce the THz signal coupling loss. Such effect has been observed in NbN HEB mixers, where more narrow devices show a high noise temperature, in particularly at higher LO frequencies (>1THz). This effect is expected to be much more critical for MgB₂ HEBs. Currently, we are working on a technique for in-situ gold contact deposition on thin MgB₂ films.

REFERENCES

-
- [1] P.Goldsmith and D.C.Lis, *Trans. IEEE THz Sci.Technol.* vol. 2, n. 4, Jul. 2012, p.383
 - [2] A. Karpov, D. A. Miller, J. A. Stern, B. Bumble, H. G. LeDuc, et al., "Low Noise 1 THz SIS Mixer for Stratospheric Observatory: Design and Characterization", *IEEE Trans.Appl.Supercond.*, vol.21, n.3, June 2011, p.616
 - [3] W. Zhang,P. Khosropanah, J. R. Gao, E. L. Kollberg, K. S. Yngvesson, T. Bansal, R. Barends, and T. M. Klapwijk, *Appl.Phys.Lett.* 96, 111113 (2010)
 - [4] H. Ekström, E. Kollberg, P. Yagoubov, G. Gol'tsman, E. Gershenzon et al. "Gain and noise bandwidth of NbN hot-electron bolometric mixers", *Appl. Phys. Lett.* 70, 3296 (1997);
 - [5] C.Risacher, R.Güsten, J.Stutzki, H.-W.Hübers, D. Büchel et al., "First Supra-THz heterodyne Array Receivers for Astronomy With the SOFIA Observatory", *Trans.IEEE THz Sci.Technol.*, v.6, n.2, pp.199-211, March, 2016.
 - [6] A. F. Loenen, P.P. Van der Werf, R.Güsten, R.Meijerink, F.P. Israel, et al., "Excitation of the molecular gas in the nuclear region of M82" *Astron. Astrophys.*, vol. 521, p. L2, 2010.
 - [7] S. Cherednichenko, V. Drakinskiy, et al, "Terahertz mixing in MgB₂ microbolometers", *Appl. Phys. Lett.*, 90 (2) pp, (2007)
 - [8] E. Novoselov, S. Bevilacqua, S. Cherednichenko, K.Ueda, T.Naito "Effect of the Critical and Operational Temperatures on the Sensitivity of MgB₂ HEB Mixers", *IEEE Trans. Terahertz Sic. Technol.* vol. 6 (2) s. 238-277 (2016)
 - [9] S. Bevilacqua, S. Cherednichenko, V. Drakinskiy, H. Shibata, Y. Tokura . "Study of IF bandwidth of MgB₂ phonon-cooled hot-electron bolometer mixers" . *IEEE Trans.THZ Sci. Technol.* v.3, n.4,pp. 409-415, Jul. 2013
 - [10] D. Cunnane, J. Kawamura, B. Karasik, M. A. Wolak, and X. X. Xi, "Development of hot-electron THz bolometric mixers using MgB₂ thinfilms", *Proc. of SPIE Vol. 9153, 91531Q.*
 - [11] D. Cunnane, J. H. Kawamura, M. A. Wolak, N. Acharya, T. Tan, X. X. Xi, and B. S. Karasik,"Characterization of MgB₂ Superconducting Hot Electron Bolometers" *IEEE Appl. Supercond.* vol. 25, no. 3, p. 2300206, June 2015
 - [12] X.X. Xi, A.V. Pogrebnayakov, S.Y. Xu, K. Chen, Y. Cui, "MgB₂ thin films by hybrid physical-chemical vapor deposition", *Physica C* 456 (2007) 22-37
 - [13] S.Cherednichenko, V.Drakinskiy, T. Berg, P. Khosropanah, and E. Kollberg "Hot-electron bolometer terahertz mixers for the Herschel Space Observatory", *Rev. Sci. Instrum.* 79, 034501 (2008).
 - [14] De Graauw T, Helmich FP, Phillips TG, et al, "The Herschel-Heterodyne Instrument for the Far-Infrared (HIFI)", *ASTRONOMY & ASTROPHYSICS* Volume: 518 Article Number: L6 , pp.1-7. 2010.
 - [15] S. Cherednichenko, M. Kroug, P. Khosropanah, A. Adam, H. Merkel, E. Kollberg, D.Loudkov, B. Voronov, G. Gol'tsman, H.-W. Huebers, H. Richter, "1.6 THz HEB mixer for far infrared space telescope (Herschel)", *Physica C*, vol.372,pp.427-431, Aug. 2002.

Paper E

Wideband THz HEB mixers using HPCVD MgB₂ thin films

E. Novoselov, N. Zhang, and S. Cherednichenko

in Proceedings of *41st International Conference on Infrared, Millimeter and Terahertz Waves*, Copenhagen, Denmark, 25-30 September 2016.

Wideband THz HEB mixers using HPCVD MgB₂ thin films

E. Novoselov, N. Zhang and S. Cherednichenko
Chalmers University of Technology, Gothenburg 41296, Sweden

Abstract— We present results of experimental study of the gain bandwidth (GBW) of MgB₂ hot electron-bolometer (HEB) mixers at 0.1THz and 0.4THz. Antenna integrated 0.25-1.5μm² area devices were made from thin MgB₂ films deposited with a custom made HPCVD system. Film as thin as 15-45nm had a T_c from 35K to 40K. The GBW was found to be independent on the bias conditions, the bath temperature, and the LO frequency. The maximum GBW of 6GHz was observed for 15nm thick HEBs. At an 0.7THz LO and a 23K bath temperature the receiver noise temperature of this mixer was 3000K (corrected for optical losses).

I. INTRODUCTION

In order to perform astronomical observations in the terahertz (THz) range (0.1-10THz) cryogenic low noise heterodyne detectors are needed due to a low intensity of incoming THz waves and a high spectral resolution requirement (>10⁶) for study of astronomical objects dynamics manifested in Doppler-shifted emission lines. Moreover, THz instruments have to demonstrate a broad instantaneous bandwidth to be able to cover fully these broadened lines. At frequencies >1THz superconducting hot-electron bolometers (HEB) are the only choice as a mixing element in high sensitivity heterodyne receivers. They have already been used in many receivers for astronomical observation programs, e.g. the Hershel Space Observatory [1], SOFIA [2], APEX [3], etc.

The gain bandwidth (GBW) of the current state-of-the-art NbN HEB mixers is <2GHz and the noise bandwidth is 4GHz, which is a significant limitation for many astronomical applications. Furthermore, a superconducting critical temperature (T_c) of thin NbN films of about 8-11K forces to use liquid helium (LHe) for device cooling, which reduces the operation time of spaceborne missions. MgB₂ HEB mixers have a potential to solve both of these problems. However, high quality thin MgB₂ films are required to achieve these goals.

II. HPCVD SYSTEM

A custom made hybrid physical chemical vapour deposition (HPCVD) system was built at Chalmers University of Technology to explore limits for MgB₂ thin films. Details of the deposition process can be found in [4], [5]. During the HPCVD process Mg is supplied by evaporation of solid magnesium (Mg) pieces, whereas boron (B) is supplied by high temperature decomposition of diborane gas (B₂H₆). In our HPCVD system a single resistive heater is used both for substrate heating and Mg evaporation. Hydrogen (H₂) as a reduce gas (400sccm), and a 5% B₂H₆ mixture with H₂ (deposition gas, 2-10sccm) were supplied to the deposition chamber using a PC controlled gas panel consisting of pneumatic valves and mass-flow controllers (MFCs). A capacitance manometer and a throttle valve were connected to the pressure controller to set the desired process pressure of 20Torr.

MgB₂ thin films described in this paper were deposited on silicon carbide (SiC) substrates. Film thicknesses, measured

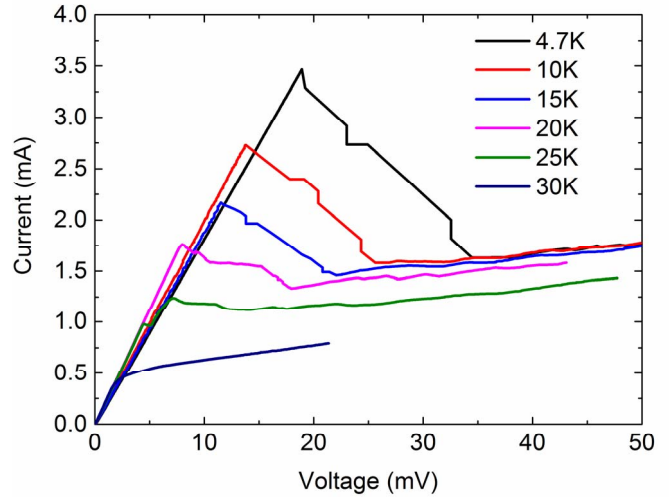


Fig. 1. I-V curve of HEB E6-7 measured in a dip-stick at various bath temperatures. At 4.7K, the critical current density is 2.3×10^7 A/cm².

with scanning probe microscope (SPM) on films etched with hydrochloric (HCl) acid, were from 15nm to 45nm depending on the deposition time and the B₂H₆ mixture gas flow. The T_c of deposited films was ranging from 35K (15nm) to 40K (45nm).

III. HEB FABRICATION AND CHARACTERIZATION

Batches E2 and E3 were fabricated using e-beam lithography, whereas batch E6 was fabricated using photolithography. In all batches, HEBs were integrated with planar spiral antennas. More details on device design and fabrication can be found in [6], [7].

TABLE I
FABRICATED DEVICES: WIDTH (W), LENGTH (L), ROOM TEMPERATURE RESISTANCE (R₃₀₀), T_c, CRITICAL CURRENT DENSITY AT 4.7K (J_c), DEPOSITION GAS FLOW AND DEPOSITION TIME.

Device	W×L, μm ²	R ₃₀₀ , Ω	T _c , K	J _c , A/cm ²	B ₂ H ₆ , sccm	t, sec
E2-2	1×1	40	39.4	6.5e7	10	120
E3-8	0.8×0.8	25	39	6.9e7	5	120
E3-2	0.5×0.5	25	39	6.7e7	5	120
E6-7	1×1.5	65	35	2.3e7	2	100
E6-4	1×1	45	35	1.6e7	2	100

First, for all fabricated devices DC tests were performed in a dip-stick placed in LHe. Selected devices were mounted in mixer blocks and placed inside a LHe cryostat for THz characterization. I-V curves for HEB E6-7 are presented in Fig. 1 as an example. Results of DC characterization, as well as film deposition parameters, are summarized in Table I.

Gain Bandwidth (GBW) measurements were performed at two LO frequencies of 0.1THz and 0.4THz, which are both below the superconducting gap frequency. We observed that the GBW is independent on both the bias voltage and the bath temperature. Fig. 2 represents I-V curves measured

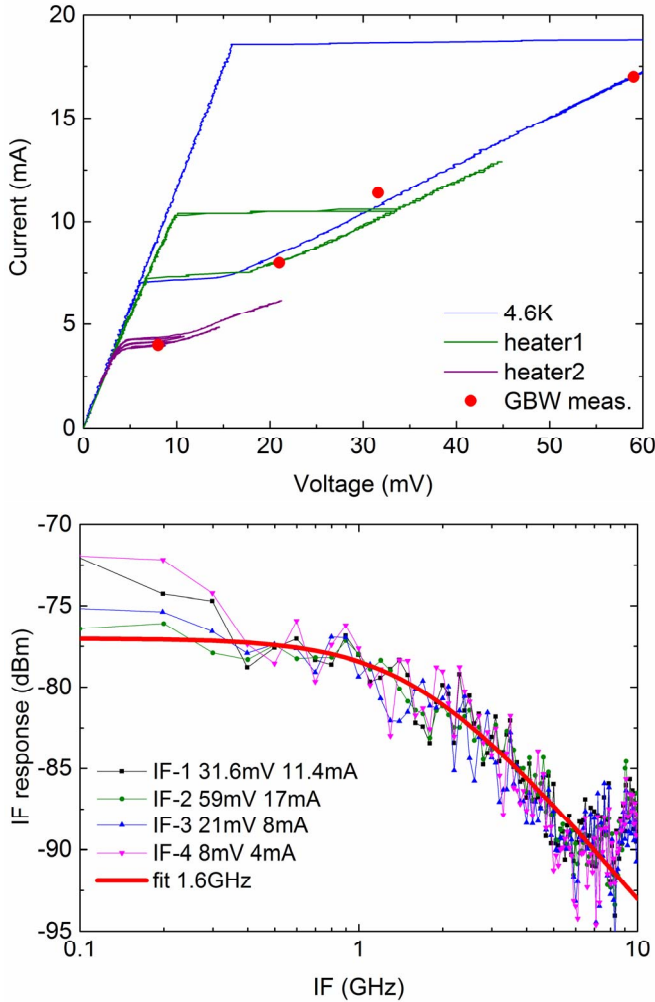


Fig. 2. (a) I-V curves measured in LHe cryostat measured at various bath temperatures and (b) IF response at 0.1THz at various bias points for HEB E2-2.

in LHe cryostat and IF response curves at 0.1THz for GBW measurements of HEB E2-2. The IF response curves taken at different bias points and bath temperatures well coincide. A higher output power of the 0.1THz LO allowed for GBW measurements of the thickest device at a wider range of bath temperatures.

Fig. 3 presents the IF response of HEBs E3-8, E3-2 and E6-7 at 0.4THz. Similar to HEB E2-2, these devices demonstrated GBWs which were almost independent on the bath temperature and the bias condition. Moreover, some devices were tested at both LO frequencies and the same GBWs were achieved. The largest GBW of 6GHz was observed for HEB E6-7 made from the thinnest MgB₂ film. This is about 2-3 times larger than for typical phonon-cooled NbN HEB mixers made of 3-5nm thick NbN films. However, the MgB₂ film thickness is 15nm and there is a room for further improvement.

Preliminary, the mixer noise temperature measurements were performed for device E6-4 using the Y-factor method. The mixer block with the device was followed by a bias-T and a cryogenic 0.1-5GHz LNA placed on the cryostat's cold plate. At 0.7THz LO (far-infrared gas laser) the maximum Y-factor was about 0.15dB at a mixer temperature of 23K. That corresponds to a receiver noise temperature of 6000K (not

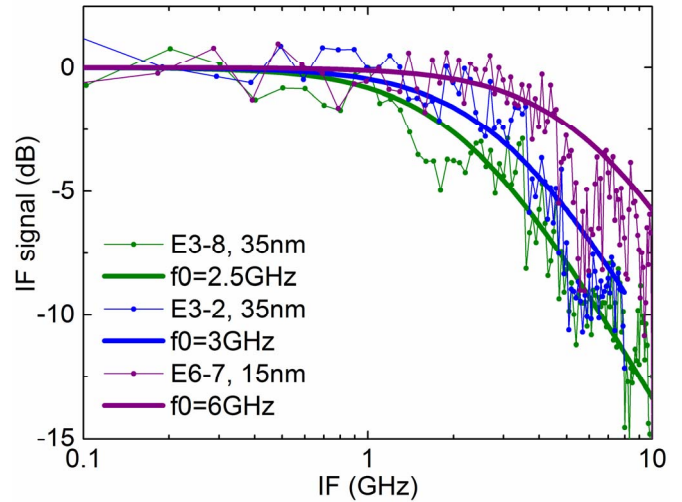


Fig. 3. The GBW of fabricated MgB₂ HEB mixers measured by mixing of radiation from BWO and multiplier source at 0.4THz.

corrected for optical losses) or about 3000K if the contribution from the known optical losses are removed (mostly, from the thick beam splitter). Testing mixers at lower temperatures was not possible at this moment due to the lack of the LO power.

IV. SUMMARY

A possibility of broadband and sensitive HEB mixers fabrication was demonstrated using Chalmers custom made HPCVD deposition system. The full development process from material growth till device THz characterization can be performed at a single place. This gives more opportunities in HEB optimization and improvement.

For our devices, a GBW of 6GHz (2-3 times the one for NbN HEB mixers) was achieved with a $1 \times 1.5 \mu\text{m}^2$ MgB₂ device made by photolithography from a 15nm thick HPCVD MgB₂ film with a T_c of about 35K. This result approximately coincides with a GBW of 8GHz reported in [8]. In order to fulfill requirements for astronomical observations, the noise temperature has to be reduced from the current 3000K to about 1000K. The most evident direction for reducing the mixer noise temperature is reduction of the MgB₂/Au interface contact resistance (between the HEB and the Au antenna).

REFERENCES

- [1]. Th. de Graauw *et al.*, "The Herschel-Heterodyne Instrument for the Far-Infrared (HIFI)," *Astron. Astrophys.*, vol. 518, p. L6, Jul.-Aug. 2010.
- [2]. S. Heyminck *et al.*, "GREAT: The SOFIA high-frequency heterodyne instrument," *Astron. Astrophys.*, vol. 542, p. L1, Jun. 2012.
- [3]. D. Meledin *et al.*, "A 1.3 THz Balanced Waveguide HEB Mixer for the APEX Telescope," *IEEE Trans. Microwave Theory and Tech.*, vol. 57, pp. 89-98, Jan. 2009.
- [4]. X. X. Xi *et al.*, "Progress in the deposition of MgB₂ thin films," *Supercond. Sci. Technol.*, vol. 17, no. 5, pp. S196-S201, May 2004.
- [5]. X. X. Xi *et al.*, "MgB₂ thin films by hybrid physical-chemical vapor deposition," *Phys. C, Supercond.*, vol. 456, no. 1/2, pp. 22-37, Jun. 2007.
- [6]. S. Bevilacqua *et al.*, "Study of IF Bandwidth of MgB₂ Phonon-Cooled Hot-Electron Bolometer Mixers," *IEEE Trans. THz Sci. Technol.*, vol. 3, pp. 409-415, Jul. 2013.
- [7]. S. Bevilacqua *et al.*, "MgB₂ Hot-Electron Bolometer Mixers at Terahertz Frequencies," *IEEE Trans. Appl. Supercond.*, vol. 25, p. 2301104, Jun. 2015.
- [8]. D. Cunnane *et al.*, "Characterization of MgB₂ Superconducting Hot Electron Bolometers," *IEEE Trans. Appl. Supercond.*, vol. 25, no. 3, pp. 2300206, Jun. 2015.

Paper F

Broadband MgB₂ hot-electron bolometer THz mixers operating up to 20 K

E. Novoselov and S. Cherednichenko

IEEE Transactions on Applied Superconductivity, vol. 27, no. 4, June 2017, Art. no. 2300504.

Broadband MgB₂ Hot-Electron Bolometer THz Mixers Operating up to 20 K

Evgenii Novoselov and Sergey Cherednichenko

Abstract—We discuss performance of submicron size hot-electron bolometer mixers made from thin MgB₂ superconducting films. With a superconducting transition temperature of ~ 30 K, such terahertz (THz) mixers can operate with high sensitivity at temperatures up to 20 K. Due to very small dimensions local oscillator power requirements are rather low. In the intermediate frequency band of 1–3 GHz, the double sideband receiver noise temperature is 1600 K at 10 K operation temperature, 2000 K at 15 K, 2500–3000 K at 20 K. The gain bandwidth of such devices is 6 GHz and the noise bandwidth is estimated to be 6–8 GHz.

Index Terms—Hot-electron bolometer (HEB), HPCVD, magnesium diboride, superconductivity, thin film.

I. INTRODUCTION

UTILIZATION of bolometers as mixers in the submillimeter (or terahertz, THz) range has been suggested back in 1960 s [1]. However only after fast electron energy relaxation was discovered in Nb-based superconducting films (hot-electron phenomenon) [2], bolometric mixers found wide applications in high spectral resolution radio astronomical instruments: on the ground (SMTO [3], APEX [4]), airborne (SOFIA [5]) and space borne (Herschel [6]) observatories. The choice for NbN was motivated by the fast electron-phonon interaction (10 ps) [7], ability to fabricate very thin films (5 nm) [8], and a convenient critical temperature, T_c (16 K in bulk, or 9–11 K in thin films). NbN HEB mixers operate in the 2–4 K temperature range, cooled (in most cases) by liquid helium. A high response rate results in ~ 2 GHz Gain Bandwidth (GBW) [9], which has also been reported by several groups. Sensitivity of NbN HEB mixers (in the units of the double sideband (DSB) receiver noise temperature) is ~ 700 – 1000 K (~ 10 times the quantum limit) as it has been experimentally obtained for frequencies ranging from 1 THz to 5 THz [10], [11]. The noise temperature increases towards higher intermediate frequencies (IF) and it doubles its value at about 4 GHz. This figure sets the so called Noise Bandwidth (NBW) $T_r(\text{IF}) = T_r(0) \times (1 + (f_{\text{IF}}/\text{NBW})^2)$ (here, f_{IF} is the intermediate frequency, $T_r(0)$ is the noise temperature at $f_{\text{IF}} = 0$) [12]. Though, for some applications these values for

the GBW and the NBW are sufficient, importance for THz mixers with a broader IF bandwidth has been emphasized: e.g. for broadband molecular line surveys, observations of extragalactic sources, pressure and Doppler broadened lines. Furthermore, necessity of LHe for cooling of NbN HEB mixers severely limits operation time of Space missions, as well as observation campaigns for ground based instruments.

In 2007 a rather broad GBW was demonstrated in HEB mixers based on 20 nm superconducting magnesium diboride (MgB₂) films [13]. Such films were made using molecular beam epitaxy [14]. Moreover, already first results showed a low noise temperature in such devices (10 000 K) at THz frequencies. Phonon transmission through the MgB₂/substrate interface was estimated to be much better than through the NbN/substrate interface. Therefore, prospects for a GBW of up to 8–10 GHz were discussed. Later, the noise performance was improved down to 700 K (at 1.6 THz [15]). However, that figure of merit was achieved for films with a T_c of 8–10 K. Degradation of the critical temperature from 39 K in bulk down to 20–25 K for 20 nm films, and then to 10 K for 10 nm films, resulted in an increased electron-phonon interaction time, and hence in a reduced GBW (2–3.5 GHz). New deposition methods were required in order to produce a high quality thin MgB₂ film. On the other hand, MgB₂ films as thin as 10 nm with a T_c above 30 K were reported deposited with a Hybrid Physical Chemical Vapor Deposition technique [16]. First MgB₂ HEB mixers made with this technique were reported with a greatly improved GBW of 8 GHz [17], [18]. Very recently, similar approach was shown in [9], where a 6 GHz GBW and a noise temperature of 3000 K were obtained. Those devices were made with the photolithography technique and hence they were 1–5 μm across. Due to the large size and the large T_c , such devices required a rather high LO power, hindering from accurate characterization at THz frequencies (output power of THz source is very limited).

In this work we present first results for submicron size MgB₂ HEB mixers made using the e-beam technique. 10 nm MgB₂ films were deposited in a custom made HPCVD system, demonstrating a T_c of 35 K. Devices as small as $300 \times 300 \text{ nm}^2$ and $500 \times 500 \text{ nm}^2$ were fabricated and characterized at 693 GHz.

II. DEVICE FABRICATION AND EXPERIMENTAL TECHNIQUES

In order to obtain thin MgB₂ films with a high T_c (the goal is $T_c > 30$ K) we utilized our home built HPCVD system. The system design and the details of the deposition process have been described in [19]. For the samples discuss in this paper, a

Manuscript received September 6, 2016; accepted December 19, 2016. Date of publication January 17, 2017; date of current version February 16, 2017. This work was supported by the European Research Council.

The authors are with the Department of Microtechnology and Nanoscience (MC2), Chalmers University of Technology, Göteborg SE-41296, Sweden (e-mail: evgenii@chalmers.se; serguei@chalmers.se).

Color versions of one or more of the figures in this paper are available online at <http://ieeexplore.ieee.org>.

Digital Object Identifier 10.1109/TASC.2017.2654861

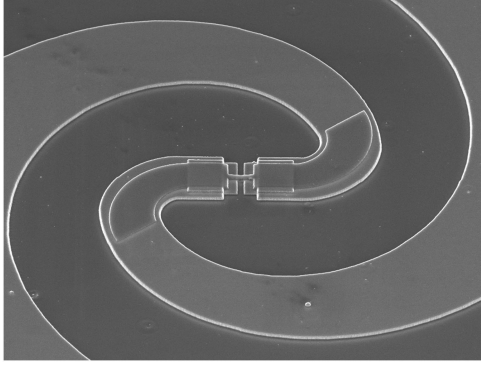


Fig. 1. A HEB mixer with a spiral antenna. The SEM image is obtained from a sample similar to the one discussed here. Gold spiral antenna is the light grey area.

TABLE I

MgB₂ HEB SIZE ($W \times L$), RESISTANCE AT 295 K AND 50 K (R_{295} AND R_{50}), CRITICAL TEMPERATURE (T_c), AND CRITICAL CURRENT AT 4.2 K (I_c)

#	$W \times L$ (nm ²)	R_{295} (Ω)	R_{50} (Ω)	T_c (K)	I_c at 4.2 K (mA)
E8-2	300 × 300	52	41	32	0.75
E8-7	500 × 500	86	67	29	0.62

deposition pressure (H_2) of 20 Torr was chosen since it provides a smooth surface, which is essential for submicron size HEBs. The diborane (5% of B_2H_6 in H_2) flow was 2 sccm and the deposition time was 120 s. Films on 10×10 mm² SiC substrates were used for the HEB fabrication. The film thickness was 10 nm as measured with a Transmission Electron Microscope (TEM). Previous measurements of the films thickness indicate that the given deposition parameters result in a 10–15 nm thick MgB₂ film. The critical temperature on the witness substrate was 35 K with a transition width of 1 K. MgB₂ films on the 10 mm × 10 mm substrates were covered with a 20 nm thick gold layer (2 nm Ti buffer) in a magnetron sputter with about 10 min MgB₂ exposure to the air during the wafer transfer.

Our previous experience shows that the equivalent sheet resistance in microstructures is approximately a factor of 2–3 larger than the sheet resistance in the continuous film (35–40 Ω /sq at room temperature). The residual resistance ratio ($R_{RR} = R_{295}/R_{50}$) for continuous films was 2 (for the discussed thickness), whereas R_{RR} was 1.3 for the ready devices. HEB mixers are essentially microbridges at the feed point of a planar spiral antenna (see Fig. 1). Antenna impedance is real (self complementary design) and it is $\sim 90 \Omega$. Microbridges were designed as squares with either a 300 nm or 500 nm side.

Resulting devices had room temperature resistances in a range of 50–80 Ω . Scattering of the resistance values we associate with some film non-uniformity on the microscale. Variation of R_{295} also correlates with the variation of the critical current (see Table I). For the THz measurements one device 300×300 nm² and one 500×500 nm² were chosen. The critical temperatures were 32 K and 29 K, correspondingly. IV-curves of the devices were recorded in a dip-stick with a 5 K interval. The critical

current values in the mixer block (during THz characterization) were used to obtain the HEB actual temperature.

In order to measure the HEB mixer sensitivity, we mounted HEB chips in a mixer block. This block consisted of a 12 mm elliptical Si lens and a coaxial contact to the HEB. This Si lens size was found to be near optimum for the THz beam coupling from the FIR gas laser, used as the LO source. The laser emission frequency was 693 GHz. The mixer block was installed in a LHe optical cryostat with some thermal insulation from the cold plate. A heater was mounted on the mixer block to be able to rise its temperature. In the cryostat, a bias-T and a 1.5–4.5 GHz Low Noise Amplifier (LNA) followed the mixer block. The noise temperature of the LNA was nominally about 2–3 K, however the total IF chain noise is higher due to the loss in the bias-T. At room temperature the IF signal was further amplified by ~ 50 dB, and measured with a microwave power meter. A tunable band-pass filter (1–9 GHz, 50 MHz bandwidth), installed just before the power meter controlled the IF frequency. A 12 μ m Milar film beam splitter combined the LO and the Signal (from the 295 K and 78 K black bodies). The receiver noise temperature was obtained from the measured Y-factor, and then corrected for a 1.3 dB loss in the cryostat window and the IR filter, a 0.5 dB loss in the beam splitter, and a 1 dB loss on the Si lens surface (the Si lens did not have any antireflection coating). These optical corrections we also utilized in our previous publications, hence a direct comparison with published results for larger HEB mixers can be done.

III. SENSITIVITY CHARACTERIZATION

MgB₂ HEB mixers were characterized in the receiver setup as described in the previous section. The choice of the LO frequency (693 GHz) was motivated by a higher output power of the utilized far-infrared (FIR) laser, as compared to other emission lines (e.g. 1.63 THz). A factor of 10 smaller area of the discussed devices compared to those e.g. presented in [9], allowed to use a thinner beam splitter and hence to increase the measured Y-factor. Current–Voltage characteristics (IV-curves) of sample E8-7 are shown in Fig. 3. By comparing the IVs measured in the dip-stick (IV-1) and in the cryostat (IV-2) we can estimate the sample temperature, 10 K. The IV under the optimal LO power (the highest Y-factor) is IV-3. The measured microwave power P_{IF} from the receiver is a sum of the HEB output noise, the IF chain noise, and the down converted signal from the input load. The resulting P_{IF} (Fig. 3, PV-1) varies with the HEB bias voltage with a maximum at about 0.5 mV. The lowest receiver noise temperature is obtained at bias voltages slightly above the maximum on the PV-curve (1–2 mV). Since the device area was very small then using a mirror (instead of the beam splitter) the LO source was able to pump the HEB into the normal state (IV-4). IV-4 is totally linear with a resistance of 50 Ω , near beginning of the superconducting transition (see Fig. 2). The IF power is also bias independent, indication that the HEB is in the normal state. As for any normal conductor the output noise of the HEB in this state is just the Johnson noise, with a characteristic noise temperature equal the HEB electron temperature, hence 32 K. How much the noise of the HEB at

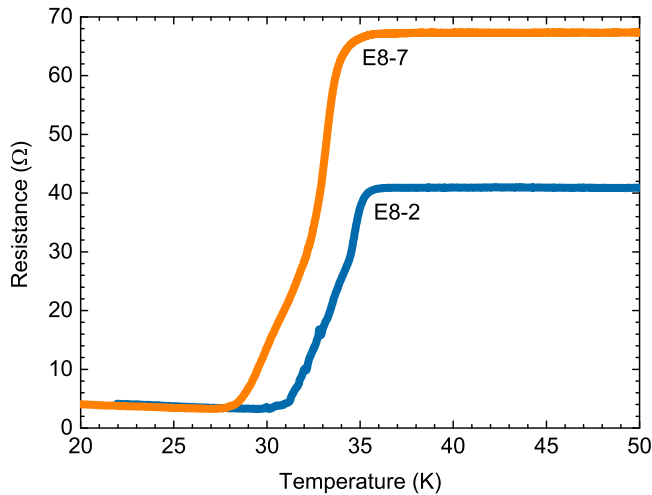


Fig. 2. R-T curves for samples E8-2 (blue) and E8-7 (orange).

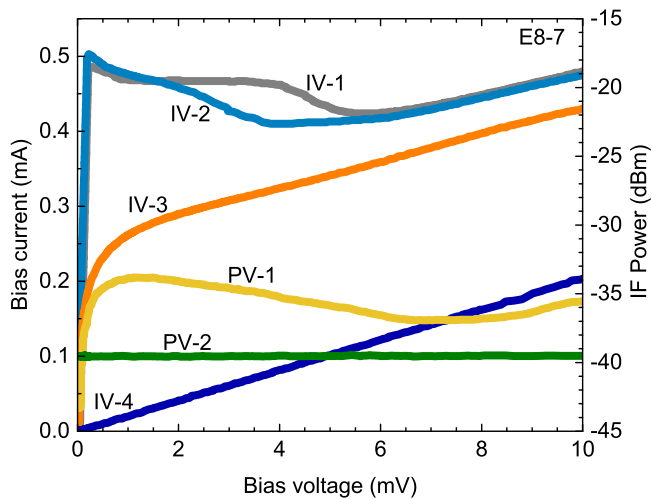


Fig. 3. Current-Voltage (IV) curves for the 500 nm \times 500 nm HEB: IV-1 -in the dip-tick at 10 K; IV-2- in the mixer block; IV-3- under the optimal LO power (693 GHz); IV-4- pumped by the LO into the normal state. IF Power-Voltage curves measured at 2 GHz: PV-1 – corresponds to the optimal LO (IV-3); PV-2- corresponds to the normal state (IV-4).

the best sensitivity point (IV-3) exceeds the noise in the normal state indicates on how well the HEB works and how low the IF LNA noise is.

The HEB receiver noise temperature across a 1.3–4.5 GHz IF band is shown in Fig. 4. For these measurements the cold load was periodically alternated with a hot load coated chopper. The scattering of the points is due to LO source instabilities, leading to Y-factor fluctuations. The noise temperature is approximately 2000 K in the range from 1.5 GHz to 3 GHz.

Recorded P_{IF} shows some falls of the receiver gain between 3 GHz and 4 GHz, and at 4.3 GHz. It is also accompanied by a rise of the noise temperature (Fig. 4). We interpret it as an LNA degradation. Two fitting curves (the dashed and dashed-dotted curves in Fig. 4) are $T_r(IF) = T_r(0)(1 + (f_{IF}/NBW)^2)$ with a NBW of 6 GHz and 8 GHz, where $T_r(0)$ is the receiver noise temperature at zero IF.

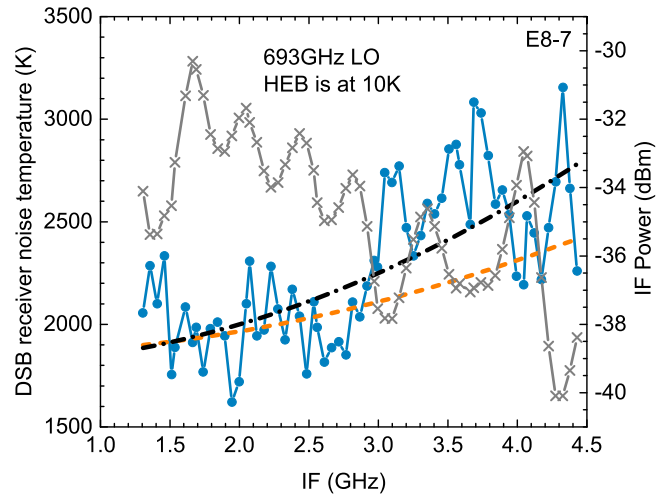


Fig. 4. The receiver noise temperature (circles) and the output power (crosses) (295 K load) as a function of the IF. The HEB mixer was at 10 K. The dashed and dashed-dotted lines are noise bandwidth fits for a 6 GHz and an 8 GHz noise bandwidth.

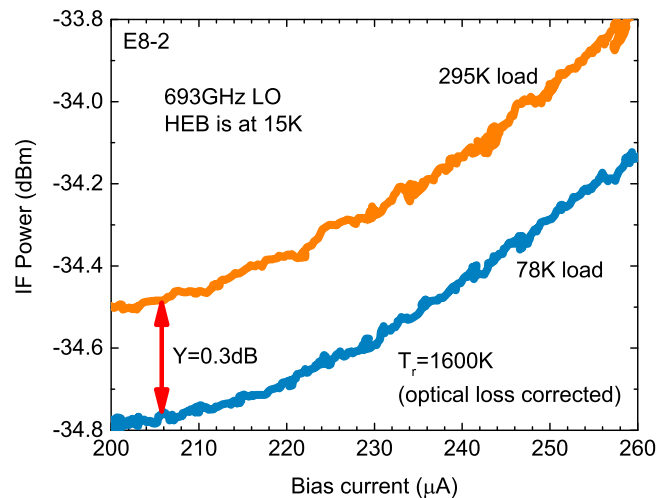


Fig. 5. IF response of sample E8-2 to the hot (295 K) and the cold (78 K) black body loads as a function of the bias current, I_0 . Variation of I_0 was achieved with a varying LO power. The bias voltage is 1 mV, and the IF is 1.3 GHz. The indicated noise temperature is corrected for the optical loss, as described in Section II. The HEB mixer was at 15 K.

In order to deal with LO source instabilities, the next sample (E8-2) was tested at a fixed IF (1.3 GHz) and a fixed bias voltage (1 mV). P_{IF} was recorded as function of the bias current. The later was achieved by varying the LO power both with the hot and the cold loads at the receiver input (Fig. 5). For the 1 mV bias point, the Y-factor was about the same from 200 μ A to 250 μ A. The resulting noise temperature is approximately 1600 K (with the optical loss removed). During this test the mixer temperature was 15 K.

IV. DISCUSSION

In the previous section we showed that a noise temperature of the order of 1600 K can be achieved at 15 K operation of an MgB₂ HEB mixer. Such mixers had a submicron size and with a 1 mW LO source a 15 dB attenuation is required in order to obtain

the optimal IV-curve if a mirror is used. It means approximately 30 μW (referenced to the output of the LO source) for the LO power requirement for the discussed devices. With a 50 μm thick Mylar beam splitter there was $\sim 7\text{--}8$ dB margin. Such a beam splitter has a reflection coefficient of 0.5 at 693 GHz which confirms the result obtained with the mirror. With the 50 μm thick Mylar beam splitter the noise temperature is approximately $\times 1.5$ higher than with the 12 μm thick beam splitter. This factor is close to the one obtained from calculations of the thin film beam splitter [20].

Apparent problem with the utilized IF LNA prevented obtaining an accurate receiver noise temperature data in the whole range up to 4.5 GHz. However, the noise bandwidth seems to be more than 6–8 GHz. This is still narrower than expected for a 6 GHz gain bandwidth obtained for devices made of similar films [9]. We believe that replacement of the LNA will solve this issue.

Another direction for improvements is optimization of the MgB_2 thin film deposition and the HEB fabrication techniques in a way to reduce the superconducting transition width. For batch E8 the transition width is approximately 4 K with a double transition structure. Such feature appears only in our thinnest films. Considering a greatly reduced RRR in the micron size HEBs (1.3 against 2 for films, see also [19]), we conclude that there is a significant concentration of defects in the film on the micrometer scale.

V. CONCLUSION

A receiver noise temperature of 1600 K has been demonstrated for MgB_2 HEB mixers at 15 K operation temperature and at a 693 GHz LO. Devices were made from a 10 nm thick film, similar to the one for which a 6 GHz gain bandwidth has been obtained [9]. The noise bandwidth is currently in a range of 6–8 GHz, limited by the IF amplifier.

REFERENCES

- [1] F. Arams *et al.*, "Millimeter mixing and detection in bulk InSb," *Proc. IEEE*, vol. 54, no. 4, pp. 612–622, Apr. 1966.
- [2] E. M. Gershenzon *et al.*, "Heating of electrons in superconductor in the resistive state due to electromagnetic radiation," *Solid State Commun.*, vol. 50, no. 3, pp. 207–212, Apr. 1984.
- [3] J. Kawamura *et al.*, "An 800 GHz NbN Phonon-cooled Hot-electron bolometer mixer receiver," *IEEE Trans. Appl. Supercond.*, vol. 9, no. 2, pp. 3753–3756, Jun. 1999.
- [4] D. Meledin *et al.*, "A 1.3 THz balanced waveguide HEB mixer for the APEX telescope," *IEEE Trans. Microw. Theory Tech.*, vol. 57, no. 1, pp. 89–98, Jan. 2009.
- [5] C. Risacher *et al.*, "First supra-THz heterodyne array receivers for astronomy with the SOFIA Observatory," *IEEE Trans. THz Sci. Technol.*, vol. 6, no. 2, pp. 199–211, Mar. 2016.
- [6] Th. de Graauw *et al.*, "The Herschel-Heterodyne Instrument for the Far-Infrared (HIFI)," *Astron. Astrophys.*, vol. 518, Jul.–Aug. 2010, Art. no. L6.
- [7] Y. Gousev *et al.*, "Broadband ultrafast superconducting NbN detector for electromagnetic radiation," *J. Appl. Phys.*, vol. 75, pp. 3695–3697, Apr. 1994.
- [8] S. Svechnikov *et al.*, "Spiral antenna NbN hot-electron bolometer mixer at submm frequencies," *IEEE Trans. Appl. Supercond.*, vol. 7, no. 2, pp. 3395–3398, Jun. 1997.
- [9] E. Novoselov *et al.*, " MgB_2 hot-electron bolometer mixers for THz heterodyne instruments," *Proc. SPIE*, vol. 9914, Jul. 2016, Art. no. 99141N.
- [10] M. Kroug *et al.*, "NbN hot electron bolometric mixers for terahertz receivers," *IEEE Trans. Appl. Supercond.*, vol. 11, no. 1, pp. 962–965, Mar. 2001.
- [11] W. Zhang *et al.*, "Quantum noise in a terahertz hot electron bolometer mixer," *Appl. Phys. Lett.*, vol. 96, Mar. 2010, Art. no. 111113.
- [12] H. Ekström *et al.*, "Gain and noise bandwidth of NbN hot-electron bolometric mixers," *Appl. Phys. Lett.*, vol. 70, Jun. 1997, Art. no. 3296.
- [13] S. Cherednichenko *et al.*, "Terahertz mixing in MgB_2 microbolometers," *Appl. Phys. Lett.*, vol. 90, no. 2, Jan. 2007, Art. no. 023507.
- [14] H. Shibata *et al.*, "Ultrathin MgB_2 films fabricated by molecular beam epitaxy and rapid annealing," *Supercond. Sci. Technol.*, vol. 26, no. 3, Mar. 2013, Art. no. 035005.
- [15] E. Novoselov *et al.*, "Effect of the critical and operational temperatures on the sensitivity of MgB_2 HEB mixers," *IEEE Trans. THz Sci. Technol.*, vol. 6, no. 2, pp. 238–244, Mar. 2016.
- [16] X. X. Xi *et al.*, " MgB_2 thin films by hybrid physical-chemical vapor deposition," *Phys. C Supercond.*, vol. 456, no. 1/2, pp. 22–37, Jun. 2007.
- [17] D. Cunnane *et al.*, "Characterization of MgB_2 superconducting hot electron bolometers," *IEEE Trans. Appl. Supercond.*, vol. 25, no. 3, Jun. 2015, Art. no. 2300206.
- [18] D. Cunnane *et al.*, "Development of hot-electron THz bolometric mixers using MgB_2 thin films," *Proc. SPIE*, vol. 9153, Jul. 2014, Art. no. 91531Q.
- [19] E. Novoselov, N. Zhang, and S. Cherednichenko, "Study of MgB_2 ultrathin films in submicron size bridges," *IEEE Trans. Appl. Supercond.*, vol. 27, no. 4, Jun. 2017, Art. no. 7500605.
- [20] P. F. Goldsmith, *Quasioptical Systems: Gaussian Beam Quasioptical Propagation and Applications*. Hoboken, NJ, USA: Wiley, 1997.

Paper G

Low noise terahertz MgB₂ hot-electron bolometer mixers
with an 11 GHz bandwidth

E. Novoselov and S. Cherednichenko

Applied Physics Letters, vol. 110, no. 3, January 2017, Art. no.
032601.

Low noise terahertz MgB₂ hot-electron bolometer mixers with an 11 GHz bandwidth

E. Novoselov^{a)} and S. Cherednichenko^{a),b)}

Terahertz and Millimetre Wave Laboratory, Department of Microtechnology and Nanoscience, Chalmers University of Technology, SE-412 96 Gothenburg, Sweden

(Received 16 December 2016; accepted 6 January 2017; published online 17 January 2017)

Terahertz (THz) hot-electron bolometer mixers reach a unique combination of low noise, wide noise bandwidth, and high operation temperature when 6 nm thick superconducting MgB₂ films are used. We obtained a noise bandwidth of 11 GHz with a minimum receiver noise temperature of 930 K with a 1.63 THz Local Oscillator (LO), and a 5 K operation temperature. At 15 K and 20 K, the noise temperature is 1100 K and 1600 K, respectively. From 0.69 THz to 1.63 THz, the receiver noise increases by only 12%. Device current-voltage characteristics are identical when pumped with LOs from 0.69 THz up to 2.56 THz, and match well with IVs at elevated temperatures. Therefore, the effect of the THz waves on the mixer is totally thermal, due to absorption in the π conduction band of MgB₂. © 2017 Author(s). All article content, except where otherwise noted, is licensed under a Creative Commons Attribution (CC BY) license (<http://creativecommons.org/licenses/by/4.0/>). [<http://dx.doi.org/10.1063/1.4974312>]

Low noise terahertz (THz) heterodyne receivers are utilized to detect the molecular emission lines from stars and interstellar medium, as well as for continuum observations, provided a large intermediate frequency (IF) bandwidth is available (several GHz). For frequencies of <1 THz, Superconductor-Insulator-Superconductor (SIS) tunnel junction mixing provides sensitivity at a level of 2–5 photon energies. However, >1 THz superconducting Hot-Electron Bolometer (HEB) mixers are the device of choice.¹ Although HEB mixers² are traditionally made of the same materials as SIS mixers, HEB mixers do not have any upper frequency operation limit and have been proven to work at least up to 5 THz.³ Despite the apparent advantage over SIS, HEB mixers show an excellent noise performance in a rather limited IF band: the 3 dB noise bandwidth (NBW) of NbN HEB mixers (currently, the most frequently used HEB mixers) is not more than 4–5 GHz.^{4–6} The IF range >5 GHz becomes unusable. The discussed limitation of NbN HEB mixers is determined by the limited HEB mixer gain bandwidth (GBW) caused by a finite electron energy relaxation rate.

Hot electrons in NbN films cool via two sequential processes: inelastic electron-phonon scattering ($\tau_{e-ph} = 12$ ps at 10 K,⁷ which is a typical critical temperature, T_c for thin NbN films) and phonon escape to the substrate ($\tau_{esc}(\text{ps}) = 10 \times d(\text{nm})$),⁸ where d is the film thickness in nm). Critical temperature drops substantially in very thin films, thus setting a technological limit for the NbN HEB mixer.

Since the electron-phonon interaction time in MgB₂ was observed to be approximately 1–2 ps,⁹ thin MgB₂ films were suggested for HEB mixers.¹⁰ With a critical temperature, T_c of 39 K in bulk films as thin as 20 nm with a T_c of 20–22 K have been fabricated using Molecular Beam Epitaxy (MBE).¹¹ Apart from a short electron-phonon interaction time, a very good acoustic match between MgB₂ films and substrates was

observed, with a gain bandwidth of 2 GHz for 20 nm thick MgB₂ films.¹⁰ Although a Double Sideband (DSB) receiver noise temperature, T_r of 700 K has been demonstrated at both 0.6 THz (Ref. 12) and 1.6 THz,¹³ these devices were made of MgB₂ films with a T_c of 9 K, and the noise bandwidth (NBW) (the IF where T_r rises $\times 2$ of its value at zero IF) did not exceed 3.5 GHz. Using 20 nm MgB₂ films with a T_c of 22 K, T_r of 1700 K was achieved with a NBW of 5 GHz.¹³ Reduction of the film thickness below 20 nm led to a drop of T_c . The next step forward was made with MgB₂ thin films deposited by Hybrid Physical Chemical Vapor Deposition (HPCVD) and 10–20 nm thick films with a $T_c = 33$ K–37 K have been obtained. This resulted in a GBW of 6–8 GHz (compared to 2–3 GHz for NbN HEB mixers).^{14,15} Further improvement in MgB₂ film deposition has been shown in Ref. 16. Initially thicker MgB₂ films (40 nm) were thinned down to 2 nm with a T_c of 28 K. Yet no mixers have been fabricated of such films. In our paper, we demonstrate MgB₂ HEB mixers made of very thin films (~6 nm). These mixers combine a low noise temperature, wide IF bandwidth, and a high operation temperature.

For MgB₂ film deposition, we utilized the HPCVD method.¹⁷ Our deposition system with the key parameter optimization has been presented in Ref. 18. The diborane (5% of B₂H₆ in H₂) and hydrogen flows were 2–5 sccm and 400 sccm, respectively, with a process pressure of 20 Torr. The substrate was SiC, with only a 0.42% lattice mismatch to the c-axis oriented MgB₂. Film thickness was proportional to the deposition time, times the diborane flow, as has been verified using Transmission Electron Microscopy (TEM) on 10 nm and 20 nm thick films, and using a profilometer and an atomic force microscope (AFM) for thicker films. At the discussed thicknesses, the deposition rate is approximately 0.8–0.9 Å/s for a diborane flow of 2 sccm. For the deposition time of 70 s, the estimated film thickness is approximately 6 nm. Unprocessed MgB₂ films had a T_c of 35–36 K, a room temperature sheet resistance, R_S of 50 Ω/sq , and a residual resistance ratio (RRR) of 2.5 (tested with films on small

^{a)}E. Novoselov and S. Cherednichenko contributed equally to this work.

^{b)}Electronic mail: serguei@chalmers.se

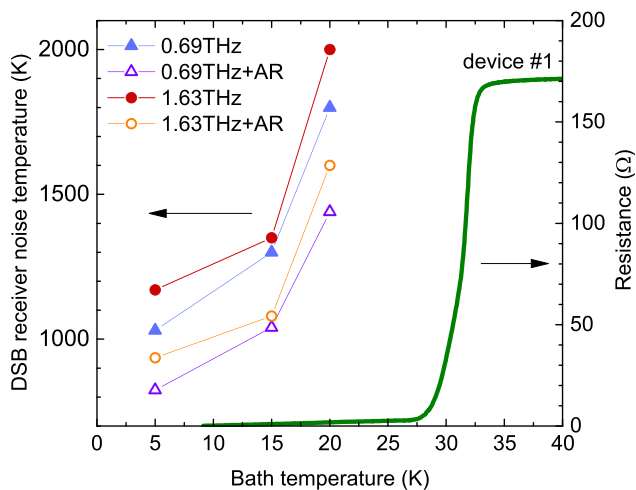


FIG. 1. Resistance versus temperature (R-T) curve for device #1 (line). Summary of the receiver noise temperature at 0.69 THz (triangles) and 1.63 THz (circles). Empty symbols are for T_r corrected for the Si lens AR coating effect.

witness substrates). Directly after MgB_2 film deposition, the substrate was transferred (with a vacuum break) to a magnetron sputtering system, where, after a 10 min Ar-ion cleaning, a 20 nm Au layer was deposited. Preliminary tests showed that a cleaning process of 25 min increases the film sheet resistance (at room temperature) by 5%–10%. This cleaning step appears to be vital for achieving low noise temperature at THz frequencies.

HEB mixers are essentially microbridges from $0.3 \mu\text{m} \times 0.3 \mu\text{m}$ to $1 \mu\text{m} \times 1 \mu\text{m}$ size, integrated with a logarithmic spiral antenna. The antenna is made of a 250 nm thick gold film. The 20 nm gold layer on top of the microbridge is removed using an ion-milling process. The exposed MgB_2 film is protected with a thin SiN_x layer. The critical temperature of the devices was 30 K (see Figure 1 for the R-T curve of device#1, however, similar R-T curves have been measured for all samples of the batch). The critical current density at 4.2 K was $(1.2\text{--}2.0) \times 10^7 \text{ A/cm}^2$ (see Figure 2). Although such a high J_c indicates thin MgB_2 films of high quality, some scattering of the critical currents and normal

state resistances probably points to some variations of film defects/thickness across the substrate. Published morphology studies of 5–10 nm thick MgB_2 films, also made with HPCVD, showed¹⁷ that MgB_2 films were not fully connected, and that there were gaps of tens of nanometers between islands of MgB_2 for films thinner than 15 nm. We have not yet been able to conduct morphology studies on our films; however, it appears that in our case, MgB_2 films merge into a continuous structure at smaller thicknesses than previously reported. This could be caused by a significantly lower deposition rate in our system, compared to e.g. (3 Å/s).¹⁹ As the result, we were able to fabricate the submicron size devices with $T_c > 30 \text{ K}$ from films thinner than 10 nm.

Two $1 \mu\text{m} \times 1 \mu\text{m}$ size mixers were tested at THz frequencies. These had room temperature resistances of 205 Ω and 230 Ω . Current-voltage (IV) characteristics for device #1 are given in Figure 2. For device #2, the $I_c(4.2 \text{ K})$ was 0.97 mA, with very similar IVs (under THz radiation), noise temperature and the bandwidth as for device #1. Therefore, a further discussion will concern only device #1. R_S obtained from the micro bridges appear to be a factor of 4 higher than for the unprocessed films (see above). The increase of R_S is in line with a reduction of T_c by 4 K. More study is needed to find out whether both effects originate in the device fabrication procedure, or are due to micro defects in the original films, which appear on the micrometer scale. 15–20 nm thick MgB_2 films did not show significant variation of film properties before or after device fabrication.

In order to measure the HEB mixer sensitivity at THz frequencies, the chip with the antenna integrated HEB was attached to the back (flat) side of a 5 mm elliptical Si lens (without an antireflection coating,²⁰ which could reduce the optical loss by 0.8 dB (Ref. 21)). Apart from the Si lens and the chip, the mixer block contained a transition to an SMA connector and a heater. In front of the mixer block, the beam was collimated with an off-axis parabolic aluminum mirror, also mounted in the cryostat. The actual HEB temperature was obtained from a comparison of the critical current, I_c in the mixer block with that obtained in the dip-stick. The IF chain consisted of a bias-T and a cryogenic Low Noise Amplifier

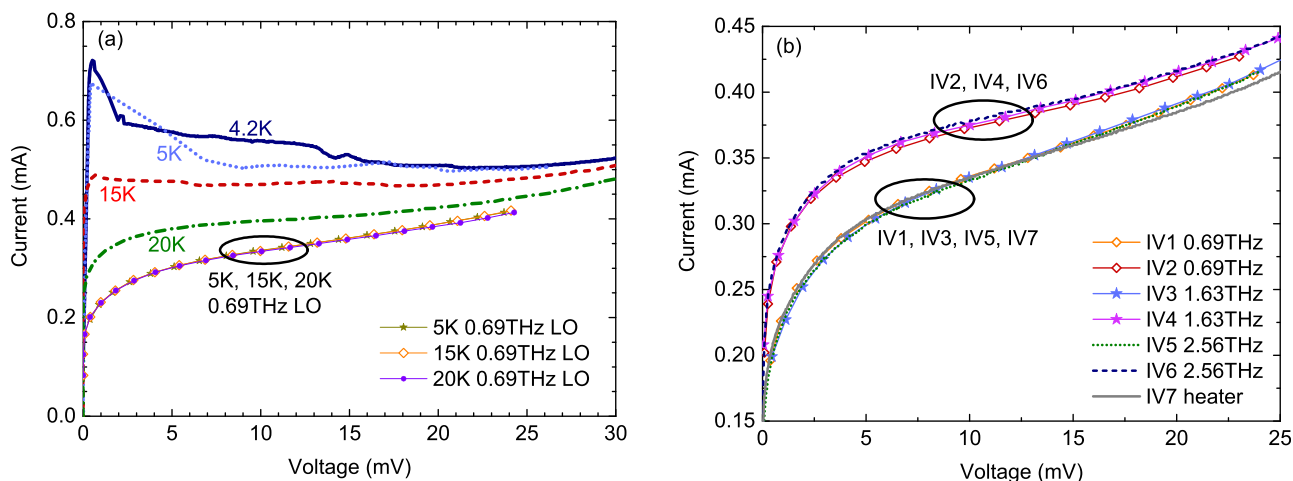


FIG. 2. (a) The mixer IV-curves (light blue dotted) without LO pumping at 4.2 K (in the dip-stick), in the cryostat at 5 K (no LO, blue solid), at 15 K (no LO, red dashed), at 20 K (no LO, green dash-dotted). Three (fully overlapping) IVs at the optimal LO power at 5 K, 15 K; and 20 K. (b) two sets of IVs at different LO power levels, all at 5 K: under the 0.69 THz, 1.63 THz, and 2.56 THz LO pumping. No difference between curves pumped with the mentioned LOs can be observed. IV7 (grey solid) is recorded for the HEB at an elevated temperature without LO pumping.

TABLE I. Optical loss included in the receiver noise temperature measurements: the 50 cm air path, the cryostat window, and the infrared filters. Calibration for Si lens reflection loss is used only in Fig. 1.

Frequency (THz)	Air path (dB)	Window (dB)	IR filters (dB)	Si Reflection (dB) ^a
0.69	0.03	0.7	0.6	1
1.63	0.55	0.7	0.6	1

^aReduction of the Si lens reflection from 1 dB to 0.2 dB can be achieved by application of Parylene C antireflection coating.²¹

(LNA) at 4.2 K, two more LNAs, a tunable band pass YIG filter (50 MHz bandwidth), and a microwave power meter at room temperature. Two sets of LNAs were used with bandwidths of 1.5–4.5 GHz and 1–9 GHz (the noise temperature is ~ 3 –5 K). A Far Infrared (FIR) gas laser was used as the local oscillator, with radiation emission frequencies of 0.69 THz, 1.63 THz, and 2.56 THz. At 2.56 THz, the output power was not sufficient to pump the mixer with a thin beam splitter and hence, it was only used with a mirror to record the IV-curves. Continuously chopped (1 Hz) emissions from 295 K/77 K black body loads were used to measure the DSB receiver noise temperature as per the Y-factor technique. It comprises the mixer noise temperature, the contributions from the IF chain and the input optics loss. A 12.5 μm thick Mylar beam splitter combined the LO and the black body loads into the cryostat. Optical losses included in receiver noise temperature calculations from the Y-factor are given in Table I. The spiral antenna polarization is elliptical, and therefore exact knowledge of the polarization ellipse is required in order to calculate the transmission loss through the beam splitter. Consequently, beam splitter loss was neglected. Although a broadband spiral antenna was used, the direct detection effect²² was not observable presumably due to a larger LO power requirement of the discussed mixers. Furthermore, because the output noise versus the bias current (for a fixed voltage) is positive, a possible (though very small) direct detection effect does not lead to an overestimation of the Y-factor.

Critical current, I_c of the mixer was measured in the dipstick to be 0.72 mA at 4.2 K, whereas I_c was 0.67 mA in the cryostat (5 K). IV curves of the mixer at 4.2 K (dip-stick), and in the cryostat at different temperatures (without LO pumping) are given in Figure 2(a). With optimal LO (0.69 THz) power, the IVs at 5 K, 15 K, and 20 K fully overlap each other, indicating that in the HEB, the LO power at 0.69 THz is absorbed independently of the temperature and the bias voltage. At 5 K, the shape of the IVs was also observed not to depend on the LO frequency from 0.69 THz to 2.56 THz (Figure 2(b)). By switching off the LO and increasing the HEB temperature, IVs can be found to fully match IVs under the LO. In MgB₂ films with a T_c of ~ 30 K (similar to those discussed here) superconducting energy gaps, $\Delta(0)$ of 2.2 meV and 5 meV have been reported for π - and σ - conduction bands, respectively.²³ With optical gaps of 2Δ , the THz photon absorption should therefore occur in the π -band (see also Ref. 24), where $2\Delta/h \approx 1$ THz, and thus explain the IVs in Figure 2(a) (h is the Planck constant). Laser output power was higher at 0.69 THz, therefore most of the experimental data were obtained at this LO frequency. A set of IVs during

LO pumping is given in Figure 3(a). The corresponding receiver output noise curves (all under the 295 K load) and the optimal noise temperature curve are given in Figure 3(b). The shapes of the curves correspond with those of low-Tc HEB mixers, e.g., made of NbN.²⁵ Being also supported by other facts (no effect of LO frequency on IVs, a weak LO frequency dependence of T_r (see below)) we may conclude that the mixing response has a bolometric nature. The minimum on the T_r -V curve was found in the 5–10 mV bias voltage range.

A summary of the measured T_r at both 0.69 THz and 1.63 THz LO frequencies at mixer temperatures of 5 K, 15 K, and 20 K is given in Figure 1. Considering a reduction of the reflection loss at the Si lens by 20% when an AR coating is used,²¹ the minimum noise temperatures at 5 K amount to 830 K (0.69 THz) and 930 K (1.63 THz). At 15 K, T_r rises by 20% from its value at 5 K. At 20 K, T_r rises by 75%. As can be noticed, the noise temperature difference between 0.69 THz and 1.63 THz is about 12%. A similar rate of T_r increase vs. LO frequency has been observed for NbN HEB mixers for LOs > 1 THz.²⁶

Detailed study of mixer conversion gain and noise versus operation temperature, and due comparison with the

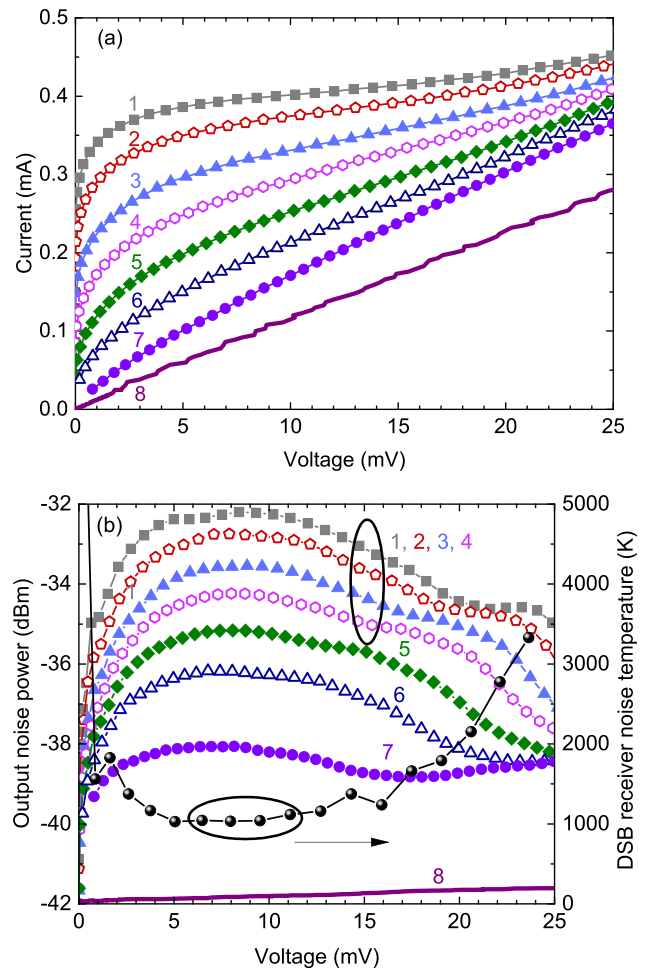


FIG. 3. (a) The mixer IV-curves at 5 K under the 0.69 THz LO pumping (curves 1–7), and without LO in the normal state (≈ 35 K) (curve 8). (b) The output power (IF = 2 GHz) versus voltage curves corresponding to the IVs in (a). IV-curves 3–5 correspond to the lowest T_r (optimal LO power). The receiver noise temperature versus voltage curve corresponds to IV-curve 3.

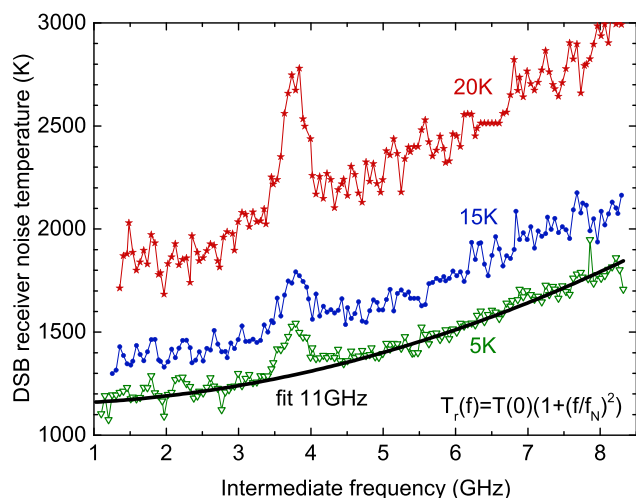


FIG. 4. The receiver noise (at 1.63 THz LO) as a function of the IF recorded at 5 K, 15 K, and 20 K operation temperatures.

theory is beyond the scope of this paper. However, it is interesting to discuss some of the data provided by Figures 3(a) and 3(b). In order to acquire intrinsic mixer parameters, a U-factor technique with a HEB in normal state (as a reference state) can be utilized.¹³ With the HEB at 5 K and at minimum noise temperature point, the U-factor is ~ 8.5 dB (Figure 3(b), curves 3 and 7), which gives a T_{out} of ~ 210 K. An output noise of 40 K–50 K has been reported for NbN HEB mixers with a T_c of 9 K.²⁶ At optimal bias point, T_{out} for HEB mixers is expected to be affected by two contributions: the temperature fluctuations noise ($\propto T_c^2$), and the Johnson noise ($\propto T_c$). Therefore, the obtained output noise temperature for MgB₂ mixers falls into the expected range. With both the receiver noise temperature and the output noise at hand, we can estimate the mixer gain to be approximately -9 dB (the optical loss is not included in this figure).

The T_{out} of 210 K is higher than the previously reported 80 K for devices made of MgB₂ film with a T_c of 22 K.¹³ We explain this fact by the higher T_c (30 K vs. 22 K) used in the current work (see discussion above). The increased mixer gain from -15 dB (from Ref. 13) to -9 dB (this work) can be attributed to the same increase of the T_c (leading to a higher LO power, and hence to the mixer gain²⁷), as well as to the reduced antenna/HEB contact resistance achieved with in-situ cleaning. High mixer gain and high output noise is a preferred combination for heterodyne receivers, because it reduces the effect of the LNA noise in the IF readout.

Perhaps, the most interesting data presented here is the IF spectrum of the receiver noise temperature. Previously, a 3 dB GBW of 6–8 GHz had been reported for devices made of 10–15 nm thick MgB₂ films.^{14,15} It has also been proven that GBW scales up inversely with film thickness.¹⁵ In our work, T_r was measured across a wide IF range using the afore mentioned two sets of LNAs. The data obtained with the 1–9 GHz LNA and the 1.63 THz LO are given in Figure 4. The data obtained with the 1.5–4.5 GHz LNA (measurements were performed for redundancy) totally repeats these curves, including the hump at 3.7 GHz, which is probably due to the mixer block or the bias-T. The fitting curve is for the noise bandwidth of 10.7 GHz. No bias point effect on the NBW has been observed within the optimal bias range.

In summary, we demonstrated that a combination of low noise temperature (~ 1000 K) and wide noise bandwidth (~ 11 GHz) can be achieved with superconducting MgB₂ HEB mixers. Current devices were made from MgB₂ films as thin as ~ 6 nm with a T_c of ~ 30 K. The small thickness provided the short phonon escape time from the film into the substrate, whereas the high T_c resulted in the short electron-phonon interaction time (which is inversely proportional to the electron temperature at the optimal operation point, $\approx T_c$). A weak dependence of T_r on LO frequency makes us optimistic with regard to the operation of current (or similar) devices at even higher frequencies (the goal is 5 THz).

This work was financially supported by the European Research Council (ERC). The authors wish to thank Professor X. X. Xi and Professor K. Chen of Temple University for valuable discussions on MgB₂ films technology; and personnel of the Nanofabrication Laboratory (Chalmers University of Technology) for technical support.

- ¹H.-W. Hübers, *IEEE J. Sel. Top. Quantum Electron.* **14**, 378–391 (2008).
- ²E. M. Gershenzon, G. N. Gol'tsman, I. G. Gogidze, Y. P. Gusev, A. I. Elant'ev, B. S. Karasik, and A. D. Semenov, *Sov. Phys. Supercond.* **3**, 1582 (1990).
- ³W. Zhang, P. Khosropanah, J. R. Gao, T. Bansal, T. M. Klapwijk, W. Miao, and S. C. Shi, *J. Appl. Phys.* **108**(9), 093102 (2010).
- ⁴S. Cherednichenko, V. Drakinskiy, T. Berg, P. Khosropanah, and E. Kollberg, *Rev. Sci. Instrum.* **79**, 034501 (2008).
- ⁵W. Zhang, W. Miao, J. Q. Zhong, S. C. Shi, D. J. Hayton, N. Vercruyssen, J. R. Gao, and G. N. Gol'tsman, *Supercond. Sci. Technol.* **27**, 085013 (2014).
- ⁶C. Risacher, R. Güsten, J. Stutzki, H.-W. Hübers, D. Büchel, U. U. Graf, S. Heyminck, C. E. Honingh, K. Jacobs, B. Klein, T. Klein, C. Leinz, P. Pütz, N. Reyes, O. Ricken, H.-J. Wunsch, P. Fusco, and S. Rosner, *IEEE Trans. Terahertz Sci. Technol.* **6**, 199–211 (2016).
- ⁷K. S. Il'in, M. Lindgren, M. Currie, A. D. Semenov, G. N. Gol'tsman, R. Sobolevski, S. I. Cherednichenko, and E. M. Gershenzon, *Appl. Phys. Lett.* **76**, 2752 (2000).
- ⁸S. Cherednichenko, P. Yagoubov, K. Il'in, G. Gol'tsman, and E. Gershenzon, in *Proceedings of 27th European Microwave Conference, Jerusalem, Israel*, 8–12 September 1997, pp. 972–977.
- ⁹Y. Xu, M. Khafizov, L. Satrapiskiy, P. Kùš, A. Plecenik, and R. Sobolevski, *Phys. Rev. Lett.* **91**, 197004 (2003).
- ¹⁰S. Cherednichenko, V. Drakinskiy, K. Ueda, and M. Naito, *Appl. Phys. Lett.* **90**, 023507 (2007).
- ¹¹H. Shibata, T. Akazaki, and Y. Tokura, *Supercond. Sci. Technol.* **26**, 035005 (2013).
- ¹²S. Bevilacqua, E. Novoselov, S. Cherednichenko, H. Shibata, and Y. Tokura, *IEEE Trans. Appl. Supercond.* **25**, 2301104 (2015).
- ¹³E. Novoselov, S. Bevilacqua, S. Cherednichenko, H. Shibata, and Y. Tokura, *IEEE Trans. Terahertz Sci. Technol.* **6**, 238–244 (2016).
- ¹⁴D. Cunnane, J. H. Kawamura, M. A. Wolak, N. Acharya, T. Tan, X. X. Xi, and B. S. Karasik, *IEEE Trans. Appl. Supercond.* **25**, 2300206 (2015).
- ¹⁵E. Novoselov, N. Zhang, and S. Cherednichenko, *Proc. SPIE* **9914**, 99141N (2016).
- ¹⁶N. Acharya, M. A. Wolak, T. Tan, N. Lee, A. C. Lang, M. Taheri, D. Cunnane, B. S. Karasik, and X. X. Xi, *APL Mater.* **4**, 086114 (2016).
- ¹⁷X. X. Xi, A. V. Pogrebnyakov, S. Y. Xu, K. Chen, Y. Cui, E. C. Maertz, C. G. Zhuang, Q. Li, D. R. Lamborn, J. M. Redwing, Z. K. Liu, A. Soukiassian, D. G. Schlom, X. J. Weng, E. C. Dickey, Y. B. Chen, W. Tian, X. Q. Pan, S. A. Cybart, and R. C. Dynes, *Phys. C* **456**, 22–37 (2007).
- ¹⁸E. Novoselov, N. Zhang, and S. Cherednichenko, "Study of MgB₂ ultra-thin films in submicron size bridges," *IEEE Trans. Appl. Supercond.* (published online).
- ¹⁹M. A. Wolak, N. Acharya, T. Tan, D. Cunnane, B. S. Karasik, and X. X. Xi, *IEEE Trans. Appl. Supercond.* **25**, 7500905 (2015).

- ²⁰A. J. Gatesman, J. Waldman, M. Ji, C. Musante, and S. Yngvesson, *IEEE Microwave Guided Wave Lett.* **10**, 264–266 (2000).
- ²¹M. Kroug, S. Cherednichenko, H. Merkel, E. Kollberg, B. Voronov, G. Gol'tsman, H.-W. Hubers, and H. Richter, *IEEE Trans. Appl. Supercond.* **11**, 962 (2001).
- ²²S. Cherednichenko, V. Drakinskiy, T. Berg, E. L. Kollberg, and I. Angelov, *IEEE Trans. Microwave Theory Tech.* **55**, 504–510 (2007).
- ²³M. Putti, M. Affronte, C. Ferdeghini, P. Manfrinetti, C. Tarantini, and E. Lehmann, *Phys. Rev. Lett.* **96**, 077003 (2006).
- ²⁴M. Ortolani, P. Dore, D. Di Castro, A. Perucchi, S. Lupi, V. Ferrando, M. Putti, I. Pallecchi, C. Ferdeghini, and X. X. Xi, *Phys. Rev. B* **77**, 100507R (2008).
- ²⁵J. Kawamura, R. Blundell, C. E. Tong, G. Gol'tsman, E. Gershenson, B. Voronov, and S. Cherednichenko, *Appl. Phys. Lett.* **70**, 1619 (1997).
- ²⁶W. Zhang, P. Khosropanah, J. R. Gao, E. L. Kollberg, K. S. Yngvesson, T. Bansal, R. Barends, and T. M. Klapwijk, *Appl. Phys. Lett.* **96**, 111113 (2010).
- ²⁷B. S. Karasik and A. I. Elantiev, *Appl. Phys. Lett.* **68**, 853 (1996).

Paper H

Gain and noise in THz MgB₂ hot-electron bolometer mixers with a 30 K critical temperature

E. Novoselov and S. Cherednichenko

submitted to *IEEE Transactions on Terahertz Science and Technology*, April 2017.

Gain and Noise in THz MgB₂ Hot-Electron Bolometer Mixers with a 30K Critical Temperature

Evgenii Novoselov and Sergey Cherednichenko

Abstract—Superconducting hot-electron bolometer mixers made from ultrathin MgB₂ films have demonstrated a low noise performance at THz frequencies with a large intermediate frequency (IF) bandwidth (11GHz). In this paper, we study variation of the mixer characteristics such as noise temperature, gain, output noise, and local oscillator (LO) power at 5K, 15K, and 20K bath temperatures, and at 0.7THz and 1.6THz Local Oscillator frequencies. The main reason for the noise temperature rising at higher temperatures is a reduction of the mixer gain, which occurs proportionally to the LO power reduction. Contrary to this, the output noise remains constant (for the same bias point).

Index Terms—Hot-electron bolometer, HPCVD, magnesium diboride, mixer, superconductivity, thin film.

I. INTRODUCTION

Superconducting hot-electron bolometer (HEB) mixers made from thin MgB₂ films have demonstrated a noise temperature of ~1000K and a noise bandwidth of 11GHz at local oscillator (LO) frequencies of 0.69THz and 1.63THz [1]. When comparing previously published results [2]-[7], this progress was made owing to advances in thin MgB₂ films deposition by Hybrid Physical Chemical Vapor Deposition (HPCVD), where films thinner than 10nm with a critical temperature (T_c) above 30K have been obtained [8]-[11]. When the mixer operation temperature was raised from 5K to 15K only a small increase of the receiver noise temperature has been observed (20%). However, when the mixer temperature was increased to 20K, the noise temperature rose by another 50%. The origin of this effect is of great importance to future HEB performance improvement. In the current paper, we study how the major HEB mixer characteristics, such as the noise temperature, the gain, the output noise, and the LO power, vary through an operation temperature range of 5K-20K. The mixer parameters most critical to mixer low noise operation up to 20K (or above) are discussed.

II. DEVICES AND SETUP

In this study, mixers from the same batch as reported in Ref.

Manuscript received Feb 20, 2017. This work was supported by the European Research Council (ERC) under the Starting Grant TERAMIX.

E. Novoselov and S. Cherednichenko are with the Department of Microtechnology and Nanoscience (MC2), Chalmers University of

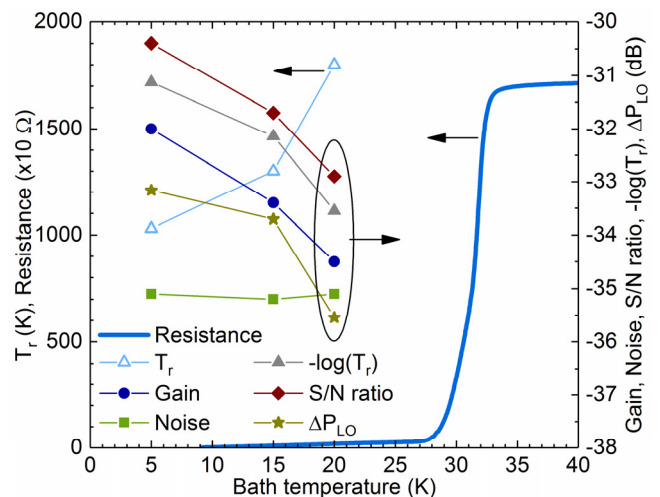


Fig. 1. The mixer noise (squares), the mixer gain (from mixing experiments) (circles), S/N ratio (diamonds), logarithm of T_r^{-1} (triangles), logarithm of LO power (ΔP_{LO}) (stars), and T_r (open triangles), at 0.69THz LO versus temperature. Resistance ($\times 10$) versus temperature (solid line). Mixer characteristics were measured at 7mV and 0.23mA bias for all temperatures.

[1] were used. In brief, MgB₂ films were deposited on SiC substrates using HPCVD [11]. HEB mixers were essentially $1\mu\text{m} \times 1\mu\text{m}$ micro bridges integrated with a 270nm thick gold planar spiral antenna [3]. The MgB₂ film thickness was measured on one of the devices from this batch using Transmission Electron Microscopy (TEM). The measured film thickness of 8nm was slightly higher than the value (6nm) estimated from the deposition rate (obtained for thicker films). The critical temperature in the devices after patterning and dicing was 30K (see Fig. 1).

HEBs were tested in a quasi-optical mixer block with an uncoated 5mm elliptical Si lens. A 30mm diameter off-axis aluminum parabolic mirror collimated the THz beam prior to exit from the cryostat. A bias-T and a low noise IF amplifier (LNA) were mounted in the cryostat. The mixer temperature was varied by means of a resistive heater mounted onto the mixer block. A far infrared (FIR) gas laser was used as the LO. Previously, we have reported [1] that LO pumped current voltage (IV) curves of the discussed devices were the same for LO frequencies of 0.69THz, 1.63THz, and 2.56THz. As the LO

Technology, SE-41296 Göteborg, Sweden (e-mail: evgenii@chalmers.se; sergeui@chalmers.se).

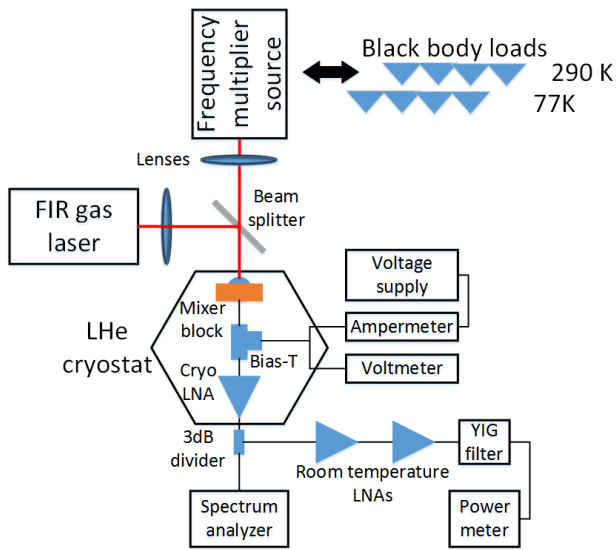


Fig. 2. Measurement setup.

frequency increases from 0.69THz to 1.63THz, rather small growth of the receiver noise temperature (from 830K to 930K) was observed. Therefore, experiments reported here were performed at 0.69THz LO, due to a higher output power being available as compared to e.g. 1.63THz, as well as due to the availability of another 0.69THz tunable source used for the mixing experiments. The receiver noise temperature was measured with the Y-factor technique, using a 295K and a 77K black body emitter (loads). The variation of the mixer (relative) gain was measured with a monochromatic THz test source, based on frequency multipliers [12]. The absolute power of the test source (including mixer-to-source beam mismatch losses) was of no importance at that stage. However, the output power of the test source was kept constant during all experiments. After the cold IF LNA, the IF signal was split into two branches outside the cryostat: 1) with an extra LNA and a tunable band-pass YIG filter (for the Y-factor and the output noise

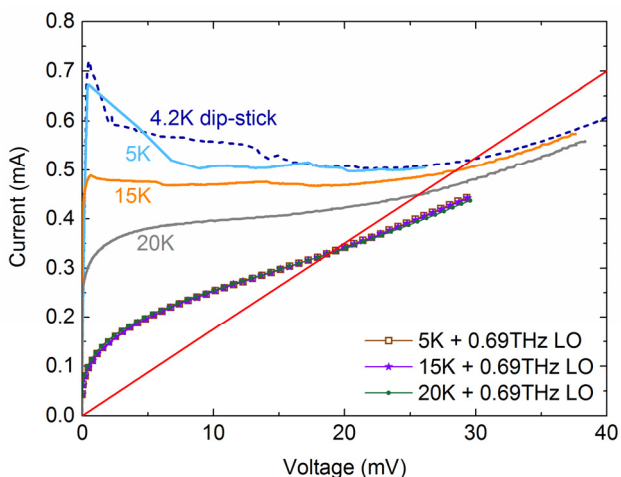


Fig. 3 The mixer IV-curves: at 4.2K (in the dip-stick, dashed); in the cryostat (≈ 5 K, no LO, blue), at 15K (no LO, orange), at 20K (no LO, grey). Three (fully overlapping) IVs at optimal LO power at 5K, 15K; and 20K (open squares, stars, and circles). A straight line is used for LO power calculations by the isothermal method.

measurements); and 2) directly fed into a spectrum analyzer. The YIG-filter was set at a 2GHz (50MHz bandwidth).

The test source frequency was 695.5GHz, i.e. 2.5GHz off-set from the LO, in order to exclude any effect from the test source on the reading from the black body source. For consistency, we accounted for losses in the optical path (the humid air absorption, the cryostat window, and the IR filter) in the receiver noise temperature measurements. Details on optical loss correction are given in Ref. [1]. Neither the Si lens reflection loss nor the beam splitter reflection loss are accounted for. The results for the two tested devices (#1 and #2) from the discussed batch were very similar. Therefore, we concentrated on results from device #1 without loss of generality.

The HEB critical current was 0.67mA at 5K, corresponding to a critical current density of $8.4 \times 10^6 \text{A/cm}^2$. At both 5K and 15K, the IV had a distinct critical current (switch-type IV), whereas at 20K a smooth flux-flow type of IV has been observed (see Fig. 3). The aforementioned critical current density is of the same order of magnitude as reported before for films of the same thicknesses ($\leq 10\text{nm}$) but obtained using a thinning-down technique [9], [10]. Room temperature and residual resistances of the discussed device are 196Ohm and 170Ohm, respectively.

III. RESULTS

A. Bias optimization

Receiver noise temperature was measured using the Y-factor technique at various LO power levels and in a bias voltage range up to 25mV. The corresponding set of IVs (each relates to a certain LO power) is given in Figs. 4a-6a for mixer temperatures 5K, 15K, and 20K. The receiver noise temperature measured along IV-3 (at 5K) is given in Fig. 4a (filled dark cyan squares, right Y-axis). For a bias voltage of 7mV, T_r as a function of mixer current (hence, LO power) is shown in red squares (top X-axis). The lowest noise temperature is obtained for voltages corresponding to the maximum output noise, i.e. 5-10mV. The IV-range for the lowest T_r is marked with the red oval. At 5K, a constant T_r is obtained at a variety of LO powers corresponding to IV-3–IV-5. As the mixer temperature increases, the optimal LO power range shrinks. At 20K the lowest T_r can be achieved at around IV-5 only. The lowest receiver noise temperatures obtained at 5K, 15K, and 20K are plotted in Fig. 1 (open triangles). They correspond to IV-5 (7mV, 200 μ A).

With the second THz source, detuned by 2.5GHz from the LO, the mixing signal P_{if} was recorded for the same IVs along with the receiver output noise power P_{out} :

$$P_{if} = P_s \cdot \frac{1}{L_{opt}} \cdot G_m \cdot G_{if} \quad (1)$$

$$P_{out} = (T_{out} + 2 \cdot 300\text{K} \cdot G_m + T_{if}) G_{if} \cdot B_{if} \quad (2)$$

where L_{opt} is optical loss, G_{if} and T_{if} is IF chain gain and noise, B_{if} is YIG-filter bandwidth, and T_{out} is HEB mixer output noise. Since the incident THz signal power P_s was constant through the

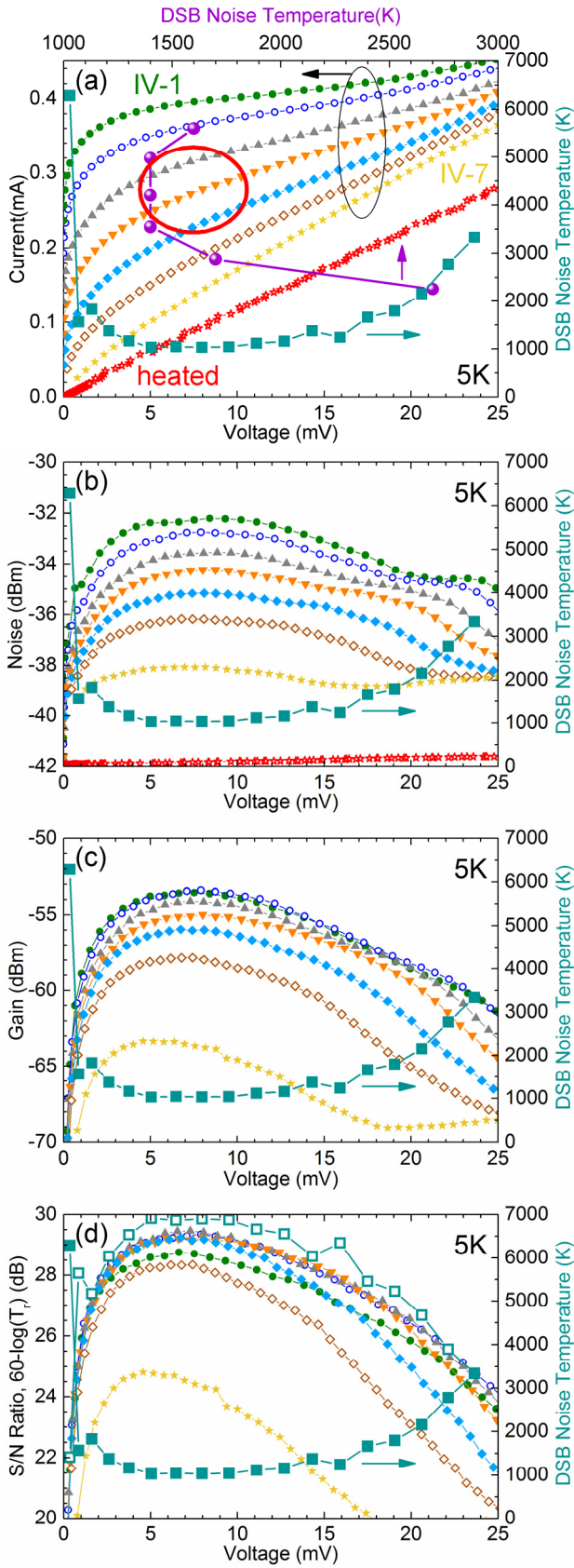


Fig. 4. LO at 0.69THz. T=5K. The area of the highest S/N ratio is marked on the I-V plane.

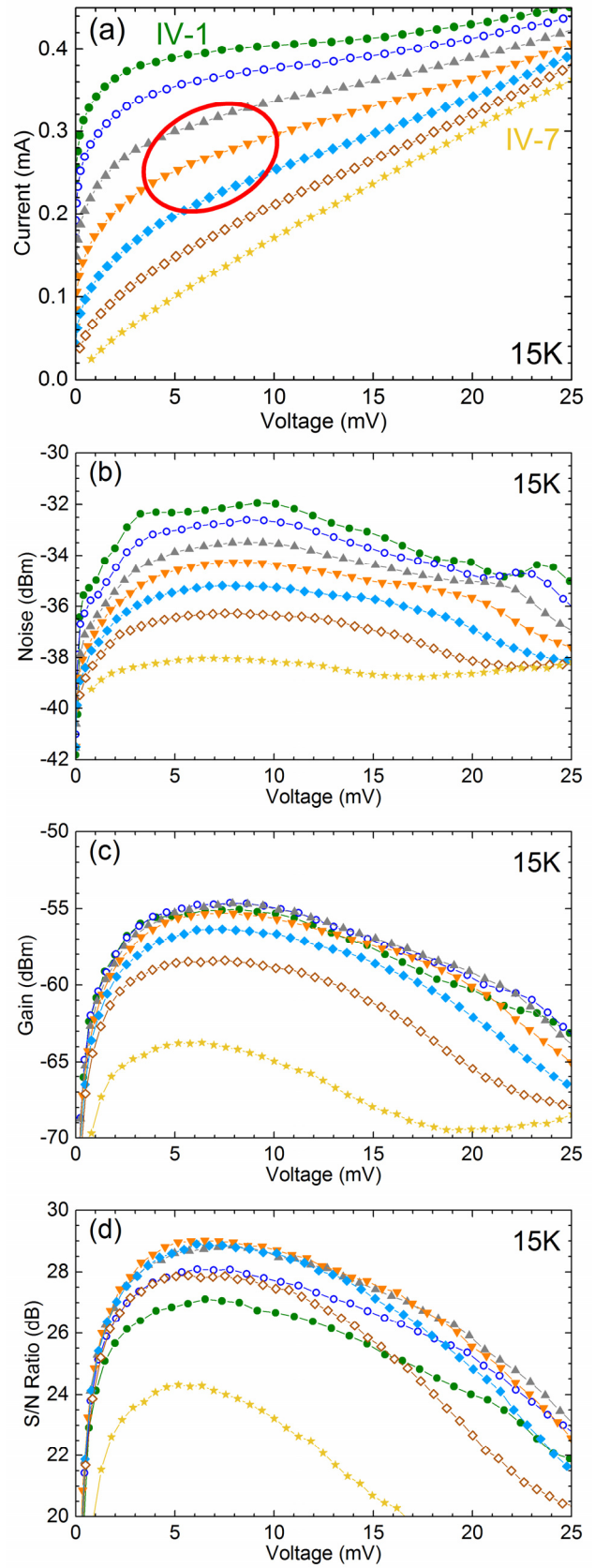


Fig. 5. LO at 0.69THz. T=15K. The area of the highest S/N ratio is marked on the I-V plane.

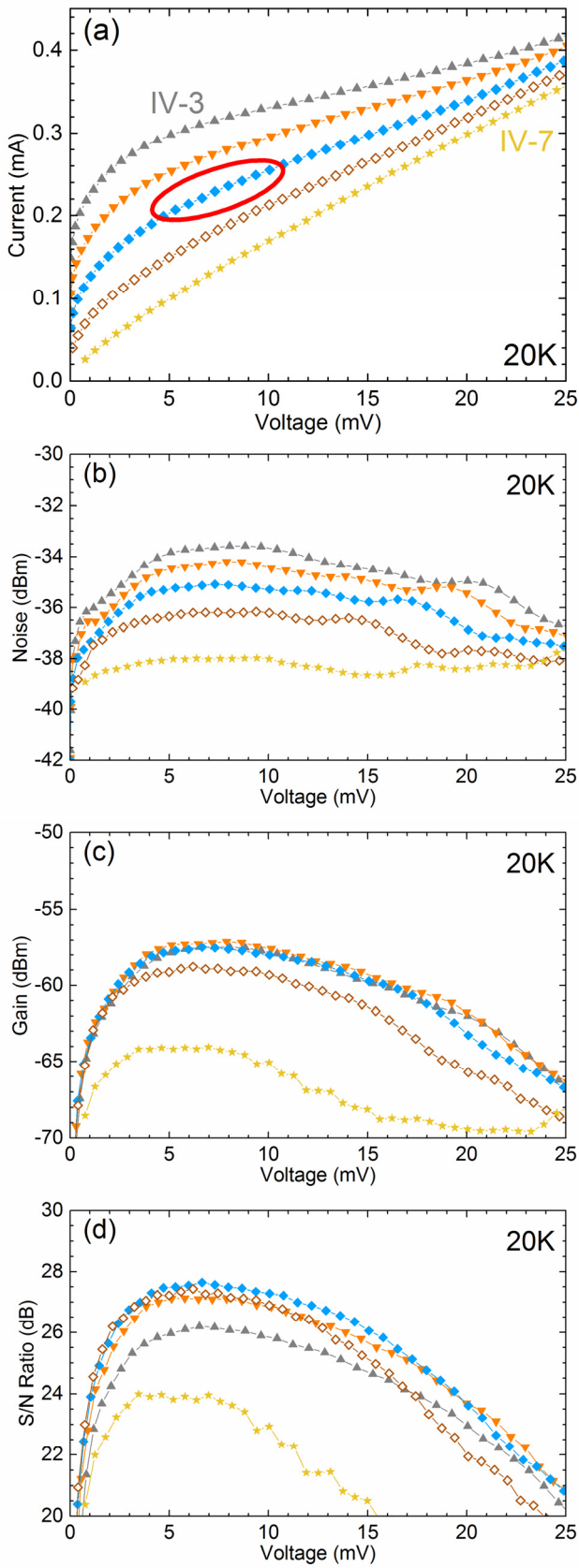


Fig. 6. LO at 0.693GHz. T=20K. The area of the highest S/N ratio is marked on the I-V plane.

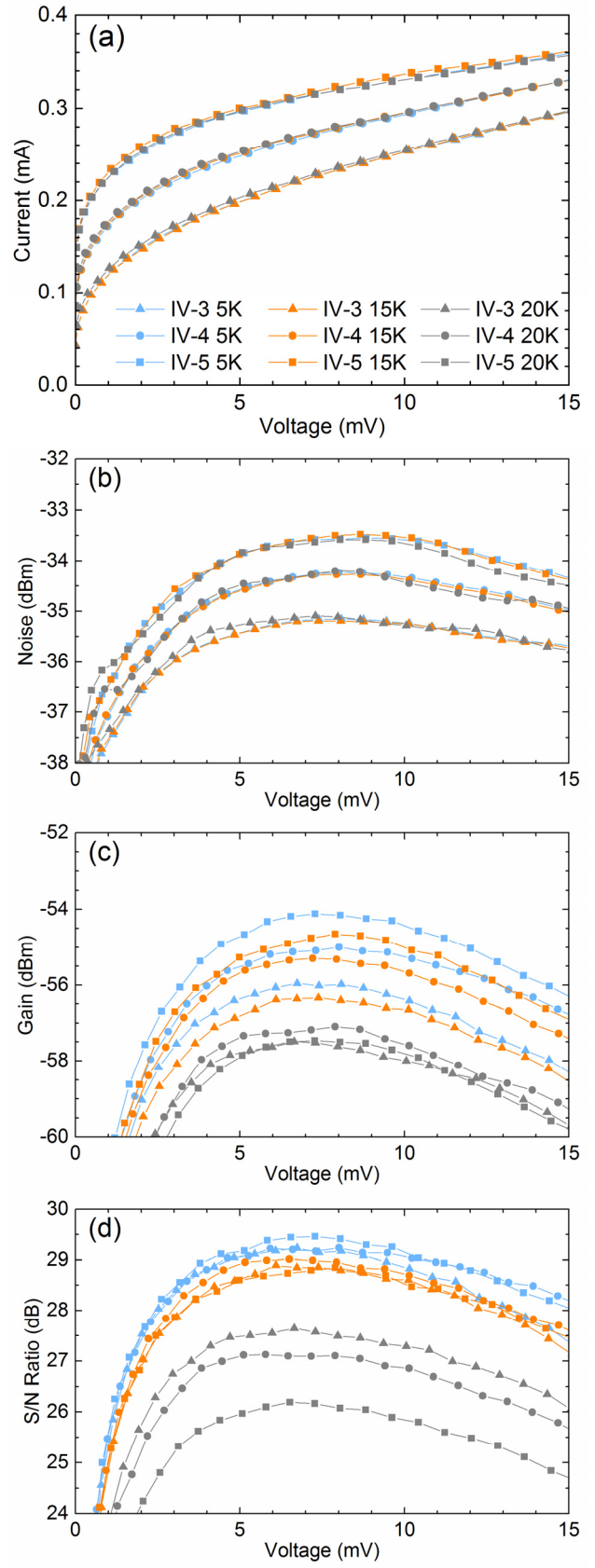


Fig. 7. LO at 0.693GHz. T=5K, 15K, and 20K. Close comparison of the I-V, P-V, G-V, and S/N-V at the bias voltages and LO power levels corresponding to the highest S/N ratio.

whole experiment, variations of the IF signal P_{if} are due to changes of the mixer gain G_m , as shown in (1). Therefore, the mixer gain (in relative units) can be compared at different LO power levels and mixer temperatures (Figs. 4c-6c). In case of $T_{if} \ll T_{out}$, receiver output noise is proportional to mixer output noise temperature, see (2). Therefore, during this experiment we measure both variations of mixer gain and output noise temperature, simultaneously.

For the given set of IVs, which more than covers the optimal LO-bias voltage range, the mixer output noise (Figs. 4b-6b) increases continuously as the LO power is reduced from IV-7 (overpumped HEB) to IV-1 (underpumped HEB). The mixer gain starts to saturate just above IV-3, hence above the optimal bias zone. The resulting signal-to-noise ratio (S/N) (Figs. 4d-6d) has a maximum at IVs-3-5. The $(A \cdot \log(T_r))$ for IV-5 is also plotted in Fig. 4d, where $A=60$ is a free coefficient used to place this curve close to the measured S/N curve. The log-function of $T_r(V)^{-1}$ closely follows the $S/N(V)$ curve, as is expected for the ideal case:

$$\log(S/N) = \log\left(\frac{P_s}{T_r \cdot B_{if} \cdot k}\right) \propto -\log(T_r) \quad (3)$$

where k is the Boltzmann constant. Comparing Fig. 4a and 4d we conclude that bias voltage–LO power optimizations for both S/N and T_r coincide across the IV-plane. This fact demonstrates that, despite the broadband antenna used with the mixer, the “direct detection” effect has no impact on the choice of mixer operation point. The discussed “direct detection” effect is a shift in the HEB bias point when the receiver input load switches from 300K to 77K. In a 3THz band, a black body at 300K (77K) emits approximately 2.8nW (1.6nW) in the single spatial mode [13]. This is about 1% of the optimal LO power for NbN HEB mixers, and hence a switch of the load temperature changes the mixer bias point. For NbN HEB mixers, this effect can be detrimental, either decreasing or increasing the Y-factor, and hence the apparent receiver noise temperature. The effect has been reported to be more pronounced at smaller bias voltages. Our results show that for discussed MgB₂ HEB mixers,

although integrated with a broadband antenna, the direct detection effect is negligible.

Measurements of the S/N ratio allows for a much larger dynamic range compared to the Y-factor. Instabilities of the LO source sometimes lead to receiver output power fluctuations as large as 0.1dB. This fact limits applicability of the Y-factor technique to mixer operation points (IV-plane) corresponding to the highest sensitivity (highest Y-factor). To verify the validity of physical models, experimental data well off the sensitive points would be required. Furthermore, the Y-factor technique can be applied mostly to mixers already having quite good sensitivity, e.g. $T_r < 10000K$ ($Y > 0.1dB$).

B. Mixer characteristics versus temperature

Two types of analyses can be performed in order to compare HEB mixer operation at different temperatures. First, the form of all corresponding I-V, P_{out} -V, and G_m -V curves at 5K, 15K, and 20K is the same (Figs. 4-6). In order to perform a more precise comparison, we plotted three sets of the curves (corresponding to IVs 3-5) on the same figure (Fig. 7). For a certain temperature we find an IV totally matching an IV at another temperature by changing the LO power (Fig. 7a) (see also a discussion in Ref. [1]). For the matching IVs, P_{out} -V curves also totally overlap each other. This may only be possible if the mixer output noise temperature, T_{out} is independent of mixer temperature (for the matching IVs). In Fig. 1, P_{out} (in dBm) is plotted as a function of mixer temperature (all for 7mV and 200 μ A (IV-5, lowest T_r point)).

In contrast to T_{out} , mixer gain decreases at higher temperatures (Fig. 7c and Fig. 1). P_{LO} (in dB) is plotted in Fig. 1 (stars) along with the mixer gain, G_m (in dB) (circles). The absorbed LO was calculated using a constant resistance line, intersecting both the LO pumped and unpumped IVs (the isothermal method [14]). It can be observed that when the bath temperature increases from 5K to 20K, reduction of mixer gain (by 2.5dB) is proportional to reduction of LO power (by 2.4dB) for the given IV, as in fact would be expected considering the classical HEB mixer model [15].

The logarithm of T_r^{-1} , measured using the Y-factor approach, follows exactly the same temperature trend as the S/N ratio, measured using the mixing approach (Fig. 1, filled triangles and diamonds).

Mixer gain (filled circles) and output noise temperature (filled squares), calculated using the U-factor technique with the HEB in the normal state as a reference [3], are plotted in Fig. 8 for 5K, 15K and 20K bath temperatures (all at the same bias point of 7mV and 0.23mA). Mixer gain is inversely proportional to the temperature, whereas output noise remains almost the same. This is also confirmed by the mixing experiment, as can be seen in Fig. 1.

As follows from Figs. 4-5 (corresponding to mixer temperatures of 5K and 15K), receiver noise temperature is constant over quite a wide range of LO power. Across this range (IV5-IV3), both mixer gain and output noise vary by a factor of 2: from 120K to 220K and from -10.7dB to -8.3dB, respectively

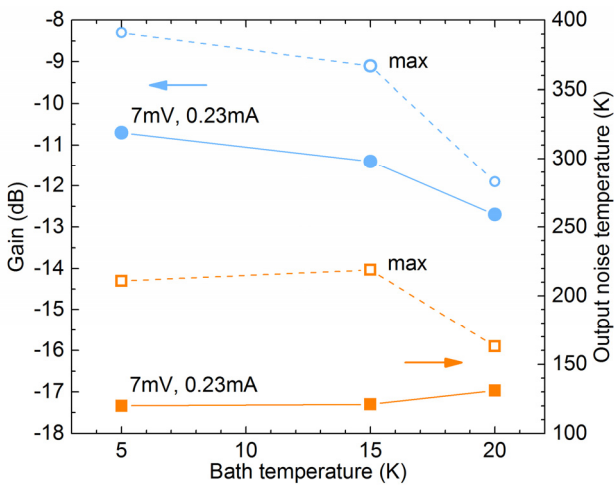


Fig. 8. The mixer gain, G_m (U-factor technique) and the output noise temperature as a function of the bath temperature. Filled symbols are at 7mV and 0.23mA bias point. Open symbols are the maximum output noise temperature and the corresponding mixer conversion gain providing the same receiver noise temperature as at the discussed bias point.

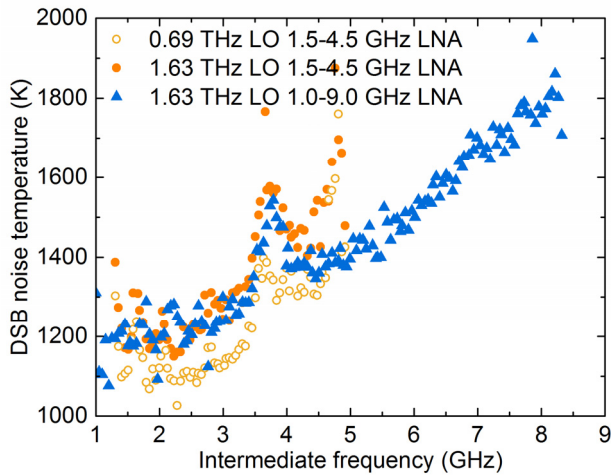


Fig. 9. The receiver noise as a function of the intermediate frequency recorded at 5K. Filled symbols: 1.63THz LO. Open symbols: 0.69THz LO. Circles: 1.5-4.5 GHz LNA. Triangles: 1.0-9.0 GHz LNA.

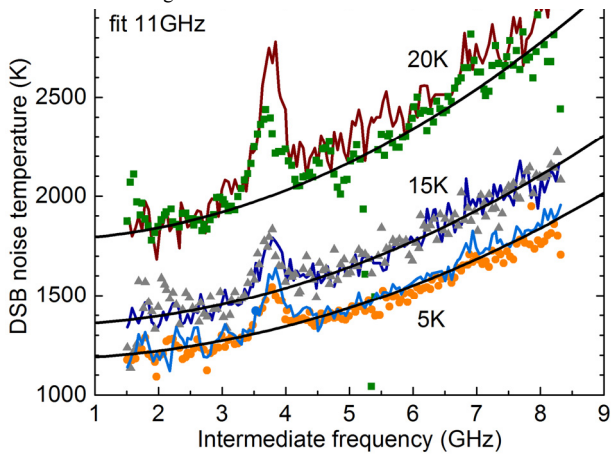


Fig. 10. The receiver noise (at 1.63 THz LO) as a function of the intermediate frequency recorded at 5K, 15K, and 20K operation temperatures. Results for mixers #10-7 (line), and #10-8 (symbols) are shown.

(Fig.8). Apart from a lower LO power, operation at IV3 has an advantage of higher output noise. With an output noise of 220K (see Fig.8), the IF LNA noise becomes much less critical to the overall receiver noise temperature:

$$T_r = \frac{1}{2} \cdot L_{opt} \cdot G_m \cdot (T_{out} + T_{if}) \quad (4)$$

This is particularly important for broadband IF LNAs. LNA optimization can now be focused on input matching rather than on noise, hence eliminating a need for an isolator. In Fig.8 both the maximum output noise temperature and the corresponding mixer gain (within the minimum T_r zone) are plotted for 5K, 15K, and 20K mixer temperatures.

C. The noise bandwidth

To obtain the HEB receiver noise bandwidth (NBW), the Y-factor was measured across a wide IF band with a IF step of 50MHz. Both a 1.5-4.5GHz and a 1.0-9.0GHz IF LNA were used for these experiments. Intentions with measurements using the 1.5-4.5GHz LNA were to verify whether HEB-LNA interference might be affecting the obtained results. In Fig. 9, we show the receiver noise temperature measured with the 1.5-4.5GHz LNA at both 0.69THz and 1.63THz LOs. The noise temperature increases proportionally over the whole IF range,

indicating that NBW is the same at both LOs, and hence supporting the idea of the bolometric nature of the heterodyne response in discussed devices. The noise temperature curve as measured with the 1.5-4.5 GHz LNA fully overlaps with the data obtained using the 1.0-9.0 GHz LNA at the corresponding IFs. The hump, seen at 3.7GHz, is present in both data sets, and hence originates from the bias-T, used for both experiments.

The noise temperature spectrum at 1.63THz LO was measured at 5K, 15K, and 20K for two HEBs from the same batch (Fig. 10). The fitting curves are for an 11GHz noise bandwidth. Curves for both devices totally overlap, hence indicating good reproducibility of results.

IV. CONCLUSIONS

HEB mixers achieve an 11GHz noise bandwidth when 8nm thick MgB_2 films are used with a T_c of $\sim 30K$. The noise bandwidth does not depend on the bath temperature up to 2/3 of T_c . When operation temperature increases, the mixer gain decreases proportionally to the LO power reduction if the same bias point is kept. Simultaneously, mixer output noise does not depend on operation temperature. A high value of the output noise ($\sim 200K$) reduces requirements for the IF LNA noise. This property might appear very useful for reduction of the IF ripples, which occur between the HEB and the LNA due to impedance mismatch. For broadband LNAs input matching (S11) could be as bad as $>3dB$. A 3dB attenuator would increase LNA noise temperature from 5K till 15K without a noticeable degradation of T_r , but will improve the HEB-LNA matching by 6dB.

Experimental verification of MgB_2 HEB mixers with both the Y-factor and mixing techniques coincide fully, thus dismissing the issue of direct detection effect on the measured Y-factor. Furthermore, mixer sensitivity data for a much broader bias voltage and LO power ranges can be obtained compared to the Y-factor technique.

Our preliminary data indicate that MgB_2 HEB mixers can be fabricated with a T_c of 33-34K (quite feasible with an improved fabrication procedure). In this case, receiver noise temperature at 20K will greatly improve. This feature is of particular interest for systems where compact mechanical cryocoolers are required (e.g. for space borne instruments).

REFERENCES

- [1] E. Novoselov and S. Cherednichenko, "Low noise terahertz MgB_2 hot-electron bolometer mixers with an 11 GHz bandwidth," *Appl. Phys. Lett.*, vol. 110, no. 3, Jan. 2017, Art. no. 032601.
- [2] S. Bevilacqua, E. Novoselov, S. Cherednichenko, S. Shibata, and Y. Tokura, " MgB_2 hot-electron bolometer mixers at terahertz frequencies," *IEEE Trans. Appl. Supercond.*, vol. 25, no. 3, Jun. 2015, Art. no. 2301104.
- [3] E. Novoselov, S. Bevilacqua, S. Cherednichenko, S. Shibata, and Y. Tokura, "Effect of the critical and operational temperatures on the sensitivity of MgB_2 HEB mixers," *IEEE Trans. THz Sci. Technol.*, vol. 6, pp. 238-244, Mar. 2016.
- [4] E. Novoselov, N. Zhang, and S. Cherednichenko, " MgB_2 hot-electron bolometer mixers for THz heterodyne instruments," *Proc. SPIE*, vol. 9914, Jul. 2016, Art. no. 99141N.
- [5] E. Novoselov and S. Cherednichenko, "Broadband MgB_2 hot-electron bolometer THz mixers operating up to 20K," *IEEE Trans. Appl. Supercond.*, vol. 27, no. 4, Jun. 2017, Art. no.
- [6] D. Cunane, J.H. Kawamura, M.A. Wolak, N. Acharya, T. Tan, X.X. Xi, and B.S. Karasik, "Characterization of MgB_2 superconducting hot

- electron bolometers," *IEEE Trans. Appl. Supercond.*, vol. 25, no. 3, Jun. 2015, Art. no. 2300206.
- [7] D. Cunnane, J.H. Kawamura, M.A. Wolak, N. Acharya, X.X. Xi, and B.S. Karasik, "Optimization of parameters of MgB₂ hot-electron bolometers," *IEEE Trans. Appl. Supercond.*, vol. 27, no. 4, Jun. 2017, Art. no.
- [8] M.A. Wolak, N. Acharya, T. Tan, D. Cunnane, B.S. Karasik, and X.X. Xi, "Fabrication and characterization of ultrathin MgB₂ films for hot-electron bolometer applications," *IEEE Trans. Appl. Supercond.*, vol. 25, no. 3, Jun. 2015, Art. no. 7500905.
- [9] N. Acharya, M.A. Wolak, T. Tan, N. Lee, A.C. Lang, M. Taheri, D. Cunnane, B.S. Karasik, and X.X. Xi, "MgB₂ ultrathin films fabricated by hybrid physical chemical vapor deposition and ion milling," *APL Mater.*, vol. 4, no. 8, Aug. 2016, Art. no. 086114.
- [10] N. Acharya, M.A. Wolak, T. Melbourne, D. Cunnane, B.S. Karasik, and X.X. Xi, "As-grown versus ion-milled MgB₂ ultrathin films for THz sensor applications," *IEEE Trans. Appl. Supercond.*, vol. 27, no. 4, Jun. 2017, Art. no. 2300304.
- [11] E. Novoselov, N. Zhang, and S. Cherednichenko, "Study of MgB₂ ultrathin films in submicron size bridges," *IEEE Trans. Appl. Supercond.*, vol. 27, no. 4, Jun. 2017, Art. no. 7500605.
- [12] Virginia Diodes, Inc [Online]. Available: <http://www.vadiodes.com>
- [13] S. Cherednichenko, V. Drakinskiy, T. Berg, E. Kollberg, and I. Angelov, "The direct detection effect in the hot-electron bolometer mixer sensitivity calibration," *IEEE Trans. Microw. Theory Tech.*, vol. 55, no. 3, pp. 504–510, Mar. 2007.
- [14] H. Ekström, B. Karasik, E. Kollberg, and K. S. Yngvesson, "Conversion gain and noise of niobium superconducting hot-electron mixers," *IEEE Trans. Microw. Theory Techn.*, vol. 43, no. 4, pp. 938–947, Apr. 1995.
- [15] F. Arams, C. Allen, B. Peyton, and E. Sard, "Millimeter mixing and detection in bulk InSb," *Proc. IEEE*, vol. 54, no. 4, pp. 612–622.



Evgenii Novoselov, was born in 1988 in Saint-Petersburg, Russia. He received his B.Sc. and M.Sc. (summa cum laude) in 2009 and 2011, respectively, from The Saint-Petersburg National Research University of Information Technologies, Mechanics and Optics (NRU ITMO).

During his studies at the university, he worked at the research center "Femtosecond optics and femtotechnology" (NRU ITMO) (2007-2011). There he participated in a number of projects on the development of terahertz spectrography and reflectometry using TDS. After completing his master degree, he joined LLC "TELROS Integration" (Saint-Petersburg, Russia) as a communication systems design engineer (2011-2013). Currently, he is a PhD student at the Terahertz Millimetre Wave Laboratory at Chalmers University of Technology, working on MgB₂ Hot Electron Bolometers.



Sergey Cherednichenko, was born in 1970 in Mariupol, Ukraine. He received his Diploma with Honours in Physics in 1993 from Taganrog State Pedagogical Institute, and Ph.D. in physics in 1999 from Moscow State Pedagogical University.

He is working at the Department of Microtechnology and Nanoscience at Chalmers University of Technology (Gothenburg, Sweden). From 2000-2006 he was involved in development of terahertz band superconducting mixers for the Herschel Space Observatory; and from 2008 till 2009 in the water vapour radiometer for ALMA. As from 2007 he has been an Associate Professor at the department of Microtechnology and Nanoscience at Chalmers University of Technology. His research interests include terahertz heterodyne receivers and mixers, photon detectors; THz antennas and optics; thin superconducting films and their application for THz and photonics; and material properties at THz frequencies.